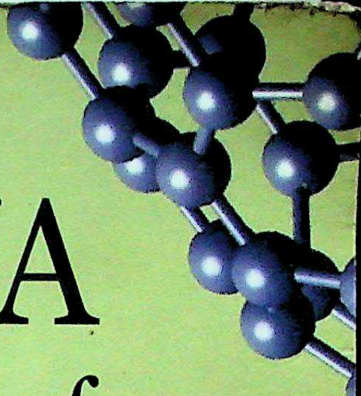

PRAMANA
journal of physics

Special Issue:

Proceedings of the Linear Collider Workshop (LCWS06) – Part I

Vol. 69, No. 5
November 2007

Indian Academy of Sciences

Springer

Pramana – journal of physics

A monthly journal of physics published by the Indian Academy of Sciences in collaboration with Indian National Science Academy and Indian Physics Association. The journal publishes refereed papers covering current research in physics, both original research articles and invited reviews. Pramana also publishes special issues devoted to (a) advances in specific areas of physics and (b) Proceedings of select high quality conferences.

Editor

H R Krishnamurthy
Indian Institute of Science, Bangalore

Associate Editor

Rohini M Godbole
Indian Institute of Science, Bangalore

Editorial Board

R C Budhani
Indian Institute of Technology, Kanpur
B K Chakrabarti
Saha Institute of Nuclear Physics, Kolkata
Charusita Chakravarty
Indian Institute of Technology, New Delhi
Subhash Chaturvedi
University of Hyderabad, Hyderabad
N K Dadhich
Inter-Univ. Centre for Astron. and Astrophys, Pune
Rajiv V Gavai
Tata Institute of Fundamental Research, Mumbai
Neelima Gupte
Indian Institute of Technology, Chennai
A M Jayannavar
Institute of Physics, Bhubaneswar
S Kailas
Bhabha Atomic Research Centre, Mumbai
Deepak Mathur
Tata Institute of Fundamental Research, Mumbai
M V N Murthy
The Institute of Mathematical Sciences, Chennai
K S Narayan
JNC for Advanced Scientific Research, Bangalore
S Phatak
Institute of Physics, Bhubaneswar
R Ramaswamy
Jawaharlal Nehru University, New Delhi
Amit Roy
Inter-University Accelerator Centre, New Delhi
K C Rustagi
Indian Institute of Technology, Mumbai
E V Sampathkumaran
Tata Institute of Fundamental Research, Mumbai
K L Sebastian
Indian Institute of Science, Bangalore
Abhijit Sen
Institute for Plasma Research, Gandhinagar
Dinesh Sharma
Indian Institute of Technology, Mumbai
Subodh R Shenoy
University of Hyderabad, Hyderabad
K Subramanian
Inter-Univ. Centre for Astron. and Astrophys, Pune
C S Sundar
Indira Gandhi Centre for Atomic Research, Kalpakkam

Editor of Publications

N Mukunda
Indian Institute of Science, Bangalore

Editorial Office

Indian Academy of Sciences, C V Raman Avenue,
P.B. No. 8005, Bangalore 560 080, India

Telephone: 80-2361 2546, 80-2361 2943; Telefax: 91-80-2361 6094

Email: pramana@ias.ernet.in

Website: http://www.ias.ac.in/pramana/ http://www.iisc.ernet.in/academy/pramana/

Editorial Staff

G Chandramohan
Cicilia Edwin
M Srimathi
Usha S Philip

Subscription

All correspondence regarding subscription within India should be addressed to The Circulation Department of the Academy. Email: orders@ias.ernet.in
Online orders within India are also accepted at Scholars without Borders (www.scholarswithoutborders.in).
Email: mail@scholarswithoutborders.in

International subscriptions are processed by Springer (www.springer.com)

The Americas (North, South, Central and the Caribbean): journals.NY@springer.com
Outside the Americas: subscriptions@springer.com

© 2007 by the Indian Academy of Sciences. All rights reserved

"Information for contributors" is printed in the last issue of every volume.

Proceedings of the
Linear Collider Workshop (LCWS06) – Part I

Indian Institute of Science
Bangalore

9–13 March 2006

Guest Editors

ROHINI M GODBOLE
ATUL GURTU

. M ollege of Education
Raipur, Bantalab
Jammu.
Acc No....5283....
Dated.....19/3/2024

Published by
Indian Academy of Sciences
Bangalore

International Advisory Committee

B Barish, Caltech
S Bertolucci, Frascati
H S Chen, IHEP, Beijing
J Dainton, Cockroft Inst.
J Dorfan, SLAC
J Engelen, CERN
B Foster, Oxford
P W-Y Huang, Taiwan
J S Kang, Korea
S Komamiya, Tokyo
F LeDiberder, France
P Oddone, Fermilab
S Ozaki, BNL
R Petronzio, Rome
V S Ramamurthy, DST, Delhi
V Rubakov, INR, Moscow
M Schocket, Chicago
A Shotter, TRIUMF
A Skrinsky, BINP
F Takasaki, KEK
G Taylor, Sydney
M Tigner, Cornell
Y Totsuka, KEK
A Wagner, DESY

National Organizing Committee

Tariq Aziz, TIFR, Mumbai
Sunanda Banerjee, TIFR, Mumbai
Rahul Basu, IMSc, Chennai
R K Bhandari, VECC, Kolkata
Debajyoti Choudhury, Delhi University
Amitava Datta, Jadavpur University
R Godbole, IISc, Bangalore
Atul Gurtu, TIFR, Mumbai
S Krishnagopal, CAT, Indore
N K Mondal, TIFR, Mumbai
B Mukhopadhyaya, HRI, Allahabad
G Rangarajan, IISc, Bangalore
S Raychaudhury, IIT, Kanpur
S Rindani, PRL, Ahmedabad
Amit Roy, NSC, Delhi
D P Roy, TIFR, Mumbai
J B Singh, Panjab University
K Sridhar, TIFR, Mumbai

Local Organizing Committee

B Ananthanarayan, IISc, Bangalore
R Godbole, IISc, Bangalore
A Patel, IISc, Bangalore
G Rangarajan, IISc, Bangalore
D Sen, IISc, Bangalore
S Vaidya, IISc, Bangalore

Programme Committee

U Baur, SUNY, Buffalo
J Brau, Oregon
T Camporesi, CERN
M Danilov, ITEP
R Godbole, IISc, Bangalore
A Gurtu, TIFR, Mumbai
R Heuer, Hamburg
J Hewett, SLAC
Y B Hsiung, Taiwan
J Jaros, SLAC
D Karlen, Victoria
A Kronfeld, Fermilab
W G Li, IHEP, Beijing
D Miller, UCL, London
A Miyamoto, KEK
Y Okada, KEK
M Oreglia, Chicago
R Patterson, Cornell
H B Park, KNU
F Richard, Orsay
R Settles, Munich
H Videau, Ecole Polytechnique
G Weiglein, IPPP, Durham
H Yamamoto, Tohoku

Foreword

The International Linear Collider Workshop in the year 2006 (LCWS06) was held in March 9–13, 2006, in Bangalore, India under the aegis of World Wide Study for Future Linear Colliders. These workshop-style conferences have been the main International fora for developing the physics case and reviewing detector designs and techniques for an electron–positron linear collider. This world-wide series of the LCWS workshops started in 1991 and have travelled all around the world. More information on the previous workshops in the series is available at the url http://www.tifr.res.in/∼lcws06/. History has taught us that electron and hadron accelerators are complementary in the exploration of new physics frontiers. The high energy physics community in the world has reached an accord that a Linear Collider operating at 0.5–1.0 TeV would provide both unique and essential scientific opportunities; it has endorsed with the highest priority the construction of such a machine. A major milestone towards this goal was the approval, by the International Committee on Future Accelerators (ICFA), of the recommendation of the International Technology Recommendation Panel (ITRP) for the cold technology of the future International Linear Collider (ILC). LCWS06 was the first International Linear Collider Workshop after the choice of this technology was announced.

Together with the Large Hadron Collider (LHC) at CERN, the ILC would allow physicists to explore energy regions beyond the reach of today's accelerators. At these energies, researchers anticipate significant discoveries that will lead to a radically new understanding of what the universe is made of and how it works. The nature of the ILC's electron–positron collisions would give it the capability to answer compelling questions that discoveries at the LHC will raise, from the identity of dark matter to the existence of extra dimensions. The ILC Global Design Effort (GDE) will establish the design of the ILC, focusing the efforts of hundreds of accelerator scientists and particle physicists in America, Europe and Asia. The ILC will be designed, funded, managed and operated as a fully international scientific project. An international effort will define the administrative and financial model for the project.

The meeting of the GDE, held concurrently with the LCWS06 for the first three days was a 'first' at the LCWS06 organised by the Indian Institute of Science, Bangalore and has been repeated since then. A discussion of the effort towards an ILC in India, meetings between the ILC community and the members of the Indian industry, which has contributed to magnet building at the LHC at CERN, Geneva, as well as those who have contributed to the detectors and an Education and Outreach Workshop for Physics Teachers conducted by the QuarkNet team from Fermilab and the Indian Academy of Sciences, were other notable features of this workshop. The report of many of these has appeared elsewhere (for example *Symmetry* (Fermilab), *Current Science* (Bangalore, India, etc.) and is not included here in these Proceedings.

The GDE pre-workshop meetings began, in fact, one day before the LCWS06, on the 8th itself. The GDE/ILC overview by Barry Barish in the joint plenary session set the tone of the meeting. The joint plenary session also had talks by Roberto Petronzio (FALC) and Ken Peach (Europe Strategic Plan) which were presented remotely. The DCR, i.e. Design Concept Report (for the LCWS) and the RDR i.e. Reference Design Report (for the GDE) documents were discussed at the workshop and have since then been finalised and both efforts have moved on. The GDE has chosen to post all its talks on the agenda at http://ilcagenda.cern.ch/conferenceOtherViews.py?view=standard &confId=6. The LCWS had its usual division into 13 parallel sessions. Included in these proceedings are some of the plenary talks such as the overview of the physics and experiments at the ILC, the detector concepts, as well as a large number of talks presented in the parallel sessions. Large number of contributions related to detectors and the machine design interface (MDI) and $\gamma\gamma, e\gamma$ option are some of the special features of these proceedings.

Our thanks are due to the following agencies in India which sponsored the Workshop: (1) Department of Science and Technology (DST), (2) Board of Research in Nuclear Sciences (BRNS), (3) Harishchandra Research Institute (HRI), (4) Institute for Mathematical Sciences (IMSc), (5) Tata Institute for Fundamental Research (TIFR) and (6) Variable Energy Cyclotron Centre (VECC). Thanks are also due to Deutsches Elektronen Synchrotron (DESY) at Hambury, for support towards participation of young researchers as well as those from the third world in the workshop.

A very special vote of thanks to Dr Anil Kakodkar, Chairman, Atomic Energy Commission for finding time in his highly busy schedule to come and inaugurate the activity. We wish to express our thanks to the members of the WWS, the program advisory committee as well as the national organizing committee. Our most sincere thanks are due to the EHEP group at TIFR which maintained the web page for the conference. Special thanks are due to Mr Desphande, EHEP group, TIFR for his valuable help in many aspects of the organization and communications at the workshop. Help from Mr Ravi from IMSc, Chennai and Mr Kulkarni from TIFR, in setting up and maintaining the network facility at the conference venue and making all the remote presentations possible, deserves a special mention. We would like to thank the staff of the Indian Academy of Sciences for their invaluable help in many aspects of organization as well as the digital library at IISc, for allowing use of their premises for conducting the Education and Outreach Workshop for Physics Teachers, held on March 10 and 11, 2006. Thanks are due to

Profs S Tonwar, B Acharya and R Verma for their help in conducting the same. A very, very special vote of thanks to Prof. G Rangarajan for helping us out of many a sticky spots. Last but not the least, a big cheer to the team of volunteers from the Centre for Theoretical Studies and the Department of Physics in the Indian Institute of Sciences Bangalore and Raman Research Institute. In addition to them some of our colleagues from different high energy physics institutes, HEP students and post-doctoral fellows provided invaluable help. There are far too many to mention all by names, but Profs S Banerjee, R Basu, S K Rai and S D Rindani deserve special mention. Without the help of the office staff of the Centre of High Energy Physics, Mr Keshava and Mr Janardhana, nothing could have been achieved. We extend our sincere thanks to them. Of course, the workshop was a success only because of the participants, hence we extend most heartfelt thanks to them.

Rohini M Godbole
Indian Institute of Science
Bangalore 560 012
Atul Gurtu
Tata Institute of Fundamental Research
Mumbai 400 005
(*Guest Editors*)

PRAMANA
— journal of
physics

© Indian Academy of Sciences

Vol. 69, No. 5
November 2007
pp. 697–702

The LDC detector concept

TIES BEHNKE, for the LDC Concept Group
Deutsches Elektronen Synchroton, Notkestrasse 65, D-22603 Hamburg, Germany
E-mail: ties.behnke@desy.de

Abstract. In preparation of the experimental program at the international linear collider (ILC), the large detector concept (LDC) is being developed. The main points of the LDC are a large volume gaseous tracking system, combined with high precision vertex detector and an extremely granular calorimeter. The main design force behind the LDC is the particle flow concept.

Keywords. International linear collider; large detector concept.

PACS No. **13.66-a**

1. Introduction

The large detector concept (LDC) detector concept group [1] was formed early in 2004. Its goal is to design a complete detector concept for the LDC, based on a gaseous central tracking detector, and on granular calorimetry. The concept is heavily based on the concept of particle flow for event reconstruction.

LDC started from the TESLA detector, developed for the TESLA TDR [2] and published in 2001. The basic philosophy of the detector and its main components are the same as for TESLA, but there has been significant development of the sub-components since then.

LDC has members from all three regions, though its biggest contributors still come from Europe. About 70% of the people subscribed to LDC are from Europe, 27% from the Americas, and only 3% from Asia.

Since its formation in 2004 one of the main tasks of LDC has been the specification of the detector, and the writing of a conceptual design report, the 'Detector Outline Document' (DOD). The DOD for LDC has been presented for the first time at this conference, and will continue to evolve until the summer of this year, when a more or less final version is expected. In figure 1, a side-view of one quarter of the LDC detector is shown.

2. The detector concept

The LDC has three main components: a high precision vertex detector, surrounding the interaction region, a large gaseous tracking system, which is backed up by

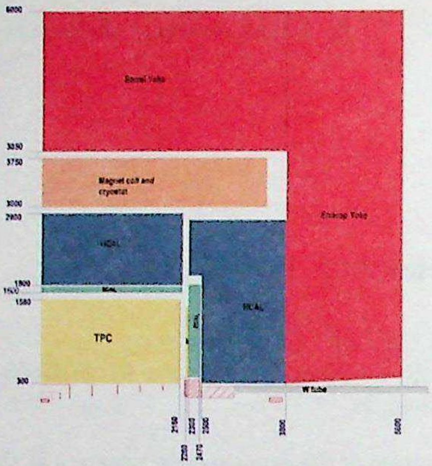

Figure 1. Side-view of the LDC detector concept.

a sophisticated system of tracking devices mostly made from silicon, and a very advanced and granular calorimeter. In the following the main components and their layout will be briefly reviewed, and the reasoning behind them will be explained.

2.1 *Vertex detector*

The vertex detector at the LDC is a SI-based pixel detector. It is installed as close as possible to the interaction point. Currently an inner radius of 1.5 cm is thought to be compatible with constraints from the accelerator. The baseline design has five layers of pixel detectors, equally spaced at a radial distance of approximately 1 cm. The innermost layer has a length of 7.5 cm, the others are twice as long.

The vertex detector has to function in the presence of significant backgrounds, mostly from beam–beam interactions. The anticipated level of background hits makes it mandatory that the vertex detector layer be read out quickly, and integrate over at most 40–50 bunch crossing.

A number of different pixel technologies are currently studied in detail by R&D collaborations. No decision has been taken as to which of these technologies will eventually be used in the LDC detector.

2.2 *Tracking detectors*

The central part of the tracking detector is a large volume TPC. This is backed up by a number of thin precision tracking devices at the inner and outer radii of the TPC.

The tracking at the ILC has to be highly efficient – efficiency is in many respects more important than precision. Particle flow requires that all particles are

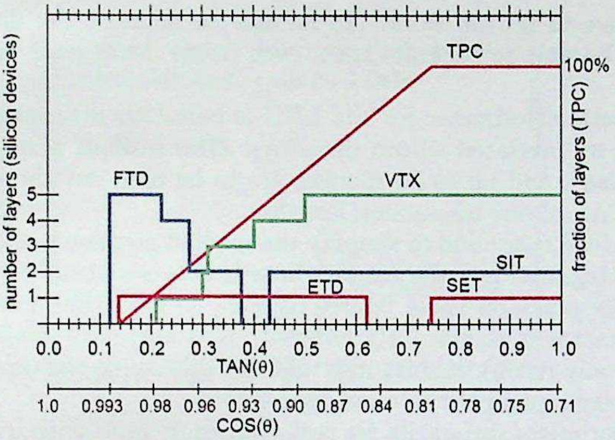

Figure 2. Number of points measured on a track as a function of $\tan(\theta)$.

reconstructed, and a highly efficient tracking system is a pre-requisite for that. The ultimate precision in tracking is needed for a number of specific reactions, in particular the reconstruction of the Higgs boson in the ZH recoil analysis.

A TPC has a number of advantages when used as a tracking detector at the ILC. It provides three-dimensional reconstruction of charged particles with a large number of points along a track. At the same time the material in a TPC is small, thus minimizing the disturbance of a particle before it reaches the calorimeter.

Compared to previously built TPCs, the ILC TPC has to have a point resolution and a double track resolution significantly improved. The current baseline design foresees a TPC with around 200 points measured along a track, and read out by a system of micro-pattern gas detectors. These novel gas amplification devices promise to provide a stable, reliable readout system, which can be realized with comparatively little material in the endplate compared to a traditional wire readout.

To breach the gap between the vertex detector and the TPC two layers of Si-based strip detectors are foreseen at intermediate radii. They provide a link between the VTX and the TPC, and improve the efficiency to find long-lived particles which decay between the VTX and the TPC. On the outer radius of the TPC, and behind the endplate, a small number of precision tracking layers are under study, to improve the linking between the tracking detectors and the calorimeters. Among the candidates for these detectors are Si strip detectors, and, in particular in the end cap direction, gaseous detectors like straw tubes of GEM-based chambers. In figure 2 the number of available points on a track as a function of the polar angle is shown. At any direction at least two points, in most cases five points, supplement the TPC measurement.

2.3 *Calorimeters*

The central piece of a detector at the ILC is the calorimeter. Particle flow works under the assumption that all particles in an event can be reconstructed individually. For charged tracks, the tracking detectors are used and for neutral ones, the calorimeters have to do the work. To be able to measure the direction and the energy, and to be able to separate them even inside dense jets, very granular devices are needed.

The electromagnetic calorimeter for the LDC is based on a tungsten absorber structure, sampled by pixelated silicon detectors. The readout pixels are of the order of 0.5×0.5 cm^2, and up to 30 samples are to be read out through the full thickness of the ECAL of one interaction lengths.

To minimize the dead space and to simplify the readout structure, the electronics is supposed to be integrated into the readout boards between absorber plates. The digitization will take place on these boards as well, so that the number of lines which leave the detector is significantly reduced. It is currently studied whether the electronics will only record the hit, or in addition determine the time of the hit, to support bunch tagging and background rejection.

The hadronic calorimeter, primarily for cost reasons, is built with iron plates as absorbers. The readout is done either through scintillator tiles, or through gas-filled resistive plate chambers or GEM-based chambers. Both options have their relative merits, and no decision has been taken so far on a technology selection.

Both ECAL and HCAL follow an octagonal geometry in the barrel region. Two endcaps close the solid angle coverage down to small angles. The very forward region is covered by two special purpose calorimeters, the beam-Cal and the lumi-Cal, which provide coverage down to approximately 3 mrad. These latter devices are, in addition, used to measure the beam–beam induced background radiation, and to determine the luminosity of the machine.

2.4 *Magnet and muon system*

Outside the calorimeters a large superconducting coil provides a magnetic field of up to 4 T, along the beam direction. The coil has been designed in such a way that it is very similar to the already built and tested CMS coil. Apart from the main field generating windings the coil will include a small number of special windings, mostly at the end of the coil, which can be used to tune the homogeneity of the field in the central region.

The magnetic flux from the field is returned through an external iron flux return. This contains the detector nearly entirely, thus ensuring proper return of the field, and, at the same time, a self-shielding detector. The iron return yoke is instrumented with a few layers of muon chambers, most probably resistive plate chambers, to measure the momentum of those muons which penetrate the calorimeter and the coil. Together the very granular calorimeters, which themselves will do an excellent job of the identification of muons, promise to provide a spectacular muon performance of the detector.

3. Detector performance

The detector performance has been studied in some detail based on a full reconstruction program developed within the GEANT4 toolkit. The MOKKA program

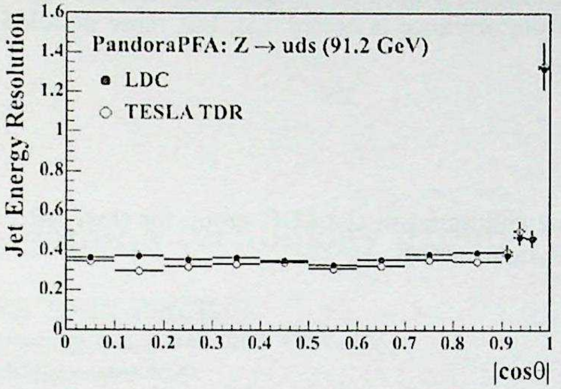

Figure 3. Simulated resolution of the LDC detector concept as a function of $\cos(\theta)$, using a particle flow approach.

provides an easy way to define geometries, and to allow the variation of most parameters at run time for systematic studies.

As stated previously the detector design has been heavily influenced by the idea of particle flow. Particle flow wants to improve the overall event reconstruction by an approach where each particle in the event is reconstructed individually. Charged particles are reconstructed by the tracking detectors. Their hits in the calorimeter are identified and removed from the event. In this way fluctuations of the total energy in the event, which are introduced by a calorimetric measurement, are removed. The remaining hits in the ECAL and in the HCAL are then searched for neutral particle candidates. Particle identification is attempted based on tracking and calorimeter information, and particles are grouped according to the photon hypothesis, the electron hypothesis, pion and neutral hadron hypothesis. A crucial role in this is played by a very granular electromagnetic and hadronic calorimeter, which is a pre-requisite to find the traces of individual particles, and to make a high quality assignment between tracker hits and calorimeter hits. The particle flow algorithms are still very much under development, and none has demonstrated the wanted performance of $30\%/\sqrt{E}$. Nevertheless significant progress has been made over the last few years, and first promising results are being presented. In figure 3 the performance of the LDC for Z events on the Z pole is shown as a function of the polar angle.

In future one of the main priorities of the LDC will be to further improve the particle flow algorithms, to reach a point where the algorithms are good and stable enough that a real detector optimization can be attempted. The results from such a study might well change the layout of the LDC detector once again.

4. Summary and outlook

The LDC concept group has presented the first version of the LDC detector at this meeting. The LDC detector has been re-optimized with respect to its size compared to earlier versions. This should result in some significant cost savings. First studies suggest that the loss of performance is acceptable, but more detailed studies will be needed in the future.

Acknowledgement

I would like to thank my colleagues in the LDC group for their help in preparing the presentation and the manuscript.

References

[1] For details, see http://www.ilcldc.org
[2] T Behnke *et al* (eds), TESLA TDR, volume 4 DESY 2001-011

PRAMANA
— journal of
physics

© Indian Academy of Sciences

Vol. 69, No. 5
November 2007
pp. 703–706

Gamma gamma technology group

ALEXANDER JOHN FINCH
Lancaster University, Lancaster, LA1 4YW, UK
E-mail: a.finch@lancaster.ac.uk

Abstract. The results presented at this conference in the $\gamma\gamma$ technology group are described.

Keywords. Laser cavity; photon linear collider; Compton scattering; emmittance; beam dump.

PACS Nos **13.60.Fz; 52.59.Wd**

1. Introduction

This report briefly describes the results presented at this conference on work to develop the technology required to build the proposed gamma gamma option, also known as the photon linear collider (PLC) [1]. Before describing the work presented at this conference I would like to put it in context. At the International Workshop on High Energy Photon Linear Colliders, 5–8 September 2005, Kazimierz Dolny, Poland, the first meeting of the Gamma Gamma Planners Group was held, chaired by David Miller. The purpose of the meeting was to form a group of people who would study the technical aspects of the photon linear collider. Various tasks were assigned, for example, A F Zarnecki agreed to look at the crossing angle and I agreed to study beam monitoring and feedback issues. A meeting was planned for October 2005 to study issues around the laser cavity design. Unfortunately one month after this David Miller suffered a major stroke which disrupted our efforts considerably. The organisation of the Laser Cavity meeting was taken over by myself and was postponed to 10 January 2006. I presented the outcome of this meeting at this conference [2]. I am happy to report that David continues to make a steady recovery and we look forward to seeing him again at future meetings.

2. Laser cavity

Klemz *et al* [3] have worked out a detailed design proposal for the laser cavity for use at the PLC. An overview of the layout is shown in figure 1. A number of people have provided written comments on the design, and a meeting was held in January 2006 to draw these people together, together with experts from outside

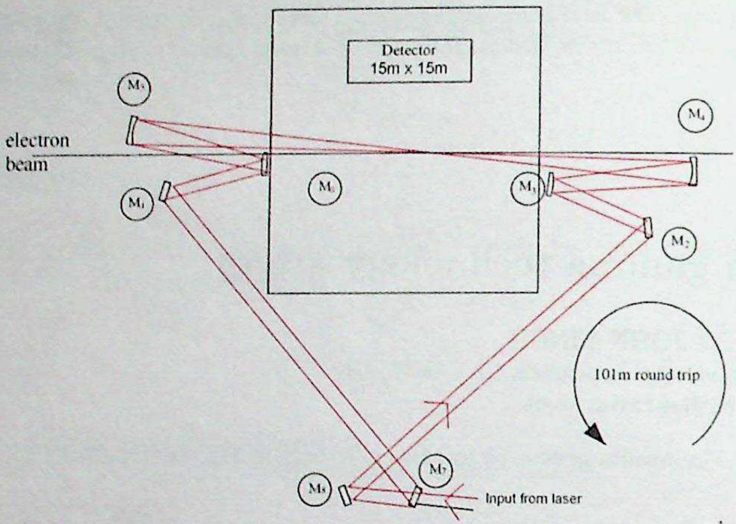

Figure 1. Proposed design for the laser cavity.

the accelerator community to discuss the feasibility of the proposed design [2]. It was very successful and helped to clarify what further studies need to be done, as well as emphasising the usefulness of making these contacts with laser and optics experts from other communities.

3. Compton-based polarized positron source for ILC

Another community with whom we hope to have fruitful collaboration is those people working on laser cavity for use in a polarized positron source. At this meeting we heard about such activity from Roychowdhury [4], on behalf of V Yakmenko, D Cline, I V Pogorelsky, and V N Litvinenko. They propose a polarized positron source based on Compton backscattering inside an optical cavity fed by a CO_2 laser beam focused on a 6 GeV e^- beam produced by a Linac. The proposal utilizes commercially available units for the laser and accelerator systems. It requires a high power picosecond CO_2 laser mode of operation developed at ATF. A three-year laser R&D program is needed to verify the laser operation in this non-standard regime.

4. Simulation of background using CAIN

Zarnecki [5] described his studies of the background at a PLC using CAIN. He studied whether backgrounds using the 20 mrad crossing angle option were acceptable by looking at the energy deposited at the face of the final dipole, 4.5 m from the interaction point. A large number of low-energy electrons are produced in the collision which are strongly deflected by the opposing beams and the detector magnetic field. An outgoing beam opening of at least 12 mrad is needed to avoid power

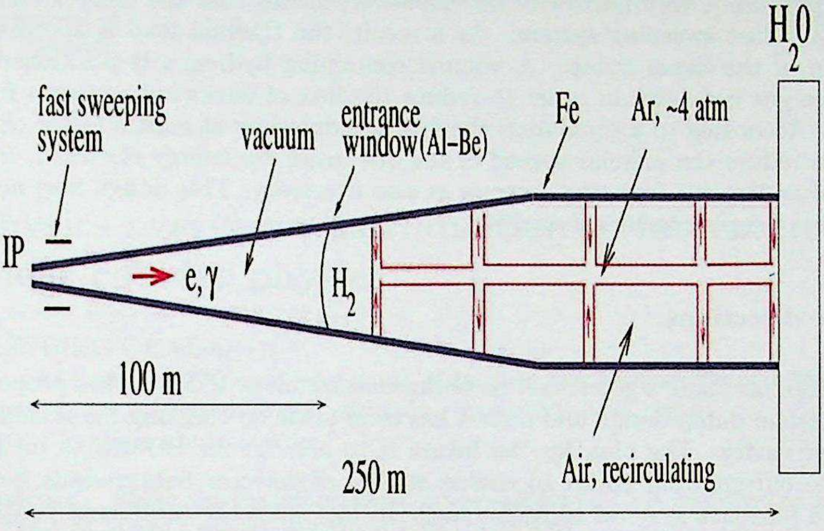

Figure 2. Proposed design for beam dump.

dissipation greater than 10 W. A new design has been proposed for the dipole which reduces its outer radius to 39 mm, combining this with an elliptical beam pipe for removing the spent beams which results in acceptable background levels for a 20 mrad crossing angle.

5. Damping ring

Telnov [6] described how the damping rings might be modified to obtain smaller emittances and thus higher luminosity at the PLC. The luminosity of the ILC is limited by beam–beam interactions and so there is no advantage in making the beams smaller than the current design. These effects are absent when one or both beams have been converted to a photon beam, and so there is a large potential gain in reducing the electron beam size. The minimum size of the beam is determined by the emittances and it might be possible to reduce these by adding more wigglers into the damping ring. This proposal needs input from damping ring experts so that the baseline configuration does not exclude this upgrade option.

6. Beam dump

A possible scheme of the beam dump for the photon collider was presented by Telnov. Having put in great efforts to produce an intense beam of high energy photons it is then a challenge to dispose them off. In the design proposed here (figure 2) the long argon gas target ensures that the photon beam produces a shower so that its density at the beam dump becomes acceptable. Approximately 10% of the electrons from the original beam are not converted into photons, and they also produce a very narrow beam. However, in this case the density can be reduced by a fast sweeping system. As a result, the thermal load is acceptable everywhere in the beam dump. A volume containing hydrogen is positioned in front of the gas converter in order to reduce the flux of backward neutrons from the dump. According to a simulation the flux is reduced by at least a factor of 10. In order to reduce the angular spread of the disrupted low energy electrons, some focusing after the exit from the detector is also necessary. This design now needs to undergo a detailed technical analysis.

7. Future directions

A F Zarnecki has made a good start on background studies, V Telnov has proposed a possible beam dump design and a start has been made on checking the feasibility of the laser cavity. The plan for the future is to arrange for BDSIM to be able to take the output from CAIN to enable studies of detector backgrounds, beam dumps and feedback systems to be pursued. In fact since the conference progress has already been made in this direction. We will also pursue the possiblity of simulating the dynamics of the laser cavity to test its feasibility.

8. Final thoughts

A quick look at the agenda of this conference reveals that 25% of the ILC-related physics talks related to the gamma gamma option. However there was no mention of the gamma gamma option in the detector concepts or DCR talks. Clearly the design of the baseline accelerator needs to take into account all the possible upgrade options. The gamma gamma community are concerned that in the rush to prepare for the e^+e^- machine, allowance is not being made for a future upgrade of the photon linear collider.

References

[1] ECFA/DESY Photon Collider Working Group: B Badelek *et al*, TESLA Technical Design Report, Part VI, Chapter 1: Photon collider at TESLA, *Int. J. Mod. Phys.* **A19**, 5097 (2004)

[2] A Finch, *These proceedings*

[3] G Klemz, K Monig and I Will, Design study of an optical cavity for a future photon collider at ILC, arXiv:physics/0507078
G Klemz and K Monig, A laser cavity for a future photon collider at ILC, *Acta Phys. Polon.* **B37**, 1257 (2006)

[4] S Roychowdhury, *These proceedings*

[5] A F Zarnecki, *These proceedings*, http://www.fuw.edu.pl/~zarnecki/

[6] V Telnov, *These proceedings*

PRAMANA
— journal of
physics

© Indian Academy of Sciences

Vol. 69, No. 5
November 2007
pp. 707–718

Physics overview: Introduction to international linear collider physics

YASUHIRO OKADA
Theory Division, KEK and Department of Particle and Nuclear Physics, The Graduate University for Advanced Studies, Tsukuba, Ibaraki 305-0801, Japan
E-mail: Yasuhiro.okada@kek.jp

Abstract. Physics at the international linear collider (ILC) is described as an introductory talk at Linear Collider Workshop 2006 (LCWS06).

Keywords. Linear collider; Higgs boson; unified theory; dark matter.

PACS Nos 29.17.+w; 14.80.Bn; 12.10.-g; 95.35.+d

1. Introduction

It has been a long time since the high energy physics community recognized the importance of the future e^+e^- linear collider with energy starting from the 500 GeV range. Physics studies of such a linear collider have been performed in international as well as regional frameworks, and there are many documents describing physics case of linear colliders [1–4]. In this talk, I will review physics potential of the International Linear Collider (ILC).

There has been much progress in understanding fundamental constituents of matter and forces acting among them throughout the last century. In fact, the development of elementary particle theory in the 20th century was a history of how we identified and understood four fundamental forces of Nature, namely gravity, electromagnetic, weak and strong interactions. In the early 1970s, so called standard model was proposed, in which three interactions except for gravity were described in a unified fashion in terms of gauge theory. Since then, a primary focus of high energy experiments has been to establish the basic principle of the standard model. Discovery of W and Z bosons at CERN in the early 1980s, increasing understanding of QCD as a fundamental theory of strong interaction and precise measurements of electroweak processes at LEP and SLC in the 1990s have led us to confidence that gauge symmetry is a guiding principle of the law of elementary particle physics.

Although the aspect of gauge invariance is well understood by recent experimental studies, there is another important ingredient in the standard model, which is the Higgs mechanism. Quarks, leptons and gauge bosons are introduced as massless fields in the standard model, and their masses are generated only through spontaneous breaking of the electroweak symmetry. Even though the concept of the spontaneous symmetry breaking in the particle physics is well established in the study of chiral symmetry of the strong interaction, we know little about how electroweak symmetry breaking occurs and what is the dynamics determining the scale of the weak interaction. This is a primary reason why we need to explore the TeV scale physics.

Finding the dynamics behind the electroweak symmetry breaking is likely to lead to physics beyond the standard model. There are many theoretical proposals for physics beyond the standard model, and each model offers different scenario for the electroweak symmetry breaking sector. In supersymmetric models the Higgs boson is accompanied by fermionic partners and the weak scale is related the supersymmetry (SUSY) breaking scale. In the little Higgs model, the Higgs boson is a composite particle arising from dynamics of new strong interaction at a more fundamental level. In the model of extra space-dimensions, the Higgs field may have some geometrical origin. Thus, the question of how the weak scale is generated could be related to physics scenario beyond the TeV scale, which may lead to unification of all forces, change our understanding of the fundamental constituents, or new concept on space and time.

Since the discovery of the cosmic microwave background of the Universe, cosmology has made a tight connection with physics laws at the microscopic world. The relationship becomes more and more important as we understand physics at smaller distance. It is likely that collider experiments play crucial roles in identifying dark matter in the Universe. Furthermore, cosmological problems such as baryogensis, inflation and dark energy require understanding physics scenario beyond the standard model.

In 2008, the LHC experiment will start its operation. This is a proton–proton collider with the center-of-mass energy of 14 TeV. The main purpose of the experiment is to discover the Higgs particle and explore physics at the TeV scale. Discovery reach of a new particle increases roughly by one order of magnitude in its mass compared to Tevatron and LEP II experiments, so that LHC is a crucial machine determining the future direction of particle physics.

The main purpose of the ILC experiment is to explore the Higgs physics and physics beyond the standard model, following the initial outcome of the LHC experiment. In this respect, once LHC finds something new, there will be more questions to be answered at ILC. LHC and ILC are two machines with different characters. Discovery reach for new particles is generally larger for LHC than ILC with 500 GeV center-of-mass energy, unless signals are suppressed in hadron collider or hidden by backgrounds. On the other hand, ILC has such advantages as initial state are elementary particles with well-defined kinematics, and the background level is less severe. The ILC's capability of beam polarization and energy scan will be important in many physics studies. ILC has several options like γ–γ, e–γ, and e^-–e^- collider modes, and the Z-pole operation. These options may become essential once new physics scenario is found out.

In the following, I will briefly review physics goals of the ILC experiment.

2. Higgs physics

Finding the dynamics of electroweak symmetry breaking and the mass generation mechanism of elementary particles is the most important issue of the current particle physics. We first have to discover the Higgs particle that is a physical excitation mode of the field responsible for the electroweak symmetry breaking. In order to show that the discovered particle is relevant for the Higgs mechanism, the coupling constants to quarks, leptons and gauge bosons have to be determined in good accuracy.

Although it is almost clear that the W and Z boson masses are generated from the spontaneous breaking of the electroweak symmetry, little is known about the Higgs sector. In the minimal standard model, only one Higgs doublet field is introduced, and consequently, we are able to make a precise prediction of the property of the Higgs boson in terms of a single parameter, the Higgs boson mass. We can even derive the upper bound of the Higgs boson mass from precise electroweak measurements together with the top quark mass, and the favored mass region is below 200 GeV [5].

The decay branching ratio and production processes of the Higgs boson crucially depend on the mass of the Higgs boson. The general property of the Higgs boson is that it couples more strongly to heavier elementary particles, because the role of the Higgs field is to generate mass terms for particles. This is quite different from the gauge interaction, where universality is a basic property.

Detailed study on the Higgs search at the LHC experiment shows that Higgs boson can be discovered independent of its mass region, as long as its production and decay properties are not much different from the standard model case [6,7]. If the mass is above two Z boson decay threshold, basic parameters of the particle like spin and width can be determined using the four lepton decay mode. On the other hand, there will be inconsistency between the indirect information on the Higgs boson mass and direct observation, if the candidate of the Higgs boson becomes much heavier than 200 GeV. In such case, an urgent question will be to find out some missing ingredients that can fill the gap. If the Higgs boson mass is lighter, an important issue will be to single out the correct model of the Higgs sector that is consistent with existence of the light Higgs boson. For example, in the minimal supersymmetric standard model (MSSM), the lightest Higgs boson mass is less than 140 GeV [8]. In such a situation, we need to determine whether or not the Higgs sector corresponds to that of the MSSM.

The goal of the Higgs physics at ILC is to determine basic properties of the Higgs particle and coupling constants related to the Higgs particle. The main production mechanism of the Higgs boson (H) at e^+e^- collider are ZH production from an s-channel virtual Z boson and $H\nu\bar{\nu}$ production from the WW fusion process. For example, the production cross-section of a 120 GeV Higgs boson through the ZH process is about 200 fb^{-1} for ILC with the center-of-mass energy of 300 GeV. This means that the number of produced Higgs bosons can be $\mathcal{O}(10^5)$ for integrated luminosity of 500 fb, which is a target number of the ILC machine. With this number, we will be able to determine the Higgs property very precisely.

The spin and parity of the Higgs boson will be determined without ambiguity at ILC using the threshold scan and the production angular distribution. These measurements are necessary to confirm that the discovered particle corresponds to the Higgs boson.

The main goal of the Higgs physics at ILC is, however, to determine the coupling constant of the Higgs boson with gauge bosons and quarks and leptons. These are directly related to mass generation mechanism of these elementary particles. In particular, ZZH and WWH coupling constants as well as $Hb\bar{b}$ coupling are determined up to a few % accuracy for the Higgs boson mass of 120 GeV, which is within a favored mass range by current global fit of the standard model parameters. The determination of ZZH and WWH coupling constants has fundamental meaning for the establishment of the Higgs mechanism because this three-point coupling can only arise after the Higgs field develops its vacuum expectation value. The magnitude of this coupling is related to the gauge boson mass. The three point coupling and the mass term are in fact originated from the same term in the original gauge invariant Lagrangian. The $Hb\bar{b}$ coupling is also important for the Higgs boson of this mass range because $H \to b\bar{b}$ is the main decay mode, and information obtained on this coupling at LHC is very limited. Indeed, LHC experiments can give useful information on some ratios of the coupling constants [9], but precise determination of absolute values of coupling constant is a major goal achievable at ILC. The precision of various coupling constants is shown in figure 1, which is taken from ref. [4]. The expected coupling determination relevant for mass-generation mechanism is plotted against a particle mass for each particle. For precise determination of the top Yukawa coupling, the energy of ILC has to be upgraded from 500 GeV. In this figure, the triple Higgs coupling constant is also included. This measurement is very important because it gives first access to the shape of the Higgs potential.

Precise measurements of Higgs coupling constants offer opportunity to search for new physics scenario. In many new physics models, extension of the Higgs sector is required, or new interaction related to the Higgs field is introduced. Thus, some Higgs coupling constants can deviate from the standard model prediction by enough amount that can be distinguished at the ILC experiment. Some of the examples are as follows:

- The ratio like $h \to WW$ and $h \to \tau\tau$ branching ratios for the lightest Higgs boson (h) in MSSM as a probe of the heavy Higgs boson mass [2,10–12].
- The ratio of $h \to bb$ and $h \to \tau\tau$ branching ratios as a probe to SUSY loop corrections to the Yukawa couplings for the large $\tan\beta$ case in MSSM [12–14].
- Radion-Higgs mixing effects on the Higgs coupling constants in models with extra space dimensions [15,16].
- Shift of the light Higgs boson branching ratios in the little Higgs model with T parity [17].
- Deviation of the Higgs triple coupling constant from the standard model prediction in models in which electroweak baryogenesis is possible such as two Higgs doublet model [18] or standard model with a low cutoff scale [19].

In this way, even if only one Higgs boson is found at the ILC experiment at the first stage, precision measurements may provide valuable information on physics at higher energy scale and point us to the next energy threshold. Just as we are now expecting a relatively low mass Higgs particle from the precise measurements

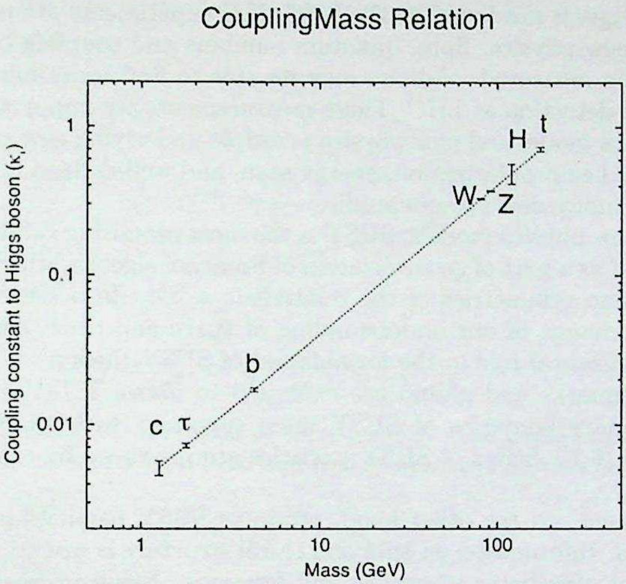

Figure 1. Precision of the coupling constant determination at ILC with $\mathcal{L} = 500\ \mathrm{fb}^{-1}$. The coupling constant κ_i is defined from the Higgs boson coupling to the "i" particle. $m_i = \kappa_i v$ holds in the standard model. The Higgs boson mass is taken to be 120 GeV. For the charm, tau, bottom, W and Z coupling measurements, $\sqrt{s} = 300$ GeV is assumed. $\sqrt{s} = 500$ GeV (700 GeV) is taken for the Higgs self-coupling ($t\bar{t}H$) coupling measurement (from ref. [4]).

on the gauge interaction, Higgs physics at ILC may determine scenario in higher energy scale.

3. Direct search for new physics

Although there are various reasons to expect physics beyond the standard model, solving the hierarchy problem has been a major theoretical motivation. Now the problem is how to explain the weak scale of $\mathcal{O}(100)$ GeV that is much smaller than the gravity scale of 10^{19} GeV in spite of the fact that this hierarchy seems to be easily destroyed by quantum corrections within the standard model. SUSY is a unique symmetry that can eliminate the quadratic divergence in the Higgs mass renormalization. The composite Higgs scenario is another way to solve the hierarchy problem, and little Higgs models proposed recently are classified in this category [20,21]. There are also attempts to change the gravity scale by considering extra spatial dimensions [22–24].

In all of these proposals, there should be some signals at the TeV scale. Search for such signals is one of main purposes of the LHC experiment. Expected signals depend on the correct new physics model and masses of new particles. In some cases, different models give similar signals at the LHC.

Once some new signals are found at the LHC, ILC experiments are necessary to figure out what is new physics. Spin, quantum numbers and coupling constants of new particles will be measured, and one may be able to find lower mass particles which have escaped detection at LHC. These measurements are important to select a correct new physics model and new physics principle underlying new phenomena. The ILC's ability of beam polarization, energy scan, and well-defined kinematics is a powerful tool for many new physics studies.

Among various new physics models, SUSY is the most promising candidate. This symmetry is realized as a part of generalization of Poincaré algebra, which is algebra formed by space–time symmetries of the relativistic world. In a sense, discovery of SUSY demands change of our understanding of space and time. Furthermore, SUSY plays a fundamental role in the formulation of SUSY theory.

Search limit of squarks and gluino are extended to above 2 TeV at the LHC experiment in ordinary scenarios of SUSY mass spectrum such as the minimal supergravity model [6,7]. Series of SUSY particles are produced by cascade decay processes.

The ILC experiment, on the other hand, produces SUSY particles in pair from lower mass particles. Information on spin and chiral structure is essential for SUSY because it is a symmetry between bosons and fermions. Electron–positron linear colliders are ideal machines, and beam polarization and threshold scan are very useful for this purpose.

By precise determination of masses, spin, quantum numbers and coupling constants of SUSY particles, we can determine various parts of SUSY Lagrangian. These measurements are essential to establish new symmetry and look for deeper structure of the theory. Examples are:

- Test of SUSY relation between electron–selectron–Bino and electron–gauge boson couplings for right-handed selectron productions [25]. The precession of this test may allow us to look for loop corrections to a tree level relation (super-oblique corrections) [26,27].
- Reconstruction of chargino and neutralino mass matrices. This is a SUSY analogy to the weak mixing angle measurement in the $SU(2) \times U(1)$ gauge boson sector. There is also a possibility to measure CP violation measurements in chargino and slepton sectors [28].
- Test of GUT relation between $SU(2)$ and $U(1)$ gaugino masses [29].
- Search for lepton flavor violation in slepton production and decays [30,31]. These measurements have potential impacts on the study of neutrino mass generation mechanism in SUSY models, along with lepton flavor violation searches in charged lepton rare decay processes.
- Determination of the left–right mixing for third generation squarks [32]. These are important parameters for the Higgs mass formula through one loop corrections.
- Tau polarization measurement which is useful to determine the composition of the lightest neutralino [25,33].

In order to understand whole structure of the SUSY model, combined analysis of LHC and ILC experiments is important. Inputs from lower mass spectrum at ILC can improve what can be extracted from LHC experiments. Squark and gluino

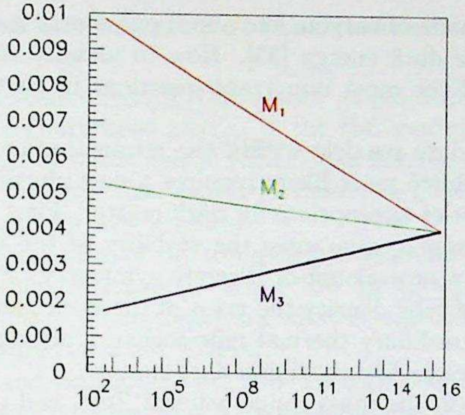

Figure 2. Evolution of three gaugino mass parameters in the SUSY GUT using inputs from LHC and ILC measurements (from ref. [34]).

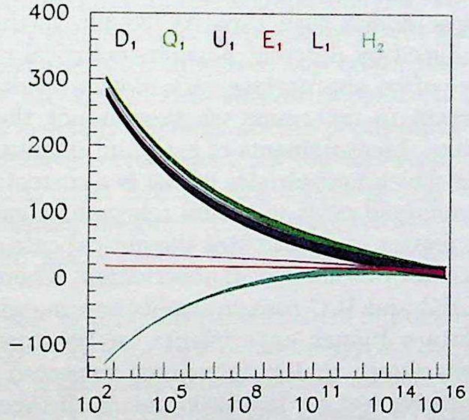

Figure 3. Evolution of scalar quark and lepton and Higgs mass parameters in a minimal supergravity point using inputs from expected results in LHC and ILC combined analysis (from ref. [34]).

masses from LHC and precise measurements on the neutralino, chargino and slepton sectors from ILC allow us to extrapolate SUSY breaking mass parameters toward the high energy scale. In this way we may be able to know the origin of SUSY breaking mechanism and test various unification scenarios. Figures 2 and 3 show how the unifications of gaugino and scalar mass parameters can be tested from combined analysis of LHC and ILC experiments [34].

4. Dark matter and collider physics

There have been significant improvements in our understanding of cosmological parameters. In particular, the recent measurement of cosmic microwave background by WMAP has shown that a large part of the energy content of the present Universe is not understood. Only 4% is made of baryon, and about one-fourth is dark matter and the rest is considered to be dark energy [35]. How to identify the nature of dark matter has become one of the most important questions in particle physics and cosmology.

Since there is no good candidate particle within the minimal standard model, solution of the dark matter problem most likely requires a new physics model. A new particle should have properties appropriate for dark matter. First of all, there should be some theoretical reason to guarantee the stability of the dark matter particle. This usually involves a new global or discrete symmetry. Furthermore, to explain the correct amount of relic density the mass of the dark matter particle is close to the weak scale in an ordinary thermal relic scenario, although different mass range is possible in other cases like the axion dark matter.

If the dark matter particle is in the mass range below 1 TeV, and produced by decays from colored particle, it is possible that some signal is obtained in the missing energy channel of the LHC experiment. Several models are proposed for such signals, for example, SUSY with R-parity, universal extra-dimension model with KK-parity [36,37], and little Higgs models with T-parity [38,39]. In these models, new parity symmetries are introduced by different phenomenological reasons, but a common feature is the existence of an appropriate dark matter candidate.

The ILC experiment is important to determine whether or not the candidate particle is actually the dark matter. Measurements of spin and quantum numbers of new particles at ILC can tell us which new physics model is a correct one. Then, we can determine coupling constants and mass spectrum relevant for calculation of thermal relic abundance of dark matter, and compare theoretical calculation with the dark matter quantity determined by cosmological observation. There have been much work on whether or not LHC and ILC measurements can match the precision obtained by WMAP and future Planck experiments for the case of typical SUSY dark matter [40,41]. It was shown that improvement expected at the ILC experiment is essential for quantitative test for the dark matter. If theoretical prediction agrees with the cosmological observation, we can conclude that the particle produced at collider experiments is indeed the dark matter and the thermal history of the Universe behind the calculation is correct. This will be a significant improvement of our understanding of cosmology.

The identification of the dark matter will also open a new area for astroparticle physics [41]. There are many experimental attempts to detect dark matter signals directly and indirectly. In indirect searches, cosmic ray particles that are supposed to be originated from annihilation of dark matter particles are detected using gamma ray, positron, anti-proton and neutrino. If the dark matter property is determined precisely at collider experiments, annihilation cross-sections in halos of galaxies as well as detection cross-sections for various detection methods are known. We then can obtain important information on how dark matter is distributed in our galaxy or in the Universe, since different methods are sensitive to the dark matter density in different regions. In this way, we may be able to improve our understanding of the Universe. Cosmic parameter determination, identification of dark matter particle at collider experiments, and direct and indirect searches for dark matter are all important in the new field, and ILC is expected to play an essential role.

5. Precision measurements of the standard model processes

Precision measurements in top quark, gauge boson and fermion pair production processes are guaranteed physics in the ILC experiment. On the one hand, precise determination of fundamental parameters like the top quark mass is important by themselves, but the other aspect is that these measurements provide new opportunities to search for new physics.

The threshold scan of the top quark production is unique for ILC. The precision of top mass measurement is about 100 MeV, which is an improvement by more than one order of magnitude from what is expected at LHC. The top quark width can be measured at a few % level.

In the standard model, the top Yukawa coupling constant is among the five dimensionless coupling constants determining the main dynamics of the theory along with the three gauge coupling constants and the Higgs self-coupling constant. Therefore, the top quark mass plays an important role in various phenomenological studies within and beyond the standard model. For example, the analysis on oblique parameters of gauge boson propagators would give a different picture for the new physics constraint with improved top quark mass and the observed Higgs boson mass. It is also known that theoretical prediction on the lightest CP-even Higgs boson mass crucially depends on the precision of top quark masses in MSSM due to large radiative corrections from top and stop loop diagrams. In addition, there is a possibility that new physics effects appear in the top width and anomalous coupling constant measurements. An interesting example is provided by the little Higgs model, where one of the essential ingredients is extension of the top quark sector.

Fermion pair production processes are important channels at ILC. These provide indirect ways to look for new particles beyond the kinematical reach for the collider. For instance, if the correct new physics model contains a new neutral gauge boson (Z'), the indirect search limit can extend to a few TeV range for 500 GeV ILC, which is comparable with direct Z' boson search limit at the LHC. If the LHC experiment finds the new gauge boson, the ILC experiment will become important to determine the coupling constants using angular distribution and initial beam polarization. One such analysis is shown in figure 4 from ref. [42]. We may be able to choose the correct model among possible candidates with an extra gauge boson by combined information on the mass and the coupling.

6. Conclusions

The LHC experiment which will be in operation soon is expected to open a new era of the high energy physics. A Higgs boson is likely to be discovered, and its mass alone provides very important information. New particles and new phenomena are also expected in various new physics scenarios.

The most urgent question of the current high energy physics is to establish the mass generation mechanism of quarks, leptons and gauge bosons, namely the Higgs physics. The discovery of a new particle is only the first step, and we have to check that the discovered particle indeed plays the role of the Higgs boson. This will be

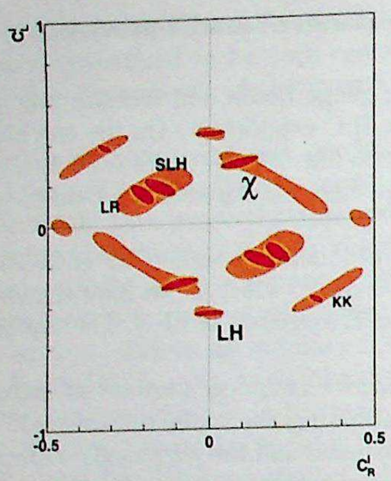

Figure 4. Resolving power (95% CL) for $M_{Z'} = 2$ TeV and $\sqrt{s} = 500$ GeV, $\mathcal{L}_{\rm int} = 1{\rm ab}^{-1}$ for leptonic couplings based on the leptonic observables $\sigma^{\mu}_{P_{e^-}P_{e^+}}$, $A^{\mu}_{\rm LR}$, and $A^{\mu}_{\rm FB}$. The largest region corresponds to the unpolarized case while the smallest region corresponds to electron and positron polarization of 80% and 60% respectively with the middle region corresponding to only electron polarization. The couplings correspond to various models with a Z' boson (E_6 χ, LR, LH, SLH and KK models) (from ref. [42]).

achieved by precise determinations of the Higgs couplings, and ILC will play an essential role for this purpose.

There are several approaches to explore physics beyond the standard model at ILC. The Higgs coupling measurements themselves are one way to find new physics effects. Direct studies of new particles and new phenomena give clear information on the new model, if new particles are kinematically accessible. Even if the collider energy is not enough to produce new particles directly at the first stage of the ILC experiment, indirect searches through processes involving only the standard model particles have great potential to provide useful information in selecting the correct model. ILC's features like clean experimental environment, availability of polarized beams, and energy scan are useful tools for precise measurements.

In this way, TeV scale physics explored at LHC and ILC is expected to help us to understand physics laws at the shortest distance and state of our Universe in the earliest time.

References

[1] ECFA/DESY LC Physics Working Group: J A Aguilar-Saavedra *et al*, arXiv:hep-ph/0106315
[2] ACFA Linear Collider Working Group: K Abe *et al*, arXiv:hep-ph/0109166
[3] American Linear Collider Working Group: T Abe *et al*, in *Proc. of the APS/DPF/DPB Summer Study on the Future of Particle Physics*, Snowmass, 2001,

edited by N Graf, SLAC-R-570 Resource book for Snowmass 2001, 30 Jun–21 Jul 2001, Snowmass, Colorado

[4] GLC project: Linear collider for TeV physics, KEK-REPORT-2003-7, available at http://lcdev.kek.jp/RMdraft/

[5] The LEP Electroweak Working Group: LEPEWWG/2006-01, available at http://lepewwg.web.cern.ch/LEPEWWG/

[6] ATLAS detector and physics performance. Technical design report, vol. 2, CERN-LHCC-99-15

[7] CMS Physics TDR, CERN/LHCC 2006-021, June 2006

[8] G Degrassi, S Heinemeyer, W Hollik, P Slavich and G Weiglein, *Euro. Phys. J.* **C28**, 133 (2003), arXiv:hep-ph/0212020

[9] M Duhrssen, S Heinemeyer, H Logan, D Rainwater, G Weiglein and D Zeppenfeld, *Phys. Rev.* **D70**, 113009 (2004), arXiv:hep-ph/0406323

[10] J Kamoshita, Y Okada and M Tanaka, *Phys. Lett.* **B391**, 124 (1997), arXiv:hep-ph/9512307

[11] M Carena, H E Haber, H E Logan and S Mrenna, *Phys. Rev.* **D65**, 055005 (2002), Erratum: *Phys. Rev.* **D65**, 099902 (2002), arXiv:hep-ph/0106116

[12] K Desch, E Gross, S Heinemeyer, G Weiglein and L Zivkovic, *J. High Energy Phys.* **0409**, 062 (2004), arXiv:hep-ph/0406322

[13] K S Babu and C F Kolda, *Phys. Lett.* **B451**, 77 (1999), arXiv:hep-ph/9811308

[14] J Guasch, W Hollik and S Penaranda, *Phys. Lett.* **B515**, 367 (2001), arXiv:hep-ph/0106027

[15] J L Hewett and T G Rizzo, *J. High Energy Phys.* **0308**, 028 (2003), arXiv:hep-ph/0202155

[16] D Dominici, B Grzadkowski, J F Gunion and M Toharia, *Nucl. Phys.* **B671**, 243 (2003), arXiv:hep-ph/0206192

[17] C R Chen, K Tobe and C P Yuan, *Phys. Lett.* **B640**, 263 (2006), arXiv:hep-ph/0602211

[18] S Kanemura, Y Okada and E Senaha, *Phys. Lett.* **B606**, 361 (2005), arXiv:hep-ph/0411354

[19] C Grojean, G Servant and J D Wells, *Phys. Rev.* **D71**, 036001 (2005), arXiv:hep-ph/0407019

[20] N Arkani-Hamed, A G Cohen, E Katz, A E Nelson, T Gregoire and J G Wacker, *J. High Energy Phys.* **0208**, 021 (2002), arXiv:hep-ph/0206020

[21] N Arkani-Hamed, A G Cohen, E Katz and A E Nelson, *J. High Energy Phys.* **0207**, 034 (2002), arXiv:hep-ph/0206021

[22] N Arkani-Hamed, S Dimopoulos and G R Dvali, *Phys. Lett.* **B429**, 263 (1998), arXiv:hep-ph/9803315

[23] I Antoniadis, N Arkani-Hamed, S Dimopoulos and G R Dvali, *Phys. Lett.* **B436**, 257 (1998), arXiv:hep-ph/9804398

[24] N Arkani-Hamed, S Dimopoulos and G R Dvali, *Phys. Rev.* **D59**, 086004 (1999), arXiv:hep-ph/9807344

[25] M M Nojiri, K Fujii and T Tsukamoto, *Phys. Rev.* **D54**, 6756 (1996), arXiv:hep-ph/9606370

[26] H C Cheng, J L Feng and N Polonsky, *Phys. Rev.* **D56**, 6875 (1997), arXiv:hep-ph/9706438

[27] E Katz, L Randall and S F Su, *Nucl. Phys.* **B536**, 3 (1998), arXiv:hep-ph/9801416

[28] S Y Choi, A Djouadi, M Guchait, J Kalinowski, H S Song and P M Zerwas, *Euro. Phys. J.* **C14**, 535 (2000)

S Y Choi, J Kalinowski, G Moortgat-Pick and P M Zerwas, *Euro. Phys. J.* **C22**, 563 (2001)

[29] T Tsukamoto, K Fujii, H Murayama, M Yamaguchi and Y Okada, *Phys. Rev.* **D51**, 3153 (1995)

[30] N V Krasnikov, *Phys. Lett.* **B388**, 783 (1996)

[31] N Arkani-Hamed, H C Cheng, J L Feng and L J Hall, *Phys. Rev. Lett.* **77**, 1937 (1996)

[32] A Finch, H Nowak and A Sopczak, hep-ph/0211140

[33] M M Nojiri, *Phys. Rev.* **D51**, 6281 (1995), arXiv:hep-ph/9412374

[34] B C Allanach, G A Blair, S Kraml, H U Martyn, G Polesello, W Porod and P M Zerwas, arXiv:hep-ph/0403133

[35] D N Spergel *et al*, arXiv:astro-ph/0603449

[36] G Servant and T M P Tait, *Nucl. Phys.* **B650**, 391 (2003), arXiv:hep-ph/0206071

[37] H C Cheng, J L Feng and K T Matchev, *Phys. Rev. Lett.* **89**, 211301 (2002), arXiv:hep-ph/0207125

[38] H C Cheng and I Low, *J. High Energy Phys.* **0309**, 051 (2003), arXiv:hep-ph/0308199

[39] H C Cheng and I Low, *J. High Energy Phys.* **0408**, 061 (2004), arXiv:hep-ph/0405243

[40] J Feng, *J. Phys.* **G32**, R1 (2006)
M Battaglia, I Hinchliffe and D Tovey, hep-ph/0406147
M Nojiri, G Polesello and D R Tovey, *J. High Energy Phys.* **0603**, 063 (2006)
H Baer *et al*, *J. High Energy Phys.* **0402**, 007 (2004)
B Allanach *et al*, *J. High Energy Phys.* **0412**, 020 (2004)
P Bambade *et al*, hep-ph/0406010
M Berggren, F Richard and Z Zhang, hep-ph/0510088
V Khotilovitch *et al*, hep-ph/0503165
T Moroi and Y Shimizu, *Phys. Rev.* **D72**, 115012 (2005)
T Moroi, Y Shimizu and A Yotsuyanagi, *Phys. Lett.* **B625**, 79 (2005)

[41] E A Baltz, M Battaglia, M E Peskin and T Wizansky, *Phys. Rev.* **D74**, 103521 (2006), arXiv:hep-ph/0602187

[42] S Godfrey, P Kalyniak and A Tomkins, arXiv:hep-ph/0511335

PRAMANA
— journal of
physics

© Indian Academy of Sciences

Vol. 69, No. 5
November 2007
pp. 719–725

Physics beyond the standard model and cosmological connections: A summary from LCWS06

K SRIDHAR
Department of Theoretical Physics, Tata Institute of Fundamental Research,
Homi Bhabha Road, Mumbai 400 005, India
E-mail: Sridhar@theory.tifr.res.in

Abstract. The international linear collider (ILC) is likely to provide us important insights into physics sector that may supersede our current paradigm, viz., the standard model. In anticipation of the possibility that the ILC may come up in the middle of the next decade, several groups are vigourously investigating its potential to explore this new sector of physics. The Linear Collider Workshop in Bangalore (LCWS06) had several presentations of such studies which looked at supersymmetry, extra dimensions and other exotic possibilities which the ILC may help us discover or understand. Some papers also looked at the understanding of cosmology that may emerge from studies at the ILC. This paper summarises these presentations.

Keywords. Beyond standard model physics; collider physics; cosmological connections.

PACS No. **12.60.-i**

1. Introduction

For several years, there has been a widespread realisation in the high energy physics community of the importance of a high-energy linear collider to study TeV-scale physics in the scattering of electrons, positrons and photons. This realisation has found concrete articulation in a project now known as the international linear collider (ILC) [1–6]. Due to the nature of the leptonic and photonic initial states, such a collider will provide a very clean environment setting the stage for probing the TeV scale with remarkably high precision. Much in the same way as the LEP experiments in CERN complemented the UA1 and UA2 experiments in understanding the gauge sector of the standard model (SM), the ILC is expected to complement the large hadron collider (LHC) in the quest to understand the nature of electroweak symmetry breaking and its ramifications [7].

Moreover, compelling theoretical arguments tell us that electroweak symmetry-breaking also holds the key to the discovery of new physics: the much sought-after ‘physics beyond the standard model’. From a purely phenomenological point of view, almost any kind of new physics can be expected at high energies that these colliders will probe. But high-energy theorists have focussed their research on the sub-class of models which are consistent with some of the following principles: symmetry, renormalizability, unitarity, naturalness etc. To these principles are added consistency with existing experimental data and also accessibility of the theoretical models in upcoming experiments. These guiding principles narrow down the field considerably and the viable models that result fall into a few distinct classes.

Supersymmetry, or more precisely, the supersymmetric extension of the standard model is the most popular of these classes of models [8,9]. Indeed, the supersymmetric extension of the standard model is in no way unique but yields a whole class of models. Further simplifying assumptions, some based on aesthetic considerations and some decidedly ugly but simplifying nonetheless, are then added to arrive at a few models which have been the subject of vigourous investigations. One of the major physics goals of the ILC will be a systematic investigation of various regions of the supersymmetric parameter space in a quest to understand the mechanism responsible for supersymmetry breaking [3].

Another class of models that has been studied as possible extensions of the SM are models based on the idea of technicolour. While the minimal versions of these models are constrained by precision electroweak data, the non-minimal versions do manage to survive all existing constraints [10]. Indeed, in recent years, there has been a resurgence of interest in these models with the realisation that they can be thought of as being dual to some TeV scale extra-dimensional models [11]. Models of TeV-scale extra dimensions have opened up new avenues for theoretical speculation in high-energy physics [12,13]. These models provide new solutions to the hierarchy problem and predict a whole host of model-dependent experimental signatures at the TeV scale [14,15]. While the ILC may not be a discovery machine for this class of models, it will definitely help in pinning down the specifics of a model by providing a window within to investigate the details of these models [16].

A major part of the preparation for the ILC involve theoretical studies and simulations of the physics that can be potentially studied at this collider [17,18]. Work has been carried out for several years now by individual researchers as well as dedicated working groups and this work includes several investigations of supersymmetry, extra dimensions, technicolour and other extensions of the SM. More recently, there has been considerable progress in understanding the interplay between collider physics and cosmology and how collider searches for dark matter candidates in supersymmetry and other models can lead us to a determination of dark matter parameters and how this precision information may influence cosmology. This paper presents a summary of the work on beyond standard model physics and cosmological connections presented at the Linear Collider Workshop 2006 (LCWS06) [19].

2. Supersymmetry and the ILC

One of the major advantages of the ILC is that it will allow several precision studies of TeV-scale supersymmetry, help determine masses, branching ratios and supersymmetric parameters to a degree of accuracy that may help pin-point the underlying mechanism of supersymmetry breaking.

A fundamental relation in SUSY is that between the gauge and the Yukawa coupling:

$$\text{Gauge coupling } g = \text{Yukawa coupling } \hat{g}. \tag{1}$$

Testing these relations via precise cross-section measurements is very important and a detailed study of how to measure these couplings at a linear collider was presented [21]. For example, selectron production at ILC and their decays into neutralinos can be studied and polarisation allows us to disentangle $SU(2)$ and $U(1)$ couplings and provides a measurement of these couplings to better than 1%. Things are more complicated with $SU(3)$ at ILC because to produce coloured states one needs reactions like $e^+e^- \to \tilde{q}\tilde{q}g$. These rates turn out to be tiny unless the ILC operates at its highest planned centre-of-mass energy of 2 TeV.

The alternative is to do a combined LHC/ILC analysis and study production of squarks and their decays through charginos at the LHC and input values of squark and chargino/neutralino BRs measured precisely at the ILC. This method gives a test of the strong coupling identity down to a 4% level.

Precision electroweak data do not yield as sensitive an estimate of supersymmetric particle masses as they did for the top quark or the Higgs boson because decoupling guarantees that low-energy observables are insensitive to the effects of supersymmetric particles. On the other hand, loop processes involving supersymmetric particles may still be useful if the processes are either rare or forbidden in the SM. In the workshop, a detailed analysis of supersymmetric models was presented [22]. This analysis has been carried out using the precision measurements of electroweak observables like m_t, M_W and $\sin^2\theta_{\text{eff}}$ from LEP and Tevatron, the bound on the lightest Higgs boson mass, loop-induced quantities like $(g-2)_\mu$ and $\text{Br}(b \to s\gamma)$ and the constraints from WMAP on the cold dark matter density $\Omega_\chi h^2$ and other cosmological observations.

The different SUSY models that have been studied include:

1. *Constrained minimal supersymmetric standard model (CMSSM)*: In this model, the universality of scalar masses, gaugino masses and trilinear parameters is assumed at the input GUT scale.
2. *Non-universal Higgs model (NUHM)*: In this model, the soft SUSY-breaking scale masses for the two Higgs doublets are not universal. As compared to the CMSSM, these are two additional parameters and, at low energies, may be taken to be the Higgs mixing parameter μ and the CP-odd Higgs boson mass, m_A.
3. *Very constrained minimal supersymmetric standard model (VCMSSM)*: This is a version of the CMSSM with additional relations between the soft tri- and bi-linear SUSY parameters: $A_0 = B_0 + m_0$.
4. *Gravitino dark-matter model (GDM)*: This is a model with a gravitino LSP so that the gravitino is the dark matter candidate. But this is done with an MSUGRA framework where the gravitino mass is taken to be equal to m_0 at the input GUT scale and again the soft tri- and bi-linear parameters are related by: $A_0 = B_0 + m_0$.

For the CMSSM, VCMSSM and GDM, it is found that $m_{1/2}$ is constrained to be of the order of a few 100 GeV and this suggests light sparticles observable at the LHC and ILC. On the other hand, m_0 values in NUHM could be considerably larger and make production of sparticles at ILC, at least at a centre-of-mass energy of 500 GeV, difficult.

One of the most promising channels for SUSY discovery at the ILC is $\tilde{\tau}$ pair production followed by the decay of the $\tilde{\tau}$ to a τ and the LSP. A work reported at the meeting [23] showed how the measurement of the polarisation of the τ in its one-prong hadronic decay channel will provide information on the underlying SUSY breaking mechanism as well as a determination of SUSY parameters. The process studied was: $e^+e^- \rightarrow \tilde{\tau}_1\tilde{\tau}_1$ with $\tau_1 \rightarrow \tau\chi_1^0$. The normalised centre-of-mass angular distribution of the τ to a pion (or a vector meson) and a neutrino allows a determination of its polarisation P_τ. The composition of χ_1^0 determines the polarisation of the τ and it is this composition that yields model-discrimination. In MSUGRA: $P_\tau = +1$, in non-universal SUGRA: $P_\tau = \cos^2\theta_\tau - \sin^2\theta_\tau$, in models of anomaly mediation one gets $P_\tau = -1$, while in gauge mediation $P_\tau = \sin^2\theta_\tau - \cos^2\theta_\tau$. Thus it is possible to distinguish different SUSY models by measuring P_τ. The work also demonstrates how P_τ may be used in a global fit for a model-independent determination of SUSY parameters.

Another study presented [24] dealt with the implications for gaugino masses of renouncing the universality of gaugino masses at the GUT scale. In the framework of $SU(5)$ GUT, for example, such non-universality may result from the vacuum expectation value of the F-term of a chiral superfield which appears in the gauge-kinetic function.

In spite of being unequal, constraints on the neutralino and chargino masses result from the grand-unified framework. Upper bounds on neutralino masses and sum rules for neutralino–chargino mass relations are obtained. Not unexpectedly, these masses have significant dependence on the representation of the GUT group. These relations can be probed in the decays of neutralinos and Higgs at the ILC.

In another presentation [25], the process $e^+e^- \rightarrow \tilde{t}_1\tilde{t}_1 \rightarrow c\chi_1^0 c\chi_1^0$ was studied in case where the stop-neutralino mass difference is small. The scenario is motivated by SUSY dark matter studies where the dark matter precision determination is dependent on the scalar mass determination through the co-annihilation process. An iterative discriminant analysis method is used to weigh each event in such a way as to optimize signal to background.

At a centre-of-mass energy of 260 GeV, for a 122 GeV stop and 107 GeV neutralino, 50 fb^{-1} luminosity and 50% efficiency, 560 signal and 200 background events are estimated using the iterative discriminant analysis. This goes towards a precise determination of the stop mass and precise prediction for dark matter.

A proposal to look for dark matter at colliders was presented [26] in the context of a model where the gravitino is the lightest-supersymmetric particle (LSP) and the dark matter candidate and the next-to-lightest supersymmetric particle (NLSP) is a $\tilde{\tau}$ with lifetimes ranging from a few seconds to several years. This is studied by looking at the decay of the $\tilde{\tau}$ via $\tilde{\tau}_1 \rightarrow \tau\tilde{G}$. At the ILC, copious $\tilde{\tau}_1$ production yields a very precise determination of the $\tilde{\tau}$ parameters with results such as

$$\begin{aligned} &\delta m_{\tilde{\tau}} \sim 10^{-3} \\ &\delta m_{\tilde{G}} \sim 10^{-1}. \end{aligned} \tag{2}$$

The analysis can be extended to the case where the NLSP is any of the other sleptons.

3. Extra dimensions

One work presented [27] studied a low-scale supersymmetry-breaking scenario. SUSY-breaking in this model is mediated by low-scale gravity in a warped extra dimension. Due to the warping SUSY breaking scale Λ is brought down to the 1–10 TeV range. Hidden sector becomes visible due to strong interaction with the visible sector fields and production of hidden sector fields, X, at collider energies becomes possible. The production and decay of X at LHC and ILC has been studied and the phenomenology is very similar to radion phenomenology. A 1 TeV ILC should probe via $e^+e^- \to ZX$ masses of $X \sim$ 1.85 TeV.

In another presentation [28], a model of universal extra dimension, where all the particles are free to propagate in a fifth dimension which is compactified on a S_1/Z_2 orbifold, was considered. Kaluza-Klein (KK) number conservation in the model yields the lightest KK particle (LKP) which is γ_1. The KK excitation of the electron E_1 has a mass equal to that of the γ_1 but the degeneracy is lifted by radiative corrections. In this work, the process $e^+e^- \to E_1^+E_1^-$ at the ILC energies is studied with $E_1 \to e\gamma_1$. This decay proceeds with a 100% BR. It is found that KK electrons give forward-peaked events due to t-channel dominance and this implies large forward–backward asymmetries which will be observed at the ILC. It is shown that it is possible to use angular distributions to obtain precise information on these KK states.

A paper which studied the modification of the standard Einstein–Hilbert action in models of TeV-scale gravity through the addition of higher curvature terms was also presented [29]. These are higher-dimensional terms which involve the curvature tensor and their introduction results in new ghost and scalar fields in D dimensions. The ghost is removed from the spectrum by fine-tuning the model parameters but KK excitations of the scalar starting around a TeV in mass result and the phenomenology of these scalars is studied. It turns out that the KK excitations of the scalar has weak couplings in both the ADD and the RS models and does not alter the phenomenology in any serious fashion. On the other hand, the higher-curvature terms also modify the relationship between the fundamental scale in D dimensions and the Planck scale in four dimensions. This leads to a modification of the KK sectors of the ADD and the RS models and can lead to $O(1)$ modifications of the cross-sections for graviton emission or exchange in both models.

4. Interface with cosmology

Another presentation [30] dealt with the issue of how to use the ILC to identify the dark matter particle and to infer dark matter properties from the measured particle spectrum and cross-sections in a minimal supersymmetric standard model study with 24 independent parameters. The scans of the 24-dimensional space was done using the Markov chain Monte Carlo technique for 4 SUSY points (LCC1–LCC4) of the LC/cosmology study group. It was found that masses and splittings in typical examples have errors smaller by a factor of 3–10 compared to LHC errors. Also polarisation at ILC may help resolve multiple solution ambiguities prevalent at the LHC (bino-, wino-, higgsino-like LSP).

Rate of production of gamma rays in galactic halos is proportional to dark matter annihilation. Determination of the annihilation cross-section allows a model independent determination of dark matter density. The study concluded that a case for a 1 TeV ILC is very strong.

In yet another study [31], it was shown that dark matter annihilation into e^+e^- yields cosmic positron signals which can be probed in experiments like Pamela and AMS-2. If dark matter is detected in these experiments it will allow for mass determination in these experiments. The signal guarantees ILC will see $\gamma+$ DM pair production leading to spin and properties determination of dark matter at ILC.

5. Conclusions

In this paper, we have summarised the presentations made at the LCWS06 in Bangalore in the sessions on beyond standard model physics and cosmological connections. While significant progress has been made, there is still a lot of concentrated effort needed in pinpointing the role of the ILC in specific model contexts. No doubt much of this will be helped by the physics that the LHC will provide us with and the synergy and the complementarity of these two colliders has been the focus of several recent studies. Another theme of recent interest has been the interplay of collider signatures of new physics with cosmology. Clearly, there is a lot of interesting physics to look forward to in the coming decade.

References

[1] ECFA/DESY LC Physics Working Group: J A Aguilar-Saavedra *et al*, arXiv:hep-ph/0106315

[2] American Linear Collider Working Group: T Abe *et al*, in *Proc. of the APS/DPF/DPB Summer Study on the Future of Particle Physics*, Snowmass, 2001, edited by N Graf, arXiv:hep-ex/0106055

[3] American Linear Collider Working Group: T Abe *et al*, in *Proc. of the APS/DPF/DPB Summer Study on the Future of Particle Physics*, Snowmass, 2001, edited by N Graf, arXiv:hep-ex/0106056

[4] American Linear Collider Working Group: T Abe *et al*, in *Proc. of the APS/DPF/DPB Summer Study on the Future of Particle Physics*, Snowmass, 2001, edited by N Graf, arXiv:hep-ex/0106057

[5] American Linear Collider Working Group: T Abe *et al*, in *Proc. of the APS/DPF/DPB Summer Study on the Future of Particle Physics*, Snowmass, 2001, edited by N Graf, arXiv:hep-ex/0106058

[6] ACFA Linear Collider Working Group: K Abe *et al*, arXiv:hep-ph/0109166

[7] LHC/LC Study Group: G Weiglein *et al*, *Phys. Rep.* **426**, 47 (2006), arXiv:hep-ph/0410364

[8] H P Nilles, *Phys. Rep.* **110**, 1 (1984)

[9] H E Haber and G L Kane, *Phys. Rep.* **117**, 75 (1985)

[10] R S Chivukula, arXiv:hep-ph/0011264

[11] R Sundrum, arXiv:hep-th/0508134

[12] N Arkani-Hamed, S Dimopoulos and G R Dvali, *Phys. Lett.* **B429**, 263 (1998), arXiv:hep-ph/9803315

[13] L Randall and R Sundrum, *Phys. Rev. Lett.* **83**, 3370 (1999), arXiv:hep-ph/9905221

[14] G F Giudice, R Rattazzi and J D Wells, *Nucl. Phys.* **B544**, 3 (1999), arXiv:hep-ph/9811291

[15] T Han, J D Lykken and R J Zhang, *Phys. Rev.* **D59**, 105006 (1999), arXiv:hep-ph/9811350

[16] K Sridhar, *Int. J. Mod. Phys.* **A15**, 2397 (2000), arXiv:hep-ph/0004053

[17] ECFA/DESY LC Physics Working Group: E Accomando *et al*, *Phys. Rep.* **299**, 1 (1998), arXiv:hep-ph/9705442

[18] S Dittmaier, arXiv:hep-ph/0308079

[19] The summary of Higgs physics, top physics, QCD studies and loop calculations can be found in ref. [20]

[20] S Heinemeyer, *These proceedings*

[21] A Freitas, *These proceedings*

[22] S Heinemeyer, *These proceedings*
J R Ellis, S Heinemeyer, K A Olive and G Weiglein, *J. High Energy Phys.* **0605**, 005 (2006), arXiv:hep-ph/0602220

[23] M Guchait, *These proceedings*
R M Godbole, M Guchait and D P Roy, *Phys. Lett.* **B618**, 193 (2005), arXiv:hep-ph/0411306

[24] P N Pandita, *These proceedings*
K Huitu, J Laamanen, P N Pandita and S Roy, *Phys. Rev.* **D72**, 055013 (2005), arXiv:hep-ph/0502100

[25] A Sopczak, *These proceedings*

[26] A B Sefkow, *These proceedings*

[27] N Okada, *These proceedings*
H Itoh, N Okada and T Yamashita, *Phys. Rev.* **D74**, 055005 (2006), arXiv:hep-ph/0606156

[28] G Bhattacharyya, *These proceedings*
G Bhattacharyya, P Dey, A Kundu and A Raychaudhuri, *Phys. Lett.* **B628**, 141 (2005), arXiv:hep-ph/0502031

[29] T Rizzo, *These proceedings*
T G Rizzo, arXiv:hep-ph/0603242

[30] M Peskin, *These proceedings* (presented by J Hewett)
E A Baltz, M Battaglia, M E Peskin and T Wizansky, *Phys. Rev.* **D74**, 103521 (2006), arXiv:hep-ph/0602187

[31] S Matsumoto, *These proceedings*
S Matsumoto and M Senami, *Phys. Lett.* **B633**, 671 (2006), arXiv:hep-ph/0512003

PRAMANA
— journal of
physics

© Indian Academy of Sciences

Vol. 69, No. 5
November 2007
pp. 727–733

The road towards the international linear collider: Higgs, top/quantum chromodynamics, loops

S HEINEMEYER
Instituto de Fisica de Cantabria (CSIC-UC), Santander, Spain
E-mail: Sven.Heinmeyer@cern.ch

Abstract. The international linear e^+e^- collider (ILC) could go into operation in the second half of the upcoming decade. Experimental analyses and theory calculations for the physics at the ILC are currently performed. We review recent progress, as presented at the LCWS06 in Bangalore, India, in the fields of Higgs boson physics and top/QCD. Also the area of loop calculations, necessary to achieve the required theory precision, is included.

Keywords. International linear collider; quantum chromodynamics; top; loop Verein; Higgs.

PACS Nos 12.15.Lk; 12.60.Fr; 14.65.Ha

1. Introduction

There is a world-wide consensus that the international linear e^+e^- collider (ILC) is the next major project in the field of high-energy physics [1]. This has most recently been confirmed by the EPP2010 report [2]. The decision about the start of construction of the ILC will be taken by the end of this decade. It could go into operation in the second half of the next decade. It will therefore take data several years after the start of the large hadron collider (LHC). The physics case for the ILC, independent of what the LHC will find, has been made in various studies in the past years [3–7]. The complementarity and the synergy of the two colliders and combined physics analyses has been discussed extensively in ref. [6].

A very important consideration with respect to the ILC physics case is the question as to what the ILC can add to the LHC (or what can a combined ILC/LHC analysis add to the LHC). It has been shown [3–7] that in all conceivable physics scenarios the ILC can add valuable and important information. In particular, it can add precision analyses, pinning down model parameters extremely precisely. Moreover, in contrast to the LHC, this can often be done in a model-independent way. Furthermore, in many scenarios the ILC can discover new states that cannot be detected at the LHC. The combination of these three capabilities (precision measurements, model-independent analyses, discovery of new particles) enables the ILC to determine the underlying physics model.

While the physics case for the ILC has been made and the physics potential of the ILC has been analyzed, there are still many tasks that have to be performed until the full potential of the ILC can be exhausted. This concerns the experimental analyses as well as the (corresponding) theoretical calculations. In many scenarios the feasibility of the experimental analyses has to be worked out in detail. Theory calculations at the level of the anticipated ILC precision still have to be performed (see e.g. refs [8–10]). Progress in both directions has to be made over the next years in order to be ready once the ILC operation starts. The status of the field and about recent progress was given at the LCWS06 in Bangalore, India. Here we briefly review the presentations about new experimental analyses and new theory calculations given at the LCWS06. We focus on the fields of Higgs physics, top/QCD and loop calculations. The overview about the other fields is given elsewhere [11].

2. Higgs physics

If a (SM-like) Higgs mechanism is realized in nature, the LHC will find a Higgs boson and measure its characteristics [12–15]. To be certain that the state observed is indeed the Higgs boson, it is necessary to measure the couplings of this state to the W and Z gauge bosons, and to fermions such as the top and bottom quarks and the tau leptons. Consequently, the measurements at the LHC include a mass determination at the per cent level and coupling constant determination at the level of 10–20%. However, in order to do this several assumptions about the realization of the Higgs mechanism have to be made. Analyses could become much more involved if the Higgs boson decay rates are strongly different from the SM rates. Interesting physics could easily hide in the 10–20% precision achievable for the Higgs boson couplings. Higgs self-couplings are extremely complicated if not impossible to measure at the LHC. On the other hand, all these problems can be overcome with the ILC measurements [3–5,7].

The progress that will be necessary to fully exploit the ILC capabilities has been summarized in ref. [7], where the main open issues are:

- analyses with full simulations of the relevant ILC processes have to be performed,
- higher precision in the theory calculations for the relevant processes are needed to match the anticipated ILC accuracy,
- analyses for SM-like Higgs bosons with 'larger' mass ($M_H \gtrsim 150$ GeV) have to be done,
- tools (encoding high-precision calculations) have to become available,
- the LHC/ILC interplay has to be worked out in more detail.

These issues have (partially) been addressed at the LCWS06. Progress has been reported e.g. about the following subjects (more details can be found in the original publications):

- Improvements in the experimental analyses of triple Higgs boson couplings [16].

- Theory calculations for Higgs production at the $\gamma\gamma$ collider in the minimal supersymmetric standard model (MSSM) at the one-loop level [17].
- Higgs production in models with universal extra dimensions [18].
- Experimental analysis for the determination of anomalous Higgs couplings at the $e\gamma$ collider [19].
- Doubly charged Higgs production at the e^+e^- collider [20].
- Measurement of $\tan\beta$ in the MSSM via heavy Higgs boson production [21].
- Progress for the MSSM Higgs tool FeynHiggs [22].

3. Top/QCD

Top and QCD physics are a guaranteed physics case for the ILC. The top quark is deeply connected to many other issues of high-energy physics:

- Is it just a heavy quark, or does it play a special role in/for electroweak symmetry breaking?
- The experimental uncertainty of m_t induces the largest parametric uncertainty in the calculation of electroweak precision observables [23] and can thus obscure new physics effects.
- In supersymmetric (SUSY) models the top quark mass is an important input parameter and drives spontaneous symmetry breaking and unification.
- Little Higgs models contain ‘heavier tops’.

The status of the field has been summarized in ref. [24]. Especially the calculations for $e^+e^- \to t\bar{t}$ at the threshold are quite advanced (see e.g. ref. [25] for a review or ref. [26] for a recent update). Also for the process $e^+e^- \to t\bar{t}H$ and the determination of the top Yukawa coupling substantial progress has been made recently (see e.g. refs [27,28]).

Advance in the field of top/QCD has been reported at the LCWS06 in the following subjects (more details can again be found in the original publications):

- Improved calculation of the cross-section $\sigma(\gamma\gamma \to \text{hadrons})$ [29].
- A new theory evaluation on how to use the lepton characteristics in top decays as probe of new physics scenarios [30].
- A calculation of $\gamma\gamma \to H, A \to t\bar{t}$ in the MSSM, including the polarization of the top quarks; this measurement can be used to test the mixing between CP-even and CP-odd Higgs bosons [31,32].

In order to exploit the full ILC capabilities for top quark physics, many improvements are still necessary. This includes a coherent treatment of electroweak effects at the $t\bar{t}$ threshold [24] or the development of tools providing the prediction of $e^+e^- \to 6f$ or $8f$ (see e.g. ref. [34]).

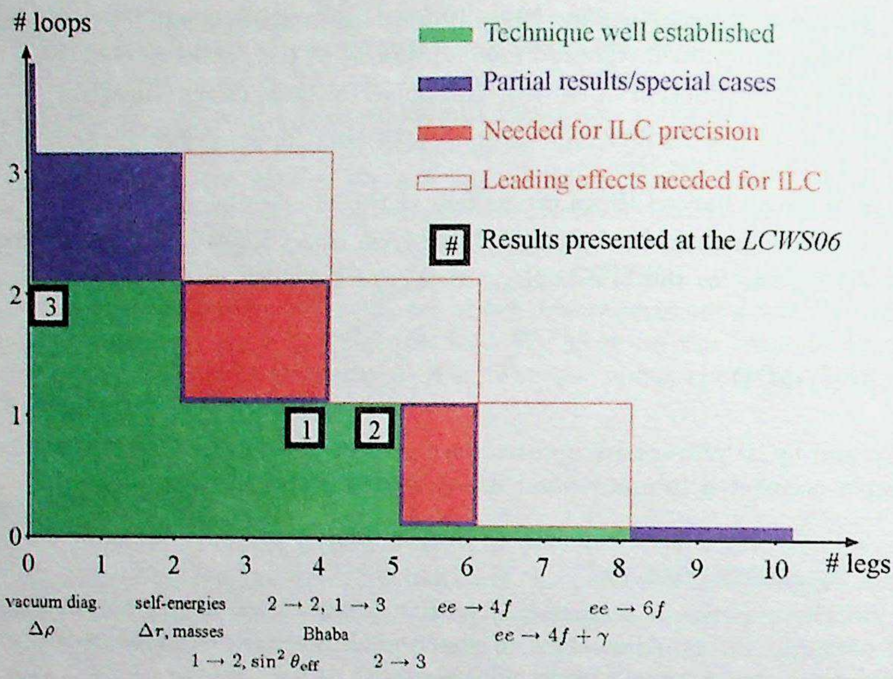

Figure 1. Status of the field of loop calculations. The orange shaded area shows what will be needed to match the anticipated ILC precision. The squares and numbers indicate the contributions presented at the LCWS06.

4. Loop calculations

The ILC will provide measurements of masses, couplings and cross-sections at (or even below) the per cent level [3–5]. A special example is the GigaZ option, which will determine the W boson mass with an error of 7 MeV and the effective leptonic weak mixing angle with a precision of 1.3×10^{-5} (see refs [35,36] and references therein). These anticipated future high precision measurements can fully be exploited only if they are matched with a theory prediction at the same level of accuracy. These theory predictions have to be obtained in the model under investigation (e.g. the SM, or the MSSM, for a recent overview see ref. [37]). The status of the field of loop calculations (including the presentations at the LCWS06) is briefly summarized in figure 1 [37a]. The complication of a higher-order loop calculation increases with the number of loops as well as with the number of external legs. On the other hand, it also increases with the number of (mass) scales appearing in the loop integral. While one-scale integrals (as in QCD) are usually the easiest possibility for a certain loop topology, two or more scales make the evaluation increasingly difficult. This poses a special problem in SUSY, where many independent mass scales can appear in one-loop diagram. In figure 1 on the horizontal axis the number of legs, and on the vertical one the number of loops is shown. Accordingly, the number of scales has to be kept in mind for the individual contributions reviewed below.

The green shaded area in figure 1 displays the number of loops and legs for which the techniques are meanwhile well established, even for an arbitrary number of scales. For these cases often public algebraic computer codes exist that do the main part of the loop calculation itself (for an overview see e.g. ref. [8]). The blue shaded area corresponds to the number of loops and legs for which partial results or calculation for special cases have been performed. This represents today's frontier of the field of loop calculations.

Compared to the situation about two years ago [9] significant progress has been made. Three examples for recent progress in the field of loop calculations are

- a complete $\mathcal{O}(\alpha)$ calculation for $e^+e^- \to 4f$ [38],
- a complete $\mathcal{O}(\alpha)$ calculation for $e^+e^- \to \nu\bar{\nu}HH$ [39],
- the automation of 2 → 3 processes at the one-loop level in the SM and the MSSM (including now also NMFV effects) [40].

In order to match the anticipated experimental precision of a future ILC, the field of loop calculations still has to advance substantially. The necessary improvement is indicated in figure 1 as the orange shaded areas, which will have to be under full control for the ILC precision [40a].

Some advances have been presented at this conference, which are shown as black rectangles (and numbers):

1. The GRACE system has been extended to 2 → 2 processes at the one-loop level in the MSSM [43].
2. Improvements in the calculation of Q_T spectra for 2 → 3 processes at the one-loop level have been obtained [44].
3. Two-loop vacuum diagrams in the MSSM with complex phases have been evaluated [45].

By comparing the necessary level of loop calculations and the current status (including the progress reported at the LCWS06), it becomes apparent that the field of loop calculations deserves a lot of attention in the next years.

5. Conclusions

There are still many tasks that have to be performed until the full potential of the ILC can be exploited. We reviewed the status of the field and the recent progress that was reported at the LCWS06 in Bangalore (India) in the fields of Higgs physics, top/QCD and loop calculations. While progress has been achieved, continuous progress over the next years will be necessary in the experimental analyses as well as the (corresponding) theoretical calculations in order to be ready once the ILC operation starts.

References

[1] See council-strategygroup.web.cern.ch/council-strategygroup/BB2/Roadmaps.html
See council-strategygroup.web.cern.ch/council-strategygroup/BB2/Roadmaps/ECFA.pdf

See council-strategygroup.web.cern.ch/council-strategygroup/ BB2/Roadmaps/Quantum_Universe_GR.pdf
See www.fnal.gov/directorate/icfa/icfa_LCstatement0204.html
See www.science.doe.gov/hep/HEPFacSub/
See ccwww.kek.jp/acfa/document/2ndLC.html
See www.science.doe.gov/hep/p5/Roadmap.html

[2] See www7.nationalacademies.org/bpa/EPP2010.html
See www.interactions.org/cms/?pid=1024118

[3] J Aguilar-Saavedra *et al*, hep-ph/0106315
See tesla.desy.de/tdr

[4] T Abe *et al*, American Linear Collider Working Group Collaboration: hep-ex/0106055, hep-ex/0106056, hep-ex/0106057, hep-ex/0106058

[5] ACFA Linear Collider Working Group Collaboration: K Abe *et al*, hep-ph/0109166
See lcdev.kek.jp/RMdraft

[6] LHC/ILC Study Group: G Weiglein *et al*, *Phys. Rep.* **426**, 47 (2006)

[7] S Heinemeyer *et al*, hep-ph/0511332

[8] S Dittmaier, hep-ph/0308079

[9] S Heinemeyer, appeared in the *Proceedings of LCWS04*, Paris, France, hep-ph/0408340

[10] More details can be found on p. 3 of: S Heinemeyer, hep-ph/0611374

[11] K Sridhar, *These proceedings.* The slides of the LCWS06 can be found at indico.cern.ch/conferenceTimeTable.py?confId=568

[12] ATLAS Collaboration: Detector and Physics Performance Technical Design Report, CERN/LHCC/99-15 (1999)
See atlasinfo.cern.ch/Atlas/GROUPS/PHYSICS/TDR/access.html

[13] S Abdullin *et al*, *Euro. Phys. J.* **C39S2**, 41 (2005)
CMS Physics TDR, see: cmsdoc.cern.ch/cms/cpt/tdr/

[14] M Dührssen, S Heinemeyer, H Logan, D Rainwater, G Weiglein and D Zeppenfeld, *Phys. Rev.* **D70**, 113009 (2004), hep-ph/0407190

[15] M Schumacher, *Czech. J. Phys.* **54**, A103 (2004), hep-ph/0410112

[16] P Gay, *These proceedings*
T Barklow, *These proceedings*
A Rosca, *These proceedings*

[17] P Niezurawski, A Zarnecki and M Krawczyk, *Acta Phys. Polon.* **B37**, 1187 (2006)

[18] S Rai, hep-ph/0608110

[19] S Biswal, R Godbole, R Singh and D Choudhury, *Phys. Rev.* **D73**, 035001 (2006), Erratum, *Phys. Rev.* **D74**, 039904 (2006), hep-ph/0509070

[20] B Mukhopadhyaya and S Rai, hep-ph/0608112

[21] A Ferrari, *These proceedings*

[22] S Heinemeyer, W Hollik and G Weiglein, *Comput. Phys. Comm.* **124**, 76 (2000); *Euro. Phys. J.* **C9**, 343 (1999)
M Frank, T Hahn, S Heinemeyer, W Hollik, H Rzehak and G Weiglein, hep-ph/0611326
T Hahn, S Heinemeyer, W Hollik, H Rzehak, G Weiglein and K Williams, hep-ph/0611373
The code is accessible via www.feynhiggs.de

[23] S Heinemeyer, S Kraml, W Porod and G Weiglein, *J. High Energy Phys.* **0309**, 075 (2003)

[24] A Juste *et al*, hep-ph/0601112

[25] A Hoang *et al*, *Euro. Phys. J. direct* **C2**, 1(2000)

[26] A Pineda and A Signer, *Nucl. Phys.* **B762**, 67 (2007)

[27] C Farrell and A Hoang, *Phys. Rev.* **D72**, 014007 (2005)

[28] A Juste, hep-ph/0512246

[29] R Godbole, A Grau, R Hegde, G Pancheri and Y Srivastava, *Pramana – J. Phys.* **66**, 657 (2006)

[30] R Godbole, S Rindani and R Singh, hep-ph/0605100

[31] R Godbole, S Kraml, S Rindani and R Singh, hep-ph/0609113

[32] E Asakawa, *These proceedings*

[33] I Campos *et al*, *Euro. Phys. J.* **C11**, 507 (1999)

[34] S Dittmaier and M Roth, *Nucl. Phys.* **B642**, 307 (2002)

[35] J Erler, S Heinemeyer, W Hollik, G Weiglein and P Zerwas, *Phys. Lett.* **B486**, 125 (2000)
R Hawkings and K Mönig, *Euro. Phys. J. direct* **C8**, 1 (1999)

[36] U Baur *et al*, hep-ph/0111314

[37] S Heinemeyer, W Hollik and G Weiglein, *Phys. Rep.* **425**, 265 (2006)

[37a] We are grateful to S Dittmaier for helpful discussions

[38] A Denner, S Dittmaier, M Roth and L Wieders, *Phys. Lett.* **B612**, 223 (2005); *Nucl. Phys.* **B724**, 247 (2005)

[39] F Boudjema *et al*, hep-ph/0510184

[40] J Küblbeck, M Böhm and A Denner, *Comp. Phys. Comm.* **60**, 165 (1990)
T Hahn, *Comp. Phys. Comm.* **140**, 418 (2001)
T Hahn and C Schappacher, *Comp. Phys. Comm.* **143**, 54 (2002)
T Hahn and M Pérez-Victoria, *Comp. Phys. Comm.* **118**, 153 (1999)
T Hahn, W Hollik, J Illana and S Penaranda, hep-ph/0512315

[40a] Progress is also needed to improve the current electroweak precision analyses, as reported in other sessions at the LCWS06 (see e.g. refs [41,42])

[41] S Heinemeyer, hep-ph/0611372

[42] S Heinemeyer, W Hollik, D Stöckinger, A M Weber and G Weiglein, *J. High Energy Phys.* **0608**, 052 (2006), hep-ph/0611371

[43] Y Yasui, *These proceedings*

[44] E Berger and J Qiu, *Phys. Rev.* **D67**, 034026 (2003)
C Balazs, E Berger, P Nadolsky and C Yuan, *Phys. Lett.* **B637**, 235 (2006)

[45] H Rzehak, *Two-loop contributions in the supersymmetric Higgs sector*, Ph.D. thesis (Technische Universität München, 2005)
See nbn-resolving.de/ with urn: nbn:de:bvb:91-diss20050923-0853568146
S Heinemeyer, talk given at the LCWS06
S Heinemeyer, W Hollik, H Rzehak and G Weiglein, in preparation

PRAMANA
— journal of
physics

© Indian Academy of Sciences

Vol. 69, No. 5
November 2007
pp. 735–741

Forward tracking detectors

KLAUS MÖNIG
DESY, Platanenallee 6, D-15738 Zeuthen, Germany
E-mail: klaus.moenig@desy.de

Abstract. Forward tracking is an essential part of a detector at the international linear collider (ILC). The requirements for forward tracking are explained and the proposed solutions in the detector concepts are shown.

Keywords. International linear collider detector; forward tracking.

PACS Nos **29.30.Aj; 29.40.Gx**

1. Introduction

At the ILC many of the most important physics reactions are central, so that the forward region, which is suppressed by the $\cos\theta$ phase space factor often is a bit neglected. However, many processes at the ILC are peaked in the forward region like Bhabha scattering or W-pair production [1]. Fermion pair production has its highest sensitivity to the forward–backward asymmetry or to the difference between effects from a Z' and from extra dimensions also in this region. In addition, the momentum of leptons from W-decays usually is high due to W-polarisation effects. A good momentum resolution in the forward region is thus essential to measure the charge and suppress the W-background in the fermion-pair analyses.

Another argument for a good forward coverage comes from the high jet multiplicity of some reactions at the ILC. There are processes with 6 jets, like $t\bar{t}$, 6–10 jets like ZHH or 8–10 jets like $t\bar{t}H$ and the chance that one jet is in the forward region is relatively high. For example, figure 1 (left) [2] shows the polar angle of the most forward jet from $t\bar{t}H$. It can be seen that full particle flow coverage down to the lowest possible angles is needed.

Apart from the events with a physics interest many calibration events also are peaked forward. The acolinearity of e^+e^- pairs from Bhabha scattering turns out to be the ideal tool to measure the luminosity spectrum at ILC [3]. The differential cross-section for small polar angles is distributed as $\mathrm{d}\sigma/\mathrm{d}\theta \propto 1/\theta^3$ so that very good forward coverage is needed to obtain sufficient statistics. The centre-of-mass energy of the e^+e^- system, $\sqrt{s'}$, can be reconstructed from the polar angle alone assuming that only one photon is radiated. The aim is to measure the beamstrahlung ($\mathcal{O}(10^{-2})$) simultaneously with the beam energy spread ($\mathcal{O}(10^{-3})$). The error on

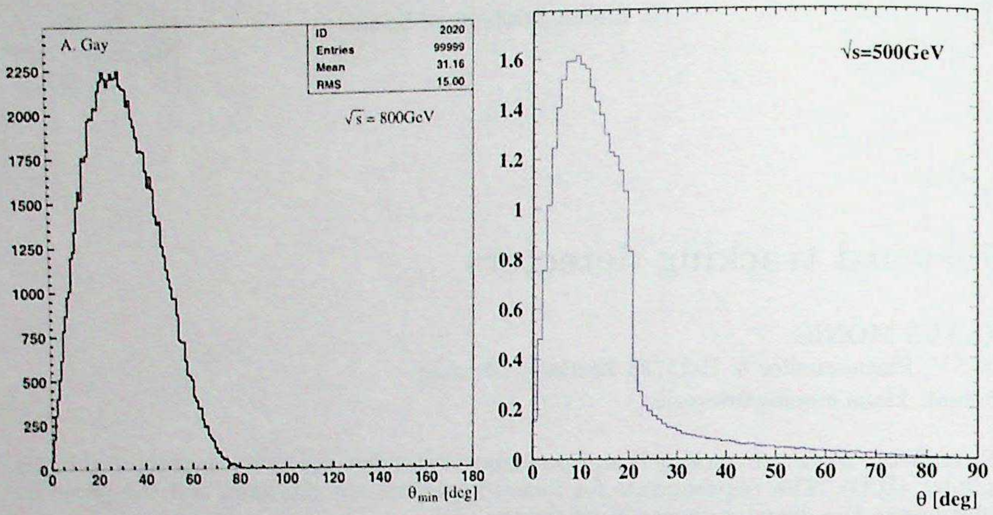

Figure 1. Left: lowest jet polar angle in $t\bar{t}H$ events [2]. Right: minimum lepton angle in radiative return events.

$\sqrt{s'}$ from the angular reconstruction method is $\Delta\sqrt{s'}/\sqrt{s'} \approx \Delta\theta/\sin\theta$ so that one needs $\Delta\theta < 10^{-4}$ in the forward region. Electrons radiate strongly in material and cylinders, like the TPC field cage are crossed under a very shallow angle so that it is important to assure a good momentum resolution in special forward detectors close to the interaction point (IP).

Another important calibration process is the radiative return to Z ($e^+e^- \to Z\gamma \to \ell^+\ell^-\gamma$). With this process the beam energy can be determined to a precision of $1.5 \cdot 10^{-4}$ using polar angles only ($\sqrt{s} = 350\,\text{GeV}, \mathcal{L} = 100\ \text{fb}^{-1}$) [4]. In the Z rest frame the lepton polar angle distribution is almost flat. However, due to the large boost in the lab system at least one lepton is again forward peaked (figure 1 right) so that here also excellent forward coverage is essential.

2. General considerations

In general, the momentum resolution of a detector scales as $\frac{\Delta p}{p} \propto \frac{p_t}{R^2}$ where the details depend on the exact detector set-up.. R denotes the radius of the detector and p_t the transverse momentum. Usually a particle physics detector has a cylindrical shape with the transition from the barrel region, where tracks leave the detector through the outer cylindrical surface to the forward region, where the tracks leave through the endplate at a given angle θ_0. In the barrel region one has $p_t = p\sin\theta$ and $R =$ const. so that $\frac{\Delta p}{p} \propto p\sin\theta$. On the contrary, in the forward region $R = l\tan\theta$ with l being the length of the detector, so that $\frac{\Delta p}{p} \propto p\sin\theta/\tan^2\theta \approx p/\tan\theta$. The momentum resolution thus deteriorates going to small polar angles.

As sketched in figure 2, in principle, there are two possible solutions to build detectors in the forward region. One possibility is to stay with the cylindrical lay-out. In this case, however, the detectors get very long and the z resolution

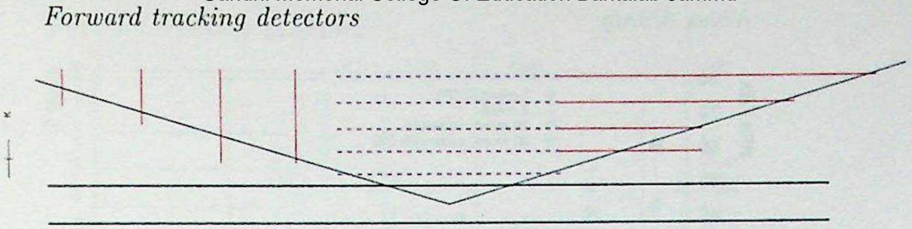

Figure 2. Possible lay-out of forward detectors close to the IP.

deteriorated with smaller angles. Another possibility is to use disks instead. In this case less material is needed and also the z resolution can be better. However, somewhere the forward tracks have to cross the material from the barrel support and cables which may be a problem for the vertex resolution.

To obtain optimal angular and momentum resolution a forward tracking system in general needs two components. A set of precise detectors close to the interaction point (IP) provides a precise measurement of the polar angle and an accurate start point for the momentum measurement. These detectors can measure the tracks before they have crossed a large amount of material. To optimise the tracking resolution, another precise space point is needed at maximum distance from the IP. This can be provided by a special detector in front of the calorimeter endplate, and also by the measurement of the central tracker. Intermediate detectors may be needed to improve the resolution and to extrapolate the track from the inner detectors to the endplate.

3. Background in the forward region

The background from e^+e^- pairs originating from the beam–beam interaction rises towards smaller polar angles [5]. There is thus a danger of many hits in the forward detectors close to the beam pipe. An additional problem arises for large crossing angles. The centre of the outgoing beam pipe is at a larger radius than the innermost forward detectors so that backscattered charged particles that follow the magnetic field direction hit the forward detectors in their sensitive area. The problem is even worse if the solenoidal field for the incoming beam is compensated by a detector integrated dipole (DID). In this case the background from the outgoing beam pipe is even guided to larger radii.

Figure 3 shows the background for different planes of the detector shown in figure 6. One can see that the direct hits as well as the backscattered background is relevant. It should be noted that the backscattered component has an about 5 m longer flight path to the detector than particles directly from the IP so that this component can be rejected if the detectors have a time resolution in the 5 ns range. Figure 4 shows the time distribution vs. the azimuthal angle ϕ for the innermost FTD disk of the LDC [6] for 20 mrad crossing angle with the DID. The gain of a good time resolution is clearly visible. Especially the large background cluster coming from backscattering near the exit hole can be suppressed.

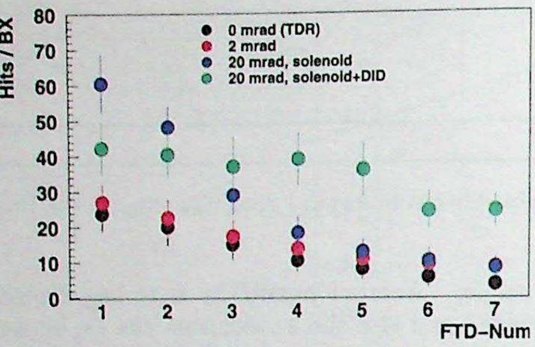

Figure 3. Background in the forward tracking disks for different assumptions on the crossing angle and the DID.

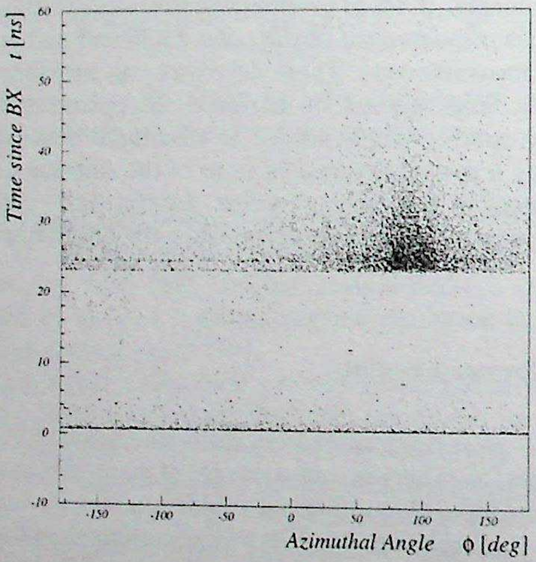

Figure 4. Arrival time vs. ϕ for background hits in the first FTD disk of the LDC.

4. Possible technologies

In the forward part not too close to the beam pipe a wide range of technologies can be used and there are no real restrictions. In the region close to the beam pipe on one hand a high precision and on the other hand a high background tolerance is required so that solid state detectors are the optimal choice. Silicon strip detectors have the advantage of being precise, fast and relatively cheap. However, they are sensitive to background and to the high track density in jets close to the IP.

Contrary to that pixel devices are much less sensitive to background and the track density, but they are significantly more expensive. Two types of pixel sensors are under consideration. The pixel technologies that are used for the vertex detector [7] are very precise and thin. However they are slow, integrating over about 100 bunch crossings increasing their background sensitivity by this factor. Another option is

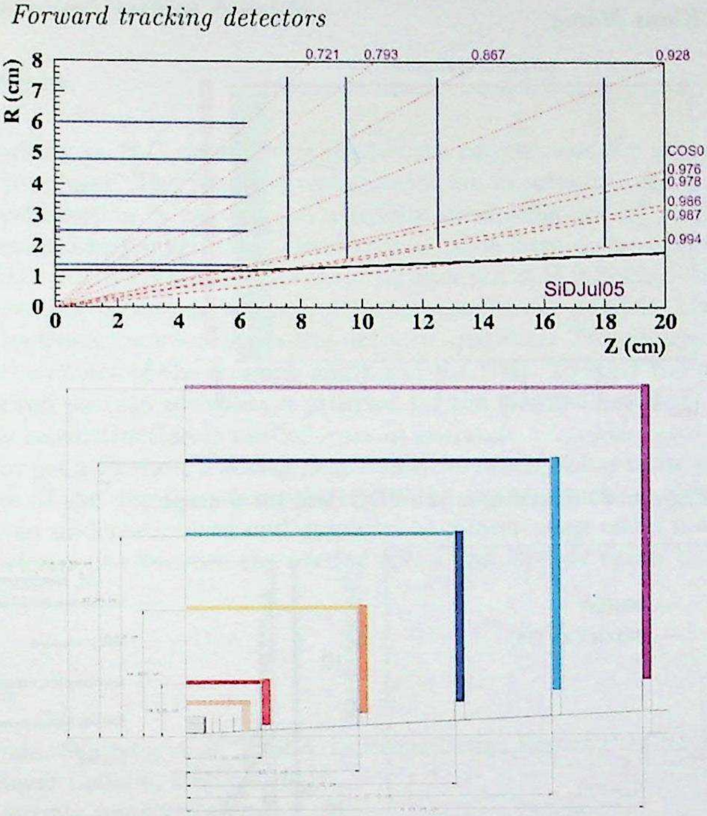

Figure 5. Forward tracking in the SID. The upper plot shows the vertex detector and the lower plot the full tracking system.

the use of hybrid pixels as they are used at the LHC, e.g. in ATLAS [8]. These devices can be very fast but have only a medium precision ($\sim (50 \times 400\ \mu\text{m}^2)/\sqrt{12}$). In addition, they are relatively thick. The ATLAS pixel detector has a thickness of $2\% X_0$ per layer. However, most of that is due to cooling and could be reduced with power cycling at the ILC.

5. Implementation of forward tracking in the concepts

At present there are two different implementations of forward tracking in the detector concepts. SID [9] (see figure 5) uses four pixel planes in the vertex detector with the same technology as the barrel. At larger distances from the IP forward tracking is completed by five disks of back-to-back silicon strips.

LDC [10] (see figure 6) and GLD [11] have similar concepts where details are still to be defined. In both concepts the main tracker is a TPC that can do stand-alone tracking down to about 10° and sees a few points down to around 5°. The vertex detector consists of cylindrical layers only to minimise the material. At small polar angles the tracking is improved by several disks where the ones closer to the IP are fast pixels, while the outer ones are strips to reduce the costs and the material in the detector. In the LDC concept at present also a tracking detector behind the

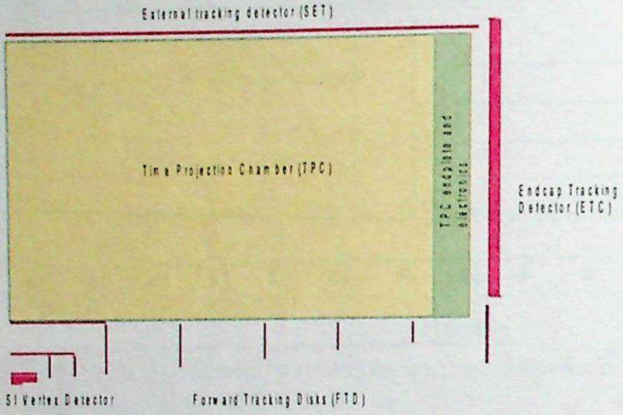
External tracking detector (SET)
Time Projection Chamber (TPC)
TPC endplate and electronics
Endcap Tracking Detector (ETC)
SI Vertex Detector
Forward Tracking Disks (FTD)

Figure 6. Tracking in the LDC detector concept.

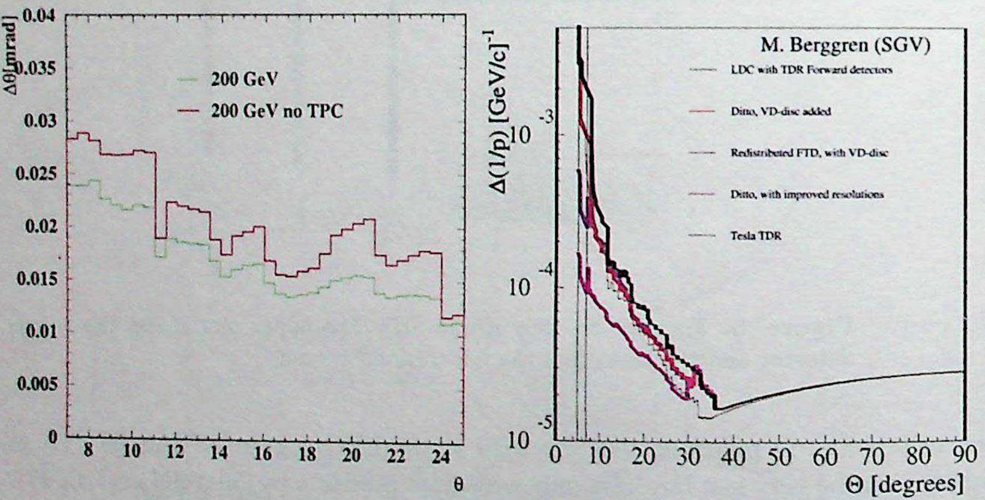

Figure 7. Angular (left) and momentum (right) resolutions of the forward tracking in LDC.

TPC is foreseen where as possible technologies silicon, MSGCs and straw tubes have been studied. The detector may however not be needed if for the TPC a resolution around 50 μm close to the endplate can be reached.

An important challenge for the forward detectors are systematic uncertainties. For the calibration processes absolute angular measurements are needed. A systematic shift in the aspect ratio R/L of the detector shifts the measured beam energy in the radiative return analysis. In order to match the statistical error of the method, the aspect ratio has to be known to $\Delta(R/L) = \Delta \tan\theta = 10^{-4}$. This is probably only possible if the detector is built on a robust mechanical support that can be precisely surveyed before installation.

With the proposed systems all concepts can reach the necessary performance. As an example, figure 7 shows the angular and momentum resolutions in the case of LDC.

6. Conclusions

Forward tracking in ILC detectors is needed for physics and for some important calibration processes. The required technologies are in principle under control but a careful optimisation is needed. A partially conflicting set of parameters like material, resolution, background tolerance and price have to be optimised where one has to take into account that the material does not only influence the resolution for the interesting processes but can also compromise the particle flow resolution because of hadronic interactions in the detector material. The optimum may also depend on the choice of the crossing angle and the DID. To start the optimisation procedure a full pattern recognition program for the forward detectors as well as a particle flow reconstruction is needed.

In order to get a forward tracking that fulfils the needs, it has to be implemented in the design of the detectors from the beginning. Past experience shows that this part was often underestimated and upgrades at a later stage could not deliver the required performance because the needed space was already taken by other parts of the detector.

References

[1] J A Aguilar-Saavedra *et al*, TESLA Technical Design Report Part III: Physics at an e^+e^- Linear Collider, DESY-01-011C
[2] A Gay, private communication
[3] K Mönig, *Measurement of the differential luminosity using Bhabha events in the forward-tracking region at TESLA*, LC-PHSM-2000-60
[4] A Hinze and K Mönig, physics/0506115
[5] C Rimbault *et al*, *Phys. Rev. ST Accel. Beams* **9**, 034402 (2006)
[6] A Vogel, private communication
[7] A Sugiyama, Tracking and vertexing summary, *These proceedings*
[8] N Wermes, *Nucl. Instrum. Methods* **A512**, 277 (2003)
[9] J Jaros, The SiD concept for an ILC detector, *These proceedings*
[10] T Behnke, The LDC outline document, *These proceedings*
[11] H Park, Global large detector concept, *These proceedings*

PRAMANA
— journal of
physics

© Indian Academy of Sciences

Vol. 69, No. 5
November 2007
pp. 743–748

Photon pairs: Quantum chromodynamics continuum and the Higgs boson

EDMOND L BERGER
High Energy Physics Division, Argonne National Laboratory, Argonne, IL 60439, USA
E-mail: berger@anl.gov

Abstract. A new QCD calculation is summarized for the transverse momentum distribution of photon pairs produced by QCD subprocesses, including all-orders soft-gluon resummation valid at next-to-next-to-leading logarithmic accuracy. Resummation is needed to obtain reliable predictions in the range of transverse momentum where the cross-section is the largest. Results are compared with data from the Fermilab Tevatron and predictions are made for the large hadron collider. The QCD continuum is shown to have a softer spectrum than the Higgs boson signal at the LHC.

Keywords. Higgs; photon pairs; quantum chromodynamics.

PACS Nos 12.15.Ji; 12.38.Cy; 13.85.Qk

1. Introduction

A Higgs boson with mass between 115 and 140 GeV may be identified at hadron colliders through its decay into a pair of energetic photons, a challenging prospect at the Large Hadron Collider in view of the intense background from hadronic production of non-resonant photon pairs. Theoretical predictions of these background processes may be of substantial value in aiding search strategies. Moreover, the perturbative quantum chromodynamics (QCD) calculation of continuum photon-pair production is of theoretical interest in its own right, and data from the Tevatron collider offer an opportunity to test results against experiment.

In this report, I focus on the transverse momentum (Q_{T}) distribution of a pair of photons from both the Higgs boson signal and the QCD continuum. This distribution is important because its behavior affects the precision of the determination of the vertex from which the Higgs boson emerges. Greater activity in Q_{T} associated with Higgs boson production allows a more precise determination of the event vertex. The expected shape of $\mathrm{d}\sigma/\mathrm{d}Q_{\mathrm{T}}$ can affect triggering and analysis strategies. Event modeling, kinematic acceptance, and efficiencies all depend on Q_{T}. Finally, as is shown here, selections on Q_{T} may be useful to enhance the signal to continuum ratio.

A new calculation of the diphoton cross-section in perturbative QCD is presented in ref. [1] and is summarized here. Contributions are included from all perturbative subprocesses (quark–antiquark, quark–gluon, antiquark–gluon, and gluon–gluon) to next-to-leading order (NLO) accuracy. In addition, to describe properly the behavior of the $Q_{\rm T}$ distribution of the pairs in the region in which $Q_{\rm T} < Q$, where Q is the invariant mass of the photon pair, all-orders resummation of initial-state soft and collinear logarithmic contributions is included, up to next-to-next-to-leading log (NNLL) accuracy. The influence of initial-state gluon radiation on the predicted transverse momentum distributions is evaluated with the Collins–Soper–Sterman (CSS) resummation procedure [2].

Good agreement of our results is obtained with data from the Collider Detector at Fermilab (CDF) collaboration at $p\bar{p}$ collision energy $\sqrt{s} = 1.96$ TeV [3]. We make suggestions for more differential analyses of the data that would allow refined tests of our calculation. Predictions are made for continuum diphoton production at the LHC, and a comparison is presented with the spectrum of photon pairs expected from Higgs boson decay.

2. Analytical calculation

Direct production of continuum photon pairs occurs from $q\bar{q}$, $\overset{(-)}{q}\,g$, and gg scattering. NLO perturbative cross-sections (i.e., cross-sections of $\mathcal{O}(\alpha_{\rm s})$ in the $q\bar{q}$ and qg channels, and $\mathcal{O}(\alpha_{\rm s}^3)$ in the gg channel are included as a part of the resummed cross-section. Singular logarithms arise in the NLO cross-sections when the transverse momentum $Q_{\rm T}$ of the $\gamma\gamma$ pair is much smaller than its invariant mass Q. These logarithms are resummed into a Sudakov exponent (composed of two anomalous-dimension functions $A(\mu)$ and $B(\mu)$) and convolutions of the conventional parton densities $f_a(x, \mu_{\rm F})$ with Wilson coefficient functions C. We include the $\mathcal{O}(\alpha_{\rm s}^3)$ expressions for $A(\mu)$, $\mathcal{O}(\alpha_{\rm s}^2)$ expressions for $B(\mu)$, and the C-functions at order $\alpha_{\rm s}$, for all subprocesses. These enhancements elevate the accuracy of the resummed prediction to the NNLL level. The resummed $Q_{\rm T}$ distribution is well-behaved as $Q_{\rm T} \to 0$, unlike its fixed-order counterpart which is singular in this limit.

A full treatment of photon pair production requires that one address the contributions from the quasi-collinear fragmentation of quarks and gluons into photons. Isolation procedures are applied by the experiments to reduce these long-distance contributions, procedures that are only approximately reproducible theoretically. The energy of the hadronic remnants is required to be less than a threshold 'isolation energy' $E_{\rm T}^{\rm iso}$ in a cone $\Delta R = \sqrt{\Delta\eta^2 + \Delta\varphi^2}$ around each photon, with $\Delta\eta$ and $\Delta\varphi$ being the separations of the hadronic remnant(s) from the photon in the plane of pseudo-rapidity η and azimuthal angle φ. The two photons must also be separated in the η–φ plane by an amount exceeding the approximate angular size $\Delta R_{\gamma\gamma}$ of one calorimeter cell. The values of $E_{\rm T}^{\rm iso}$, ΔR, and $\Delta R_{\gamma\gamma}$ serve as crude characteristics of the actual measurement, and the size of the fragmentation contributions depends on the assumed values of these parameters. We find it sufficient in our work to use a simplified fragmentation model to represent the isolated cross-section. We regularize the fragmentation region by imposing a combination of a sharp cut-off $E_{\rm T}^{\rm iso}$ on the transverse energy $E_{\rm T}$ of the final-state quark or gluon and smooth cone isolation [4].

We use two-loop expressions for the running electromagnetic and strong couplings $\alpha(\mu)$ and $\alpha_{\rm s}(\mu)$, as well as the NLO parton distribution function set CTEQ6M [5].

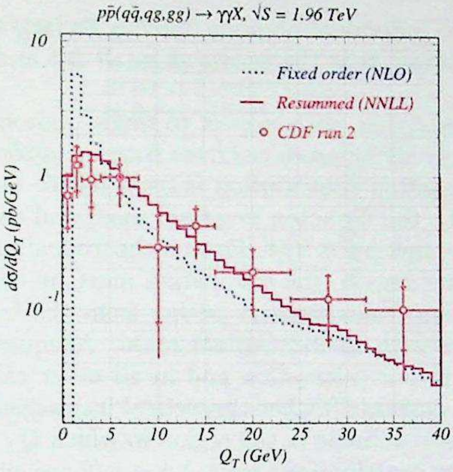

Figure 1. Transverse momentum distributions of diphotons. The dotted histogram shows the result of the next-to-leading order calculation and the solid histogram the result after resummation at NNLL accuracy. The data are from the CDF measurement.

For the renormalization and factorization scales we set $\mu_{\mathrm{R}} = \mu_{\mathrm{F}} = Q$ in the finite-order perturbative expressions.

3. Comparison with Tevatron data

Our analysis provides the triple-differential cross-section $\mathrm{d}\sigma/\mathrm{d}Q\mathrm{d}Q_{\mathrm{T}}\mathrm{d}\Delta\phi$ ($\Delta\phi$ is the difference of the angles of the two photons in the transverse plane). The calculation is especially pertinent for the transverse momentum distribution in the region $Q_{\mathrm{T}} \le Q$, for fixed values of diphoton mass Q. It would be best to compare our multi-differential distribution with experiment, but the collider data tend to be presented in the form of single-differential distributions in Q, Q_{T}, and $\Delta\phi$, after integration over the other variables. We follow suit in order to make comparisons with the Tevatron data, but we comment on the features that can be explored if more differential studies are made. For calculations appropriate at Tevatron energies, we impose cuts $|y_\gamma| < 0.9$ on the rapidity of each photon, and $p_{\mathrm{T}}^{\gamma} > p_{\mathrm{Tmin}}^{\gamma} = 14$ (13) GeV on the transverse momentum of the harder (softer) photon in each $\gamma\gamma$ pair. We choose $E_{\mathrm{T}}^{\mathrm{iso}} = 1$ GeV, $\Delta R = 0.4$, and $\Delta R_{\gamma\gamma} = 0.3$.

The Q_{T} distribution is shown in figure 1. The NLO calculation displays an unphysical logarithmic singularity as $Q_{\mathrm{T}} \to 0$. The result after NNLL resummation is in reasonable agreement with the absolute rate and overall shape of the cross-section. In the two highest-Q_{T} bins, the CDF central values lie above the theory predictions. While the observed excess in this 'shoulder' region is not statistically significant, it has been discussed as a possible indication of enhanced fragmentation contributions in the Tevatron data [3,6].

Our calculations show that most of the shoulder events populate a limited volume of phase space characterized by $\Delta\phi \lesssim 1$ rad, $Q < 27$ GeV, and $Q_{\mathrm{T}} \gtrsim 25$ GeV. The location of the shoulder is sensitive to the value of the cut on the minimum transverse momentum, p_T^γ, of the individual photons, moving to larger Q_T if these cuts are raised. We note, in addition, that the excess at small $\Delta\phi$ and large Q_T is characterized by $Q_T \gtrsim Q$.

A new feature of diphoton production, with respect to single photon production, is the prospect that both photons may be produced from fragmentation of the same final-state parton. This fragmentation contribution is expected to be most influential in the region in which both the diphoton invariant mass and the separation $\Delta\phi$ are relatively small, $Q < Q_T$ and $\Delta\phi < \pi/4$. From a theoretical point of view, when $Q_T > Q$, as in the shoulder region, the calculation must be organized in a different way [7] in order to resum contributions arising from the fragmentation of partons into a pair of photons with small invariant mass. Adequate treatment of the light $\gamma\gamma$ pairs is missing in our calculation and in all other calculations at present. This interesting region warrants further theoretical investigation.

Our theoretical treatment is most reliable in the region in which $Q_T < Q$. When the $Q_T < Q$ selection is made, the contributions from $\Delta\phi < \pi/2$ are efficiently suppressed, and dependence on tunable isolation parameters and factorization scales is reduced. Our resummed cross-section provides an accurate description of the rate at small values of Q_T. After the selection $Q_T < Q$, we expect that the large Q_T shoulder will disappear in the experimental Q_T distribution.

Predicted distributions in the invariant mass Q of the photon pair and the separation in $\Delta\phi$ may be found in ref. [1]. An important consequence of the resummation formalism is a logarithmic dependence on the diphoton invariant mass Q. We urge the CDF and D0 collaborations to verify this predicted broadening of the Q_T distribution as Q increases.

4. Results for the LHC

To obtain predictions for pp collisions at $\sqrt{s} = 14$ TeV, we require transverse momentum $p_T^\gamma > 25$ GeV and rapidity $|y_\gamma| < 2.5$ for each photon. We impose a somewhat looser isolation restriction than for the Tevatron study, requiring less than $E_T^{\text{iso}} = 10$ GeV of extra transverse energy inside a cone with $\Delta R = 0.7$ around each photon. Figure 2 shows our resummed transverse momentum distributions for various selections of the diphoton invariant mass at the LHC. The plot shows the predicted broadening of the Q_T distribution with increasing mass. Additional predictions for the LHC are presented in ref. [1].

5. Comparison with the Higgs boson signal

Differences arise between the production spectrum for the Higgs boson signal and the QCD continuum. We focus on the dominant gluon fusion mechanism for production of the signal, $gg \to H \to \gamma\gamma$, and we calculate the signal with the same order of precision in the QCD contributions as for the continuum. We include fixed order initial-state QCD corrections at $O(\alpha_s^3)$ (NLO) and resummation at NNLL accuracy. These contributions are coded in the same numerical program used to compute the continuum, and we apply the same cuts for both the signal and the continuum. Use of one code minimizes potential deviations than can arise from

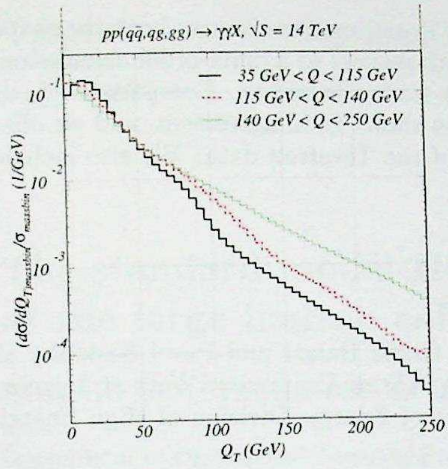

Figure 2. Transverse momentum distributions of diphotons at the LHC for different selections on the invariant mass of the pair of photons.

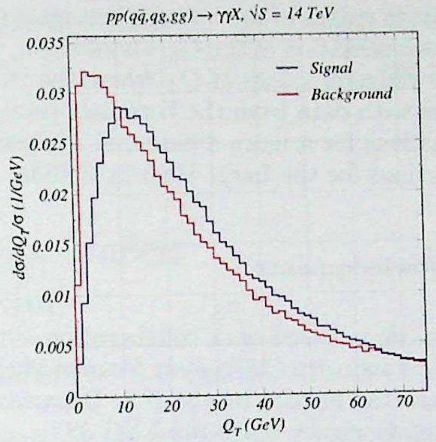

Figure 3. Comparison of the transverse momentum distributions for the Higgs boson signal and diphoton continuum at the LHC, both computed at NNLL accuracy. The continuum is calculated for $128 < Q < 132$ GeV, and the Higgs boson mass is taken to be $m_{\mathrm{H}} = 130$ GeV.

codes with different physics content, parton densities, and numerical implementations. We compute the continuum in the range $128 < Q < 132$ GeV and the signal at a fixed Higgs boson mass $m_{\mathrm{H}} = 130$ GeV. We use $\mu_{\mathrm{R}} = \mu_{\mathrm{F}} = Q$ for both the signal and the continuum and the CTEQ6M parton distributions.

The cross-section times branching ratio for the Higgs boson signal is substantially smaller than the continuum. We present distributions normalized to the respective total rates in figure 3. The signal and continuum peak at about 12 and 5 GeV, respectively. The dominant Sudakov exponent $C_{\mathrm{F}} = A_{q\bar{q}}^{(1)} = A_{qg}^{(1)}$ that controls gluon radiation for the $q\bar{q}$ and $qg + \bar{q}g$ initial states is less than $A_{gg}^{(1)} = C_A$ that controls the gg case. More gluon radiation in the gg case explains the broader Q_{T} spectrum for the Higgs boson signal. The comparison in figure 3 suggests that the signal-to-background ratio would be enhanced if a cut is made to restrict $Q_{\mathrm{T}} > 10$ GeV. Additional differences between the signal and continuum are shown in ref. [1], including the rapidity difference of the two photons [8], the scattering angle in the Collins–Soper frame $\tanh((y_1^\gamma - y_2^\gamma)/2) = \cos\theta^*$, and the difference between the azimuthal angles of the photons.

6. Summary

A new QCD calculation is presented of the transverse momentum distribution of photon pairs produced at hadron colliders, including all-orders resummation of initial-state soft-gluon radiation valid at next-to-next-to-leading logarithmic accuracy. This calculation is most appropriate for values of $\gamma\gamma$ transverse momentum

Q_{T} not in excess of the $\gamma\gamma$ invariant mass Q. Resummation changes both the shape and normalization of the Q_{T} distribution, with respect to a finite-order calculation, in the range of values of Q_{T} where the cross-section is largest. Comparison of our results with data from the Fermilab Tevatron shows good agreement, and we offer suggestions for a more differential analysis of the Tevatron data. We also include predictions for the Large Hadron Collider.

Acknowledgments

This work is based on a collaboration with Csaba Balazs and Pavel Nadolsky at Argonne and with Chien-Peng Yuan of Michigan State University. Work at Argonne is supported in part by the U.S. Department of Energy, Division of High Energy Physics, Contract W-31-109-ENG-38.

References

[1] C Balazs, E L Berger, P Nadolsky and C P Yuan, *Phys. Lett.* **B637**, 235, (2006), arXiv:hep-ph/0603037; *Phys. Rev.* **D76**, 013008 (2007), arXiv:hep-ph/0702003; *Phys. Rev.* **D76**, 013009 (2007), arXiv:0704.001 [hep-ph]
[2] J C Collins, D E Soper and G Sterman, *Nucl. Phys.* **B250**, 199 (1985)
[3] CDF Collaboration: D Acosta, *et al*, *Phys. Rev. Lett.* **95**, 022003 (2005)
[4] S Frixione, *Phys. Lett.* **B429**, 369 (1998)
[5] J Pumplin *et al*, *J. High Energy Phys.* **07**, 012 (2002)
[6] T Binoth, J-P Guillet, E Pilon and M Werlen, *Phys. Rev.* **D63**, 114016 (2001)
[7] E L Berger, L E Gordon and M Klasen, *Phys. Rev.* **D58**, 074012 (1998)
E L Berger, J Qiu and X Zhang, *Phys. Rev.* **D65**, 034006 (2002)
[8] Z Bern, L J Dixon and C R Schmidt, *Phys. Rev.* **D66**, 074018 (2002)

PRAMANA
— journal of
physics

© Indian Academy of Sciences

Vol. 69, No. 5
November 2007
pp. 749–752

The standard model Higgs search at the large hadron collider

SATYAKI BHATTACHARYA, on behalf of the CMS and the ATLAS Collaborations
Department of Physics and Astrophysics, University of Delhi, Delhi 110 009, India
E-mail: Bhattacharya.satyaki@gmail.com

Abstract. The experiments at the large hadron collider (LHC) will probe for Higgs boson in the mass range between the lower bound on the Higgs mass set by the experiments at the large electron positron collider (LEP) and the unitarity bound (~1 TeV). Strategies are being developed to look for signatures of Higgs boson and measure its properties. In this paper results from full detector simulation-based studies on Higgs discovery from both ATLAS and CMS experiments at the LHC will be presented. Results of simulation studies on Higgs coupling measurement at LHC will be discussed.

Keywords. Higgs; large hadron collider; CMS; ATLAS.

PACS Nos **10.30.Pb; 10.30.Qc; 12.60.Fr; 12.60.Jv; 14.80.Bn; 14.80.Cp**

1. Introduction

Higgs boson, the massive scalar particle responsible for giving mass to gauge bosons and fermions and for the renormalizability of the standard model (SM) of particle physics has remained elusive so far. The large electron positron collider program at CERN, Geneva concluded with no definitive discovery signal of Higgs. The Tevatron data have not revealed any signature of Higgs boson so far. The large hadron collider (LHC), under construction at CERN will collide protons at a center-of-mass energy of 14 TeV. The LHC is expected to start operating in the year 2007. The design startup luminosity is 2×10^{33} cm^{-2}/s. Search for Higgs boson is the most important physics goal of the experiments at the LHC. Two experiments at the LHC, CMS and ATLAS will carry out searches for Higgs bosons. Detailed search strategies are being designed to look for signatures of Higgs. Studies have also been done on measurement of Higgs properties such as coupling, spin etc. at the LHC. The existing LEP lower limit on SM Higgs mass is 114.4 GeV, at 95% CL. The experiments at the LHC are capable of scanning a Higgs mass range starting from the LEP lower bound up to more than a TeV. It is strongly expected that experiments at the LHC will discover Higgs if it exists. In the following sections we will give an overview of the results obtained from simulation studies done by the CMS [1] and the ATLAS on Higgs search at the LHC.

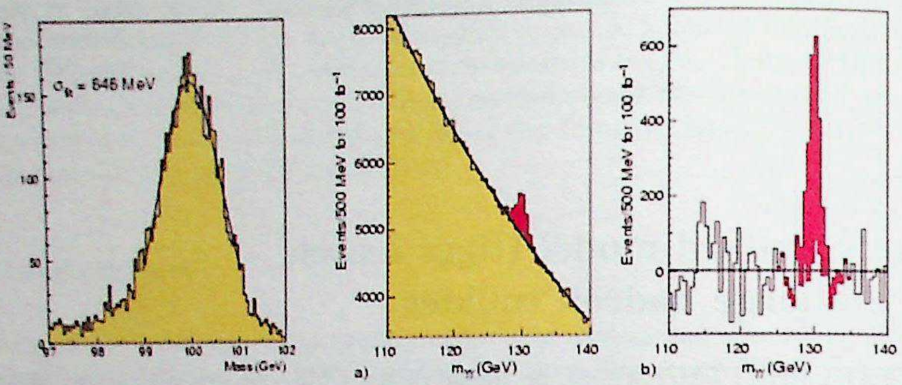

Figure 1. Mass distribution from a Pythia simulated sample of 100 GeV Higgs decaying to two photons (left). A signal (in red) + background (yellow) mass distribution for a 130 GeV Higgs (center) and background subtracted signal peak (right) are also shown.

2. Search for SM Higgs boson

SM Higgs boson production proceeds mainly via gluon–gluon fusion at low x, due to high gluon flux at LHC energies. Other important mechanisms for Higgs production are $qq \rightarrow Hqq$ via vector boson fusion (VBF), associated production of Higgs with $t\bar{t}$ or $b\bar{b}$.

2.1 *Low mass region*

Below the $W^{\pm}$ and Z^0 boson pair production thresholds, $H^0 \rightarrow b\bar{b}$ has the highest branching fraction followed by Higgs decay to $\tau^+\tau^-$. Beyond $2m_W(2m_Z)$, $W^{\pm}(Z^0)$ pair production becomes dominant. For $m_H > 2m_{\text{top}}$, $H^0 \rightarrow t\bar{t}$ becomes significant.

Higgs can also decay to two photons through loop process (predominantly through top or $W^{\pm}$ triangle). In spite of small branching fraction $H^0 \rightarrow \gamma\gamma$ is foreseen to be an important search channel in the so-called low mass range (roughly below $2m_W$) due to its clean signature of two isolated photons in the electromagnetic calorimeter. If the Higgs is produced via VBF channel, two additional forward–backward jets are present [2]. Monte Carlo studies predict that CMS can make a 5σ discovery of a 120 GeV Higgs with 15 fb^{-1} data or about 9 months of running at low luminosity. With its high precision electromagnetic calorimetry, CMS can achieve ~650 MeV mass resolution for a 100 GeV Higgs (see figure 1).

2.2 *Intermediate-high mass region*

In this mass region the WW and ZZ decay modes of Higgs open up and become the dominant decay modes. ZZ decay to four (isolated) leptons (e/μ) gives the highest sensitivity in the Higgs mass range 200–500 GeV (see figure 3). Discovery

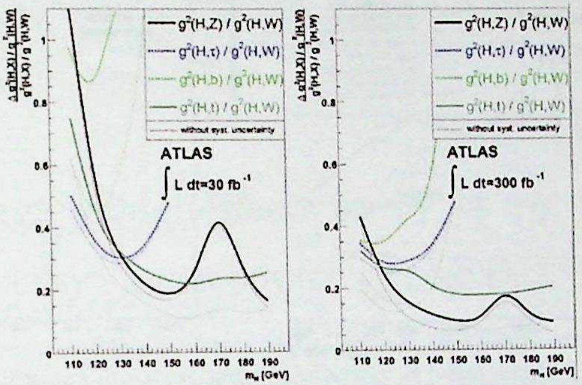

Figure 2. Relative error for the measurement of relative couplings. The dashed lines give the expected relative error without systematic uncertainties.

of luminosity in this channel decreases rapidly with the Higgs mass approaching the ZZ pair production threshold. For a 140 GeV Higgs one expects to get a 5σ discovery with about 15 fb^{-1}(31 fb^{-1}) in the $4\mu(4e)$ final state.

Figure 3 shows the discovery significance (number of sigmas) for 30 fb^{-1} integrated luminosity. In the entire mass range, CMS can make a more than 5σ discovery with 30 fb^{-1}. W^+W^- mode with both Ws decaying leptonically gives a high sensitivity in the mass range 150–180 GeV. If $m_H \approx 2m_W$ one can expect to make a 5σ discovery in this channel with 2 fb^{-1}.

3. Higgs coupling measurement

All Higgs decays and productions depend on the Higgs couplings $g_W, g_Z, g_b, g_t, g_\tau$ and it should be possible to determine the relative values of these couplings from the measured Higgs decay rates at the LHC. ATLAS has studied a method of global maximum likelihood fit to extract relative values of coupling constants from the measured ratio of partial width [3]. The study indicates that it should be possible to measure $\Gamma_\tau/\Gamma_W, \Gamma_\gamma/\gamma_W, \Gamma_Z/\Gamma_W$ within 15–60% accuracy with 30$\sim$ fb^{-1} of data. Corresponding ratios of coupling constant squares $g_\tau^2/g_W^2, g_\gamma^2/g_W^2, g_Z^2/g_W^2$ can be determined within 15–50% accuracy if Higgs mass is above 125 GeV. With 300 fb^{-1} one can expect to measure g_t^2/g_W^2 at 30% accuracy (see figure 2).

4. Summary

In this paper we discussed the search strategies of a SM Higgs boson in three broadly divided mass regions. We have discussed some of the dominant discovery modes as examples of MC studies of the MSSM Higgs search at the LHC.

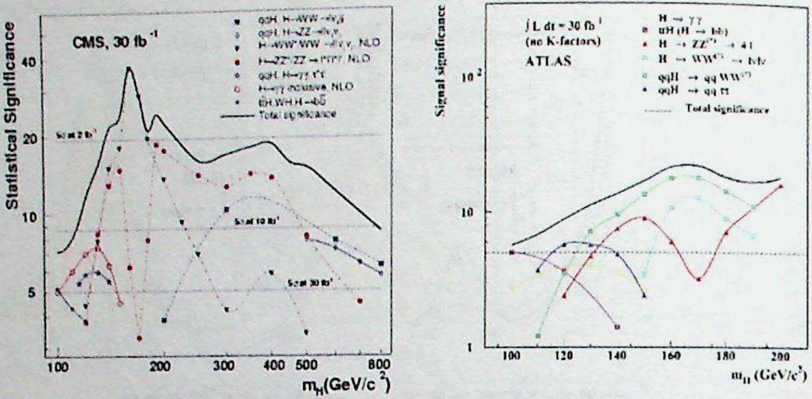

Figure 3. Discovery significance for 30 fb^{-1} of data from CMS (left) and ATLAS (right) Monte Carlo studies. The black line represents combined significance of all channels.

Full detector simulation-based studies have been performed in both the CMS and the ATLAS experiments for all major discovery channels in each mass region. Some promising channels, namely $H \to \gamma\gamma, H \to ZZ \to 4$ leptons (e/μ) in the low mass region, and $H \to WW \to ll$ (dilepton), $H \to ZZ \to lljj$ (dilepton+dijet) channels have been discussed in this paper. It is expected that the LHC will be able to discover Higgs with mass between the LEP limit and the perturbative bound within the first year of running at the design luminosity and center-of-mass energy. In the low mass region Higgs decay to two photons will play a significant role, while in the intermediate-high mass region $H \to WW$ and $H \to ZZ$ with W and Z decaying leptonically are the most promising search channels. For a low-intermediate mass Higgs it should be possible to measure the Higgs mass within few hundred MeV from the $H \to \gamma\gamma, H \to ZZ \to 4$ leptons (e/μ) channels. Higgs properties, such as coupling and CP should be measurable with 100 fb^{-1} of data.

References

[1] S Abdullin *et al*, Summary of the CMS potential for the Higgs boson discovery, CMS NOTE 2003/033, 10 December 2003. For details of the individual searches, please see the references therein

[2] J Cammin and M Schumacher, The ATLAS discovery potential for the channel $ttH, H \to b\bar{b}$, ATLAS-phys-2003-024, 16 July 2003

[3] Michael Duhrssen, Prospects for the measurement of Higgs boson coupling parameters in the mass range from 110 to 190 Gev/c^2, ATLAS-phys-2003-030

PRAMANA
— journal of
physics

© Indian Academy of Sciences

Vol. 69, No. 5
November 2007
pp. 753–757

Little Higgs model effects in $\gamma\gamma \to \gamma\gamma$

S RAI CHOUDHURY[1], ASHOK GOYAL[2], A S CORNELL[3]
and NAVEEN GAUR[4,*]
[1]Centre for Theoretical Physics, Jamia Millia Islamia, New Delhi 110 025, India
[2]Department of Physics & Astrophysics, University of Delhi, Delhi 110 007, India
[3]Yukawa Institute of Theoretical Physics (YITP), Kyoto, Japan
[4]Theory Group, KEK, Tsukuba, Ibaraki 305-0801, Japan
*E-mail: naveen@physics.du.ac.in

Abstract. Though the predictions of the standard model (SM) are in excellent agreement with experiments, there are still several theoretical problems associated with the Higgs sector of the SM, where it is widely believed that some new physics will take over at the TeV scale. One beyond the SM theory which resolves these problems is the Little Higgs (LH) model. In this work we have investigated the effects of the LH model on $\gamma\gamma \to \gamma\gamma$ scattering [1].

Keywords. Little Higgs model; linear collider.

PACS Nos **12.60.Cn; 12.60.-i; 14.80.Cp**

1. Introduction

It has been known for some time that the $\gamma\gamma \to \gamma\gamma$ scattering amplitude at high energies will be a very useful tool in the search for new particles and interactions in an e^+e^- linear collider operated in the $\gamma\gamma$ mode. In the SM the $\gamma\gamma \to \gamma\gamma$ amplitudes will have one-loop contributions mediated by charged fermions (leptons and quarks) and W-bosons. At large energies ($\sqrt{s_{\gamma\gamma}} \geq 250$ GeV) it is known that the W contributions dominate over the fermionic contributions and that the dominant amplitudes are predominantly imaginary. Therefore, we expect that any new physics effects in the $\gamma\gamma \to \gamma\gamma$ process may come from the interference terms between the predominantly imaginary SM amplitudes and new physics effects to these amplitudes.

The SM has been very successful in explaining all electroweak interactions probed so far, where the SM requires a Higgs scalar field to achieve the electroweak symmetry breaking. Note that the mass of the Higgs scalar is not protected by any symmetry. In fact the Higgs mass diverges quadratically when quantum corrections in the SM are taken into account.. This gives rise to a 'fine tuning' problem in the SM. The precision electroweak data demands the lightest Higgs boson mass to be $\sim$200 GeV! In order for this to happen we need to invoke some symmetries which will protect the Higgs mass to a much higher scale (possibly GUT scale). To resolve the 'fine tuning' problem it is expected that some new physics should takeover from the SM at the TeV scale. The favoured model, supersymmetry, addresses this problem by introducing a symmetry between bosons and fermions. Recently, a new approach has been advocated, the approach popularly known as the 'little Higgs models', which addresses some of the problems in the SM by making the Higgs boson a pseudo-Goldstone boson of a symmetry which is broken at some higher scale Λ. For a review of the LH models, see refs [2,3]. However, LH models were severely constrained by precision EW data. The basic problem with these kinds of models was the way in which new physics was coupled to the SM. To resolve these problems, a class of models with another symmetry, named T-parity, was introduced. These classes of models were investigated in ref. [3]. These T-parity models had another advantage in that they provided a very useful dark matter candidate. In our work [1] we have analyzed $\gamma\gamma \to \gamma\gamma$ in both the LH and LH with T-parity models.

2. The $\gamma\gamma \to \gamma\gamma$ cross-sections

The process $\gamma(p_1, \lambda_1)\gamma(p_2, \lambda_2) \to \gamma(p_3, \lambda_3)\gamma(p_4, \lambda_4)$ can be represented by 16 possible helicity amplitudes $F_{\lambda_1\lambda_2\lambda_3\lambda_4}(\hat{s}, \hat{t}, \hat{u})$, where p_i and λ_i represent the respective momenta and helicities; $\hat{s}$, $\hat{t}$ and $\hat{u}$ are the usual Mandelstam variables. By the use of Bose statistics, crossing symmetries and demanding parity and time-invariance, these 16 possible helicity amplitudes can be expressed in terms of just three amplitudes, namely (the relationships between the various helicity amplitudes is given in Appendix A of our paper [1]) $F_{++++}(\hat{s}, \hat{t}, \hat{u}), F_{+++-}(\hat{s}, \hat{t}, \hat{u}), F_{++--}(\hat{s}, \hat{t}, \hat{u})$. As such, the cross-section for this process can be expressed as [4]

$$\begin{aligned}\frac{\mathrm{d}\sigma}{\mathrm{d}\tau \mathrm{d}\cos\theta^*} = \frac{\mathrm{d}\bar{L}_{\gamma\gamma}}{\mathrm{d}\tau}\bigg\{ & \frac{\mathrm{d}\bar{\sigma}_0}{\mathrm{d}\cos\theta^*} + \langle\xi_2\xi_2'\rangle\frac{\mathrm{d}\bar{\sigma}_{22}}{\mathrm{d}\cos\theta^*} + [\langle\xi_3\rangle\cos 2\phi + \langle\xi_3'\rangle\cos 2\phi] \\ & \times\frac{\mathrm{d}\bar{\sigma}_3}{\mathrm{d}\cos\theta^*} + \langle\xi_3\xi_3'\rangle\left[\frac{\mathrm{d}\bar{\sigma}_{33}}{\mathrm{d}\cos\theta^*}\cos 2(\phi+\phi') + \frac{\mathrm{d}\bar{\sigma}_{33}'}{\mathrm{d}\cos\theta^*}\cos 2(\phi-\phi')\right] \\ & + [\langle\xi_2\xi_3'\rangle\sin 2\phi' - \langle\xi_3\xi_2'\rangle\sin 2\phi']\frac{\mathrm{d}\bar{\sigma}_{23}}{\mathrm{d}\cos\theta^*}\bigg\}, \end{aligned} \tag{1}$$

where $\mathrm{d}\bar{L}_{\gamma\gamma}$ describes the photon–photon luminosity in the $\gamma\gamma$ mode and $\tau = s_{\gamma\gamma}/s_{ee}$. Note that ξ_2, ξ_2', ξ_3 and ξ_3' are the Stokes parameters. To obtain the total cross-section from the above expressions, the integration over $\cos\theta^*$ has to be done in the range $0 \leq \cos\theta^* \leq 1$. However, the whole range of θ^* will not be experimentally observable. Hence, for our numerical estimates we will restrict the scattering angle to $|\cos\theta^*| \leq \sqrt{3}/2$. The process $\gamma\gamma \to \gamma\gamma$ proceeds through the mediation of charged particles. In the SM these charged particles were charged gauge bosons (W), quarks and charged leptons. In the LH model, in addition to the charged gauge bosons and fermions, we also have charged scalars. The analytical expressions of the contributions from fermions, gauge bosons and scalars to the helicity amplitudes are given in ref. [4] and are quoted in Appendix A of our paper [1]. In our work we have analyzed the effects of the LH models on various polarized cross-sections defined in eq. (1).

3. Results and conclusions

As the $\gamma\gamma \to \gamma\gamma$ scattering proceeds through loops, both in the SM and in the LH models (where these loops intermediate particles are pair produced), in the SM these are dominated by W loops, leading to a peak in the SM cross-sections around the threshold of the W pair production [4]. Similarly, in the LH model, the dominant contribution will come from the new heavy W-boson and the Higgs particles (especially those that are doubly charged, as the amplitudes are proportional to the fourth power of the charge), once we exceed the threshold for the pair production of these particles. As such, we have plotted the various cross-sections for a range of energies ($\sqrt{s_{\gamma\gamma}}$) well above the threshold for the SM W-bosons, but in the vicinity of the pair production energy for the new particles in the LH models. Note further, that we have integrated our differential cross-sections in the angular range $30° \leq \theta^* \leq 150°$.

As expected, the deviation in the SM value of the cross-sections becomes visible around the threshold of the pair production of LH particles, where the present constraints on the LH models force the masses of all the new heavy particles to be of the order of TeV.

In all cases we can get substantial deviations in the cross-sections due to LH effects. However, σ_3 and σ'_{33} provide the most interesting results (as given in figures 1 and 2), where σ_3 is the only cross-section with pronounced 'dips'. The location of these 'dips' is dependent on the model parameters. The other feature of note in these plots is the pronounced peaks in the σ'_{33} cross-section. The SM values of the cross-sections σ_3 and σ'_{33} are relatively small as compared to the other cross-sections. However, the LH effects in these two cross-sections are very striking. These effects mainly depend upon the LH parameter f (the symmetry breaking scale of the global symmetry).

Though the results we have presented are rather generic, they can be used as a probe for heavy charged gauge bosons and charged scalars. In our results we have tried to focus ourselves to the range of cm energy ($\sqrt{s_{\gamma\gamma}}$) which is close to the threshold of the pair production of the particles. The deviations from SM results as shown will not be observable in the proposed international linear collider (ILC), but will be easily probed in a multi-TeV e^+e^- compact linear collider (CLIC); where it is proposed to build an e^+e^- linear collider with a center-of-mass energy from 0.5 to 3 TeV. Generically such a mode should lead to $\gamma\gamma$ collisions at cm energies $E_{\text{cm}}^{\gamma\gamma} \leq 0.8 E_{\text{cm}}^{ee}$. Furthermore, the polarized cross-sections σ_3 and σ'_{33} can be used to test the spin structure of the particle loops which are responsible for the $\gamma\gamma \to \gamma\gamma$ process [4]. In summary the $\gamma\gamma \to \gamma\gamma$ process is a very clean process which shall provide a very useful tool for testing LH-type models.

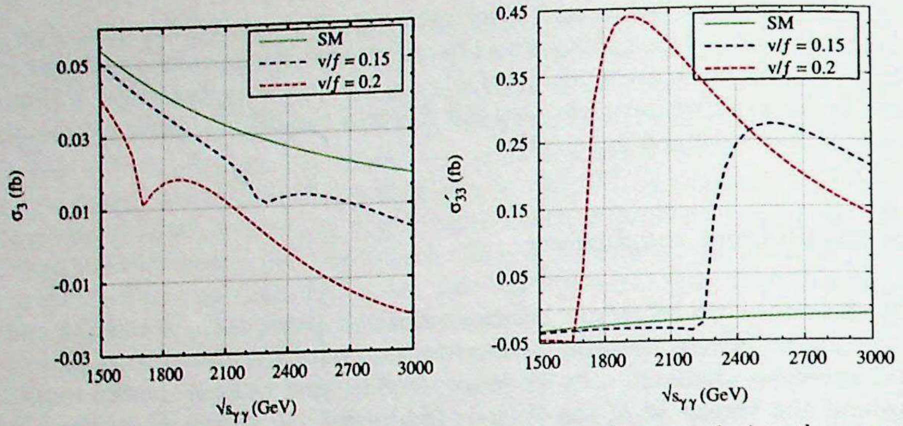

Figure 1. Results for the cross-sections integrated in the range $30 \leq \theta^* \leq 150$ for various values of v/f. Other LH model parameters are: $x_L = 0.2, s = s' = 0.6$.

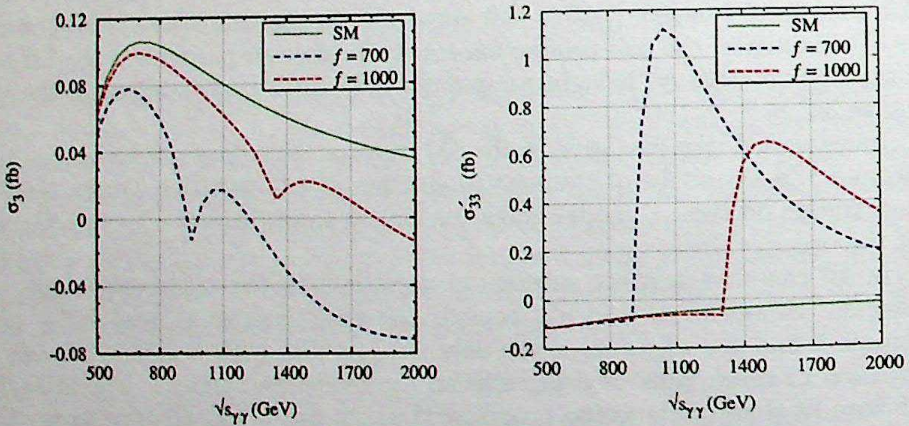

Figure 2. Results for the cross-sections integrated in the range $30 \leq \theta^* \leq 150$ for various values of v/f in LH model with T-parity.

Acknowledgements

The work of SRC, NG and AG was supported by the Department of Science & Technology (DST), India under grant No. SP/S2/K-20/99. The work of ASC was supported by the Japan Society for the Promotion of Science (JSPS), under fellowship No. P04764. The work of NG was supported by JSPS, under fellowship No. P06043.

References

[1] S R Choudhury, A S Cornell, N Gaur and A Goyal, *Phys. Rev.* **D73**, 115002 (2006), arXiv:hep-ph/0604162

[2] M Schmaltz and D Tucker-Smith, *Ann. Rev. Nucl. Part. Sci.* **55**, 229 (2005), arXiv:hep-ph/0502182
M Perelstein, arXiv:hep-ph/0512128
R Casalbuoni, A Deandrea and M Oertel, *J. High Energy Phys.* **0402**, 032 (2004), arXiv:hep-ph/0311038
M Asano, S Matsumoto, N Okada and Y Okada, arXiv:hep-ph/0602157
S R Choudhury, N Gaur and A Goyal, *Phys. Rev.* **D72**, 097702 (2005), arXiv:hep-ph/0508146

[3] J Hubisz, P Meade, A Noble and M Perelstein, *J. High Energy Phys.* **0601**, 135 (2006), arXiv:hep-ph/0506042
J Hubisz and P Meade, *Phys. Rev.* **D71**, 035016 (2005), arXiv:hep-ph/0411264
H C Cheng and I Low, *J. High Energy Phys.* **0309**, 051 (2003), arXiv:hep-ph/0308199; *J. High Energy Phys.* **0408**, 061 (2004), arXiv:hep-ph/0405243

[4] G J Gounaris, P I Porfyriadis and F M Renard, *Euro. Phys. J.* **C9**, 673 (1999), arXiv:hep-ph/9902230
G Jikia and A Tkabladze, *Phys. Lett.* **B323**, 453 (1994), arXiv:hep-ph/9312228
G J Gounaris, P I Porfyriadis and F M Renard, *Phys. Lett.* **B452**, 76 (1999); Erratum, *Phys. Lett.* **B513**, 431 (2001), arXiv:hep-ph/9812378

[5] S R Choudhury, A S Cornell and G C Joshi, *Phys. Lett.* **B481**, 45 (2000), arXiv:hep-ph/0001061
S R Choudhury, A S Cornell and G C Joshi, *Phys. Lett.* **B492**, 148 (2000), arXiv:hep-ph/0007347
S R Choudhury, A S Cornell and G C Joshi, arXiv:hep-ph/0012043

PRAMANA
— journal of
physics

© Indian Academy of Sciences

Vol. 69, No. 5
November 2007
pp. 759–763

Charged and neutral minimal supersymmetric standard model Higgs boson decays and measurement of tan β at the compact linear collider

E CONIAVITIS and A FERRARI*
Department of Nuclear and Particle Physics, Uppsala University, 75121 Uppsala, Sweden
*E-mail: ferrari@tsl.uu.se

Abstract. The minimal supersymmetric extension of the standard model (MSSM) predicts the existence of new charged and neutral Higgs bosons. The pair creation of these new particles at the multi-TeV e^+e^- compact linear collider (CLIC), followed by decays into standard model particles, were simulated along with the corresponding background. High-energy beam–beam effects such as ISR, beamstrahlung and hadronic background were included. We have investigated the possibility of using the ratio between the number of events found in various decay channels to determine the MSSM parameter tan β and we have derived the corresponding statistical error from the uncertainties on the measured cross-sections and Higgs boson masses.

Keywords. Minimal supersymmetric standard model; heavy Higgs bosons; compact linear collider.

PACS Nos 12.60.Fr; 13.66.Hk; 14.80.Cp

1. Introduction

In the standard model (SM), one doublet of scalar Higgs fields is needed to break the electroweak gauge symmetry. On the other hand, in several extensions of the SM, and in particular supersymmetry, the Higgs sector may consist of at least two isodoublets of scalar fields. The theoretical framework of this study is the minimal supersymmetric extension of the standard model (MSSM), where the symmetry breaking through two complex Higgs doublets leads to five physical states. Two of them are charged (H^+, H^-) and, among the three neutral Higgs bosons, two are CP-even states, h^0 and H^0, and one is CP-odd, A^0. At tree level, the MSSM Higgs sector is entirely determined with only two independent parameters, generally taken as the mass m_A and the ratio of the two vacuum expectation values tan β. In this paper, we consider the production of charged and neutral Higgs bosons at the compact linear collider (CLIC) [1], through $e^+e^- \to H^+H^-$ and $e^+e^- \to A^0H^0$. These two processes were already analysed separately in previous studies [2,3].

Here, we consider all hadronic decays of the charged and neutral Higgs bosons, either via a pair of third generation quarks or via final states with one or two τ-leptons decaying into hadrons. We present a combined sensitivity study of the two processes at CLIC, with an updated description of the beam–beam effects and of the various background processes. In addition, we estimate the accuracy with which various cascade decays of H^+H^- and A^0H^0 can be measured, and we discuss the derivation of $\tan\beta$ from these measurements.

2. Discovery limits for charged and neutral MSSM Higgs bosons at CLIC

In e^+e^- collisions, charged and neutral Higgs bosons can be produced in pairs via an intermediate photon or Z boson. At CLIC, prior to the initial state radiation of photons (ISR), one must take into account several high-energy beam–beam effects, which lead in particular to a long low-energy tail in the center-of-mass energy spectrum via emission of beamstrahlung photons at the interaction point. In turn, high-energy collisions between the beamstrahlung photons may lead to the production of additional hadrons. With the beam parameters considered for this study [4], the nominal center-of-mass energy is 3 TeV, the luminosity is 6.5×10^{34} cm^{-2} s^{-1}, the average energy loss of a beam particle due to beamstrahlung is 16%, and one expects 0.73 hadronic events per bunch crossing (we integrate the hadronic background over 75 bunch crossings, i.e. 20 ns). After the generation of A^0H^0 and H^+H^- pairs with PYTHIA, a fast detector simulation is performed with SIMDET [6] using its default parametrizations for CLIC. The b- and τ-tagging efficiencies are both set to 70% and are implemented by hand in the reconstruction procedure.

2.1 *Estimation of the SM backgrounds*

The most significant SM background processes for the pair production and hadronic decays of MSSM charged and neutral Higgs bosons are those which lead to genuine $bbbb$, $tttt$, $bb\tau\tau$, $tt\tau\tau$, $tbtb$ and $tb\tau\nu_\tau$ final states. MadGraph and MadEvent [7] were used to generate the SM background processes and to calculate the associated cross-sections (a separate Monte-Carlo program was written to include the energy spectrum of the incoming electrons and positrons). Then, the quark fragmentation and the inclusion of final state radiation (FSR) effects are performed using the relevant PYTHIA subroutines, prior to fast detector simulation and event reconstruction with SIMDET.

2.2 *Charged Higgs boson discovery contour*

In order to reconstruct $e^+e^- \to H^+H^- \to tbtb$ events, which can occur for all values of $\tan\beta$, we proceed as follows. First, the presence of two W bosons decaying hadronically is tested and t quarks are reconstructed from a W candidate paired with one of the four b-tagged jets. After assignment of the t candidates and the remaining b jets to their correct H^+H^- pair, a mass constrained kinematical fit is applied. Some cuts on $m_{\rm rec}(tt)$ and $m_{\rm rec}(bb)$ allow to further reduce the SM background. As for $e^+e^- \to H^+H^- \to tb\tau\nu_\tau$, which has a significant branching ratio for the large values of $\tan\beta$ only, we first search for one charged Higgs boson decaying into tb. Then, since a full reconstruction of the other charged Higgs boson is not possible due to the presence of missing transverse energy in the final state, we reconstruct its transverse mass $m_{\rm T}$ instead. In that case, the dominant background is $e^+e^- \to tb\tau\nu_\tau$, which mostly arises from the pair production of top quarks, where one of them decays through $t \to bW \to b\tau\nu_\tau$. However, it is efficiently reduced by appropriate cuts, in particular on the missing transverse energy and $m_{\rm T}$. The left-hand side plot of figure 1 shows how the CLIC discovery limit varies with $\tan\beta$ for $H^+H^- \to tbtb$, $H^+H^- \to tb\tau\nu_\tau$ and the combination of these two processes. The discovery limit for charged Higgs bosons at CLIC lies between 1.22 TeV and 1.25 TeV.

2.3 *Neutral Higgs boson discovery contour*

After the discovery of heavy charged Higgs bosons at CLIC, one should explore the neutral Higgs sector. For this purpose, we focus on the three cascade decays leading to t and/or b quarks in the final state. One major challenge in the Higgs sector is to reduce not only the SM background, but also the background arising from $e^+e^- \to H^+H^-$ events, for which the production cross-section is about 2.5 times larger than for $e^+e^- \to A^0H^0$. For small values of $\tan\beta$, both A^0 and H^0 mainly decay into a tt pair and, after reduction of all backgrounds, one expects a CLIC discovery limit of 0.97 TeV. At large $\tan\beta$, the search for $A^0H^0 \to bbbb$ events yields a higher discovery limit, namely 1.30 TeV. Finally, for the intermediate values of $\tan\beta$, some $e^+e^- \to A^0H^0$ events lead to $ttbb$ final states, just like most of the $e^+e^- \to H^+H^-$ events. However, in order to reconstruct the neutral Higgs bosons, one pairs two t candidates on the one hand and two b-tagged jets on the other hand, while two tb pairs are searched for when reconstructing the charged Higgs bosons. At $\tan\beta \simeq 7.6$, where the fraction of A^0H^0 pairs decaying into $ttbb$ final states is the largest, the discovery limit is 0.89 TeV. The CLIC discovery contour associated to these three cascade decays of the A^0H^0 pairs is shown in the right-hand side plot of figure 1.

3. Estimation of the signal rates and measurement of $\tan\beta$

The decay widths of the MSSM charged and neutral Higgs bosons depend directly on $\tan\beta$ [8], and so do the number of observed events for each cascade decay. In order to minimize the effect of luminosity and cross-section uncertainties for $\tan\beta$ determination, we consider the ratio between two decay widths (i.e. between two signal rates of the same Higgs boson pair). The statistical uncertainty on m_A was derived from a χ^2-analysis. Since it usually remains smaller than 1%, it does not significantly affect the $\tan\beta$ determination. Figure 2 shows the expected positive

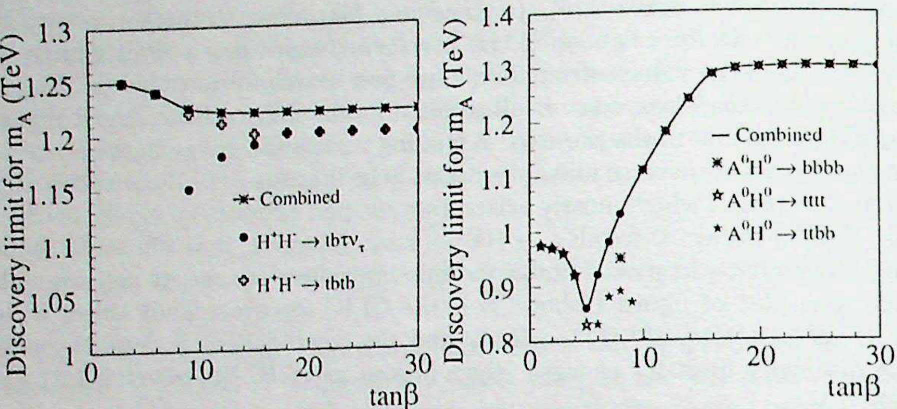

Figure 1. Discovery contours of charged and neutral Higgs bosons at CLIC, with an integrated luminosity of 3000 fb^{-1}: for a discovery, one requires the signal S to be at least ten events and it must exceed five statistical fluctuations of the background B.

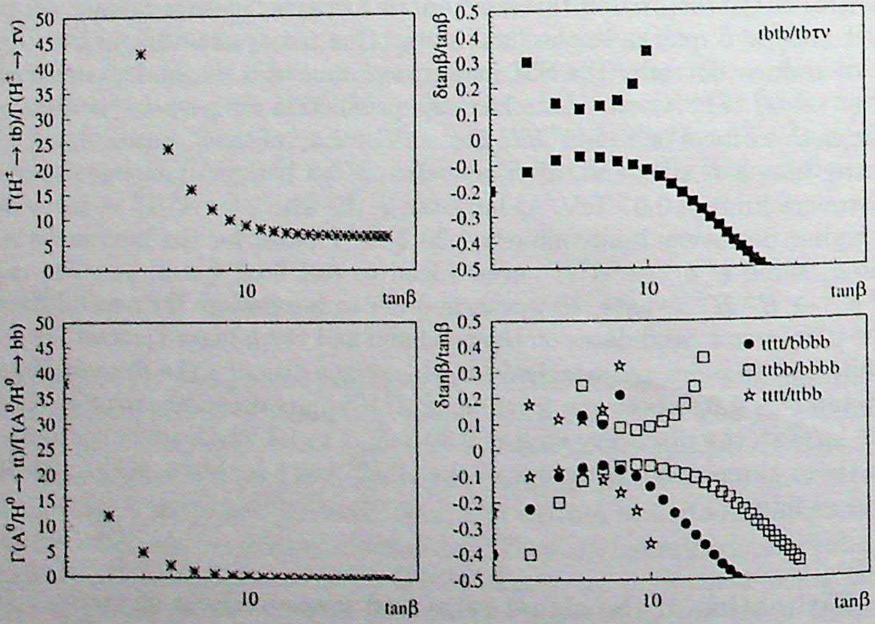

Figure 2. Variation with $\tan\beta$ of the expected statistical error on $\tan\beta$ when deriving this parameter from the ratio between various signal rates, for $m_A = 700$ GeV and an integrated luminosity of 3000 fb^{-1}.

and negative relative uncertainties on $\tan\beta$. We neglect the relative error on the luminosity, and so the signal rate uncertainty is $\sqrt{S+B}/S$.

The statistical errors on $\tan\beta$ are always smallest for values of $\tan\beta$ in the 5–8 region. For other $\tan\beta$ values, the relative error on the ratio of the signal rates is much larger, either because one of the cascade decays has a vanishing cross-section, or because of the asymptotic behaviour of the ratio between the signal rates (especially at large $\tan\beta$).

4. Conclusion

The discovery limit for MSSM charged and neutral Higgs bosons at CLIC lies beyond 1 TeV and, in contrast to the LHC, does not significantly depend on $\tan\beta$. In addition, by comparing the signal rates of different cascade decays, one may be able to measure $\tan\beta$ with a good accuracy in the intermediate region, which is not accessible through standard decays of the MSSM Higgs bosons at the LHC.

References

[1] The CLIC Study Team, CERN 2000-008
[2] A Ferrari, LC-PHSM-2003-051
[3] A Ferrari, LC-PHSM-2004-008
[4] F Tecker *et al*, CLIC note 627
[5] T Sjöstrand, P Eden, C Friberg, L Lonnblad, G Miu, S Mrenna and E Norrbin, *Comput. Phys. Commun.* **135**, 238 (2001)
[6] M Pohl and H J Schreiber, DESY 99-030
[7] F Maltoni and T Stelzer, hep-ph/0208156
W F Long and T Stelzer, *Comput. Phys. Commun.* **81**, 357 (1994)
K Hagiwara, H Murayama and I Watanabe, KEK Report 91-11
[8] A Djouadi, J Kalinowski and M Spira, *Comput. Phys. Commun.* **108**, 56 (1998)

PRAMANA
— journal of
physics

© Indian Academy of Sciences

Vol. 69, No. 5
November 2007
pp. 765–769

Power losses in the international linear collider 20 mrad extraction line at 1 TeV

A FERRARI[1,*] and YURI NOSOCHKOV[2]
[1]Department of Nuclear and Particle Physics, Uppsala University, 75121 Uppsala, Sweden
[2]Stanford Linear Accelerator Center, USA
*E-mail: ferrari@tsl.uu.se

Abstract. We have performed a detailed study of the power losses in the post-collision extraction line of a TeV e^+e^- collider with a crossing angle of 20 mrad at the interaction point. Five cases were considered: four luminosity configurations for ILC and one for CLIC. For all of them, the strong beam–beam effects at the interaction point lead to an emittance growth for the outgoing beam, as well as to the production of beamstrahlung photons and e^+e^- coherent pairs. The power losses along the extraction line, which are due to energy deposition by a fraction of the disrupted beam, of the beamstrahlung photons and of the coherent pairs, were estimated in the case of ideal collisions, as well as with a vertical position or angular offset at the interaction point.

Keywords. Extraction line; international linear collider; compact linear collider; beam losses.

PACS Nos 29.27.-a; 29.17.+w; 41.75.Ht; 41.85.-p

1. Introduction

In a high-energy e^+e^- linear collider, the beams must be focused to extremely small spot sizes in order to achieve high charge densities and, in turn, to reach the desired luminosity. Because of the extremely small transverse dimensions of the colliding beams, electrons and positrons experience very strong transverse electromagnetic fields at the interaction point. The subsequent bending of their trajectories leads to the emission of hard beamstrahlung photons, which can then turn into coherent pairs. A careful design of the extraction line must be performed in order to transport the outgoing charged beams and beamstrahlung photons from the interaction point to their dump. In this study, we estimate the beam losses in the extraction line of a 1 TeV e^+e^- linear collider with a 20 mrad crossing angle. This may correspond either to the early stage of the multi-TeV compact linear collider (CLIC) or to an upgraded version of the international linear collider (ILC).

Table 1. Beam parameters for various configurations of a 1 TeV e^+e^- linear collider.

Configuration at 1 TeV	CLIC	ILC nominal	ILC hl1	ILC hl2	ILC hl3
Particles per bunch N_b (10^{10})	0.256	2.0	2.0	2.4	2.0
Bunches per RF pulse, n	220	2820	2820	2820	2820
Bunch spacing (ns)	0.267	307.7	307.7	307.7	307.7
Beam current (A)	1.5	0.0104	0.0104	0.0125	0.0104
Repetition frequency f (Hz)	150	4	4	4	4
Primary beam power (MW)	6.8	18.1	18.1	21.7	18.1
$(\beta\gamma)\epsilon_x$ in 10^{-6} mrad	0.660	10	10	10	10
$(\beta\gamma)\epsilon_y$ in 10^{-6} mrad	0.001	0.04	0.03	0.023	0.023
σ_x (nm)	94	554	320	550	470
σ_y (nm)	1.0	3.5	2.5	2.7	2.7
σ_z (μm)	30.8	300	150	300	300
Luminosity (10^{34} cm^{-2}s^{-1})	2.8	2.8	7.8	5.7	4.6
Photons per e^+ or e^-	0.9	1.4	2.2	1.7	1.7
Beamstrahlung loss δ_B	9.0%	4.8%	17.6%	6.7%	6.5%

2. Beam parameters and extraction line layout

Several machine configurations are being studied to reach the ILC luminosity goals [1,2]. Here, we consider four sets of parameters at 1 TeV. One is referred to as nominal and the other three (hl1, hl2 and hl3) correspond to various high luminosity configurations. As for CLIC, an optimization of the machine design at 1 TeV was recently performed [3]. More details are given in table 1.

At an e^+e^- linear collider with a 20 mrad crossing angle, one uses a dedicated line to transport the disrupted beam and the beamstrahlung photons from the interaction point to their dump. In its present design, the ILC 20 mrad extraction line consists of a DFDF quadruplet, followed by two vertical chicanes for energy and polarization measurements and a field-free region that allows the beam to grow naturally, with two collimators located 200 m and 300 m downstream of the interaction point, in order to reduce the maximum beam size at the dump [4].

3. Power losses in the case of ideal e^+e^- collisions

Knowing the incoming beam parameters, the outgoing beam distributions at the interaction point can be obtained with GUINEA-PIG [5]. These were then tracked to the dump with DIMAD [6]. Using the number of lost particles in the extraction line, as well as their energy (in GeV), one can calculate the power loss (in W) using the following formula:

$$P_{\text{loss}} = 1.602 \times 10^{-10} \frac{N_b n f}{N_{\text{tracks}}} \sum_{i=1}^{N_{\text{loss}}} E_i.$$

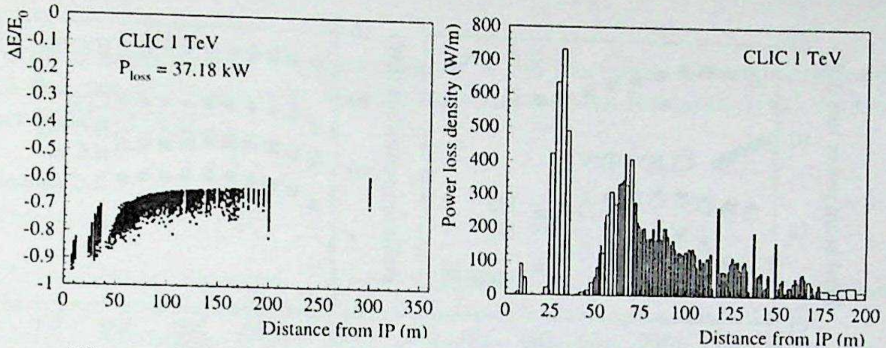

Figure 1. Relative energy spread of the lost particles as a function of the position of loss in the 20 mrad extraction line (left) and loss density upstream of the collimators (right), obtained when tracking the disrupted beam of the 1 TeV CLIC case.

Table 2. Total power losses for various configurations of a 1 TeV e^+e^- linear collider.

Configuration at 1 TeV	CLIC	ILC nominal	ILC hl1	ILC hl2	ILC hl3
Disrupted beam losses (kW)	37.2	0.9	202.7	4.1	3.6
Beamstrahlung photon losses (kW)	$< 10^{-3}$	$< 10^{-3}$	1.2	$< 10^{-3}$	$< 10^{-3}$
Coherent pair losses (kW)	0.2	–	–	–	–

The particle tracking clearly shows that most of the power losses come from the low-energy tail of the disrupted beam (see figure 1). Indeed, the ILC 20 mrad extraction line accepts most of the electrons and positrons with $E/E_0 > 40\%$. As for the beamstrahlung photons, they lead to significant power losses on the first round collimator in the ILC hl1 configuration only, for which one has a large horizontal photon cone size at the interaction point. Finally, our tracking studies suggest that about 75% of the particles coming from the coherent pairs do not reach the dump at the end of the extraction line. These losses mostly occur due to over-focusing of low-energy particles in the quadrupoles and they do not significantly depend on the particle charge. Note that only the CLIC case leads to a non-negligible amount of e^+e^- coherent pairs. A summary of our results is given in table 2 (see also ref. [7] for more details).

4. Power losses with a vertical offset in position or angle

Let us introduce a vertical position or angle offset at the interaction point, which can occur during initial tuning. GUINEA-PIG simulations clearly show a blow-up of the emittance with such a beam-to-beam offset. Also, there are more particles in the low-energy tail of the disrupted beam, which are then likely to be lost in the extraction line. Figure 2 shows how the disrupted beam losses vary with a vertical offset in position or angle.

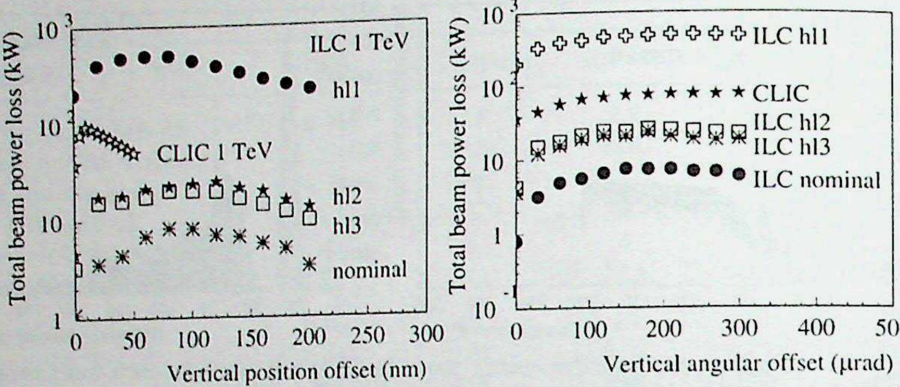

Figure 2. Disrupted beam power losses in the extraction line as a function of the position offset Δy (left) or the angular offset $\Delta y'$ (right), for various ILC and CLIC configurations at 1 TeV.

More beamstrahlung photons are produced with a vertical beam-to-beam offset and their angular distribution is wider than for ideal collisions. In the ILC hl1 configuration, the power loss due to beamstrahlung photons on the collimators is maximal when $\Delta y = 80$ nm and it reaches 62 kW. With a vertical angular offset at the interaction point, tails appear in the y'-distribution of the beamstrahlung photons (while its x'-distribution is unaffected). Together with an increased number of beamstrahlung photons per e^+e^- collision, this leads to additional power losses (mostly on the collimators). However, the maximal losses due to the vertical angular offset are about twice smaller than the maximal losses due to the vertical position offset. Finally, the number of coherent pairs per bunch crossing may be up to about six times larger than in the case of ideal collisions, but their contribution to the power losses along the extraction line still remains negligible.

5. Conclusion

A detailed study of the beam losses along the 20 mrad extraction line of a TeV e^+e^- collider was performed, for various CLIC or ILC configurations. More than 99% of these losses are due to the low-energy tail of the disrupted beams. In the 1 TeV ILC nominal configuration, the power losses are less than 1 kW and their distribution along the 20 mrad extraction line appears acceptable. The recently proposed ILC high luminosity hl2 and hl3 configurations should also allow to keep the power losses at a reasonable level in the extraction line, although these are three to five times larger than in the ILC nominal case. On the other hand, the beam losses become too large for the ILC high luminosity hl1 and CLIC configurations. The power losses in the 20 mrad extraction beam line were also studied as a function of a vertical position or angular offset at the interaction point. It was found that the strongest beam–beam effects, and in turn the maximal power losses, occur when the vertical position offset is 10–30σ_y or when the vertical angular offset reaches about 200 μrad.

Acknowledgements

This work is supported by the Commission of the European Communities under the 6th Framework Programme 'Structuring the European Research Area', contract number RIDS-011899.

References

[1] T Raubenheimer, *Suggested ILC beam parameter range*, 28 February 2005 (available at http://www-project.slac.stanford.edu/ilc/acceldev/beamparameters.html)

[2] A Seryi, *Alternative 1 TeV high luminosity parameters*, 26 July 2005 (available at http://www-project.slac.stanford.edu/lc/bdir/Meetings/beamdelivery/2005-07-26/index.htm)

[3] F Tecker *et al*, CLIC note 627

[4] R Arnold, K Moffeit, Y Nosochkov, W Oliver, A Seryi, E Torrence and M Woods, Design of ILC extraction line for 20 mrad crossing angle, *Proceedings of PAC 2005*, Knoxville, USA

[5] D Schulte, TESLA-97-08 (1996)

[6] http://www.slac.stanford.edu/accel/ilc/codes/dimad

[7] A Ferrari and Y Nosochkov, EUROTeV-Report-2005-025

PRAMANA
— journal of
physics

© Indian Academy of Sciences

Vol. 69, No. 5
November 2007
pp. 771–775

Probing CP-violating Higgs contributions in $\gamma\gamma \rightarrow f\bar{f}$

ROHINI M GODBOLE[1], SABINE KRAML[2], SAURABH D RINDANI[3] and RITESH K SINGH[4,*]
[1]Center for High Energy Physics, Indian Institute of Science, Bangalore 560 012, India
[2]Theory Division, Department of Physics, CERN, Switzerland
[3]Physical Research Laboratory, Ahmedabad 380 009, India
[4]Laboratoire de Physique Théoretique, 91405 Orsay Cedex, France
*E-mail: ritesh.singh@th.u-psud.fr

Abstract. We discuss the use of fermion polarization for studying neutral Higgs bosons at a photon collider. To this aim we construct polarization asymmetries which can isolate the contribution of a Higgs boson ϕ in $\gamma\gamma \rightarrow f\bar{f}$, $f = \tau/t$, from that of the QED continuum. This can help in getting information on the $\gamma\gamma\phi$ coupling in case ϕ is a CP eigenstate. We also construct CP-violating asymmetries which can probe CP mixing in case ϕ has indeterminate CP. Furthermore, we take the MSSM with CP violation as an example to demonstrate the potential of these asymmetries in a numerical analysis. We find that these asymmetries are sensitive to the presence of a Higgs boson as well as its CP properties over a wide range of MSSM parameters.

Keywords. CP-violating Higgs; polarization; photon collider.

PACS Nos 14.80.Cp; 14.60.Fg; 12.60.Jv

At a photon collider, fermion-pair production proceeds through the standard QED t-channel as well as through s-channel Higgs mediation. The Higgs boson, ϕ, in general can be CP violating as the case in the MSSM with nonvanishing CP phases. The QED vertex $\gamma f\bar{f}$ conserves chirality, whereas the $\phi f\bar{f}$ coupling mixes different chiralities and hence it can affect, in principle, the polarization of the produced fermions. With unpolarized photons in the initial state, the QED contribution leads to unpolarized fermions in the final state. The same is true for the Higgs exchange should the Higgs boson(s) be a CP eigenstate; CP violation (CPV) in the Higgs sector leads to a net, though very small, polarization of the fermions, even with the unpolarized initial beams. With polarized initial-state photons, the QED contribution alone gives rise to a finite polarization. The additional chirality-mixing contribution from the Higgs boson exchange diagram causes a change in this polarization for both, the CP-conserving and the CP-violating, cases. It is thus possible to construct observables involving the polarizations of the initial-state

Table 1. Polarization observables, interactions and the form-factor combinations that they can probe.

Observable	Type of interaction	Combinations probed
P_f^U	P/CP violating	y_i's
$\delta P_f^+ = P_f^{++} - (P_f^{++})^{\rm QED}$	Chirality mixing	x_i's, y_i's
$\delta P_f^- = P_f^{--} - (P_f^{--})^{\rm QED}$	Chirality mixing	x_i's, y_i's
$\delta P_f^{\rm CP} = P_f^{++} + P_f^{--}$	P/CP violating	y_i's

photons and those of the final-state fermions (τ/t), which can probe the Higgs boson couplings, including possible CP violation in the Higgs sector.

The fermion polarization is defined as the fractional surplus of positive helicity fermions over negative helicity ones, $P_f^{ij} = (N_+^{ij} - N_-^{ij})/(N_+^{ij} + N_-^{ij})$, where the superscript ij stands for the polarizations of the parent e^+e^- beams $(P_e, P_{\bar{e}})$ of the ILC. N_+ and N_- stand for the number of fermions with positive and negative helicities, respectively. The polarization of anti-fermions, $\bar{P}_f^{ij}$, is defined analogously; conservation of linear and angular momenta implies $P_f^{ij} = \bar{P}_f^{ij}$.

We know that the chirality mixing amplitudes in pure QED are proportional to the fermion mass m_f. Hence these are small for light fermions. Further, the Higgs-exchange diagram contributes only when the helicities of the colliding photons are equal; at the same time the QED contribution can be suppressed by choosing $\lambda_1 = \lambda_2$. For the case of the polarized, peaked photon spectrum [1] this amounts to choosing $(P_e, P_{\bar{e}}) = (\pm, \pm)$ for the parent e^+/e^- beams.

The final-state fermion polarization with unpolarized initial state, P_f^U, is zero should the Higgs boson have a definite CP quantum number. Nonzero values of P_f^U only arise for $y_i \neq 0$, thus it is a signal of CP violation in the Higgs sector. For polarized initial states, the final-state fermion polarization is always nonzero. Regardless of whether CP is violated or not, any deviation of P_f^{++} and P_f^{--} from their QED predictions probes the Higgs boson contribution. Moreover, since P-invariance implies $P_f^{++} = -P_f^{--}$ for the QED contribution, $P_f^{++} + P_f^{--} \neq 0$ is a signal of CP violation. The polarization observables are summarized in table 1. Here note that $\delta P_f^{\rm CP} = \delta P_f^+ + \delta P_f^-$. In the following, we choose δP_f^- and $\delta P_f^{\rm CP}$ as the independent observables.

We demonstrate the utility of our polarization observables, by performing a numerical analysis for $\gamma\gamma \to \tau^+\tau^-$ and $\gamma\gamma \to t\bar{t}$ in the CPX scenario [2]. We vary $M_{H^\pm} = 150$–500 GeV and $\tan\beta = 3$–40 and consider different phases Φ_A. The Higgs boson masses, couplings and widths are computed with both CPsuperH [3] and FeynHiggs [4]. For the polarized photon beams, we use the ideal Compton-backscattered photon spectrum of [1]. The beam energy $E_{\rm b}$ for the parent e^+e^- collider is chosen such that the peak in the spectrum of the $\gamma\gamma$ invariant mass corresponds to the relevant Higgs boson mass(es). This choice explores the ultimate potential of the polarization observables; we call it the 'peak E_B' choice. In general, $P_f^U \neq 0$ would be a clear signal of CPV. However, P_f^U is found to be very small, well below experimental sensitivity. So we have to work with polarized beams and consider δP_f^- and $\delta P_f^{\rm CP}$.

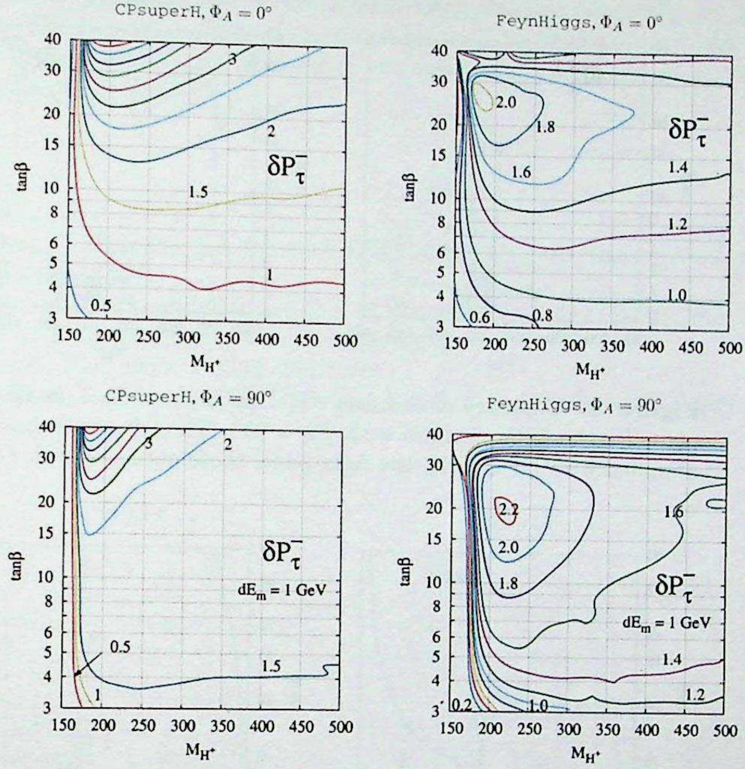

Figure 1. Contours of constant δP_τ^- in units of 10^{-2} in the $\tan\beta$-$M_{H^\pm}$ plane for the CPX scenario with $\Phi_A = 0°$ (top panel) and $\Phi_A = 90°$ (bottom panel) with $\mathrm{d}E_m = 1$ GeV. The left panels show the results obtained with CPsuperH, the right panels those obtained with FeynHiggs.

Let us start with $f = \tau$. Due to the small τ mass, the contribution to the τ polarization from the Higgs boson exchange diagram is very small unless one puts a cut on the $\tau^+\tau^-$ invariant mass. We use a cut $|m_{\tau\tau} - M_{H_1}| \leq \max(\mathrm{d}E_m,\ 5\ \Gamma_{H_1})$ with $\mathrm{d}E_m = 1$ GeV. In figure 1 we show δP_τ^- for both CPsuperH and FeynHiggs for zero and maximal phase Φ_A. The $e^\pm$ beam energy is chosen such that $\sqrt{s}_{\gamma\gamma}$ at the peak of the photon spectrum is equal to the mass of the lightest Higgs boson H_1. The deviation in the polarization due to the H_1 exchange is large for both $\Phi_A = 0$ and 90°. δP_τ^- increases with $\tan\beta$ because the τ Yukawa coupling increases. However, it turns out that $\delta P_\tau^+ \simeq \delta P_\tau^-$, so that $\delta P_\tau^{\mathrm{CP}} \simeq 0$ over all the $\tan\beta$–$M_{H^\pm}$ plane. The difference between CPsuperH and FeynHiggs in figure 1 can be traced to somewhat different predictions of the masses, couplings and decay widths as a result of the different approximations used in the two programs.

In the case of $t\bar{t}$ production, it is the heavier Higgs bosons $H_{2,3}$ which contribute. Since the masses of $H_{2,3}$ are in general close to each other, we choose the beam energy such that the mean value $(M_{H_2} + M_{H_3})/2$ matches with $\sqrt{s}_{\gamma\gamma}$ at the peak of the photon spectrum. We find that the top polarization is sensitive not only to the

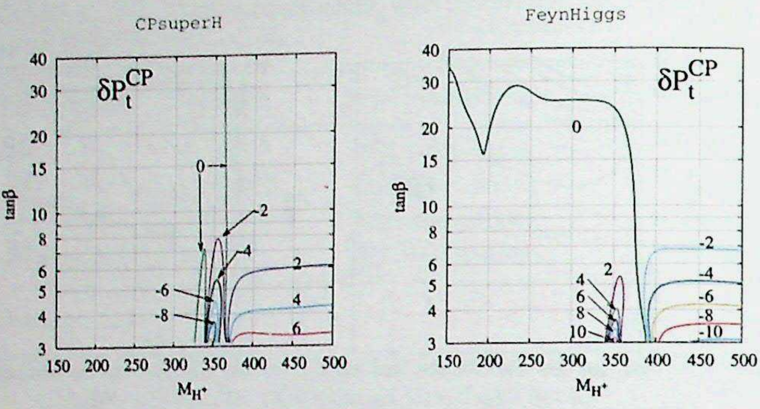

Figure 2. Contours of constant δP_t^{CP} in units of 10^{-2} in the $\tan\beta$–$M_{H\pm}$ plane for the CPX scenario with $\Phi_A = 90°$. The left panel shows the results obtained with CPsuperH, the right panel those obtained with FeynHiggs.

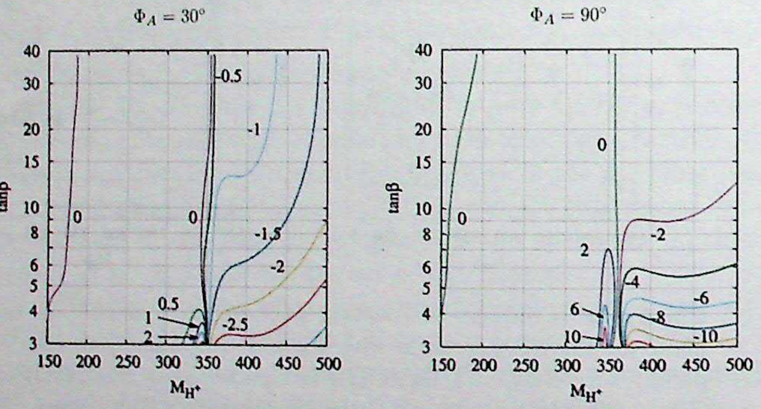

Figure 3. Contours of constant $\mathcal{A}_3$ for $\Phi_A = 30°$ and $90°$; computed with CPsuperH.

Higgs contribution in general ($\delta P_t^{\pm}$) but also to CP violation (δP_t^{CP}). In figure 2 we show contours of constant δP_t^{CP} in the $\tan\beta$–$M_{H\pm}$ plane for $\Phi_A = 90°$. Of course one needs $M_{H\pm} \geq 2m_t$. Since the top Yukawa coupling decreases with $\tan\beta$, δP_t^{CP} is only sizable for small values of $\tan\beta$. Note that due to the large top-quark mass, no cut on the $t\bar{t}$ invariant mass is needed to increase the sensitivity. The difference in the sign of δP_t^{CP} in the two panels in figure 2 is due to different conventions in CPsuperH and FeynHiggs leading to the opposite signs of y_i, $i = 1, \ldots, 4$, for the same input MSSM parameters. Further, we also investigate the asymmetries defined at the level of leptons as constructed in ref. [5]. These are sensitive to the CP violation in the Higgs sector. We show the corresponding countours in figure 3 for $\Phi_A = 30°$ and $90°$. We see that the lepton asymmetry $\mathcal{A}_3$ is large and observable for small $\tan\beta$, large $m_{H\pm}$, only for large enough CP phase Φ_A.

In summary, the polarization of heavy fermions is a good probe of the coupling of the Higgs boson including CP violation. We have analyzed this in the MSSM with CPV in the CPX scenario. We find that the polarization of τ-leptons may be used to probe the couplings of the lightest Higgs boson, especially in the large $\tan\beta$ region. The t-quark polarization, which is sensitive to the contribution of the two heavier Higgs bosons, can be used in the low $\tan\beta$ and large $M_{H^\pm}$ region of the MSSM parameter space.

References

[1] I F Ginzburg, G L Kotkin, S L Panfil, V G Serbo and Valery I Telnov, *Nucl. Instrum. Methods* **A219**, 5 (1984)
[2] M Carena, J R Ellis, A Pilaftsis and C E M Wagner, *Phys. Lett.* **B495**, 155 (2000)
[3] J S Lee *et al*, *Comput. Phys. Commun.* **156**, 283 (2004)
[4] S Heinemeyer, *Eur. Phys. J.* **C22**, 521 (2001)
[5] Rohini M Godbole, Saurabh D Rindani and Ritesh K Singh, *Phys. Rev.* **D67**, 095009 (2003)

PRAMANA
— journal of
physics

© Indian Academy of Sciences

Vol. 69, No. 5
November 2007
pp. 777–782

Anomalous VVH interactions at a linear collider

SUDHANSU S BISWAL[1,*], DEBAJYOTI CHOUDHURY[2],
ROHINI M GODBOLE[1] and RITESH K SINGH[3]
[1]Centre for High Energy Physics, Indian Institute of Science, Bangalore 560 012, India
[2]Department of Physics and Astrophysics, University of Delhi, New Delhi 110 007, India
[3]Laboratoire de Physique Théoretique, 91405 Orsay Cedex, France
[*]E-mail: sudhansu@cts.iisc.ernet.in

Abstract. We examine, in a model independent way, the sensitivity of a linear collider to the couplings of a light Higgs boson to a pair of gauge bosons, including the possibility of CP violation. We construct several observables that probe the various possible anomalous couplings. For an intermediate mass Higgs, a collider operating at a center of mass energy of 500 GeV and with an integrated luminosity of 500 fb^{-1} is shown to be able to constrain the ZZH vertex at the few per cent level, with even higher sensitivity for some of the couplings. However, lack of sufficient number of observables as well as contamination from the ZZH vertex limits the precision to which anomalous part of the WWH coupling can be probed.

Keywords. Anomalous Higgs couplings; linear collider.

PACS Nos 13.66.Fg; 14.80.Cp; 14.70.Fm; 14.70.Hp

1. Introduction

The standard model (SM) of particle physics has been tested up to a high degree of accuracy, but the direct experimental verification of the phenomenon of spontaneous symmetry breaking is still pending. Various extensions of the SM have more than one Higgs boson whose CP parity and hypercharges may differ from those of the SM Higgs boson. The minimal supersymmetric standard model (MSSM) is one example of such an extended Higgs sector [1]. To establish the experimental observation of the SM Higgs boson it will be therefore, necessary to establish its properties such as hypercharge, CP parity etc. At an e^+e^- collider the dominant Higgs production processes are $e^+e^- \to f\bar{f}H$, which proceed via the VVH coupling with $V = W, Z$ and f any light fermion. Demanding Lorentz invariance, the VVH couplings can be parameterized as

$$\Gamma_{\mu\nu} = g_V \left[a_V g_{\mu\nu} + \frac{b_V}{m_V^2}(k_{1\nu}k_{2\mu} - g_{\mu\nu}k_1 \cdot k_2) + \frac{\tilde{b}_V}{m_V^2}\, \epsilon_{\mu\nu\alpha\beta}k_1^\alpha k_2^\beta \right], \qquad (1)$$

where k_i denote the momenta of the two W's (Z's); $g_W^{\rm SM} = e \cot\theta_W M_Z$ and $g_Z^{\rm SM} = 2eM_Z/\sin 2\theta_W$. In general, all these anomalous couplings can be complex. For simplicity we assume a_V to be real and close to its SM value. For processes involving VVH coupling alone we can choose, without loss of generality, $g_V = g_V^{\rm SM}$ and $a_V = 1 + \Delta a_V$. We further assume $\Delta a_W = \Delta a_Z$ and keep terms up to linear order in the anomalous couplings. The analysis will be made for the ILC with center of mass energy 500 GeV and a Higgs boson of mass 120 GeV. We will use $H \to b\bar{b}$ final state and further assume b-quark detection efficiency of 0.7. The largest contribution comes from the process, $e^+e^- \to \nu_e\bar{\nu}_e H$. This process contains two missing neutrinos in the final state. However, this receives contributions from both the WWH and ZZH vertices. Hence one needs to look at $e^+e^- \to Z^*H \to f\bar{f}H$ to constrain ZZH anomalous couplings and then make use of this information while probing WWH couplings.

2. Observables and kinematical cuts

We have constructed various momentum combinations $\mathcal{C}_i$ by taking dot and scalar triple products of different linear combinations of momenta. These combinations have been listed in table 1 with their transformation properties under discrete symmetries C, P and T̃, where the pseudotime reversal operator (T̃) reverses the momenta and spins of particles without interchanging their initial and final states. Then we construct observables ($\mathcal{O}_i$) by taking the expectation values of the signs of various $\mathcal{C}_i$'s, i.e. $\mathcal{O}_i = \langle \mathrm{sign}(\mathcal{C}_i)\rangle$. Most of these observables have definite CP and T̃ properties and hence can be used directly to probe the anomalous coupling which has the same CP and T̃ properties. In our analysis we keep the terms only upto linear order in anomalous couplings $\mathcal{B}_i$. So all observables can be written down as

$$\mathcal{O}(\{\mathcal{B}_i\}) = \sum O_i \mathcal{B}_i.$$

Measurements of these observables may be used to constrain the anomalous couplings. The possible sensitivity of these observables to the different anomalous couplings $\mathcal{B}_i$, at a given degree of statistical significance f, can be obtained by demanding $|\mathcal{O}(\{\mathcal{B}_i\}) - \mathcal{O}(\{0\})| \le f\,\delta\mathcal{O}$. Here $\mathcal{O}(\{0\})$ is the SM value of $\mathcal{O}$ and $\delta\mathcal{O}$ is the statistical fluctuation in $\mathcal{O}$.

Table 1. List of momentum correlators, their discrete transformation properties and anomalous couplings they probe. $\vec{P}_e = \vec{p}_{e^-} - \vec{p}_{e^+}$, $\vec{P}_f^+ = \vec{p}_f + \vec{p}_{\bar{f}}$, $\vec{P}_f^- = \vec{p}_f - \vec{p}_{\bar{f}}$.

	Correlator	C	P	CP	T̃	CPT̃	Probe of
$\mathcal{C}_0$	1	+	+	+	+	+	a_V, $\Re(b_V)$
$\mathcal{C}_1$	$\vec{P}_e \cdot \vec{P}_f^+$	−	+	−	+	−	$\Im(\tilde{b}_V)$
$\mathcal{C}_2$	$[\vec{P}_e \times \vec{P}_f^+] \cdot \vec{P}_f^-$	+	−	−	−	+	$\Re(\tilde{b}_V)$
$\mathcal{C}_3$	$\left[[\vec{P}_e \times \vec{P}_f^+] \cdot \vec{P}_f^-\right][\vec{P}_e \cdot \vec{P}_f^+]$	−	−	+	−	−	$\Im(b_V)$
$\mathcal{C}_4$	$\left[[\vec{P}_e \times \vec{P}_f^+] \cdot \vec{P}_f^-\right][\vec{P}_e \cdot \vec{p}_f]$	×	−	×	−	×	$\Im(b_V)$, $\Re(\tilde{b}_V)$

Statistical fluctuation in cross-section and in an asymmetry can be written as

$$\Delta\sigma = \sqrt{\sigma_{\text{SM}}/\mathcal{L} + \epsilon^2\sigma_{\text{SM}}^2}, \tag{2}$$

$$(\Delta A)^2 = \frac{1 - A_{\text{SM}}^2}{\sigma_{\text{SM}}\mathcal{L}} + \frac{\epsilon^2}{2}(1 - A_{\text{SM}}^2)^2. \tag{3}$$

Here σ_{SM} and A_{SM} are the SM value of cross-section and asymmetry respectively.

We choose the integrated luminosity $\mathcal{L} = 500\ \text{fb}^{-1}$, fractional systematic error $\epsilon = 0.01$ and $f = 3$.

Various kinematical cuts we impose, to suppress dominant background to the signal, are $5^\circ \le \theta_0 \le 175^\circ$; $E_b,\ E_{\bar{b}}, E_{l^-}, E_{l^+} \ge 10$ GeV; $p_{\text{T}}^{\text{missing } \nu} \ge 15$ GeV; $\Delta R_{q_1 q_2} \ge 0.7$; $\Delta R_{l^- l^+} \ge 0.2$; $\Delta R_{l^- b},\ \Delta R_{l^- \bar{b}},\ \Delta R_{l^+ b},\ \Delta R_{l^+ \bar{b}} \ge 0.4$.

Here $(\Delta R)^2 \equiv (\Delta\phi)^2 + (\Delta\eta)^2$ when $\Delta\phi$ and $\Delta\eta$ denote the separation between the two jets in azimuthal angle and rapidity respectively.

We additionally impose cuts on the invariant mass of the $f\bar{f}$ system:

$$R1 \equiv \left|m_{f\bar{f}} - M_Z\right| \le 5\,\Gamma_Z \qquad \text{select } Z\text{-pole}, \tag{4}$$

$$R2 \equiv \left|m_{f\bar{f}} - M_Z\right| \ge 5\,\Gamma_Z \qquad \text{de-select } Z\text{-pole}. \tag{5}$$

These enhance or suppress the contribution from Z resonance in the Bjorken process respectively. Γ_Z in the above is the width of Z boson.

3. ZZH couplings

To probe the anomalous ZZH couplings we consider $f\bar{f}$ final state, where f is any light fermion other than neutrinos. As outlined above we can construct observables with definite CP and $\tilde{\text{T}}$ properties and thus can maximize sensitivity to the anomalous couplings for a chosen final state. One can use some of these variables to probe the anomalous couplings [1a].

Cross-section: (observable $\mathcal{O}_0$ corresponding to correlator $\mathcal{C}_0$). Total rates are CP and $\tilde{\text{T}}$ even quantities. Hence these can be used to constrain Δa_Z and $\Re(b_Z)$. Total rates with $R1$ cut and $f = \mu, u, d, c, s$ can be used to probe $|\Re(b_Z)| > 0.48 \times 10^{-2}$. Similarly total cross-section for $f = e$ with $R2$ cut, $\sigma(R2; e)$ can probe Δa_Z to $|\Delta a_Z| > 0.038$ at 3σ level. Figure 1a shows that the sensitivity to $\Re(b_Z)$ is correlated with Δa_Z, whereas the reverse is not true.

Forward–backward asymmetry (A_1): We define the FB asymmetry A_1 with respect to the polar angle of Higgs boson. Since A_1 is CP odd and $\tilde{\text{T}}$ even, $A_1(R1; \mu, q)$ can be used to probe $\Im(\tilde{b}_Z)$. We find that this measurement can probe $|\Im(\tilde{b}_Z)| > 0.042$.

Up–down asymmetry (A_2): A_2 is the up–down asymmetry corresponding to f being above or below the H-production plane. It is a CP odd and $\tilde{\text{T}}$ odd observable and a real probe of $\Re(\tilde{b}_Z)$. Since this asymmetry requires charge determination of the final-state fermions, we cannot consider quarks in the final state. Hence using $A_2^{R2}(e)$ one will be able to constrain $|\Re(\tilde{b}_Z)| \le 0.064$ and it is shown by vertical lines in figure 1b.

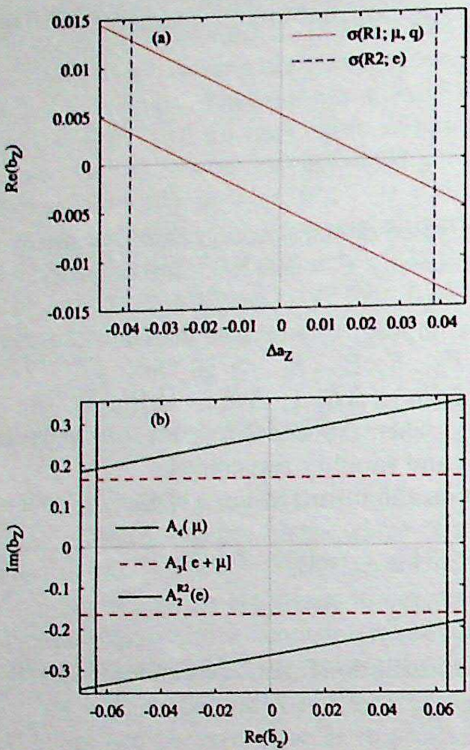

Figure 1. Simultaneous 3σ limits on anomalous couplings with $L = 500$ fb^{-1}: (a) Δa_Z–$\Re(b_Z)$ plane using cross-sections; (b) $\Re(\tilde{b}_Z)$–$\Im(b_Z)$ plane using various asymmetries.

Polar–azimuthal asymmetry (A_3): A_3 is a mixed polar–azimuthal asymmetry combining polar angle of Higgs boson and azimuthal angle of f with respect to Higgs production plane and is CP even and $\tilde{\mathrm{T}}$ odd. So it is sensitive only to $\Im(b_Z)$. This asymmetry requires charge measurement of f, hence suitable only for $f = e, \mu$. This can give a sensitivity at 3σ level as $|\Im(b_Z)| \leq 0.17$. The region inside the horizontal lines in figure 1b shows 3σ variation in A_3.

Another combined asymmetry (A_4): We construct this combined asymmetry with respect to the polar and azimuthal angles of final state f. Although A_4 is $\tilde{\mathrm{T}}$ odd, it does not have any definite CP property. So it is sensitive to both $\Im(b_Z)$ and $\Re(\tilde{b}_Z)$. Also A_4 requires charge determination of f and hence we cannot consider quarks in the final-state for this observable. But we consider only $f = \mu$, because for $f = e$ many anomalous couplings contribute significantly with $R1$ cut. The corresponding constraint is shown in figure 1b with slant lines.

In table 2 we list all the achievable limits obtained above. We emphasize that all of them, except for Δa_Z and $\Re(b_Z)$, are independent of other anomalous couplings. Table 2 shows that the constraint on $\Re(b_Z)$ depends on Δa_Z. Also $\tilde{\mathrm{T}}$-odd observables require charge measurement of final-state fermions and hence quarks in the final-state cannot be considered to probe $\tilde{\mathrm{T}}$-odd couplings leading to rather poor sensitivity to them.

Table 2. Sensitivity achievable at 3σ level for various anomalous couplings with $L = 500$ fb^{-1}.

Coupling	3σ Bound	Observable used
$\lvert\Delta a_Z\rvert$	0.038	σ with $R2$ cut; $f = e^-$
$\lvert\Re(b_Z)\rvert$	0.0048 ($\Delta a_Z = 0$) 0.013 ($\lvert\Delta a_Z\rvert = 0.038$)	σ with $R1$ cut; $f = \mu, q$
$\lvert\Im(b_Z)\rvert$	0.17	A_3 with $R1$ cut; $f = \mu^-, e^-$
$\lvert\Re(\tilde{b}_Z)\rvert$	0.064	$A_2(\phi_{e^-})$ with $R2$ cut
$\lvert\Im(\tilde{b}_Z)\rvert$	0.042	$A_1(c_H)$ with $R1$ cut; $f = \mu, q$

Table 3. Individual 3σ limits of sensitivity.

Coupling		Limit	Observable used
$\lvert\Delta a\rvert$	$\leq$	0.018	σ_{R2}
$\lvert\Re(b_W)\rvert$	$\leq$	0.098	σ_{R2}
$\lvert\Im(b_W)\rvert$	$\leq$	0.62	σ_{R1}
$\lvert\Re(\tilde{b}_W)\rvert$	$\leq$	1.6	$A^1_{FB}(c_H)$
$\lvert\Im(\tilde{b}_W)\rvert$	$\leq$	0.39	$A^2_{FB}(c_H)$

Table 4. Simultaneous 3σ limits of sensitivity.

Coupling		$\Delta a = 0$	$\Delta a \neq 0$
$\lvert\Delta a\rvert$	$\leq$	–	0.038
$\lvert\Re(b_W)\rvert$	$\leq$	0.10	0.31
$\lvert\Im(b_W)\rvert$	$\leq$	1.6	1.6
$\lvert\Re(\tilde{b}_W)\rvert$	$\leq$	3.2	3.2
$\lvert\Im(\tilde{b}_W)\rvert$	$\leq$	0.44	0.44

4. *WWH* couplings

Due to missing neutrinos in the final state here one can only construct two observables: cross-section and forward–backward asymmetry with respect to polar angle of Higgs boson. Any deviation from SM value for cross-section largely depends on Δa_V and $\Re(b_V)$ (CP even, $\tilde{\text{T}}$ even). Similarly, FB asymmetry receives a large contribution from $\Im(\tilde{b}_V)$ (CP odd, $\tilde{\text{T}}$ even). Hence there is no other direct observable to probe the remaining anomalous couplings. Assuming $\Delta a_Z = \Delta a_W = \Delta a$, we calculate the expressions for both the observables with $R1$ and $R2$ cuts. In table 3 we list the individual limits of sensitivity on the various anomalous couplings at 3σ level. To see what the sensitivity will be when all the anomalous couplings were to be nonzero, we construct a nine-dimensional region in parameter space and take a point from that region and calculate all the observables simultaneously. If the difference from their SM values due to these anomalous couplings is within the statistical fluctuation in SM values of these observables, then we say that the point is inside the blind region. The points on the boundary of this region give us the simultaneous limit of sensitivity of these measurements to the anomalous couplings. These are listed in table 4. These tables show that the lack of a specific observable to probe $\tilde{\text{T}}$-odd couplings results in rather poor sensitivity to them. For more details, see [2].

5. Conclusion

We have analyzed the sensitivity of the process $e^+e^- \to f\bar{f}H$, f being a light fermion and probe different anomalous couplings. We implement various kinematical cuts on the different final-state particles so as to reduce background and also take into account finite b-tagging efficiency. When these effects are removed, our analysis reproduces the results of [4]. Although the observables constructed using optimal observable analysis [3] have maximum sensitivity to the anomalous couplings, they are a little opaque to the physics that is being probed. The observables that we have constructed by taking expectation values of sign of the correlators are simple to construct and most of them have definite CP and $\tilde{\mathrm{T}}$ properties thus probing specific anomalous couplings. Apart from $\Re(b_V)$ and Δa_V, constraints on all the other anomalous couplings can be obtained using asymmetries and hence are robust to the effects of radiative corrections.

References

[1] See, for example, M Drees, R M Godbole and P Roy, *Theory and phenomenology of sparticles* (World Scientific, Singapore, 2004)

[1a] For detailed definition, see [2]

[2] Sudhansu S Biswal, Debajyoti Choudhury, Rohini M Godbole and Ritesh K Singh, *Phys. Rev.* **D73**, 035001 (2006)

[3] K Hagiwara, S Ishihara, J Kamoshita and B A Kniehl, *Euro. Phys. J.* **C14**, 457 (2000)

[4] T Han and J Jiang, *Phys. Rev.* **D63**, 096007 (2001)

PRAMANA
— journal of
physics

© Indian Academy of Sciences

Vol. 69, No. 5
November 2007
pp. 783–788

Testing the minimal supersymmetric standard model with the mass of the W boson

S HEINEMEYER[1,*], W HOLLIK[2], D STÖCKINGER[3], A M WEBER[2]
and G WEIGLEIN[3]
[1]Instituto de Fisica de Cantabria (CSIC-UC), Santander, Spain
[2]Max-Planck-Institut für Physik, Föhringer Ring 6, D-80805 Munich, Germany
[3]IPPP, University of Durham, Durham DH1 3LE, UK
*E-mail: Sven.Heinemeyer@cern.ch

Abstract. We review the currently most accurate evaluation of the W boson mass, M_W, in the minimal supersymmetric standard model (MSSM). It consists of a full one-loop calculation, including the complex phase dependence, all available MSSM two-loop corrections as well as the full standard model result. We analyse the impact of the phases in the scalar quark sector on M_W and compare the prediction for M_W based on all known higher-order contributions with the experimental results.

Keywords. Minimal supersymmetric standard model; W boson; precision observables.

PACS Nos 11.30.Pb; 12.38.Ex; 14.70.Fm

1. Introduction

The relation between the massive gauge-boson masses, M_W and M_Z, in terms of the Fermi constant, G_μ, and the fine structure constant α, is of central importance for testing the electroweak theory:

$$\frac{G_\mu}{\sqrt{2}} = \frac{e^2}{8\left(1-\frac{M_W^2}{M_Z^2}\right) M_W^2} (1+\Delta r) \ . \tag{1}$$

It is usually employed for predicting M_W in the model under consideration, where the loop corrections enter via Δr. This prediction can then be compared with the corresponding experimental value. The current experimental accuracy for M_W, obtained at LEP and the Tevatron, is $\delta M_W = 29$ MeV (0.04%) [1,2]. This experimental resolution provides a high sensitivity to quantum effects involving the whole structure of a given model. The M_W–M_Z interdependence is therefore an important tool for discriminating between the standard model (SM) and its minimal supersymmetric extension (MSSM) [3] (see ref. [4] for a recent review). Within the MSSM the W boson mass, supplemented with other electroweak precision observables, exhibits a certain preference for a relatively low scale of supersymmetric particles (see e.g. refs [5,6]). Consequently, a precise theoretical prediction for M_W in terms of the model parameters is of utmost importance for present and future electroweak precision tests. A precise prediction for M_W in the MSSM is also needed as a part of the 'SPA Convention and Project' (see ref. [7]).

In ref. [8] the currently most up-to-date evaluation of M_W (i.e. Δr) in the MSSM has been presented. It consists of the full one-loop calculation, taking into account the complex phase dependence (the phases had been neglected so far in all previous calculations), the full SM result [9] and all available MSSM two-loop contributions [10–13]. The corresponding Fortran program for the calculation of precision observables within the MSSM will be made publicly available [14].

In the numerical analysis below, except for the parameter scan in §3, for simplicity we choose all soft SUSY-breaking parameters in the diagonal entries of the sfermion mass matrices to be equal ($\equiv M_{\tilde{f}}$). In the neutralino sector the GUT relation $M_1 = 5/3\, s_\mathrm{w}^2/c_\mathrm{w}^2\, M_2$ has been used (for real values). We have fixed the SM input parameters as [14a]

$$\begin{aligned}
&G_\mu = 1.16637 \times 10^{-5}, \quad M_Z = 91.1875 \text{ GeV}, \quad \alpha_s(M_Z) = 0.117, \\
&\alpha = 1/137.03599911, \quad \Delta\alpha_\mathrm{had}^{(5)} = 0.02761, \quad \Delta\alpha_\mathrm{lep} = 0.031498, \\
&m_t = 172.5 \text{ GeV [16]}, \quad m_b = 4.7 \text{ GeV}, \quad m_\tau = m_c = \cdots = 0. \qquad (2)
\end{aligned}$$

The complex phases appearing in the MSSM are experimentally constrained by their contribution to low energy observables such as electric dipole moments (see ref. [4] and references therein). Accordingly (using the convention that $\phi_{M_2} = 0$), in particular the phase ϕ_μ is tightly constrained [17], while the bounds on the phases of the third generation trilinear couplings are much weaker. The Higgs sector parameters are obtained from the program FeynHiggs2.2 [18].

2. Dependence on the complex phases in the squark sector

Here we show the dependence of M_W on the phases of the scalar quark sector. The physical phases are $\phi_{A_t} + \phi_\mu$ and $\phi_{A_b} + \phi_\mu$, where $A_{t,b}$ are the trilinear Higgs-$\tilde{t}, \tilde{b}$ coupling and μ is the Higgs mixing parameter. We focus here on the mass shift δM_W arising from changing Δr by the amount Δr^SUSY,

$$\delta M_W = -\frac{M_W^\mathrm{ref}}{2} \frac{s_\mathrm{w}^2}{c_\mathrm{w}^2 - s_\mathrm{w}^2} \Delta r^\mathrm{SUSY}. \qquad (3)$$

Here Δr^SUSY represents the one-loop contribution from the supersymmetric particles of the considered sector of the MSSM and $M_W^\mathrm{ref} = 80.425$ GeV (see ref. [8] for more details).

The leading one-loop SUSY contributions to Δr arise from the $\tilde{t}/\tilde{b}$ doublet. The complex parameters in the $\tilde{t}/\tilde{b}$ sector are μ, A_t and A_b, entering via the off-diagonal entries of the $\tilde{t}$ and $\tilde{b}$ mass matrices, $X_{t,b}$. In ref. [8] it has been shown at the analytical level that the phases $\phi_{X_{t,b}}$ drop out entirely in the full one-loop calculation of Δr and have no influence on M_W. Hence, the phases and absolute values of μ,

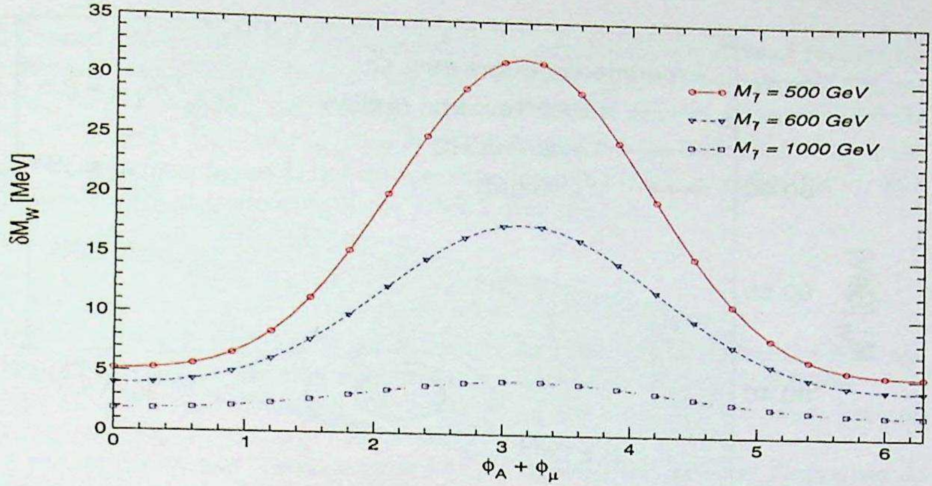

Figure 1. Squark contribution to δM_W as a function of the phase $(\phi_A + \phi_\mu)$, where $\phi_A \equiv \phi_{A_t} = \phi_{A_b}$, for different values of the common sfermion mass $M_{\tilde{f}}$ = 500, 600, 1000 GeV. The other relevant SUSY parameters are set to $\tan\beta = 5$, $|A_{t,b}| = 2M_{\tilde{f}}$, $|\mu| = 900$ GeV.

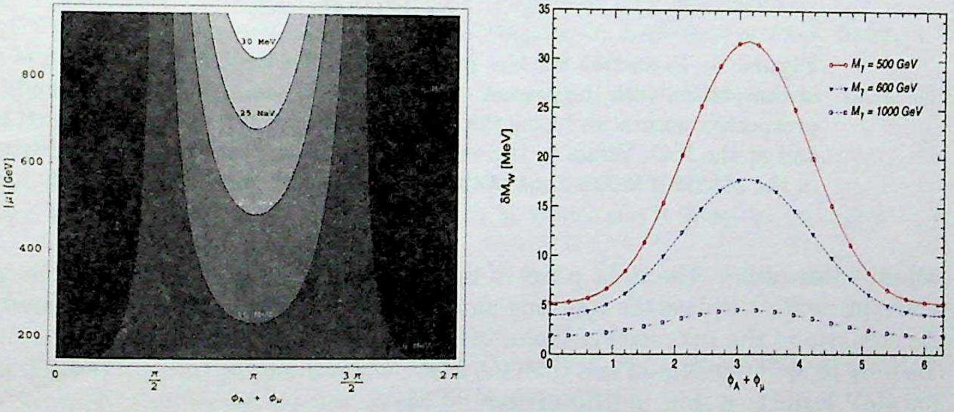

Figure 2. Contour lines of the squark contributions to δM_W in the plane of $(\phi_A + \phi_\mu)$ and $|\mu|$, where $\phi_A \equiv \phi_{A_t} = \phi_{A_b}$. The left plot shows a scenario with $\tan\beta = 5$, $M_{\tilde{f}}$ = 500 GeV, $|A_{t,b}|$ = 1000 GeV, while in the right plot $\tan\beta = 30$, $M_{\tilde{f}}$ = 600 GeV, $|A_{t,b}|$ = 1200 GeV.

A_t and A_b enter the sfermion-loop contributions (at one-loop order) only via a shift in the $\tilde{t}$ and $\tilde{b}$ masses and mixing angles.

The phase dependence is illustrated in figures 1 and 2. Figure 1 shows the effect on δM_W from varying the phase $(\phi_A + \phi_\mu)$ for a fixed value of $|\mu| = 900$ GeV and $M_{\tilde{f}}$ = 500, 600, 1000 GeV, while in figure 2 the squark sector contributions to δM_W are shown as contour lines in the plane of $(\phi_A + \phi_\mu)$ and $|\mu|$. In the scenario with $\tan\beta = 5$ (figure 1 and left panel of figure 2) the variation of $(\phi_A + \phi_\mu)$ can amount to a shift in M_W of more than 20 MeV. The most pronounced phase dependence is obtained for the largest sfermion mixing, i.e. the smallest value of $M_{\tilde{f}}$ and the

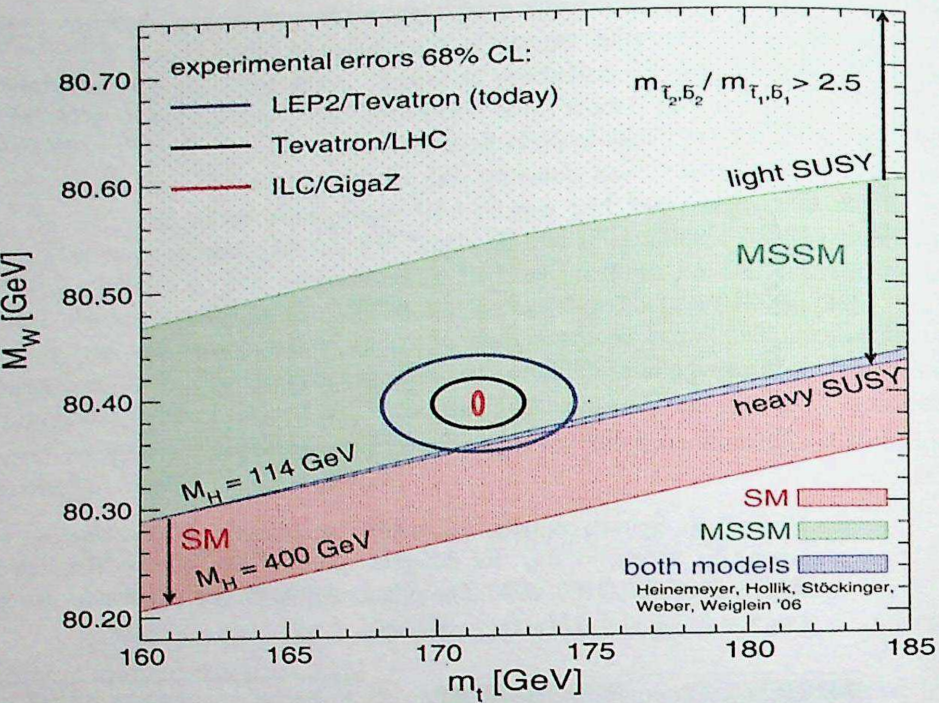

Figure 3. Prediction for M_W in the MSSM and the SM as a function of m_t in comparison with the present experimental results for M_W and m_t and the prospective accuracies (using the current central values) at the Tevatron/LHC and at the ILC. Values in the very light shaded region can only be obtained in the MSSM if at least one of the ratios $m_{\tilde{t}_2}/m_{\tilde{t}_1}$ or $m_{\tilde{b}_2}/m_{\tilde{b}_1}$ exceeds 2.5.

largest value of $|\mu|$. The right panel of figure 2 shows a scenario with $\tan\beta = 30$. The plot clearly displays the resulting much weaker phase dependence compared to the scenario in the left panel of figure 2. The variation of the complex phase gives rise only to shifts in M_W of less than 0.5 MeV, while changing $|\mu|$ between 100 and 500 GeV leads to a shift in M_W of about 2 MeV.

3. The MSSM parameter scan

Here we show the overall behaviour of M_W in the MSSM by scanning over a broad range of the SUSY parameter space. All relevant SUSY parameters are varied independently of each other (see ref. [8] for details). We have taken into account the constraints on the MSSM parameter space from the LEP Higgs searches [19,20] and the lower bounds on the SUSY particle masses from ref. [21].

In figure 3 we compare the SM and the MSSM predictions for M_W as a function of m_t as obtained from the scatter data (the plot shown here is an update of refs [4,8,22]). The predictions within the two models give rise to two bands in the m_t–M_W plane with only a relatively small overlap region (indicated by a dark-shaded (blue) area in figure 3). The very light-shaded (light green), the light shaded (green) and the dark-shaded (blue) areas indicate allowed regions for the unconstrained MSSM. In the very light-shaded region at least one of the ratios $m_{\tilde{t}_2}/m_{\tilde{t}_1}$ or $m_{\tilde{b}_2}/m_{\tilde{b}_1}$ exceeds 2.5. The current 68% C.L. experimental results $m_t^{\rm exp} = 171.4 \pm 2.1$ GeV and $M_W^{\rm exp} = 80.392 \pm 0.029$ GeV are indicated in the plot. As can be seen from figure 3, the current experimental 68% C.L. region for m_t and M_W exhibit a slight preference of the MSSM over the SM.

References

[1] The ALEPH, DELPHI, L3, OPAL, SLD Collaborations: the LEP Electroweak Working Group, the SLD Electroweak and Heavy Flavour Groups, hep-ex/0509008
The ALEPH, DELPHI, L3 and OPAL Collaborations: the LEP Electroweak Working Group, hep-ex/0511027

[2] F Spano, *Electroweak interactions and unified theories*, talk given at Rencontres de Moriond, La Thuile, Italy, March 2006
See also lepewwg.web.cern.ch/LEPEWWG/Welcome.html

[3] H Nilles, *Phys. Rep.* **110**, 1 (1984)
H Haber and G Kane, *Phys. Rep.* **117**, 75 (1985)
R Barbieri, *Riv. Nuovo Cim.* **11**, 1 (1988)

[4] S Heinemeyer, W Hollik and G Weiglein, *Phys. Rep.* **425**, 265 (2006)

[5] J Ellis, S Heinemeyer, K Olive and G Weiglein, *J. High Energy Phys.* **0502**, 013 (2005), hep-ph/0508169

[6] J Ellis, S Heinemeyer, K Olive and G Weiglein, *J. High Energy Phys.* **0605**, 005 (2006)
S Heinemeyer, *These proceedings*

[7] J Aguilar-Saavedra *et al*, *Euro. Phys. J.* **C46**, 43 (2006)

[8] S Heinemeyer, W Hollik, D Stöckinger, A M Weber and G Weiglein, to appear in *J. High Energy Phys.*, hep-ph/0604147

[9] M Awramik, M Czakon, A Freitas and G Weiglein, *Phys. Rev.* **D69**, 053006 (2004)

[10] A Djouadi, P Gambino, S Heinemeyer, W Hollik, C Jünger and G Weiglein, *Phys. Rev. Lett.* **78**, 3626 (1997); *Phys. Rev.* **D57**, 4179 (1998)

[11] S Heinemeyer, *Two-loop calculations in the MSSM*, Ph.D. Thesis, University Karlsruhe, Shaker Verlag, Aachen, 1998, ISBN 3826537874
See www-itp.physik.uni-karlsruhe.de/prep/phd/
G Weiglein, hep-ph/9901317

[12] J Haestier, S Heinemeyer, D Stöckinger and G Weiglein, *J. High Energy Phys.* **0512**, 027 (2005)

[13] S Heinemeyer and G Weiglein, *J. High Energy Phys.* **0210**, 072 (2002), hep-ph/0301062

[14] A M Weber *et al*, `SUSY-POPE`, to be available from the authors

[14a] Using the most up-to-date value for the top quark mass, $m_t = 171.4$ GeV [15], would lead to slightly lower absolute M_W values, while the impact on δM_W is negligible.

[15] See www-cdf.fnal.gov/physics/new/top/top.html

[16] Tevatron Electroweak Working Group, hep-ex/0603039

[17] V Barger, T Falk, T Han, J Jiang, T Li and T Plehn, *Phys. Rev.* **D64**, 056007 (2001)

[18] S Heinemeyer, W Hollik and G Weiglein, *Comput. Phys. Commun.* **124**, 76 (2000); *Euro. Phys. J.* **C9**, 343 (1999)
G Degrassi, S Heinemeyer, W Hollik, P Slavich and G Weiglein, *Euro. Phys. J.* **C28**, 133 (2003)

T Hahn, S Heinemeyer, W Hollik and G Weiglein, hep-ph/0507009
M Frank, T Hahn, S Heinemeyer, W Hollik, H Rzehak and G Weiglein, *in preparation*
T Hahn, S Heinemeyer, W Hollik, H Rzehak, G Weiglein and K Williams, *These proceedings*
The code is accessible via www.feynhiggs.de

[19] ALEPH, DELPHI, L3, OPAL Collaborations and LEP Working Group for Higgs boson searches, hep-ex/0602042

[20] ALEPH, DELPHI, L3, OPAL Collaborations and LEP Working Group for Higgs Boson Searches: G Abbiendi *et al*, *Phys. Lett.* **B565**, 61 (2003)

[21] Particle Data Group Collaboration: S Eidelman *et al*, *Phys. Lett.* **B592**, 1 (2004)

[22] P Chankowski, A Dabelstein, W Hollik, W Mösle, S Pokorski and J Rosiek, *Nucl. Phys.* **B417**, 101 (1994)

PRAMANA
— journal of
physics

© Indian Academy of Sciences

Vol. 69, No. 5
November 2007
pp. 789–793

Partially composite two-Higgs doublet model

DONG-WON JUNG
School of Physics, KIAS Seoul 130-722, Korea
E-mail: dwjung@kias.re.kr

Abstract. In the extra dimensional scenarios with gauge fields in the bulk, the Kaluza–Klein (KK) gauge bosons can induce Nambu–Jona–Lasinio (NJL) type attractive four-fermion interactions, which can break electroweak symmetry dynamically with accompanying composite Higgs fields. We consider a possibility that electroweak symmetry breaking (EWSB) is triggered by both a fundamental Higgs and a composite Higgs arising in a dynamical symmetry breaking mechanism induced by a new strong dynamics. The resulting Higgs sector is a partially composite two-Higgs doublet model with specific boundary conditions on the coupling and mass parameters originating at a compositeness scale Λ. The phenomenology of this model is discussed including the collider phenomenology at LHC and ILC.

Keywords. Dynamical electroweak symmetry breaking; technicolor and composite models; Higgs physics.

PACS Nos 12.60.Fr; 12.60.Rc

1. Introduction

Although the standard model (SM) has been successful to describe the physics up to $E \sim 200$ GeV, the origin of the electroweak symmetry breaking (EWSB) still remains a mystery. Among the various models for the EWSB, the extra dimensional scenarios have many interesting characteristics. Under this extra dimensional setup, the EWSB can occur in various ways. It can be accomplished by fundamental Higgs bosons, and/or some dynamical way by bulk QCD, and/or nontrivial boundary conditions, etc. It is an interesting observation that in the extra dimensional scenarios the EWSB can be achieved by both fundamental Higgs boson and dynamical fermion condensates. With this philosophy in mind, we study an extension of Bardeen–Hill–Lindner (BHL) scenario [1]. The BHL scenario is particularly interesting since the heavy top mass is intimately related with a new strong dynamics that condenses the $t\bar{t}$ bilinear, and breaks the EW symmetry. The original version of BHL scenario predicts that the top mass should be larger than ~200 GeV, which is no longer viable. The extension of BHL with two composite Higgs doublets has a similar shortcoming [2]. In our model [3], a fundamental scalar particle is introduced in addition to the $t\bar{t}$ condensate, and we successfully fit the top and bottom quark masses simultaneously. Our model predicts $\tan\beta$ between 0.45 and 1. In addition, our model can be tested in the future collider experiments.

2. Model description

We introduce a strong dynamics to the standard model at some high scale Λ, which is effectively described by the NJL-type four-fermion interaction term.

$$\mathcal{L} = \mathcal{L}_{\rm SM} + G(\bar{\psi}_{\rm L} t_{\rm R})(\bar{t}_{\rm R}\psi_{\rm L}), \tag{1}$$

where

$$\mathcal{L}_{\rm SM} = \mathcal{L}_{\rm gauge} + \mathcal{L}_f + \mathcal{L}_\phi + (y_{t0}\ \bar{\psi}_{\rm L} t_{\rm R}\tilde{\phi} + \text{H.c.}) + (y_{b0}\ \bar{\psi}_{\rm L} b_{\rm R}\phi + \text{H.c.}) \tag{2}$$

and $\tilde{\phi} \equiv i\sigma_y\phi^*$. Introducing an auxiliary scalar doublet field $\Phi(x)$, we can rewrite the NJL term in eq. (1) as

$$\mathcal{L} = \mathcal{L}_{\rm SM} + g_{t0}(\bar{\psi}_{\rm L} t_{\rm R}\tilde{\Phi} + \text{H.c.}) - M^2\Phi^\dagger\Phi, \tag{3}$$

where $G = g_{t0}^2/M^2$ and g_{t0} is a newly defined Yukawa coupling. The mass scale M will be generally of order Λ. The new scalar field Φ describes the composite scalar bosons that appear when the $\langle\bar{t}t\rangle$ develops nonvanishing VEV and breaks the electroweak symmetry. Then we have one fundamental scalar field ϕ and one composite scalar field Φ, although Φ is not a dynamical field at the scale Λ. Far below the scale Λ, the Φ field will develop the kinetic term due to quantum corrections and become dynamical. The resulting low energy effective field theory will be two-Higgs doublet model. The large FCNC problem can be avoided by assigning a Z_2 discrete symmetry [4]

$$(\Phi,\ \psi_{\rm L},\ U_{\rm R}) \to +(\Phi,\ \psi_{\rm L},\ U_{\rm R}),\ (\phi, D_{\rm R}) \to -(\phi, D_{\rm R}).$$

Then the Yukawa term $(y_{t0}\bar{\psi}_{\rm L} t_{\rm R}\phi + \text{H.c.})$ is forbidden and only the y_{b0} coupling term remains. From now on, we will rename y_{b0} as g_{b0}. As a consequence, our model becomes the Type-II two-Higgs doublet model. We write the effective Lagrangian far below Λ as

$$\begin{aligned}\mathcal{L} = {}& \mathcal{L}_{\rm gauge} + \mathcal{L}_f + (D_\mu\phi)^\dagger(D^\mu\phi) + (D_\mu\Phi)^\dagger(D^\mu\Phi)\\ &+(g_b\bar{\psi}_{\rm L} b_{\rm R}\phi + \text{H.c.}) + (g_t\bar{\psi}_{\rm L} t_{\rm R}\tilde{\Phi} + \text{H.c.}) - V(\phi,\Phi),\end{aligned} \tag{4}$$

where the most general Higgs potential is given by

$$\begin{aligned}V(\phi,\Phi) = {}& \mu_1^2\phi^\dagger\phi + \mu_2^2\Phi^\dagger\Phi + (\mu_{12}^2\phi^\dagger\Phi + \text{H.c.}) + \frac{1}{2}\lambda_1(\phi^\dagger\phi)^2\\ &+\frac{1}{2}\lambda_2(\Phi^\dagger\Phi)^2 + \lambda_3(\phi^\dagger\phi)(\Phi^\dagger\Phi) + \lambda_4|\phi^\dagger\Phi|^2\\ &+\frac{1}{2}[\lambda_5(\phi^\dagger\Phi)^2 + \text{H.c.}].\end{aligned} \tag{5}$$

In the scalar potential, we have introduced a dimension-two μ_{12}^2 term that breaks the Z_2 discrete symmetry softly in order to generate the nonzero mass for the CP-odd Higgs boson. This μ_{12}^2 parameter will be traded with m_A^2. The renormalized at low energy is given by

$$\begin{aligned}\mathcal{L}_{\text{ren}} &= Z_\phi (D_\mu \phi)^\dagger (D^\mu \phi) + Z_\Phi (D_\mu \Phi)^\dagger (D^\mu \Phi) - V(\sqrt{Z_\phi}\phi, \sqrt{Z_\Phi}\Phi) \\ &\quad + \sqrt{Z_\Phi} g_t (\bar{\psi}_{\text{L}} t_{\text{R}} \tilde{\Phi} + \text{H.c.}) + \sqrt{Z_\phi} g_b (\bar{\psi}_{\text{L}} b_{\text{R}} \phi + \text{H.c.}), \end{aligned} \tag{6}$$

and matching the Lagrangian with eq. (3) at the compositeness scale Λ, we obtain the matching condition

$$\begin{aligned} &\sqrt{Z_\phi} \to 1, \quad \sqrt{Z_\Phi} \to 0, \quad Z_\phi \mu_1^2 \to m_0^2, \qquad Z_\Phi \mu_2^2 \to M^2, \\ &Z_\phi \lambda_1 \to \lambda_{10}, \qquad Z_\Phi^2 \lambda_2 \to 0, \quad Z_\phi Z_\Phi \lambda_{i=3,4,5} \to 0, \end{aligned} \tag{7}$$

as the scale $\mu \to \Lambda$. Note that our model has nonvanishing $\sqrt{Z_\phi}$ and $Z_\phi \lambda_1$ unlike the Luty's model, and we can fit both the bottom and top quark masses.

3. Particle spectrum

Our model is defined in terms of three parameters: Higgs self-coupling λ_{10}, the compositeness scale Λ (where λ_{10} and the NJL interaction are specified), and the CP-odd Higgs boson mass m_A. Using the field redefinition

$$\phi \to Z_\phi^{-1/2} \phi, \quad \Phi \to Z_\Phi^{-1/2} \Phi, \tag{8}$$

we rewrite the matching condition given in eq. (2.7) as

$$g_b \to g_{b0}, \quad g_t \to \infty, \quad \lambda_1/g_b^4 \to \lambda_{10}/g_{b0}^4, \quad \lambda_{2,3,4,5} \to 0, \tag{9}$$

for the rescaled couplings. These conditions are the boundary conditions for the RG equations. We will use the one-loop RG equations given in ref. [5]. After numerical analysis, we find that the allowed parameter space is rather restricted as Λ increases. Since m_A is a free parameter in our model, other Higgs boson masses can be calculated in various parameter regions. Again, we can get rather narrow band for the Higgs masses as a function of m_A. For $\Lambda \sim 10^{15}$ GeV, m_h larger than 250 GeV is predicted. Also the charged Higgs can be lighter than h, and could be the first signal of our model at future colliders. Generally charged Higgs boson is lighter than the CP-odd Higgs.

4. Higgs production at LHC and ILC

The ratio of self-couplings to the SM values $\lambda_{hhh}/\lambda_{hhh}^{\text{SM}}$, $\lambda_{hhhh}/\lambda_{hhhh}^{\text{SM}}$ are enhanced for the small mass of the light Higgs boson h. In most parameter region, our triple gauge coupling is negative and it can lead to many interesting phenomenology [3].

The cross-sections predicted in our model are modified from those in the SM by factors [6],

$$\begin{aligned} &\sigma(pp \to gg \to h^0) = \left(\frac{\cos\alpha}{\sin\beta}\right)^2 \sigma_{\text{SM}}(pp \to gg \to h^0), \\ &\sigma(e^+e^- \to Z + h^0/H^0) = \sin^2/\cos^2(\beta-\alpha)\sigma_{\text{SM}}(e^+e^- \to Z + h^0/H^0), \\ &\sigma(e^-e^+ \to \bar{\nu}_e \nu_e + h^0/H^0) = \sin^2/\cos^2(\beta-\alpha)\sigma_{\text{SM}}(e^-e^+ \to \bar{\nu}_e \nu_e + h^0/H^0). \end{aligned} \tag{10}$$

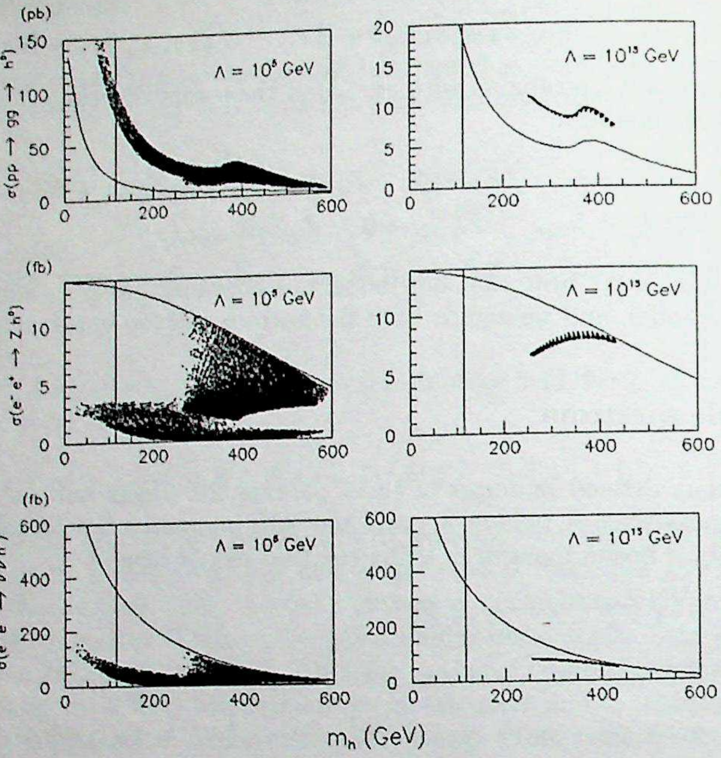

Figure 1. Production cross-section of the neutral Higgs boson at the LHC and ILC. $\sqrt{s} = 14$ TeV for the LHC and $\sqrt{s} = 1$ TeV for the ILC are assumed. The solid curves denote the SM predictions.

In figure 1, we show the single Higgs boson production cross-sections at the LHC and the ILC for different Λ and m_h, etc. For higher Λ, the allowed m_h has a narrow region. Therefore, the cross-sections are almost definitely determined for large Λ, and they will be a strong signature of our model.

5. Summary

We considered an interesting possibility that the Higgs boson produced at the future colliders is neither a fundamental scalar nor a composite scalar, but a mixed state of them. This scenario could be easily realized, if we embed the SM in a higher dimension with bulk gauge interactions. We have constructed the simplest model with the NJL-type four-fermion interaction of top quarks as the strong dynamics inspired by the BHL and study the phenomenology of the two-Higgs doublets model with the compositeness condition as the low energy effective theory. The resulting theory can accommodate the observed top mass, and give specific predictions for neutral and charged Higgs masses at a given value of Λ. The charged Higgs boson is always lighter than the CP-odd Higgs neutral boson, although the mass difference is very small. For $\Lambda \sim 10^{15}$ GeV, the allowed parameter region is rather restricted, and we predict $m_h > 250$ GeV. The cross-sections for the Higgs boson production are modified in our model, and it will be observed in the future colliders, i.e., LHC and ILC.

References

[1] W A Bardeen, C T Hill and M Lindner, *Phys. Rev.* **D41**, 1647 (1990)
C T Hill, Report No. FERMI-CONF-90/170-T

[2] M Luty, *Phys. Rev.* **D41**, 2893 (1990)

[3] Byungchul Chung, Kang Young Lee, Dong-Won Jung and Pyungwon Ko, *J. High Energy Phys.* **05**, 010 (2006)

[4] S L Glashow and S Weinberg, *Phys. Rev.* **D15**, 1958 (1977)

[5] C T Hill, C N Leung and S Rao, *Nucl. Phys.* **B262**, 517 (1985)

[6] See, for example, recent reviews and references therein: A Djouadi, arXiv:hep-ph/0503172; arXiv:hep-ph/0503173

PRAMANA
— journal of
physics

© Indian Academy of Sciences

Vol. 69, No. 5
November 2007
pp. 795–800

Probing anomalous Higgs couplings at an $e\gamma$ collider using unpolarised beams

DEBAJYOTI CHOUDHURY[1] and MAMTA[2]
[1]Department of Physics and Astrophysics, University of Delhi, Delhi 110 007, India
[2]S.G.T.B. Khalsa College, University of Delhi, Delhi 110 007, India
E-mail: debchou@physics.du.ac.in; mdahiya@physics.du.ac.in

Abstract. We examine the sensitivity of $e\gamma$ colliders (based on e^+e^- linear colliders of c.m. energy 500 GeV) to the anomalous couplings of the Higgs to W-boson via the process $e^-\gamma \longrightarrow \nu WH$. This has the advantage over e^+e^- collider in being able to dissociate WWH vertex from ZZH. We are able to construct several dynamical variables which may be used to constrain the various couplings in the WWH vertex.

Keywords. Higgs; anomalous couplings; photon collider.

PACS Nos 12.60.Fr; 14.80.Br; 13.66.Fg

1. Introduction

The dominant neutral Higgs production modes at a linear collider proceed via its coupling with a pair of gauge bosons ($VV,\ V = W, Z$), and hence these are expected to be sensitive to the VVH couplings (see refs [1,2]). It is possible to obtain $\gamma\gamma$ and $e\gamma$ colliders with real photons from the high energy ee colliders using the Compton back-scattering of laser light [4]. Thus, one may now consider a process such as $e^- + \gamma \longrightarrow \nu_e + W^- + H$ to probe WWH vertex.

Demanding only Lorentz and gauge invariance, the most general coupling structure involving the Higgs boson and a pair of gauge bosons may be expressed as

$$\Gamma^V_{\mu\nu} = g_V \left[a_V g_{\mu\nu} + \frac{b_V}{m_V^2} (k_{2\mu} k_{1\nu} - g_{\mu\nu} k_1 \cdot k_2) + \frac{\beta_V}{m_V^2} \epsilon_{\mu\nu\alpha\beta} k_1^\alpha k_2^\beta \right], \qquad (1)$$

where k_1^μ and k_2^ν are the momenta of two W's (or Z's) with $g_W^{\rm SM} = e \cot\theta_W M_Z$ and $g_Z^{\rm SM} = 2eM_Z/\sin 2\theta_W$. In the context of the SM, at the tree level, $a_W^{\rm SM} = a_Z^{\rm SM} = 1$, while the other couplings vanish identically. The general structure of these anomalous couplings can be obtained from dimension-6 operators in an effective theory [3].

Table 1. Transformation properties of the terms in the Lagrangian corresponding to the various couplings given by eq. (1).

Trans.	a_W	$\mathcal{R}(b_W)$	$\mathcal{R}(\beta_W)$	$\mathcal{I}(b_W)$	$\mathcal{I}(\beta_W)$
C	+	+	+	+	+
P	+	+	−	+	−
$\hat{T}$	+	+	−	−	+

2. The process and cross-sections

To the lowest order, Higgs production at an $e\gamma$ collider – the process $e^- + \gamma \rightarrow \nu_e + W^- + H$ – receives contributions from three Feynman diagrams. Retaining contributions only up to the lowest non-trivial order in the anomalous couplings, the cross-section may be written as

$$\sigma = (1 + 2\Delta a_W)\sigma_0 + \mathcal{R}(b_W)\sigma_1 + \mathcal{R}(\beta_W)\sigma_2 + \mathcal{I}(b_W)\sigma_3 + \mathcal{I}(\beta_W)\sigma_4, \quad (2)$$

where we have assumed that $a_W \equiv 1 + \Delta a_W$ is close to its SM value. Being odd under $\hat{T}$ (table 1), some of the terms in eq. (1) would not contribute, at the linear order, to the total rate.

To be quantitative, we shall choose to work with a Higgs boson of mass 120 GeV and a parent e^+e^- machine operating at a center of mass energy of 500 GeV. The final state comprises of four jets and missing momentum. Of the jets, two must be b-like and these must reconstruct to m_H and the other two must reconstruct to m_W. To be detectable, we consider the events characterized by the following acceptance cuts:

$$\begin{array}{rcll} p_{\mathrm{T}}^{\mathrm{miss}} & \geq & 20\,\mathrm{GeV}, & \\ -3.0 \leq \eta_j & \leq & 3.0, & \text{for rapidity of each jet,} \\ p_{\mathrm{T}} & \geq & 10\,\mathrm{GeV}, & \text{for each jet,} \\ \Delta R_{j_1 j_2} & \geq & 0.7, & \text{for each pair of jets,} \end{array} \quad (3)$$

where $(\Delta R_{j_1 j_2})^2 \equiv (\Delta\phi)^2 + (\Delta\eta)^2$ with $\Delta\phi$ and $\Delta\eta$ denoting the separation between the two jets in azimuthal angle and rapidity respectively.

A statistical measure of agreement with the SM expectations is given by $(\delta\sigma)^2 = \sigma_{\mathrm{SM}}/(\mathcal{L} + \epsilon^2\sigma_{\mathrm{SM}}^2)$. Here σ_{SM} is the SM value of the cross-section, $\mathcal{L}$ is the integrated luminosity of the machine and ϵ is the fractional systematic error. We shall, henceforth, consider $\epsilon = 0.01$.

3. $\hat{T}$ even couplings $\Delta a_W, \mathcal{R}(b_W)$ and $\mathcal{I}(\beta_W)$

The relative contribution of the couplings can be enhanced or reduced by using different cuts on kinematic observables. A partial list of such cuts and the corresponding cross-sections are displayed in table 2. The set of cuts $\mathcal{C}_{3,4}$ eliminate the

Table 2. Various cuts and the corresponding rates, in femtobarns, for unpolarised scattering with $\sqrt{s_{ee}} = 500$ GeV.

	Cut	σ_0	σ_1	σ_4
$\mathcal{C}_0$	Acceptance cuts	4.15	−16.10	−1.96
$\mathcal{C}_1$	$p_T(W) \geq 80$ GeV and $\lvert \sin\phi_{HW} \rvert \geq 0.4$	0.25	−2.58	−0.73
$\mathcal{C}_2$	$p_T(W) \geq 80$ GeV and $p_T^{\text{miss}} \geq 60$ GeV	0.19	−2.37	−0.74
$\mathcal{C}_3$	$p_T(W) \leq 80$ GeV and $\lvert \sin\phi_{HW} \rvert \leq 0.4$	1.11	−2.55	0.18
$\mathcal{C}_4$	$p_T(W) \leq 80$ GeV and $\lvert \cos\theta_H \rvert \leq 0.8$	1.89	−5.56	0.044
$\mathcal{C}_5$	$p_T(W) \geq 80$ GeV and $\lvert \sin\phi_{HW} \rvert \leq 0.4$	0.50	−3.49	−0.62

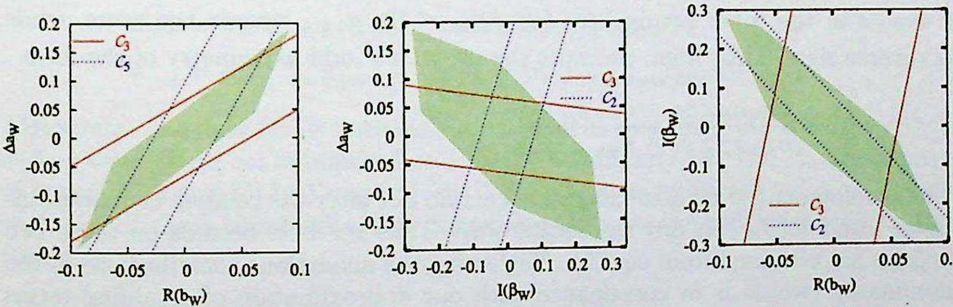

Figure 1. The pairs of oblique lines denote the region allowed by the corresponding cut, at the 3σ level, when the third anomalous coupling is identically zero. Intersection of strips, thus, gives the area allowed by both the observables. The shaded regions constitute the projections of the parameter space that leads to observables indistinguishable from the SM expectations for each of the cuts of table 2 when all three couplings are allowed to be non-zero. In each case, an integrated luminosity of 500 fb^{-1} has been used.

bulk of the $\mathcal{I}(\beta_W)$ contribution, while the cuts $\mathcal{C}_{1,2}$ serve to enhance the effect of $\mathcal{I}(\beta_W)$. If we make the simplifying assumption that only one anomalous coupling may be non-zero, the corresponding individual limits are easy to obtain. In figure 1, we display the regions allowed at 3σ level in the three different planes corresponding to each of the three pairs of anomalous couplings. The individual and simultaneous limits of these couplings are listed in table 3.

Table 3. Achievable upper limits (3σ) on $\hat{T}$ even couplings. Individual limits are obtained under the assumption that only one of the couplings is non-zero. The simultaneous limits are based on the shaded regions of figure 1.

Coupling	Individual limit	Observable used	Simultaneous limit
$\lvert\Delta a_W\rvert$	0.050	σ with C_4	0.19
$\lvert\mathcal{R}(b_W)\rvert$	0.035	σ with C_4	0.09
$\lvert\mathcal{I}(\beta_W)\rvert$	0.078	σ with C_2	0.27

4. $\hat{T}$ odd couplings $\mathcal{I}(b_W)$ and $\mathcal{R}(\beta_W)$

On restricting the W-boson to lie above the plane of production of the Higgs (defined in conjunction with the beam axis), i.e. ($\sin\phi_{HW} \geq 0$), we have, for the corresponding partial cross-section,

$$\begin{aligned}\sigma(\sin\phi_{HW} \geq 0) = 2.07(1 + 2\Delta a_W) - 8.04\mathcal{R}(b_W) - 0.982\mathcal{I}(\beta_W)\\ +1.50\mathcal{I}(b_W) - 3.11\mathcal{R}(\beta_W).\end{aligned} \tag{4}$$

For events in the other hemisphere ($\sin\phi_{HW} \leq 0$), $\sigma_{0,1,4}$ remain the same, while $\sigma_{2,3}$ reverse sign. This, then, prompts the use of a $\hat{T}$-odd asymmetry of the form

$$\mathcal{A} \equiv \frac{\sigma_{\sin\phi_{HW}\geq 0} - \sigma_{\sin\phi_{HW}\leq 0}}{\sigma_{\sin\phi_{HW}\geq 0} + \sigma_{\sin\phi_{HW}\leq 0}}. \tag{5}$$

The employment of further kinematic cuts do not alter the relative contributions of $\mathcal{I}(b_W)$ and $\mathcal{R}(\beta_W)$ in any significant way. Thus the best bounds on these two couplings are obtained from eq. (5). Neglecting the anomalous contributions in the denominator (which is in consonance with our approximation of retaining terms which are at best linear in the anomalous couplings) and assuming that only one of these couplings is non-zero, the corresponding 3σ bounds are

$$|\mathcal{I}(b_W)| \leq 0.092 \quad \text{and} \quad |\mathcal{R}(\beta_W)| \leq 0.045 \tag{6}$$

for an integrated luminosity of 500 fb^{-1}.

5. Use of the $e^+\gamma$ initial state

We now consider the action of the composite discrete symmetry $P\hat{T}$. This is best achieved by comparing the results obtained until now using the $e^-\gamma$ colliders with those expected from the conjugate process, namely $e^+\gamma \longrightarrow \bar{\nu}W^+H$. The total cross-section for the conjugate process is related to that obtained earlier in a simple fashion:

$$\begin{aligned}\sigma_{e^+\gamma} = [\sigma_0(1 + 2\Delta a_W) + \sigma_1\mathcal{R}(b_W) + \sigma_2\mathcal{R}(\beta_W)]_{e^-\gamma}\\ -[\sigma_3\mathcal{I}(b_W) + \sigma_4\mathcal{I}(\beta_W)]_{e^-\gamma}.\end{aligned} \tag{7}$$

Table 4. Limits on anomalous couplings at 3σ level using unpolarised beams with an integrated luminosity of 250 fb^{-1} for each of the $e^-\gamma$ and $e^+\gamma$ modes.

Coupling	$3\delta\mathcal{A}$ bound	Observable used
$\vert\mathcal{I}(\beta_W)\vert$	0.092	$\mathcal{A}_1$ with $\mathcal{C}_1$
$\vert\mathcal{I}(b_W)\vert$	0.096	$\mathcal{A}_3$ with acceptance cuts
$\vert\mathcal{R}(\beta_W)\vert$	0.046	$\mathcal{A}_2$ with acceptance cuts

This leads us to construct the asymmetries

$$\begin{aligned}\mathcal{A}_1 &\equiv \frac{\sigma_{e^+\gamma}-\sigma_{e^-\gamma}}{\sigma_{e^+\gamma}+\sigma_{e^-\gamma}},\\ \mathcal{A}_2 &= \frac{(\sigma_{++}-\sigma_{+-})-(\sigma_{-+}-\sigma_{--})}{(\sigma_{++}+\sigma_{+-})+(\sigma_{-+}+\sigma_{--})},\\ \mathcal{A}_3 &= \frac{(\sigma_{++}-\sigma_{--})-(\sigma_{+-}-\sigma_{-+})}{(\sigma_{++}+\sigma_{--})+(\sigma_{+-}+\sigma_{-+})},\end{aligned} \tag{8}$$

where

$$\begin{aligned}&\sigma_{++} = \sigma_{e^+\gamma,\,\sin\phi_{HW}>0}, \quad \sigma_{+-} = \sigma_{e^+\gamma,\,\sin\phi_{HW}<0},\\ &\sigma_{-+} = \sigma_{e^-\gamma,\,\sin\phi_{HW}>0}, \quad \sigma_{--} = \sigma_{e^-\gamma,\,\sin\phi_{HW}<0}.\end{aligned} \tag{9}$$

Again retaining only terms linear in the anomalous couplings, $\mathcal{A}_1$ contains only the $\mathcal{I}(\beta_W)$ term (if no cut is imposed on $\sin\phi_{HW}$). Similarly, $\mathcal{A}_2$ and $\mathcal{A}_3$ are functions of only $\mathcal{I}(b_W)$ and $\mathcal{R}(\beta_W)$ respectively. This allows us to obtain a direct bound on each one of these couplings alone, something that we were hitherto unable to do (table 4).

6. Conclusions

Since the WWH couplings are not contaminated by the ZZH couplings in the process studied, $e\gamma$ colliders can be used to constrain the anomalous WWH couplings independent of the ZZH couplings. Thus $e\gamma$ colliders are better equipped than e^+e^- colliders to study these couplings.

Comparing our results to those of ref. [1], we find that we obtain better individual limits for all couplings, bar Δa_W. Furthermore, in ref. [1], the authors were unable to construct observables that depend on only one of the couplings. Hence their limits on WWH couplings are not independent of each other. However, using the process $e^-\gamma \longrightarrow \nu W^- H$ in conjunction with the conjugate process $e^+\gamma \longrightarrow \bar{\nu} W^+ H$, and using the $P\hat{T}$ properties of various contributions to the total rate, we are able to construct observables that are functions of only one of the couplings. Thus we are able to derive constraints on each of the couplings $\mathcal{I}(\beta_W)$, $\mathcal{I}(b_W)$ and $\mathcal{R}(\beta_W)$ independent of the value of any other coupling. Δa_W and $\mathcal{R}(b_W)$, however, cannot be constrained independent of each other.

References

[1] S S Biswal, D Choudhury, R M Godbole and R K Singh, *Phys. Rev.* **D73**, 035001 (2006), arXiv: hep-ph/0509070

[2] R Rattazzi, *Z. Phys.* **C40**, 605 (1988)
K Hagiwara and M L Stong, *Z. Phys.* **C62**, 99 (1994)
H J He, Y P Kuang, C P Yuan and B Zhang, *Phys. Lett.* **B554**, 64 (2003), arXiv:hep-ph/0211229
K Hagiwara, S Ishihara, R Szalapski and D Zeppenfeld, *Phys. Rev.* **D48**, 2182 (1993)
K Hagiwara, R Szalapski and D Zeppenfeld, *Phys. Lett.* **B318**, 155 (1993), arXiv:hep-ph/9308347
T Han and J Jiang, *Phys. Rev.* **D63**, 096007 (2001)

[3] M C Gonzalez-Garcia, *Int. J. Mod. Phys.* **A14**, 3121 (1999), arXiv:hep-ph/9902321

[4] I F Ginzburg, G L Kotkin, V G Serbo and V I Telnov, *Nucl. Instrum. Methods* **205**, 47 (1983)

PRAMANA
— journal of
physics

© Indian Academy of Sciences

Vol. 69, No. 5
November 2007
pp. 801–807

Search for Higgs boson in beyond standard model scenarios at large hadron collider

KAJARI MAZUMDAR, on behalf of the ATLAS and CMS Collaborations
Tata Institute of Fundamental Research, Homi Bhabha Road, Mumbai 400 005, India
E-mail: mazumdar@tifr.res.in

Abstract. The principal physics motivation of the LHC experiments is to search for the Higgs boson and to probe the physics of TeV energy scale. Potential of discovery for Higgs bosons in various scenarios beyond standard model have been estimated for both CMS and ATLAS experiments through detailed detector simulations. Main results from the recently published studies of CMS collaboration are only included in this write-up.

Keywords. Higgs; beyond standard model; large hadron collider.

PACS Nos 12.15.-y; 12.60.Fr; 12.60.Jv; 12.10.-g; 12.10.Dm

1. Introduction

The general-purpose experiments, CMS and ATLAS, at the large hadron collider (LHC) are fully equipped to probe the nature of the electroweak symmetry breaking. There are a number of ideas which try to address the issues of the mass hierarchy and naturalness in standard model (SM), notably, supersymmetry (SUSY), extra dimensions, little Higgs models and so on. There is ernest hope that the LHC will be able to elucidate on the possible mechanism at work by discovering at least some of the new particles these models evoke.

Discovery potential of various scenarios have been estimated realistically with detailed detector simulation (using GEANT4) followed by full reconstruction including trigger selections. It is assumed that during initial years of LHC the instantaneous luminosity (2×10^{33} s^{-1} cm^{-2}) will correspond to an average event pile-up of about five minimum bias events in the detector. The key issues for experimental identification and subsequent discovery include sufficient signal rate, efficient trigger, control of background and signal-to-background ratio.

At the time of writing this report, the latest studies from CMS collaboration has been published in the Physics TDR Vol. 2 [1] and we present them here briefly. Other results discussed during the presentation have been mostly omitted.

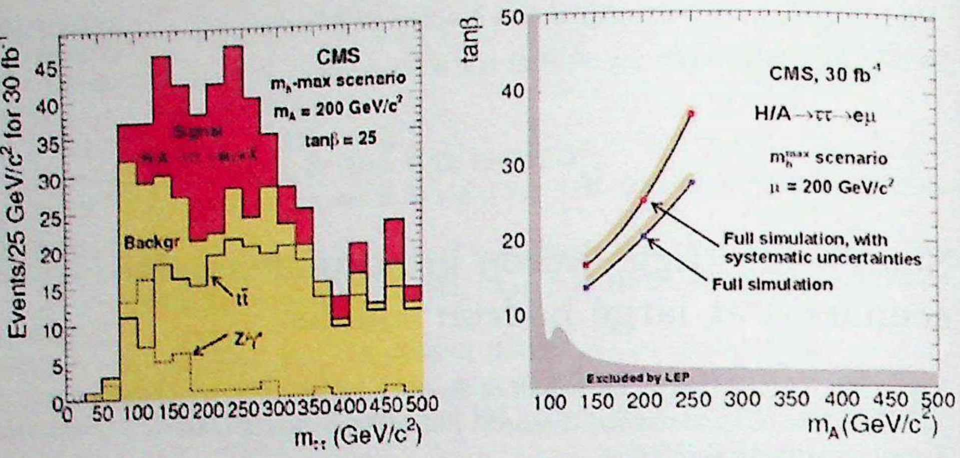

Figure 1. $\tau\tau$ reconstructed mass after all selection and the discovery region for $gg \to b\bar{b}H/A, H/A \to \tau\tau \to e\mu + X$ in $M_A, \tan\beta$ plane for 30 fb^{-1}.

2. SUSY Higgses

The most studied scenario beyond SM is its minimal supersymmetric extension (MSSM) with five elementary Higgs particles $h, H, A, H^{\pm}$ whose masses and decay branchings mainly depend on two parameters, typically m_A and $\tan\beta$. For a wide range of SUSY parameters the lightest Higgs boson mass m_h is expected to be less than 150 GeV/c^2 whereas $m_A \sim m_h$ for $m_A \leq 120$ GeV/c^2 and $m_A \sim m_H$ for $m_A \geq 120$ GeV/c^2. Thus the search of low mass SUSY Higgs boson is similar to SM Higgs boson and studied processes are: $h \to \gamma\gamma$, $h \to ZZ^* \to 4\ell$ in inclusive productions, $h \to \gamma\gamma$ and $b\bar{b}$ in Wh production while $h \to b\bar{b}$ in the case of $t\bar{t}H$ production. For vector boson fusion (VBF) processes, $qq \to qqh$, the suitable modes are: $h \to \gamma\gamma, h \to \tau\tau \to \ell+$ jets. For m_A in the range of 90–130 GeV/c^2 the above channels are not useful and special methods to tag and trigger b-jets and τs are used to utilise the process $gg \to b\bar{b}H, H \to \mu^+\mu^-, \tau^+\tau^-$.

The productions of heavy, neutral Higgs boson, H/A, though weak at LHC, are larger than SM Higgs and they are produced directly for low $\tan\beta$ values whereas they are produced in association for high $\tan\beta$ values through $gg \to b\bar{b}H/A$. Fortunately, the branching ratios to experimentally suitable decay modes are large for all $\tan\beta$ and they are best detected through $H, A \to \mu^+\mu^-$ and $H, A \to \tau\tau \to e\mu$, $\ell^+\ell^-, \ell +$ jet, 2 jets modes. The leptonic decay modes are cleaner and the τ-mass reconstruction is possible assuming the neutrinos to be collinear. Subsequently Higgs mass is reconstructed for events where the charged leptons are not back-to-back. The $\tau\tau$ reconstructed mass for $m_H = 200$ GeV/c^2 with 30 fb^{-1} and the discovery region in $H, A \to \tau\tau \to e\mu$ channel is shown in figure 1. The systematic uncertainties taken into account are: lepton identification (2%), b-tagging efficiency (5%), mistagging efficiency (5%), theoretical prediction for $t\bar{t}$ cross-section (5.8%), luminosity (3%) etc. The jet energy and missing energy scale uncertainties contribute to an uncertainty of 7.3% on the dominant $t\bar{t}$ background.

The discovery curves for the light, neutral Higgs boson h from inclusive $pp \to h + X, h \to \gamma\gamma$ channel and for neutral Higgs produced in VBF mode are

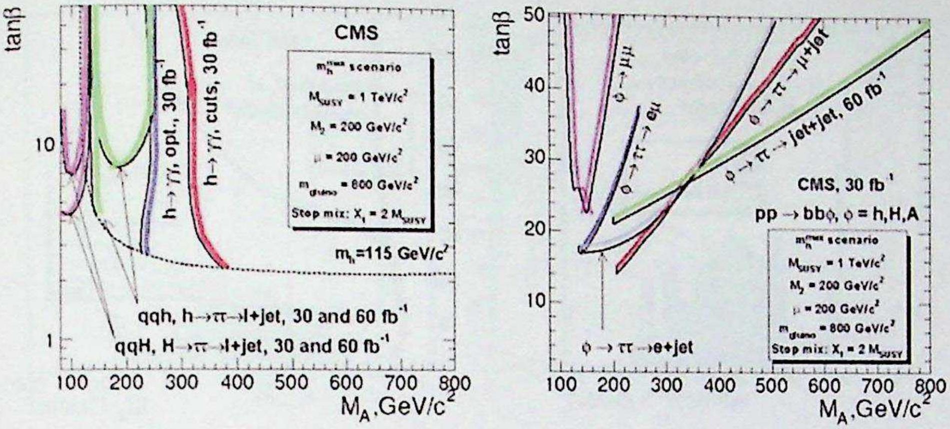

Figure 2. Left: 5σ discovery regions for the light, neutral Higgs boson in inclusive process and light and heavy Higgs bosons in VBF process. Right: 5σ discovery regions for neutral Higgs boson (ϕ) in $pp \to b\bar{b}\phi$ process.

shown in figure 2 (left). The discovery regions for the neutral Higgs bosons $\phi(\phi = h, H, A)$ produced in $pp \to b\bar{b}\phi$ with $\phi \to \mu\mu, \tau\tau$ are displayed in figure 2 (right). It may be possible to discriminate SM vs. SUSY via $h(H) \to \gamma\gamma$ channel through absolute rate estimates, though it is limited by luminosity measurements to 5%, while rates differ by less than 10% for $m_A \geq 550$ GeV/c^2. However, the ratio of the decay branchings, $h \to \gamma\gamma$ and $h \to b\bar{b}$ is about 15% for $m_A \geq 550$ GeV/c^2 and it is not limited by luminosity. It is also hoped that the distinction between A and H masses may be possible for mass difference of more than 5 GeV/c^2 for $\tan\beta \geq 30$.

For charged Higgs boson ($H^{\pm}$), which can be lighter than W-mass, two mass regions are distinguished in searches. For $M_H^{\pm} \leq m_t$ the suitable process is $t\bar{t} \to H^{\pm}W^{\mp}b\bar{b}$ with $H^{\pm} \to \tau^{\pm}\nu, \tau \to \nu+$hadrons and $W^{\mp} \to \ell^{\mp}\nu$. The low mass study is mainly systematics dominated which may be reduced through alternative approaches. For heavier mass region ($M_H^{\pm} \geq m_t$) the channel $gg \to tbH^{\pm}$, with decays $H^{\pm} \to \tau^{\pm}\nu, \tau \to \text{hadrons} + \nu$ and $t \to qqb$ is probed where the signal pions from τ deacys are more energetic due to opposite polarisation of $\tau^{\pm}$ from $H^{\pm}$ vs. than that from $W^{\pm}$. Figure 3 shows the transverse mass of τ after all selections and the reach for 30 fb^{-1} in $m_A, \tan\beta$ plane.

2.1 *tan β measurement*

The sensitivity of the width of Higgs boson, $\Gamma_{H/A}$ on tan β can be utilised for its determination. Also, since the production cross-section for H/A has large sensitivity to tan β values, the effective value defined through relation: $\sigma \times \text{BR} \sim \tan^2\beta_{\text{eff}}$, is a significant observable for global fit to determine SUSY parameters. Figure 4 gives the uncertainties in the measurement using two methods.

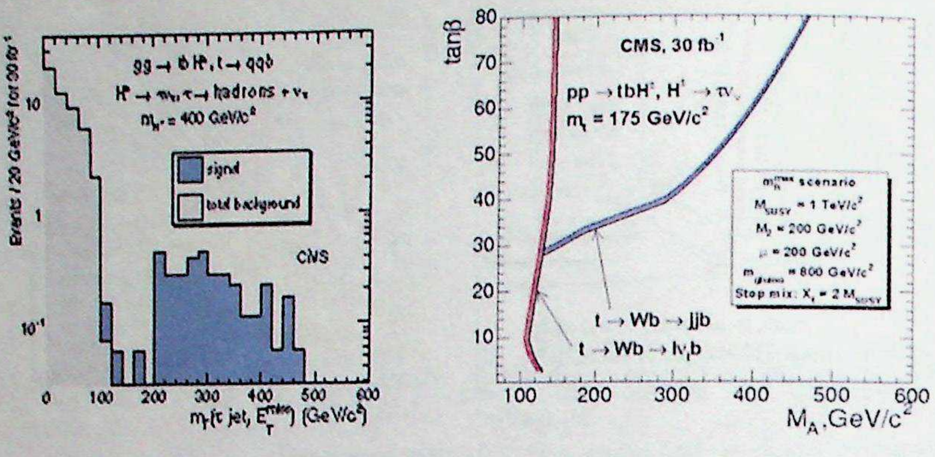

Figure 3. Left: Reconstructed transverse τ mass after all selections from signal ($gg \to tbH^{\pm}$) superposed with background. Right: 5σ discovery reach of $H^{\pm}$.

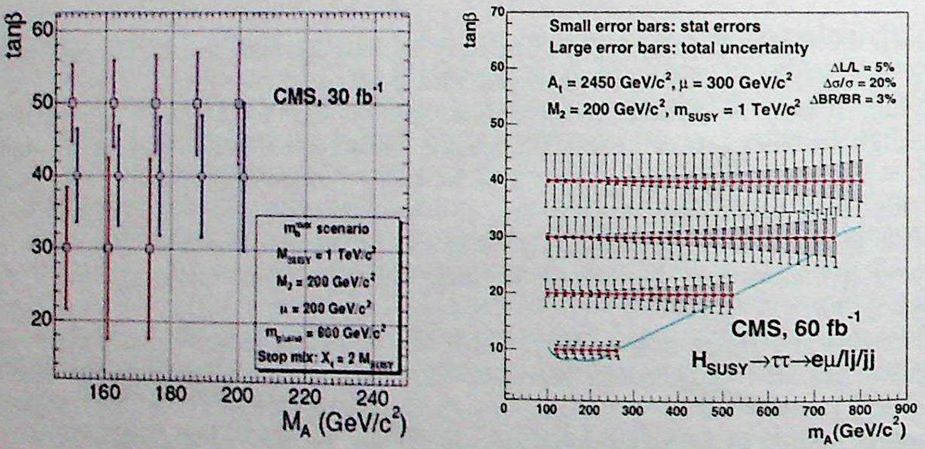

Figure 4. Uncertainty on tan β measurement obtained from the estimate of Higgs boson width and from exploiting the dependence of cross-section in $H \to \tau\tau$ channel where experimental systematics and statistical uncertainties have been taken into account.

2.2 *Observation of Higgs bosons in decay to gauginos and Higgs bosons from gaugino decays*

The region around tan $\beta = 5$ and $m_A = (130, 150)$ GeV/c^2 in M_A, tan β plane remains uncovered by standard searches and hence special strategies are employed. The channel $H, A \to \chi_2^0 \chi_2^0 \to 4\ell$ covers this special zone and the invariant mass spectrum of four leptons can be studied. However, the spectrum being featureless,

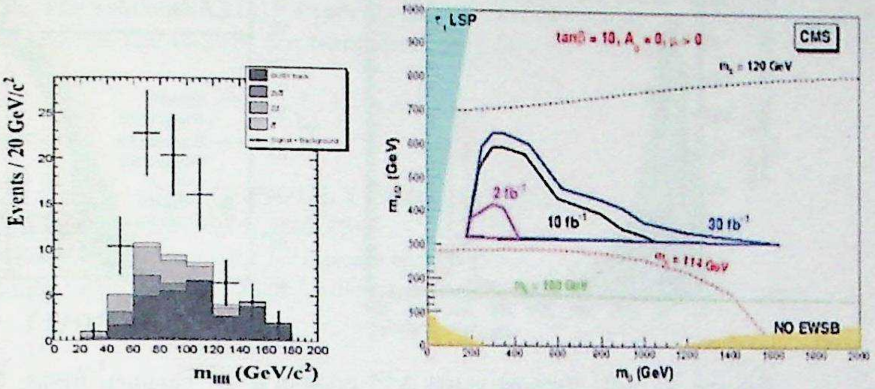

Figure 5. Left: Four lepton invariant mass distribution for paramaters $m_0 = 50\ \mathrm{GeV/c^2}$, $m_{1/2} = 150\ \mathrm{GeV/c^2}$, $\tan\beta = 5$. Right: Higgs discovery reach in SUSY cascades as a function of luminosity.

a good knowledge of SM and SUSY backgrounds is necessary as shown in figure 5 (left). Large rate for gaugino productions in cascade decays of squarks and gluinos can be effectively utilised to study h productions of mass $\leq 250\ \mathrm{GeV/c^2}$ in some portions of parameter space, specially through $b\bar{b}$ decays since the events can be triggered by inclusive SUSY signatures. Similarly $H^{\pm}$ can also be searched in top decays. These methods give the unique possibility to measure couplings of SUSY particles to the Higgs bosons and also the intense coupling region can be probed as shown in figure 5 (right).

3. Little Higgs model

In this scenario the Higgs field is treated as pseudo-Goldstone boson resulting from a broken global symmetry at a scale of about 10 TeV and a new set of particles are invoked. There are three types of Higgs scalars (neutral, singly charged and doubly charged) of mass $M_\phi \leq 10\ \mathrm{TeV/c^2}$. The doubly charged Higgs (ϕ^{++}) can be produced via W^+W^+ fusion, and it can also decay via $W^+W^+ \rightarrow \ell^+\nu\ \ell^+\nu$. The transverse mass reconstruction of ϕ^{++} is possible at very high luminosity. A typical distribution of invariant mass of same sign di-muons is presented in figure 6 (left). The ratio of confidence levels for the signal and background hypothesis $\mathrm{CL_S} = \mathrm{CL_{S+B}}/\mathrm{CL_B}$, interpreted as the probability of excluding an existing signal [2] is shown in figure 6 (right).

4. Probing extra dimensions in Randall–Sundrum (RS) model

In this case all SM particles are assumed to reside in one brane while the fluctuations in fifth dimension produces a scalar field radion (ϕ) which can mix with SM Higgs boson. The characteristic parameters of the model with an additional scalar field

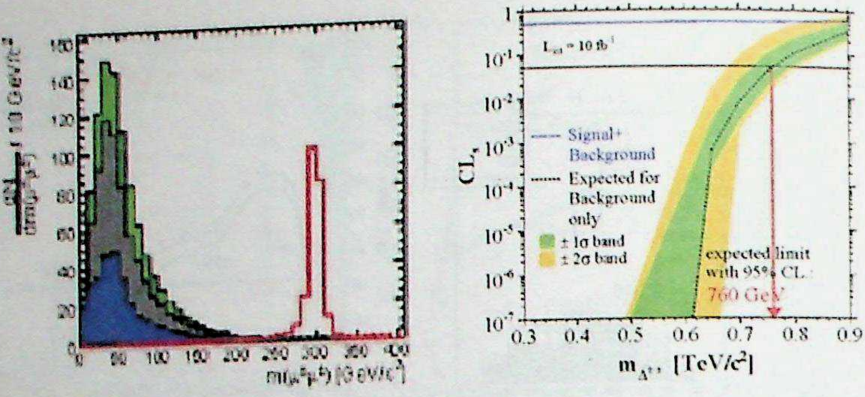

Figure 6. Left: Reconstructed $\Delta^{\pm\pm}$ mass in $\mu^{\pm}\mu^{\pm}$ channel. Right: CLs as a function of $\Delta^{\pm\pm}$ mass (see text for definition of CLs).

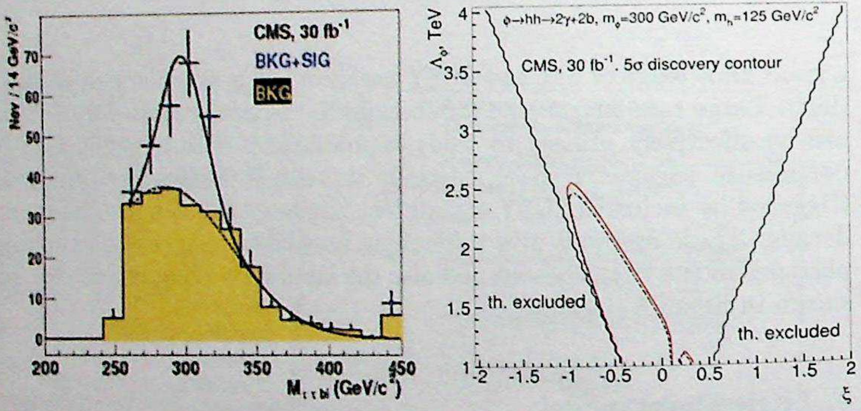

Figure 7. Left: Invariant mass distribution of $\tau^+\tau^- bj$ system for radion production and decay assuming maximum signal rate. Right: 5σ discovery contour for $\phi \to \tau\tau bb$ channel.

radion (ϕ) are: m_h, m_ϕ, ξ (mixing), Λ_ϕ (VEV of radion field) with typical branching ratio of $\mathrm{Br}(\phi \to hh) = 30\%$, for $m_h = 120$ GeV/c², $m_\phi = 350$ GeV/c² and $\Lambda_\phi = 5$ TeV. Studies have been made in channels $\phi \to hh \to \gamma\gamma b\bar{b}, \tau^+\tau^- b\bar{b}$ and $4b$ modes. Requiring only one jet to be b-tagged, the invariant mass distribution of $\tau^+\tau^- bj$ system is shown in figure 7 (left). The right plot shows 5σ discovery contour for $\phi \to \gamma\gamma b\bar{b}$ channel where the reach in parameter space is the maximum.

5. Conclusion

LHC machine and the experiments are ready to start taking data in 2007. Both CMS and ATLAS experiments are capable of discovering what lies ahead of standard model. Typical uncertainties for CMS experiment have been quoted only for a particular analysis though all results include both statistical and systematic errors [3]. The reach of ATLAS experiment in terms of various discoveries are similar and sometimes the studies are complementary [4].

References

[1] CMS Collaboration: CERN/LHCC **2006-021** (2006)

[2] A L Read, *J. Phys.* **G28**, 2693 (2002)

[3] CMS Collaboration: http://cms.cern.ch/iCMS/

[4] ATLAS Collaboration: http://cdsweb.cern.ch/collection/ATLAS%20Notes

PRAMANA
— journal of
physics

© Indian Academy of Sciences

Vol. 69, No. 5
November 2007
pp. 809–813

Associated single photons and doubly-charged scalars at linear e^-e^- colliders

BISWARUP MUKHOPADHYAYA* and SANTOSH KUMAR RAI
Harish-Chandra Research Institute, Chhatnag Road, Jhunsi, Allahabad 211 019, India
*E-mail: biswarup@mri.ernet.in

Abstract. Doubly-charged scalars, predicted in many models having exotic Higgs representations, can in general have lepton-number violating (LFV) couplings. We show that by using an associated monoenergetic final state photon seen at a future linear e^-e^- collider, we can have a clear and distinct signature for a doubly-charged resonance. The strength of the $\Delta L = 2$ coupling can also be probed quite effectively as a function of the recoil mass of the doubly-charged scalar.

Keywords. Doubly-charged Higgs; associated photon; initial state radiation.

PACS Nos 12.60.Fr; 14.80.Cp

Doubly-charged scalars arise in a number of physics scenarios [1,2], the most common models to accommodate such scalars are those with triplet Higgs. An added feature often associated with doubly-charged Higgs is the possibility of lepton-number violation. This basically consists of $\Delta L = 2$ couplings with leptons of the form

$$L_Y = ih_{ij}\Psi^T_{iL}C\tau_2\Phi\Psi_{jL} + \text{h.c.}, \tag{1}$$

where $i, j = e, \mu, \tau$ are generation indices, the Ψ's are the two-component left-handed lepton fields, and Φ is the triplet with $Y = 2$ weak hypercharge. This leads to mass terms for neutrinos once the neutral component ϕ^0 of Φ acquires a vacuum expectation value (VEV):

$$M^\nu_{ij} \sim h_{ij}v' \tag{2}$$

v' being the triplet VEV. Constraints on the ρ-parameter put strong limits on the triplet VEV [3] translating into limits on the L-violation Yukawa couplings from the expected ranges of neutrino masses. Such limits usually constrain the collider signals for doubly-charged scalars sought through $\Delta L = 2$ interactions.

We point out the usefulness of looking for doubly-charged scalars in an e^-e^- collider, in the radiative production channel. Resonant production of ϕ^{--} requires one to know its mass with reasonable accuracy to start with, and tune the center-of-mass energy of the colliding electrons accordingly. In addition, precise identification of a doubly-charged resonance will also depend on its decay products, which depend on the parameters of the L-violating sector. In general, one can have the decays

$$\phi^{--} \to W^-W^-, l^-l^-, W^-\phi^-, \phi^-\phi^- .$$

A degeneracy among the triplet components is often a consequence of theories, albeit in a model-dependent fashion. If we thus neglect the last two channels listed above, we still have the W^-W^- and l^-l^- channels, of which the first is controlled by the triplet VEV v' and the second, by the coupling h_{ll}. When the first mode is dominant, it requires careful analysis of the W-decay products in order to isolate signatures of resonant production. It is thus desirable to have supplementary channels in mind while looking for doubly-charged scalars. With this in view, we have calculated the rates for the process

$$e^-e^- \longrightarrow \phi^{--}\gamma \longrightarrow X\gamma$$

at a $\sqrt{s} = 1$ TeV e^-e^- machine, concentrating on the hard single photon in the final state. This photon will be monochromatic if a doubly-charged resonance is produced, irrespective of what it decays into. Furthermore, one is no more required to tune the electron–electron center-of-mass energy at a fixed value. For our analysis, taking the radiative production of the scalar ϕ^{--} as the benchmark process, we concentrate only on the flavor diagonal coupling h_{ee}. In our numerical estimate, we have chosen the coupling strength to be $h_{ee} = 0.1$ which respects the most stringent bounds coming from muonium–antimuonium conversion results which for flavor diagonal coupling is $h < 0.44 M_\phi^{\pm\pm}$ TeV^{-1} at 90% CL. The on-shell radiative production of a doubly-charged scalar gives an almost monochromatic photon of energy

$$E_\gamma = \frac{s - M^2_{\phi^{--}}}{2\sqrt{s}} \tag{3}$$

which stands out against the continuum background of the standard model (SM). We assume that the h_{ii} couplings are of equal strength. The total decay width of ϕ^{--} thus obtained is very miniscule (~1.2 GeV) for a 1 TeV scalar mass when compared to the machine energy and allows one to use the narrow-width approximation.

The major SM background that contributes to the above process is the radiative Moller scattering process: $e^- + e^- \to \gamma + e^- + e^-$ which, although a continuum background, could *prima facie* be large enough to wash away the monochromatic peak. The event selection criteria, therefore, are largely aimed at suppressing this continuum background. We impose the following set of cuts.

- Rapidity cut on the final state particles: $|\eta(e^-)| < 1.5$ and $|\eta(\gamma)| < 2.5$
- Minimum cut on energies: $E(\gamma) > 20$ GeV, $E(e^-) > 5$ GeV
- To ensure that the final state particles are well separated in space for the detectors to resolve events: $\delta R > 0.2$

Using the above cuts we make an estimate of the SM background and the signal. We focus on the main trigger, viz. the photon. In figure 1a we show the distribution of the photon energy, where we have superposed the differential cross-section for

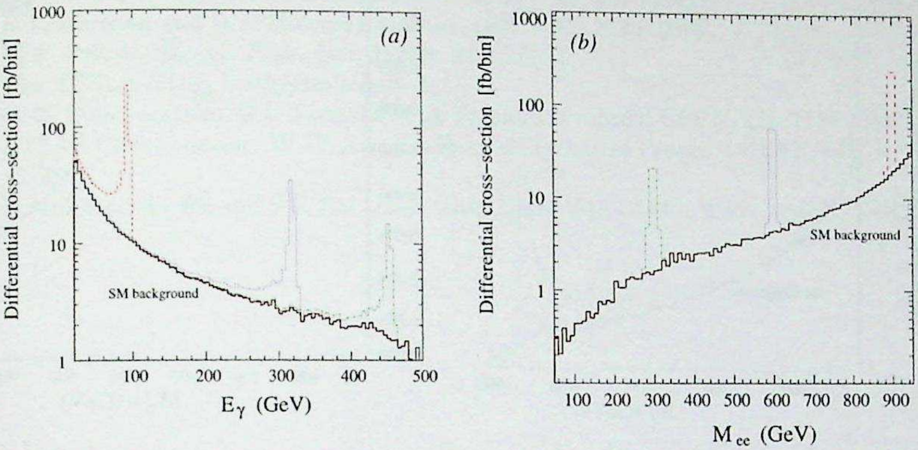

Figure 1. Differential cross-sections against (a) photon energy E_γ and (b) invariant mass of electron pair M_{ee}. The dash-dot-dash (green) line corresponds to $M_{\phi^{--}} = 300$ GeV, dotted (blue) line corresponds to $M_{\phi^{--}} = 600$ GeV and the dashed (red) line corresponds to $M_{\phi^{--}} = 900$ GeV respectively. The bin size is chosen to be 5 GeV in (a) and 10 GeV in (b).

signal+background in each bin over the SM background. A pronounced peak can be seen in the photon energy distribution, due to the monochromaticity of the photon, corresponding to the recoil energy against the scalar resonance through the relation of eq. (3). To make our analysis realistic, we have smeared the photon energy by a Gaussian function whose half-width is guided by the resolution of the electromagnetic calorimeter [4,5] and also incorporated the effects of ISR which often results in substantial broadening of the peak. We show the resulting peak for three choices of scalar mass (300, 600, 900 GeV). Alternatively, in figure 1b, we also show the invariant mass distribution of the *ee* pair for the above choice of parameters and as expected the distribution peaks corresponding to the mass of scalar.

In figure 2a we plot the energy distribution of the photon once again but here we only look at the final state hard transverse photon in $e^-e^- \to \gamma + \phi^{--} \to \gamma + X$. The distribution again shows peaks corresponding to the recoil against the massive scalars, irrespective of the knowledge of the decay products of the scalar. In fact, our signal here receives a relative boost as it is not suppressed by considering any further decay since $\mathrm{BR}(\phi^{--} \to X) = 100\%$. The fact that looking at a single photon against the backdrop of a continuum background makes it possible to identify a LFV $(\Delta L = 2)$ process in a model independent way, makes this signal worth studying at a future e^-e^- collider and running the linear collider in this mode.

Since the rates for the signal depend directly on the eeH coupling squared, in figure 2b we show the strength of the coupling for which the peaks would stand out against the fluctuations in the SM background. In our analysis we have assumed a luminosity of $\mathcal{L} = 100$ fb^{-1}. The fact that we are not looking at any specific final state arising from ϕ^{--} decay improves the reach of this search channel. However, if a direct resonance is excited then that would invariably translate into a much

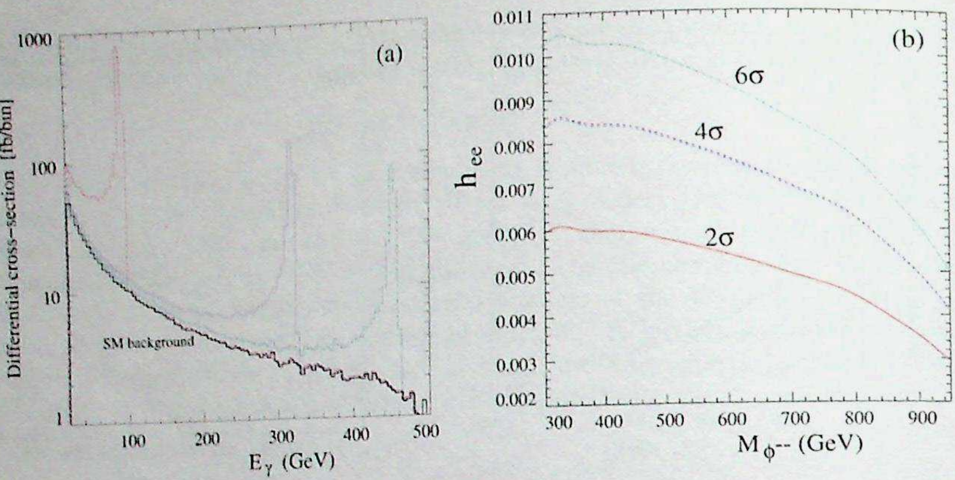

Figure 2. (a) Differential cross-sections against photon energy E_γ when $\phi^{--} \to X$ (anything). The dash-dot-dash (green) line corresponds to $M_{\phi^{--}} = 300$ GeV, dotted (blue) line corresponds to $M_{\phi^{--}} = 600$ GeV and the dashed (red) line corresponds to $M_{\phi^{--}} = 900$ GeV respectively. (b) Illustrating the reach of the coupling constant at which the resonances in the E_γ distribution can be identified over the fluctuations in the SM background. The assumed luminosity is 100 fb^{-1}.

stronger probe of the coupling strength. Nonetheless, our analysis is not dependent on the tuning of $\sqrt{s}$ of the machine to hit a resonance and hence serves as a more robust proposition. For luminosity higher than what we have used, this reach can be further enhanced.

To summarise, the cleanliness of central photon detection at a high energy linear collider can be very helpful in identifying a doubly-charged scalar. The peaks in the hard photon energy can be helpful in two ways. First, one does not need to tune the two electron beams, and can therefore work without a prior knowledge of the ϕ^{--} mass. Secondly, this method is shown to work even if the ϕ^{--} dominantly decays into states that are not clean enough for the resonance to be identified. Thus, as soon as one succeeds in reducing the SM backgrounds, one can clearly see $\Delta L = 2$ interactions, just by looking at the accompanying hard photon. Not only doubly-charged scalars but also more exotic resonances such as bileptons are amenable to detection in this manner.

This talk was based on an earlier work and for further details one is suggested to look at ref. [6].

References

[1] J Schechter and J W F Valle, *Phys. Rev.* **D23**, 1666 (1981)
G B Gelmini and M Roncadelli, *Phys. Lett.* **B99**, 411 (1981)
[2] J C Pati and A Salam, *Phys. Rev.* **D10**, 275 (1974)
R N Mohapatra and J C Pati, *Phys. Rev.* **D11**, 566 (1975)
G Senjanovic and R N Mohapatra, *Phys. Rev.* **D12**, 1502 (1975)

R N Mohapatra and D P Sidhu, *Phys. Rev. Lett.* **38**, 667 (1977)
R E Marshak and R N Mohapatra, *Phys. Lett.* **B91**, 222 (1980)

[3] LEP Collaborations: *Phys. Lett.* **B276**, 247 (1992)

[4] The TESLA TDR, http://tesla.desy.de/

[5] CMS Collaboration: G L Bayatian *et al*, Technical Proposal CERN/LHCC 94-38, 1994
ATLAS Collaboration: W W Armstrong *et al*, Technical Proposal CERN/LHCC/94-43, 1994

[6] B Mukhopadhyaya and S K Rai, *Phys. Lett.* **B633**, 519 (2006), arXiv:hep-ph/0508290

PRAMANA
— journal of
physics

© Indian Academy of Sciences

Vol. 69, No. 5
November 2007
pp. 815–818

Identifying new physics contributions in the Higgs sector at linear e^+e^- colliders

SANTOSH KUMAR RAI
Harish-Chandra Research Institute, Chhatnag Road, Jhunsi, Allahabad 211 019, India
E-mail: santosh.rai@helsinki.fi

Abstract. Loop-driven decay modes of the Higgs are sensitive to new physics contributions because of new particles in the loops. To highlight this we look at the dilepton–dijet signal in the dominant Higgs production channel at a linear e^+e^- collider. We show that by taking a simple ratio between cross-sections of two different final states such contributions can be very easily identified.

Keywords. Higgs; universal extra dimension; linear collider.

PACS Nos 11.10.Kk; 13.66.Fg

1. Introduction

Higgs boson discovery will prove to be a crucial ingredient towards understanding the mechanism of electroweak symmetry breaking. Once discovered, a major goal would be to determine its other intrinsic properties, couplings and its total width with high accuracy in a model independent way. The proposed future e^+e^- linear colliders would be instrumental in achieving very precise measurements of the Higgs boson properties.

The partial width of the Higgs decaying to the massless gauge boson is of special interest, since there are no tree level couplings of the Higgs to them and any contribution is generated at the one-loop level. The di-photon partial width gets contribution through massive charged particles in the loops while the gluon–gluon partial width gets contributions from the heavy quarks running in the loops. The effective loop-induced couplings of $H\gamma\gamma$ and Hgg are sensitive to new contributions from particles which appear in various extensions of the SM. Not only do these decay modes provide for a possible probe of new physics particles which are too heavy to be produced directly but they are also sensitive to scales far beyond the Higgs mass. We take up the case of the enhancement in the partial decay width of $H \to gg$ due to additional contributions coming from particles from theories of beyond SM (BSM) physics. Such additional heavy particles are predicted in many different models of BSM physics and here we consider the model of universal extra dimensions (UED) [1] where all the quark flavors of the SM have heavy Kaluza–Klein (KK) excitations. These heavy KK states will modify the form factors which in turn will affect the partial width $\Gamma(H \to gg)$. The UED model, in its simplest form [2], has all the SM particles propagating in a single extra dimension, which is compactified on an S_1/Z_2 orbifold with R as the radius of compactification. The KK tower resulting on the four-dimensional space-time has a tree level mass given by

$$m_n^2 = m^2 + \frac{n^2}{R^2}, \tag{1}$$

where n denotes the nth level of the KK tower and m corresponds to the mass of the SM particle in question.

Since $H \to gg$ proceeds through diagrams containing fermion triangle loops and the coupling is proportional to the zero-mode mass of the fermion even in the case of UED, we consider contributions of the KK tower of the top quark only. The partial decay width for $H \to gg$ with SM and UED contribution is [3],

$$\Gamma(H \to gg) = \frac{G_{\mathrm{F}} m_H^3}{36\sqrt{2}\pi} \left(\frac{\alpha_{\mathrm{s}}(m_H)}{\pi}\right)^2 \; |I_q + \sum_n \tilde{I}_{t^{(n)}}|^2, \tag{2}$$

where G_{F} is the Fermi constant, $\alpha_{\mathrm{s}}(m_H)$ is the running QCD coupling evaluated at m_H and $I_g = \sum_q I_q$, I_q being the contributions of the loop integrals involving the different quark flavors and $\tilde{I}_{t^{(n)}}$ are the additional contributions of the loop integrals for the UED case. These functions are given in ref. [3]. The UED contribution is summed over the first few levels of the KK tower, till the effects of the higher modes decouple and hardly contribute to the amplitude anymore.

2. Channel of interest

We consider the case of a 500 GeV linear e^+e^- collider and calculate the production of a Higgs in association with a Z boson through a process of the form

$$e^+e^- \to Z + H, \tag{3}$$

where Z decays leptonically. In the preceding paragraph we discuss the final states relevant for our study.

1. $e^+e^- \to \ell^+\ell^- +$ two jets, which arises when the Higgs boson decays to a pair of quarks or gluons [3a], which then undergo fragmentation to form a pair of hadronic jets. Clearly, for a Higgs boson in the SM, final state will receive contributions mainly from the decays $H \to b\bar{b}$ and $H \to c\bar{c}$, with a minuscule contribution due to $H \to gg$. However, due to the increase in the partial width for $H \to gg$ due to the extra contribution coming from the additional KK excitations of the top quark in the loops, there will be an enhancement in the overall branching ratio to jets.
2. $e^+e^- \to \ell^+\ell^- + b\bar{b}$, which simply means that the final state in the above contains two tagged b-jets. The decay width for $H \to b\bar{b}$ is roughly the same in SM as well as UED, although the change of the two-gluon decay mode will have a small effect on the branching ratio for the $b\bar{b}$ mode.

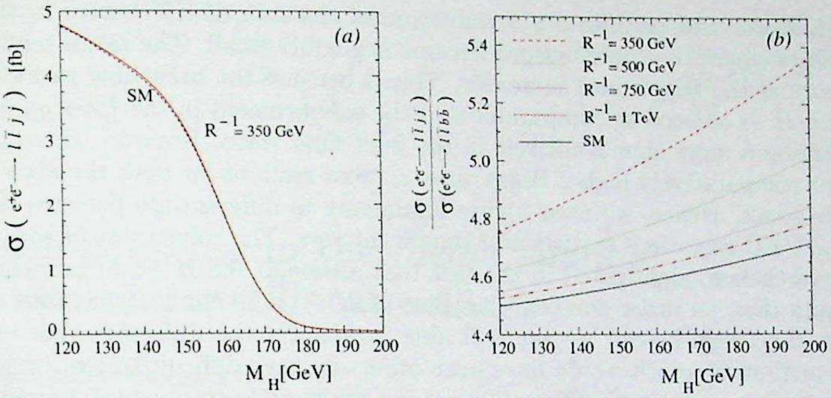

Figure 1. The curves are generated for $\sqrt{s} = 500$ GeV linear e^+e^- collider. (**a**) Shows the cross-section. (**b**) Shows the ratio of cross-sections between two final states for different values of the compactification radius.

In our subsequent analysis, we have imposed a few kinematic acceptance cuts on the final-state particles, viz.,

1. The final-state leptons should have transverse momentum $p_T^{(\ell)} > 10$ GeV and pseudo-rapidity $\eta^{(\ell)} < 3.0$. The final-state jets should have transverse momentum $p_T^{(J)} > 10$ GeV and pseudo-rapidity $\eta^{(J)} < 2.5$.
2. The final-state jets should be clearly separated from each other, so we impose a cut: $\Delta R_{JJ} (\equiv \sqrt{\Delta\eta_{JJ}^2 + \Delta\phi_{JJ}^2}) > 0.4$.

In figure 1a, we illustrate our result for the process discussed above, namely,

$$e^+e^- \to \ell^+\ell^- + \text{two jets}$$

at a $\sqrt{s} = 500$ GeV, e^+e^- collider. The solid line denotes the UED-included cross-section where we have chosen the value of $R^{-1} = 350$ GeV which gives a greater enhancement compared to values of R^{-1} greater than the above, while the dashed line denotes the SM contribution only. It should be noted that the graph shows the excess cross-section after removing the non-Higgs part of the standard model contributions (such as $e^+e^- \to ZZ, ZZ^*$ etc.). The continuum background ($\gamma^*\gamma^*$, Z^*Z^*) too can be easily neglected as it lies below 10^{-3} fb (in the bins of $b\bar{b}$ invariant mass) and would hardly affect the rates for the signal in consideration. The cross-section shown in figure 1a makes it clear that it is very hard to see the differences by just looking at the rates. The cross-sections for $\ell^+\ell^-$ + two jets final state are almost identical in the two cases. As the cross-sections look very similar, it would require very precise measurements to form a distinction between the two cases. However, if we consider the ratio of the two processes, viz. $\frac{\sigma(e^+e^- \to \ell^+\ell^- + \text{two jets})}{\sigma(e^+e^- \to \ell^+\ell^- + b\bar{b})}$ we can see that the difference between the two cases becomes more prominent. In figure 1b we plot this ratio for different values of the compactification scale R^{-1}. We find that the ratio differs from that of the SM throughout the mass range of 120 GeV $\leq m_H \leq$ 200 GeV with the lines converging towards the SM value as R^{-1} is increased. In fact this highlights the decoupling nature of the higher levels of the

KK tower and justifies our termination of the sum of KK towers in the loop, to values where the contributions become negligibly small. The ratios tend to diverge more as the Higgs mass increases. This is because the branching ratios of $H \to gg$ and $H \to b\bar{b}$ become comparable and the enhancement in the $H \to gg$ mode starts playing a more significant role in the 2-jet final state. However, there is a caveat. For comparatively higher Higgs masses, cross-sections for both the above processes are small. Hence, we need higher luminosity to differentiate between the SM and the UED cases in a statistically significant way. The robustness of this method is, nevertheless, highlighted in the fact that although the $H \to gg$ branching ratio is more than an order smaller than that of $H \to b\bar{b}$ in the intermediate mass range for the Higgs boson, we are still able to identify the difference due to the UED contribution which would have been otherwise very difficult to see, by just looking at the cross-sections. The ratios are not susceptible to uncertainties like different efficiency factors associated with particle identifications as they would cancel out. The efficiency factors will however give a more realistic estimate of the events that will be observed at the experiments and which gives us an estimate of the uncertainties in the statistics.

In fact the above analysis can be used to identify other new physics scenarios which play a similar role in modifying the partial width of the Higgs to massless gauge bosons. It can also be used to distinguish scalars of other theories which behave similar to the Higgs boson. Radions predicted in models of warped extra dimensions [4] have similar couplings like the Higgs boson. A major difference is the enhanced coupling of radion to gluons through the trace anomaly. The above analysis proves useful in distinguishing radions from Higgs boson quite effectively [5].

3. Summary

This talk was based on the work done with Anindya Datta and further details can be obtained from ref. [6].

References

[1] I Antoniadis, *Phys. Lett.* **B246**, 377 (1990)

[2] T Appelquist, H C Cheng and B A Dobrescu, *Phys. Rev.* **D64**, 035002 (2001)

[3] F J Petriello, *J. High Energy Phys.* **0205**, 003 (2002)

[3a] We exclude $H \to \tau^{\pm}$ decays because these produce narrow jets which can be identified as $\tau^{\pm}$ with 80–90% efficiency

[4] L Randall and R Sundrum, *Phys. Rev. Lett.* **83**, 3370 (1999); *Phys. Rev. Lett.* **83**, 4690 (1999)

[5] P K Das, S K Rai and S Raychaudhuri, *Phys. Lett.* **B618**, 221 (2005)

[6] A Datta and S K Rai, arXiv:hep-ph/0509277

PRAMANA
— journal of
physics

© Indian Academy of Sciences

Vol. 69, No. 5
November 2007
pp. 819–822

Higgs self-coupling in the fusion channel at the international linear collider

K MOENIG[1] and A ROSCA[2,*]
[1]DESY, Zeuthen, D15738, Germany
[2]West University of Timisoara, Timisoara, RO 300223, Romania
*E-mail: ars@ifh.de

Abstract. We investigate the Higgs pair production process at the international linear collider (ILC), focusing on the measurement of the trilinear self-coupling of the Higgs boson in the fusion channel. The sensitivity of this measurement is discussed in the Higgs mass range 140–200 GeV at a center-of-mass energy between 1 TeV and 1.5 TeV.

Keywords. Higgs; self-coupling.

PACS Nos 13.66.Fg; 13.66.Jn; 14.80.Bn

1. Introduction

In order to verify the role of the Higgs boson in the spontaneous breaking of the electroweak symmetry [1] we need to reconstruct experimentally the Higgs potential, $V = \lambda(\Phi^+\Phi - v^2/2)^2$ [2]. A probe of the shape of this potential requires the measurement of the triple and quartic self-couplings of the Higgs boson. These self-couplings are defined in the standard model through the Higgs potential

$$V_H = \frac{M_H^2}{2}H^2 + \frac{M_H^2}{2v}H^3 + \frac{M_H^4}{8v^2}H^4 \qquad (1)$$

and are uniquely determined by the mass of the Higgs boson: $\lambda_{HHH} = 3M_H^2/v$ and $\lambda_{HHHH} = 3M_H^2/v^2$, where v is the vacuum expectation value of the Higgs boson, $v = (\sqrt{2}G_{\mathrm{F}})^{1/2} = 246$ GeV. A precision test of this relation may reveal an extended nature of the Higgs sector [3].

The triple self-coupling λ_{HHH} is accessible directly in double Higgs production at high energy at future colliders. Several mechanisms that are sensitive to λ_{HHH} can be exploited for this task. At the ILC a pair of Higgs particles is produced in e^+e^- interactions via either the double Higgsstrahlung mechanism [4–7] or WW/ZZ boson fusion processes [8–11]. Moreover, two Higgses can be produced in $\gamma\gamma$ collisions [12] as well, singly or together with a W boson pair through a mechanism equivalent to the WW boson fusion in e^+e^-. Unfortunately, not all the possible subprocesses contributing to double Higgs production contain the triple Higgs vertex. Most of

Table 1. Signal rates at $\sqrt{s}$ = 0.5, 1.0 and 1.2 TeV, for 1000 fb^{-1}, 80% electron beam and 40% positron beam polarization.

	N		
m_H	$\sqrt{s} = 0.5$ TeV	$\sqrt{s} = 1.0$ TeV	$\sqrt{s} = 1.2$ TeV
140	14.5	146.7	252.6
180	1.9	63.3	124.8

these subprocesses involve standard electroweak gauge vertexes and constitute an irreducible background for the λ_{HHH} measurement. The presence of such an irreducible background makes the measurement intrinsically difficult.

The double Higgsstrahlung process is strongly investigated elsewhere [13]. Therefore, in this work we examine only the feasibility of the triple Higgs self-coupling measurement in the WW fusion process.

2. The cross-sections

The cross-sections for double Higgs production in the WW boson fusion process are presented in figure 1 (left) as a function of the center-of-mass energy, for four different values of the Higgs mass. The cross-sections are shown for unpolarized electrons and positrons; they increase by a factor 4 for polarized electron and positron beams. The cross-sections increase with rising energy and their values become sizable at energies above 1 TeV. To compute the cross-sections we employed the Whizard [14] generator.

In table 1 the number of signal events is given for several center-of-mass energies and Higgs masses of 140 GeV and 180 GeV, assuming 80% electron beam polarization and 40% positron beam polarization.

The sensitivity to the HHH self-coupling is demonstrated by varying the trilinear coupling within the range $\delta\lambda = -1$ and $+1$. Here we introduce an effective coupling which includes an anomalous contribution as $\lambda_{HHH} = (1+\delta\lambda)\lambda^{\text{SM}}_{HHH}$. The dimensionless anomalous coupling $\delta\lambda$ is normalized in such a way that $\delta\lambda = -1$ exactly cancels the SM HHH coupling. The cross-sections for various values of $\delta\lambda$ are shown in figure 1 (right), for polarized beams and $\sqrt{s} = 0.5$, 1, 1.2 and 1.5 TeV. The cross-sections decrease with increase in triple Higgs self-coupling due to a negative interference with the gauge part of the amplitude.

From the values of the cross-section, assuming an integrated luminosity of 1000 fb^{-1}, a detection efficiency of 100% and no backgrounds the accuracy on the coupling can reach at its best 4–5% for polarized beams, as is shown in figure 1 (bottom).

The sensitivity to the triple Higgs vertex may be enhanced by studying discriminating variables, as for example the invariant mass of the Higgses and the angle of a Higgs boson in the rest frame of the HH system with the HH direction.

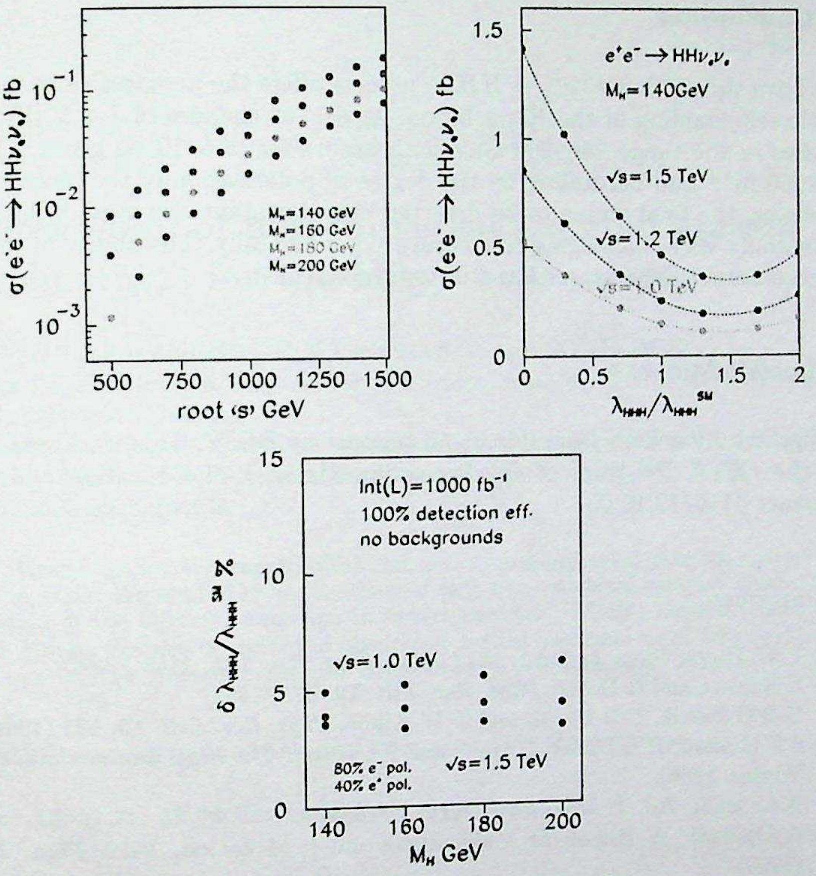

Figure 1. Top, left: Dependence of the cross-section for Higgs pair production on the center-of-mass energy for several Higgs mass values and unpolarized beams. Top, right: Dependence of the $HH\nu\bar{\nu}$ cross-section on the triple Higgs coupling, normalized to its SM value, for $M_H = 140$ GeV, several $\sqrt{s}$ values and polarized beams. Down: Accuracy on λ_{HHH} as a function of Higgs mass for several $\sqrt{s}$ values and polarized beams.

2.1 *The background processes*

However, one has to prove that the signal for two-Higgs boson production can be extracted in the presence of a large multi-channel background. We intend to study two mass values, 140 GeV and 180 GeV. The dominant decay channels are then: $b\bar{b}$, WW^* and WW, giving rise to complex final states with up to ten fermions. Whizard generator can be used to simulate these processes. The backgrounds are many and include processes such as: $e^+e^- \to W^+W^-W^+W^-$, $W^+W^-Z^0Z^0$, $Z^0Z^0Z^0Z^0$, $e^+e^- \to W^+W^-Z^0$, $Z^0Z^0Z^0$, $\nu\bar{\nu}W^+W^-$, $\nu\bar{\nu}Z^0Z^0$, νeWZ, $e^+e^-W^+W^-$, $e^+e^-Z^0Z^0$, $t\bar{t}H$. The cross-sections of the background processes are larger than those of the signal and one has to verify whether they can be reduced applying kinematic cuts.

3. Conclusions

We have shown that $e^+e^- \to HH\nu\bar{\nu}$ process offers the perspective to measure the triple self-coupling of the Higgs boson, λ_{HHH}, at energies of 1–1.5 TeV for Higgs masses in the range 140–200 GeV with accuracies of 5–10 %, given a luminosity of 1000 fb^{-1} and depending on the degree of polarization of the incoming beams. However, the final states to be detected experimentally are very complicated and potentially very challenging to measure experimentally. The ability of the detector to reconstruct these states has still to be confirmed.

Acknowledgments

AR gratefully acknowledges financial support by DESY. This work was supported by the CEEX Program of the Romanian Ministry of Education and Research, contract 3176/12.10.05.

References

[1] P W Higgs, *Phys. Lett.* **12**, 132 (1964); *Phys. Rev.* **145**, 1156 (1966)
F Englert and R Brout, *Phys. Rev. Lett.* **13**, 321 (1964)
G S Guralnik, C R Hagen and T W Kibbe, *Phys. Rev. Lett.* **13**, 585 (1964)
[2] J F Gunion, H E Haber, G Kane and S Dawson, *The Higgs hunter's guide* (Addison-Wesley, 1990)
A Djouadi, *Int. J. Mod. Phys.* **A10**, 1 (1995)
[3] A Djouadi, W Kilian, M Muhlleitnera and P M Zerwas, *Euro. Phys. J.* **C10**, 45 (1999)
[4] G Gounaris, D Schildknecht and F Renard, *Phys. Lett.* **B83**, 191 (1979)
G Gounaris, D Schildknecht and F Renard, *Phys. Lett.* **B89**, 437 (1980)
V Barger, T Han and R J N Phillips, *Phys. Rev.* **D38**, 2766 (1988)
[5] V A Ilyin A E Pukhov, Y Kurihara, Y Shimizu and T Kaneko, *Phys. Rev.* **D54**, 6717 (1996)
[6] A Djouadi, H E Haber and P M Zerwas, *Phys. Lett.* **B375**, 203 (1996)
[7] D J Miller and S Moretti, *Euro. Phys. J.* **C13**, 459 (2000)
[8] F Boudjema and E Chopin, *Z. Phys.* **C73**, 85 (1996)
[9] V Barger and T Han, *Mod. Phys. Lett.* **A5**, 667 (1990)
[10] A Dobrovolskaya and V Novikov, *Z. Phys.* **C52**, 427 (1991)
[11] D A Dicus, K J Kallianpur and S S D Willenbrock, *Phys. Lett.* **B200**, 187 (1988)
A Abbasabadi, W W Repko, D A Dicus and R Vega, *Phys. Rev.* **D38**, 2770 (1988)
A Abbasabadi, W W Repko, D A Dicus and R Vega, *Phys. Lett.* **B213**, 386 (1988)
[12] G Jikia, *Nucl. Phys.* **B412**, 57 (1994)
R Belusevic and G Jikia, *Phys. Rev.* **D70**, 073017 (2004)
[13] C Castanier, P Gay, P Lutz and J Orloff, LC-PHSM-2000-061, hep-ex/0101028
P Gay, *These proceedings*
T Barklow, *These proceedings*
[14] W Kilian, LC-TOOL-2001-039

PRAMANA
— journal of
physics

© Indian Academy of Sciences

Vol. 69, No. 5
November 2007
pp. 823–827

Phenomenology of non-universal gaugino masses and implications for the Higgs boson decay

K HUITU[1,2], J LAAMANEN[1,2], P N PANDITA[3,*] and SOUROV ROY[2]
[1]High Energy Physics Division, Department of Physical Sciences, University of Helsinki, P.O. Box 64, FIN-00014, Finland
[2]Helsinki Institute of Physics, University of Helsinki, P.O. Box 64, FIN-00014, Finland
[3] Department of Physics, North-Eastern Hill University, Shillong 793 022, India
*E-mail: pandita@sancharnet.in

Abstract. Grand unified theories (GUTs) can lead to non-universal gaugino masses at the unification scale. We study the implications of such non-universal gaugino masses for the composition of the lightest neutralino in supersymmetric (SUSY) theories based on $SU(5)$ gauge group. We also consider the phenomenological implications of non-universal gaugino masses for the phenomenology of Higgs bosons in the context of large hadron collider.

Keywords. Supersymmetry; non-universal gaugino masses; Higgs bosons.

PACS Nos 12.60.Jv; 11.30.Er; 14.80.Ly

1. Introduction

It is widely expected that some of the supersymmetric partners of the standard model (SM) particles will be produced at the CERN large hadron collider (LHC), which is going to start operation in a few years time. In the experimental search for supersymmetry the lightest SUSY particle will play a crucial role since the heavier SUSY particles will decay into it. In SUSY models with R-parity conservation, the lightest SUSY particle is absolutely stable [1]. In most of the SUSY models the lightest neutralino ($\tilde{\chi}_1^0$), which is an admixture of gauginos and higgsinos, is the lightest SUSY particle (LSP). Such an LSP is also a particle dark matter candidate [2]. From the point of view of experimental discovery of supersymmetry at a collider like the LHC, the LSP is the only SUSY particle in the final product of the cascade decay of a heavy SUSY particle.

In this work [3] we will assume that the LSP is the lightest neutralino, and that it escapes the collider experiments undetected. The cascade chain will typically contain other neutralinos ($\tilde{\chi}_j^0$, $j = 2,3,4$) as well as charginos ($\tilde{\chi}_i^{\pm}$, $i = 1,2$). The charginos are an admixture of charged gauginos and charged higgsinos. The composition and mass of the neutralinos and charginos will play a key role in the

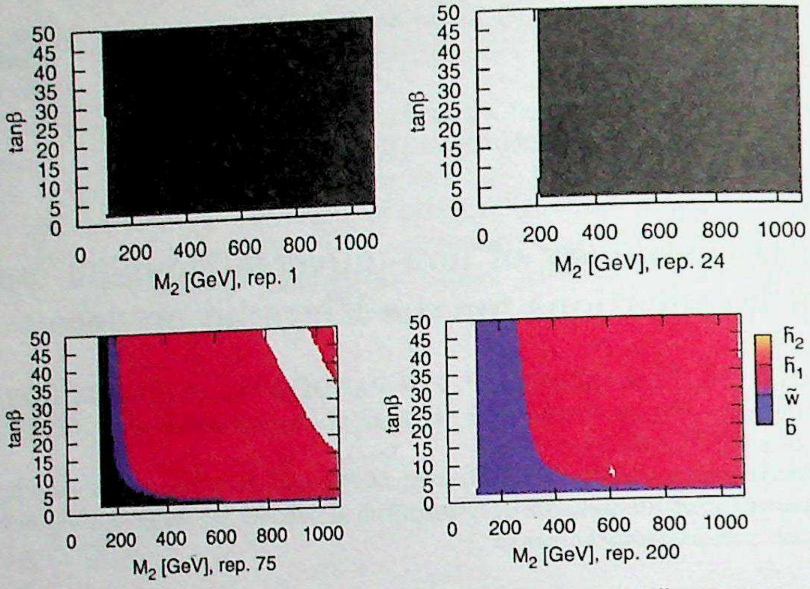

Figure 1. Main component of the lightest neutralino in different representations of $SU(5)$ that arise in the product (2).

search for SUSY particles. The mass patterns of the neutralinos in different SUSY models were considered in detail in [4,5].

Although most of the phenomenological studies involving neutralinos and charginos have been performed with universal gaugino masses at the GUT scale, there is no compelling theoretical reason for such a choice. Thus, it is important to investigate the changes in the experimental signals for supersymmetry with the changes in the composition of neutralinos and charginos that may arise because of the changes in the underlying boundary conditions at the grand unification scale. In this paper we shall study the implications of the non-universal gaugino masses for the phenomenology of neutral Higgs bosons in a $SU(5)$ supersymmetric grand unified theory.

2. Non-universal gaugino masses in supersymmetric $SU(5)$

The masses and the compositions of neutralinos and charginos are determined by the soft SUSY breaking gaugino masses M_i ($i = 1, 2, 3$), the Higgs mixing parameter μ, and the ratio of the Higgs vacuum expectation values $\tan\beta$. In general, the gaugino masses need not be equal at the GUT scale. In SUSY models, such as $SU(5)$ grand unified models, non-universal gaugino masses are generated by a non-singlet chiral superfield Φ^n that appears linearly in the gauge kinetic function $f(\Phi)$ which is an analytic function of the chiral superfields Φ in the theory [6]. When the F-component of Φ, F_Φ, gets a VEV $\langle F_\Phi \rangle$, it generates the gaugino masses ($\lambda^{a,b}$ are gaugino fields):

Table 1. Ratios of the gaugino masses at the GUT scale, and at the electroweak scale in the normalization $M_3(\text{GUT}) = 1$, $M_3(\text{EW}) = 1$.

F_Φ	M_1^{G}	M_2^{G}	M_3^{G}	M_1^{EW}	M_2^{EW}	M_3^{EW}
1	1	1	1	0.14	0.29	1
24	−0.5	−1.5	1	−0.07	−0.43	1
75	−5	3	1	−0.72	0.87	1
200	10	2	1	1.44	0.58	1

$$\mathcal{L}_{\text{g.k.}} \supset \frac{\langle F_\Phi \rangle_{ab}}{M_{\text{P}}} \lambda^a \lambda^b + \text{ h.c.}, \tag{1}$$

where g.k. stands for gauge kinetic term. Since the gauginos belong to the adjoint representation of $SU(5)$ with

$$(\mathbf{24} \otimes \mathbf{24})_{\text{symm}} = \mathbf{1} \oplus \mathbf{24} \oplus \mathbf{75} \oplus \mathbf{200}, \tag{2}$$

Φ and F_Φ can belong to, besides the singlet, any of the non-singlet representations **24**, **75** and **200** of $SU(5)$. For the non-singlet case these gaugino masses are unequal but related to one another [7]. In table 1, we show the ratios of the resulting gaugino masses at the GUT scale and the electroweak scale. In figure 1, we show the dominant component of the lightest neutralino (LSP) for the four representations as a function of $\tan\beta$ and M_2 (calculated at the electroweak scale) for the value of soft SUSY breaking scalar mass $m_0(\text{GUT}) = 1$ TeV. For the case of the singlet and **24** representation, the dominant component is always the bino. For the **75** dimensional representation, the situation is complicated, and for the **200** dimensional representation the LSP is either a wino or a higgsino, depending on the values of M_2, μ and $\tan\beta$.

3. Higgs detection using $H^0, A^0 \to \tilde{\chi}_2^0 \tilde{\chi}_2^0 \to 4l$

It is usually assumed that SUSY partners are too heavy so that Higgs bosons cannot decay into SUSY particles. However, it may be that for the heavy Higgs bosons H^0, A^0 and $H^\pm$ the decays to SUSY particles are important or even dominant. Here we will study the decay chain

$$H^0, A^0 \to \tilde{\chi}_2^0 \tilde{\chi}_2^0, \;\; \tilde{\chi}_2^0 \to \tilde{\chi}_1^0 l^+ l^-, \;\; l = e, \mu, \tag{3}$$

for four different representations of $SU(5)$ in (2). The decay $\tilde{\chi}_2^0 \to \tilde{\chi}_1^0 l^+ l^-$ depends on the parameters M_2, M_1, μ and $\tan\beta$, which control the neutralino masses and the mixing parameters, and also on the slepton masses $m_{\tilde{l}}$. As long as the direct decay of $\tilde{\chi}_2^0$ into $\tilde{\chi}_1^0 + Z^0$ is suppressed and the sleptons are heavier than $\tilde{\chi}_2^0$, three-body decays of $\tilde{\chi}_2^0$ into charged leptons and $\tilde{\chi}_1^0$ will be significant. In figure 2 we show a typical branching ratio of the three-body decay (3) as a function of $\tan\beta$ for the **1**, **75** and **200** representations, respectively. In this figure the initial value of $\tan\beta$ is 4.5, since for a lower value of $\tan\beta$ the light Higgs mass m_h is less

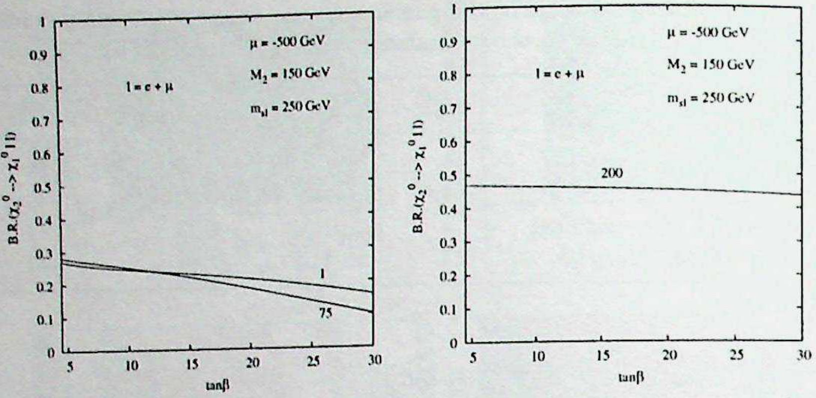

Figure 2. Branching ratio as a function of $\tan\beta$, with $m_{\tilde{l}} > m_{\tilde{\chi}_2^0}$, for the representations **1**, **75** and **200**.

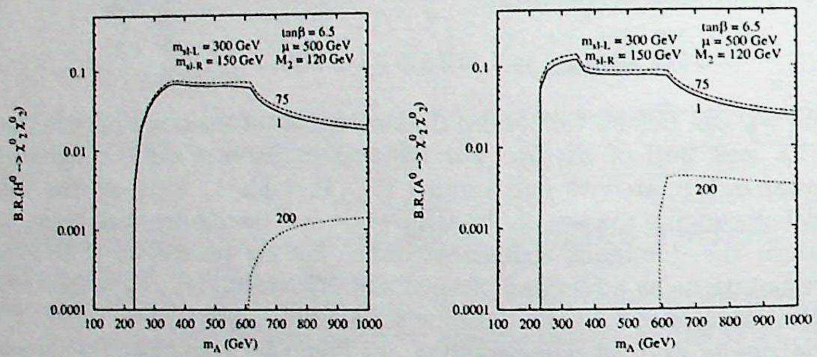

Figure 3. The branching ratio of $H^0, A^0 \to \tilde{\chi}_2^0\tilde{\chi}_2^0$ as a function of m_A for three different $SU(5)$ representations in (2). Here $\tan\beta$ is taken to be 6.5.

than 114.4 GeV, which is the lower limit of LEP [8]. We see from the figure that for higher values of $\tan\beta$ this branching ratio decreases since the branching ratio $\tilde{\chi}_2^0 \to \tilde{\chi}_1^0\tau^+\tau^-$ increases with $\tan\beta$ due to a larger Yukawa coupling.

4. Decay of heavy Higgs bosons into a pair of neutralinos: $H^0, A^0 \to \tilde{\chi}_2^0\tilde{\chi}_2^0$

Here we study the branching ratios of the heavy Higgs bosons H^0 and A^0 into a pair of second lightest neutralinos. The decay widths and the branching ratios depend on the ratio of M_1 and M_2 along with other MSSM parameters. We have calculated the branching ratio of $H^0, A^0 \to \tilde{\chi}_2^0\tilde{\chi}_2^0$ for different $SU(5)$ representations that arise in the product (2). As an example, in figure 3, we have shown the dependence of branching ratio $\mathrm{BR}(H^0, A^0 \to \tilde{\chi}_2^0\tilde{\chi}_2^0)$ on m_A for a particular choice of MSSM parameters. We can see that for this choice of the parameter set and for $m_A <$ 350 GeV, the branching ratio of the decay of A^0 is larger than that of the decay of the heavy Higgs scalar H^0 for the representations **1** and **75**. This is due to the fact that for H^0 the total decay width is larger due to the increase in the number of available channels to the SM particles, which leads to a smaller branching ratio to sparticles. In the case of **200** dimensional representation the threshold opens up for heavier m_A, and once again the branching ratio of A^0 is larger than that of the H^0. The results for the representation **24** is not shown here due to the fact that it results in the lightest neutralino mass below the current experimental limits.

References

[1] M Drees and M Peskin, *Proceedings of SUSY04*, Tsukuba, Japan (http://www-conf.kek.jp/susy04/plenary.html)

[2] See, for e.g. G Jungman, M Kamionkowski and K Griest, *Phys. Rep.* **267**, 195 (1996)

[3] K Huitu, J Laamanen, P N Pandita and Sourov Roy, *Phys. Rev.* **D72**, 055013 (2005)

[4] P N Pandita, *Phys. Rev.* **D53**, 566 (1996)

[5] K Huitu, J Laamanen and P N Pandita, *Phys. Rev.* **D67**, 115009 (2003)

[6] E Cremmer, S Ferrara, L Girardello and A Van Proeyen, *Phys. Lett.* **B116**, 231 (1982)

[7] J R Ellis, K Enqvist, D V Nanopoulos and K Tamvakis, *Phys. Lett.* **B155**, 381 (1985)

[8] R Barate *et al*, *Phys. Lett.* **B565**, 61 (2003)

PRAMANA
— journal of
physics

© Indian Academy of Sciences

Vol. 69, No. 5
November 2007
pp. 829–833

Low-scale gravity mediation in warped extra dimension and collider phenomenology on hidden sector*

H ITOH[1], N OKADA[1,†] and T YAMASHITA[2]
[1]Theory Division, KEK, Oho 1-1, Tsukuba 305-0801, Japan
[2]SISSA, via Beirut 4, I-34014 Trieste, Italy
[†]E-mail: okadan@post.kek.jp

Abstract. We propose a new scenario of gravity-mediated supersymmetry breaking (gravity mediation) in a supersymmetric Randall–Sundrum model, where the gravity mediation takes place at a low scale due to the warped metric. We investigate collider phenomenology involving the hidden sector field, and find a possibility that the hidden sector field can be produced at the LHC and the ILC. The hidden sector may no longer be hidden.

Keywords. Supersymmetry; supersymmetry breaking; collider.

PACS Nos 12.60.Jv; 11.30.Qc

1. Introduction

Supersymmetric (SUSY) extension of the standard model is one of the most promising ways to solve the gauge hierarchy problem of the standard model. However, since no superpartner has been observed in the current experiments, SUSY should be broken at low energies. The origin of SUSY breaking and its mediation mechanism to the visible (MSSM) sector is one of the most important issues in any supersymmetric phenomenological models.

The simplest model of SUSY breaking is the Polonyi model, where a chiral superfield singlet under the standard model gauge group is introduced and SUSY is broken by its non-zero F-term. After SUSY is broken, the SUSY breaking is transmitted to the visible sector through some mechanism. One simple mechanism is the

---

[*] Talk presented by N Okada. The talk is based on the work of H Itoh, N Okada and T Yamashita, hep-ph/0606156.

gravity mediation in the minimal supergravity scenario [1], where SUSY breaking is transmitted through higher dimensional contact operators between the hidden sector and the visible sector superfields. In the scenario, the scale of the SUSY breaking mediation is the Planck scale which is nothing but the cutoff scale of (four-dimensional) supergravity.

In this work, we propose a new scenario of the gravity mediation in a supersymmetric Randall–Sundrum model. Due to the warped metric, the gravity mediation takes place at the low-scale, and we call this scenario 'low-scale gravity mediation'. We investigate collider phenomenology involving the hidden sector field, when the gravity mediation scale is low enough.

2. Low-scale gravity mediation

We consider a supersymmetric Randall–Sundrum model, where the fifth dimension is compactified on the orbifold S^1/Z_2 with two branes, ultraviolet (UV) and infrared (IR) branes, sitting on each orbifold fixed point. The system is a slice of a AdS$_5$ with the warped metric [2], $\mathrm{d}s^2 = \mathrm{e}^{-2kr|y|}\eta_{\mu\nu}\mathrm{d}x^\mu \mathrm{d}x^\nu - r^2\mathrm{d}y^2$, where k is the AdS curvature, and r and y are the radius and the angle of S^1, respectively.

The set-up of our model is that both the hidden and visible sectors reside on the IR brane. We introduce the Polonyi model with a singlet chiral superfield (X) as the hidden sector. Then, we consider the gravity mediation on the IR brane, namely SUSY breaking is transmitted through contact operators between the visible sector and the hidden sector superfields. In four-dimensional models, the contact operators are suppressed by the four-dimensional Planck mass (M_{P}), which is nothing but the cutoff of four-dimensional supergravity. In our case, because of the warped metric, the effective cutoff scale on the IR brane is warped down to a low scale, $\Lambda_{\mathrm{IR}} = \omega M_{\mathrm{P}}$, where $\omega = \mathrm{e}^{-\pi k r}$ is the warp factor. Therefore, the gravity mediation occurs at the low scale, $\Lambda_{\mathrm{IR}} \ll M_{\mathrm{P}}$.

In effective four-dimensional theory, the contact operators relevant to the gravity mediation are described as

$$\begin{aligned}\mathcal{L}^{\mathrm{eff}}_{\mathrm{contact}} = & -\int \mathrm{d}^4\theta \left(c_A \frac{X + X^\dagger}{\Lambda_{\mathrm{IR}}} + c_0 \frac{X^\dagger X}{\Lambda_{\mathrm{IR}}^2} \right) Q_i^\dagger Q_i \\ & -\frac{1}{4}\int \mathrm{d}^2\theta \; c_a \frac{X}{\Lambda_{\mathrm{IR}}} \mathcal{W}^{a\alpha}\mathcal{W}^a_\alpha, \end{aligned} \tag{1}$$

where Q_i denotes matter and Higgs chiral superfields in the MSSM, c_A, c_0 and c_a are dimensionless parameters naturally of order one (flavor universality has been assumed, for simplicity), and $a = 3, 2, 1$ corresponds to the standard model gauge groups $SU(3) \times SU(2) \times U(1)$. Plugging non-zero F-term of the hidden sector field ($X = \theta^2 F_X$) into the above contact operators, we obtain soft SUSY breaking terms in the MSSM (scalar squared masses, A-parameter and gaugino masses) such as

$$\tilde{m}^2 = (c_A^2 + c_0)\frac{|F_X|^2}{\Lambda_{\mathrm{IR}}^2}, \quad A = 3c_A \frac{F_X}{\Lambda_{\mathrm{IR}}}, \quad M_a = \frac{1}{2}c_a \frac{F_X}{\Lambda_{\mathrm{IR}}}. \tag{2}$$

3. Collider phenomenology involving the hidden sector field

If the effective cutoff scale $\Lambda_{\rm IR}$ is low enough, higher dimensional interactions suppressed by $\Lambda_{\rm IR}$ have an impact on collider physics. Note that the contact operators relevant to the gravity mediation also provide contact interactions between the hidden sector scalar field and the standard model fields. From the operator giving masses to gauginos in eq. (1), we can extract interactions among the hidden sector scalar and the standard model gauge bosons such that

$$\mathcal{L}_{\rm int} = -\frac{1}{4}\int {\rm d}^2\theta\; c_a \frac{X}{\Lambda_{\rm IR}} \mathcal{W}^{a\alpha}\mathcal{W}^a_\alpha \supset -\frac{c_a}{4\sqrt{2}}\frac{\chi}{\Lambda_{\rm IR}}\mathcal{F}^{a\mu\nu}\mathcal{F}^a_{\mu\nu}, \tag{3}$$

where χ is the real component of the hidden scalar field X, and $\mathcal{F}^a$ is the field strength of the corresponding standard model gauge fields. The operators in eq. (1) also give interactions between the hidden scalar and standard model fermions,

$$\mathcal{L}_{\rm int} = \int {\rm d}^4\theta\; c_A \frac{X + X^\dagger}{\Lambda_{\rm IR}} Q_i^\dagger Q_i \supset \sqrt{2} c_A \frac{\chi}{\Lambda_{\rm IR}} \mathcal{L}^{\rm fermion}_{\rm kin}, \tag{4}$$

where $\mathcal{L}^{\rm fermion}_{\rm kin}$ is the kinetic term for each standard model fermion.

Now we investigate collider phenomenologies involving the hidden scalar based on the above interactions. If χ is light enough and $\Lambda_{\rm IR}$ is low enough, it may be possible to produce the hidden scalar at future colliders through the interactions in eq. (3). At the LHC, the dominant χ production process is the gluon fusion process. Note that the process is the same as the dominant production process for the Higgs boson (h) of the standard model through the effective interaction, $\mathcal{L}_{\rm eff} \sim -\frac{\alpha_s}{16\pi}\frac{h}{v}G^{a\mu\nu}G^a_{\mu\nu}$, of the same form as eq. (3). Therefore, in the production process, the hidden scalar χ behaves like the Higgs boson in the standard model. Comparing coefficients of their interactions, we find that their production cross-sections become comparable for $\Lambda_{\rm IR} \simeq 10$ TeV, assuming the same masses for them.

When we consider the decay process of χ, we find a big difference between χ and the Higgs boson. The branching ratio of the χ decay into the standard model particles is depicted in figure 1. Note that the branching ratio of $\chi \to \gamma\gamma$ is large, ${\rm Br}(\chi \to \gamma\gamma) \simeq 0.1$, while the branching ratio of the Higgs boson into two photons is at most 10^{-3} even when the Higgs boson is light, $m_{\rm h} < 2m_W$.

At the LHC, the most important channel for the search of the lightest Higgs boson in the MSSM is its decay process into two photons. Therefore, the χ production and the large branching ratio of its decay into two photons have a great impact on the Higgs boson search at the LHC. The ratio between two-photon events from the χ decay and the Higgs boson decay is found to be

$$\frac{\sigma(gg \to \chi){\rm Br}(\chi \to \gamma\gamma)}{\sigma(gg \to h){\rm Br}(h \to \gamma\gamma)} \simeq 100 \left(\frac{\Lambda_{\rm IR}}{10\ {\rm TeV}}\right)^{-2}, \tag{5}$$

for $c_1 = c_2 = c_3 = c_A = 1$ and $m_\chi = m_{\rm h} = 120$ GeV. If $\Lambda_{\rm IR}$ is around 10 TeV, the hidden sector scalar χ can be discovered at the LHC with a very clean signature.

Next, let us investigate phenomenology at the ILC, the linear e^+e^- collider. The most clean channel of the Higgs boson production at the ILC is the associated

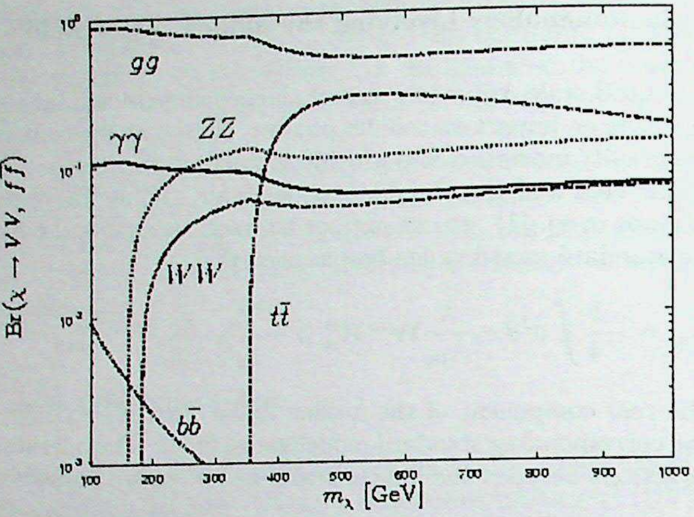

Figure 1. The branching ratio of the hidden scalar (χ) as a function of its mass m_χ for $c_1 = c_2 = c_3 = c_A = 1$.

Higgs production (Higgsstrahlung production), $e^+e^- \to Zh$, through the standard model interaction $\mathcal{L}_{\text{int}} = \frac{m_Z^2}{v} hZ^\mu Z_\mu$. Since the hidden sector scalar χ has the vertex among Z-boson in eq. (3), we can consider the same associated process for the χ production. At the ILC with the collider energy $\sqrt{s} = 1$ TeV, the ratio of the total cross-sections between χ and Higgs boson productions is found to be

$$\frac{\sigma(e^+e^- \to Z\chi)}{\sigma(e^+e^- \to Zh)} \simeq \left(\frac{\Lambda_{\text{IR}}}{1.3\ \text{TeV}}\right)^{-2}, \tag{6}$$

for $c_1 = c_2 = c_3 = c_A = 1$ and $m_\chi = m_{\text{h}} = 120$ GeV.

The coupling manner among χ and the Z-boson pair is different from that of the Higgs boson, and this fact reflects into the difference of the angular distribution of the final state Z-boson. In the high energy limit, we find $\frac{\mathrm{d}\sigma}{\mathrm{d}\cos\theta}(e^+e^- \to Z\chi) \propto 1 + \cos^2\theta$, while $\frac{\mathrm{d}\sigma}{\mathrm{d}\cos\theta}(e^+e^- \to Zh) \propto 1 - \cos^2\theta$. Therefore, even if $m_\chi = m_{\text{h}}$ and the cross-sections of χ and Higgs boson productions are comparable ($\Lambda_{\text{IR}} \sim 1$ TeV), we can distinguish the χ production from the Higgs boson by the difference of the angular dependences. Of course, detecting two photons from the χ decay with the sizable branching ratio $\mathrm{Br}(\chi \to \gamma\gamma) \sim 0.1$ would be an easy way to distinguish χ from Higgs boson, as discussed in the case of the LHC.

4. Summary

We have proposed the low-scale gravity mediation scenario with the warped extra dimension. In this scenario, the effective cutoff on the IR brane is warped down, so that the gravity mediation takes place at low energies. The contact operators relevant to the gravity mediation also provide contact interactions among the hidden sector scalar and the standard model particles. In the case where the effective cutoff scale is low enough, we have investigated collider physics involving the hidden sector scalar field. We have found the possibility that the hidden sector scalar can be discovered at the LHC and the ILC. The hidden sector may be no longer hidden.

References

[1] For a review, see H P Nilles, *Phys. Rep.* **110**, 1 (1984), and references therein
[2] L Randall and R Sundrum, *Phys. Rev. Lett.* **83**, 3370 (1999), arXiv:hep-ph/9905221

PRAMANA
— journal of
physics

© Indian Academy of Sciences

Vol. 69, No. 5
November 2007
pp. 835–838

Model-independent approach for dark matter phenomenology: Signatures in linear colliders and cosmic positron experiments

SHIGEKI MATSUMOTO* and NOBUCHIKA OKADA
Theory Group, KEK, Oho 1-1, Tsukuba, Ibaraki 305-0801, Japan
*E-mail: smatsu@post.kek.jp

Abstract. We have studied the phenomenology of dark matter at the ILC and cosmic positron experiments based on model-independent approach. We have found a strong correlation between dark matter signatures at the ILC and those in the indirect detection experiments of dark matter. Once the dark matter is discovered in the positron experiments such as the PAMELA, its nature will be investigated in detail at the ILC.

Keywords. Dark matter; collider signature; indirect detection using cosmic positrons.

PACS No. 95.35.+d

1. Introduction

Precise measurements of the cosmological parameters have achieved amazing progress in recent years. Especially, the observation of cosmic microwave background anisotropies by the WMAP has revealed the existence of a non-baryonic cold dark matter (DM) [1]. In order to detect the DM, many experiments have been performed and are now on-going. However, the DM has not been discovered yet and its nature still remains a mystery. On the other hand, the LHC experiment may give a clue for the DM, but it is still difficult to investigate its nature in detail.

On the theoretical side, many candidates of the DM have been proposed so far, for example, the lightest supersymmetric particle in the minimal supersymmetric standard model (MSSM) [2], and the lightest Kaluza–Klein particle in the universal extra-dimension model (UED) [3]. However, all these models have not been confirmed experimentally. Thus we do not know what kind of model provides the DM.

The ILC is expected to be an ultimate experiment to investigate the nature of the DM. Therefore, we consider a signature of the DM at the ILC based on model-independent approach. In particular, we focus on the DM pair production associated with a photon. Furthermore, we point out that there is a strong correlation between the signal in this process and that in the indirect detection of the DM using cosmic positrons. The result of the cosmic experiment will give important information for the DM search at the ILC, e.g. its mass and the typical size of the cross-section for the DM pair production.

In the analysis, we postulate that the DM is a weakly interacting massive particle (WIMP), and its cosmological abundance is determined by the thermal relic scenario. The possibility of coannihilations is ignored. Then, the abundance is given by $\Omega_{\rm DM}h^2 \simeq 2 \times 10^{-26}\ {\rm cm}^3/{\rm s}/\langle\sigma v\rangle$, where $\langle\sigma v\rangle$ is the thermal averaged annihilation cross-section of the DM at the freeze-out temperature, $T \sim m/20$. Since the motion of the DM is non-relativistic at the temperature, the cross-section can be expanded by the relative velocity as $\sigma v = \sigma_0 + \sigma_1 v^2 + \sigma_2 v^4 + \cdots$, where σ_0 receives a contribution from s-wave annihilation. Hence, the approximation $\sigma v \simeq \sigma_0$ can be used unless the s-wave annihilation is highly suppressed [4]. The abundance is precisely determined by the WMAP as $\Omega_{\rm DM}h^2 \simeq 0.112$. Thus the cross-section is estimated as $\sigma_0 \simeq 2 \times 10^{-26}\ {\rm cm}^3/{\rm s}$.

Following the paper [5], we introduce two parameters for the model-independent analysis. One is the mass of the DM, m, and the other is the annihilation fraction into e^+e^-, which is defined as $\kappa_e \equiv \sigma v(2{\rm DM} \to e^+e^-)/\sigma_0$. For instance, κ_e is 0.2–0.3 for the Kaluza–Klein DM in the UED.

2. DM signature at the ILC

Since the DM cannot be measured directly by the detector, we need at least one detectable particle associated with the DM pair production [6]. Here we consider the γ associated DM pair production at the ILC. In general, there is no model-independent relation between DM pair productions and those associated with γ. However, since emitted γ is either soft or collinear with the beam, we have such a relation. This method has been developed [5] in the context of the model-independent approach.

The differential cross-section for the energy of the signal γ is

$$\frac{{\rm d}\sigma}{{\rm d}E_\gamma} = \frac{(2s_{\rm DM}+1)^2}{8\sqrt{s}} \left(1 - \frac{4m^2}{(1-2E_\gamma/\sqrt{s})s}\right)^{1/2} \times \int {\rm d}c_\gamma H(2E_\gamma/\sqrt{s}, c_\gamma)\ \kappa_e \sigma_0\ , \tag{1}$$

where s is the center-of-mass energy, $s_{\rm DM}$ is the spin of the DM, and c_γ is the angle between the photon and the incoming beam. The function $H(x, \sin\theta)$ is called the dressing function, and defined as $H(x,c) = (\alpha/\pi)\{1+(1-x)^2\}/x/(1-c^2)$. In figure 1a, some results are shown in cases $m = 150$ GeV with $\sqrt{s} = 500$ GeV and $m = 350$ GeV with $\sqrt{s} = 1$ TeV. We set $s_{\rm DM} = 1$ and $\kappa_e = 0.2$ in both results. In this process, the background comes from $e^+e^- \to \nu\bar{\nu}\gamma$. In figure 1b, the statistical significance for detecting the signal is depicted in the case of 500 fb^{-1} luminosity with $\sqrt{s} = 100$–1000 GeV. From the figure, it seems to be difficult to detect the signal when $\kappa_e < 0.5$. However, if the polarized electron beam is available, the background photon is drastically reduced. Then we will detect the signal even if $\kappa_e \sim 0.1$.

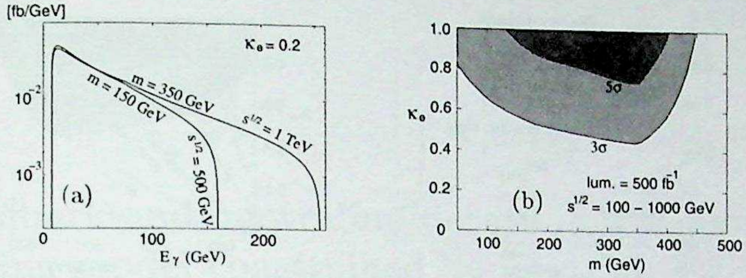

Figure 1. (a) Cross-section for the process $e^+e^- \to 2\mathrm{DM}+\gamma$ as a function of the photon energy E_γ. (b) The statistical significance for detecting the signal.

3. DM signature in cosmic positron experiments

In the present Universe, the DM makes up a halo associated with a galaxy. In the halo, the DM often annihilates and produces high energy positrons. In indirect detection measurement of DM using anti-particles, people try to observe such positrons to explore the nature of DM. In this measurement, main background comes from the cosmic ray (CR). As a result, the signal of DM in the measurement is expected to be observed as the anomalous excess of positrons in CR measurements.

Since the inverse process of the dark matter pair production at the ILC is nothing but the DM annihilation into positrons, we can expect a strong correlation between these signals. Using model-independent parameters, the flux of signal positrons is given by

$$\frac{\mathrm{d}\Phi^{(S)}_{e^+}}{\mathrm{d}E} = \mathrm{BF}\int \mathrm{d}E' G(E,E')\kappa_e\sigma_0. \qquad (2)$$

All information for the modification of the positron spectrum due to the propagation in the galaxy is encoded in the function $G(E,E')$ [8]. As a result, it depends on several astrophysical parameters such as the strength of the magnetic field. Since the positron is absorbed and loses its energy through the propagation in the galaxy, the flux at the earth mostly originates within a few kpc. Hence, the function depends only on the parameters near the solar system, and its ambiguity is small. On the other hand, a relatively large ambiguity comes from the DM density around the solar system. Recent N-body simulations show that the DM is clustered at the local scale, and it leads to an enhancement of the flux. This effect is represented in the boost factor, BF, and its value is expected to be 2–5 [9].

In figure 2a, the cosmic positron fractions are shown in cases of $m = 150$ GeV and 350 GeV with BF = 5. The fraction is defined as the ratio of the positron flux (signal + background) to the combined electron and positron fluxes. We find the clear signature of the DM annihilation at the threshold ($E \sim m$) in this figure. In fact, in the PAMELA [11] (on-going experiment) and the AMS-02 [12] (future experiment), the signal can be discriminated from the background unless κ_e is tiny (see figure 2b).

In realistic cases, high energy positrons from the DM annihilation are also produced through cascade processes, e.g. $2\mathrm{DM}\to b\bar{b} \to e^+$s in addition to the direct

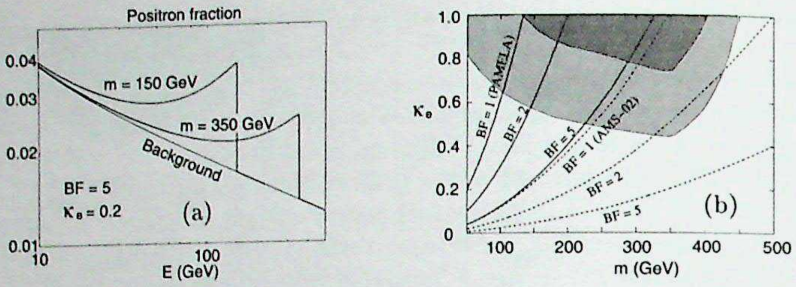

Figure 2. (**a**) Positron fraction as a function of the positron energy. (**b**) The statistical significance for detecting the signal in the PAMELA and the AMS-02 experiments in several cases of BF. In the region above a line, the signal can be discriminated from the background at the 5σ level.

production 2DM$\to e^+e^-$. One might think that these contributions smear the clear signature in figure 2. However, the spectrum of positrons from these cascade decays are very soft, and does not contribute to the signal at the threshold region unless $\kappa_e \ll 1$.

4. Summary

We have performed the model-independent analysis for the DM signatures at the ILC and cosmic positron experiments, and shown that there is a strong correlation between signals in these experiments. Cosmic experiments such as the PAMELA and the AMS-02 will give important information for the DM production at the ILC through the observation of the 'dip' at the threshold region.

References

[1] WMAP Collaboration: D N Spergel *et al*, *Astrophys. J. Suppl.* **148**, 175 (2003)
[2] For review, see G Jungman, M Kamionkowski and K Griest, *Phys. Rep.* **267**, 195 (1996)
[3] T Appelquist, H C Cheng and B A Dobrescu, *Phys. Rev.* **D64**, 035002 (2001)
M Kakizaki, S Matsumoto and M Senami, *Phys. Rev.* **D74**, 023504 (2006)
[4] These DMs are called s-annihilators, and a typical example is higgsino(wino)-like neutralino in the MSSM or the first KK photon in the UED. On the other hand, the example of the DM whose s-wave annihilation is suppressed is bino-like neutralino in the MSSM (for more details, see refs [5,6]).
[5] A Birkedal, K Matchev and M Perelstein, *Phys. Rev.* **D70**, 077701 (2004)
[6] A Birkedal, K T Matchev, M Perelstein and A Spray, arXiv:hep-ph/0507194
[7] Because of the stability of the DM, it will be produced with a pair at colliders.
[8] The function has a very complex form. See ref. [10] for its concrete expression
[9] V Berezinsky, V Dokuchaev and Y Eroshenko, *Phys. Rev.* **D68**, 103003 (2003)
[10] E A Baltz and J Edsjo, *Phys. Rev.* **D59**, 023511 (1999)
J Hisano, S Matsumoto, O Saito and M Senami, *Phys. Rev.* **D73**, 055004 (2006)
[11] PAMELA Collaboration: M Circella, *Nucl. Instrum. Methods* **A518**, 153 (2004)
[12] AMS-02 Collaboration: F Barao, *Nucl. Instrum. Methods* **A535**, 134 (2004)

PRAMANA
— journal of
physics

© Indian Academy of Sciences

Vol. 69, No. 5
November 2007
pp. 839–842

Top squark and neutralino decays in a R-parity violating model constrained by neutrino oscillation data

SUJOY PODDAR
Department of Physics, Jadavapur University, Kolkata 700 032, India
E-mail: sujoy@juphys.ernet.in

Abstract. In a R-parity violating (RPV) model of neutrino mass with three bilinear couplings μ_i and three trilinear couplings λ'_{i33}, where i is the lepton index, we find six generic scenarios each with a distinctive pattern of the trilinear couplings consistent with the neutrino oscillation data. These patterns may be reflected in direct RPV decays of the lighter top squark or in the RPV decays of the lightest superparticle, assumed to be the lightest neutralino. Typical signal sizes at the Tevatron RUN II and the LHC have been estimated and the results turn out to be encouraging.

Keywords. ν-oscillation; R-parity violation; supersymmetry; collider physics.

PACS Nos 11.30.Pb; 13.85.-t; 14.60.Pq; 14.80.Ly

1. Introduction

Neutrino oscillations have confirmed that the neutrinos have tiny masses, several orders of magnitude smaller than other fermion masses in the standard model (SM). The SM being unable to naturally explain the origin of very small neutrino masses, R-parity violating (RPV) supersymmetry (SUSY) could be a viable alternative. In the lepton number violating version of this model, the neutrino masses (Majorana type) and mixing angles [1] can naturally arise without requiring the right-handed neutrinos.

The general R-parity violating superpotential of our interest takes the form:

$$W = W_{\text{MSSM}} + W_{\not{R}_p}, \tag{1}$$

$$W_{\not{R}_p} = \lambda'_{ijk}\epsilon_{ab}L_i^a Q_j^b D_k^c + \mu_i \epsilon_{ab} L_i^a H_2^b. \tag{2}$$

Here, W_{MSSM} is the usual superpotential of the MSSM containing the terms which give mass to the SM fermions [2]. In our work we select a benchmark scenario [3] with a minimal set of six RPV parameters (μ_i, λ'_{i33}; $i = 1, 2, 3$). For the choice of the RPC parameters we have considered some well-motivated models like the gaugino-dominated model, mixed type model, etc. [2].

The tree level and the loop level neutrino mass matrices are given below [1,3]:

$$\mathcal{M}^{\text{tree}}_{\nu_{ij}} = C\mu_i\mu_j, \tag{3}$$

and C is given by

$$C = g_2^2 \frac{(M_1 + \tan^2\theta_W M_2)}{4\det M}\, v_d^2. \tag{4}$$

The one-loop mass matrix is given by

$$\mathcal{M}^{\text{loop}}_{\nu} = \begin{pmatrix} K_2\lambda'^2_{133} & K_2\lambda'_{133}\lambda'_{233} & K_2\lambda'_{133}\lambda'_{333} \\ K_2\lambda'_{133}\lambda'_{233} & K_2\lambda'^2_{233} & K_2\lambda'_{233}\lambda'_{333} \\ K_2\lambda'_{133}\lambda'_{333} & K_2\lambda'_{233}\lambda'_{333} & K_2\lambda'^2_{333} \end{pmatrix}. \tag{5}$$

The neutrino mass eigenstates and the mixing angles are obtained by diagonalizing the full neutrino mass matrix numerically and the oscillation parameters can be calculated. We have generated several billions of sets of RPV parameters for several representative choices of the RPC parameters (C and K_2), out of which only a few sets are allowed by the neutrino oscillation data [4]. Examining the entire allowed parameter space (APS) consistent with the oscillation data we have classified the allowed solutions in six generic scenarios [2].

For $\mu_1 \ll \mu_2, \mu_3$; (a$_1$) $\lambda'_{333} > \lambda'_{133} \geq \lambda'_{233}$, (a$_2$) $\lambda'_{233} > \lambda'_{133} \geq \lambda'_{333}$.

For $\mu_2 \ll \mu_1, \mu_3$; (b$_1$) $\lambda'_{133} \approx \lambda'_{233} \gg \lambda'_{333}$, (b$_2$) $\lambda'_{233} > \lambda'_{333} \gg \lambda'_{133}$.

For $\mu_3 \ll \mu_1, \mu_2$; (c$_1$) $\lambda'_{333} > \lambda'_{133} \gg \lambda'_{233}$, (c$_2$) $\lambda'_{333} > \lambda'_{233} \gg \lambda'_{133}$.

Each scenario has a characteristic hierarchy of λ' couplings which will be reflected in the observed BRs of different RPV decay modes.

2. The lighter top squark decay

In [2], we have considered the lighter top squark to be the next lightest supersymmetric particle (NLSP). The relevant RPV and RPC decay channels of $\tilde{t}_1$ are

$$\text{(a)}\ \ \tilde{t}_1 \to l_i^+ b, \quad \text{(b)}\ \ \tilde{t}_1 \to c\tilde{\chi}_1^0, \quad \text{(c)}\ \ \tilde{t}_1 \to b\tilde{\chi}_1^0 f\bar{f}'. \tag{6}$$

The BRs of the $\tilde{t}_1$ decay modes and competition among the RPV and RPC decays would be highly indicative of the underlying model. In case of the gaugino-like model [2], the RPV decay modes do not dominate although the combined BR of the three RPV modes is appreciable (20–30%) over most of the APS. For the mixed type model [2], most of the allowed solutions have RPV BRs dominating over the RPC BRs [2]. We have also computed the number of several signal events assuming $\int \mathcal{L}\,\mathrm{d}t = 9000\,\mathrm{pb}^{-1}$ corresponding to different dileptonic final states at the Tevatron

Table 1. BRs of the competing decay modes of the lighter top squark in the gaugino-dominated model. Three sets of λ' couplings consistent with oscillation data have been considered: (A) $\lambda'_{133} = 3.72 \times 10^{-5}$, $\lambda'_{233} = 3.3 \times 10^{-5}$ and $\lambda'_{333} = 8.5 \times 10^{-5}$, (B) $\lambda'_{133} = 4.2 \times 10^{-5}$, $\lambda'_{233} = 1.3 \times 10^{-5}$ and $\lambda'_{333} = 8.3 \times 10^{-5}$ and (C) $\lambda'_{133} = 4.2 \times 10^{-5}$, $\lambda'_{233} = 8.6 \times 10^{-5}$ and $\lambda'_{333} = 1.8 \times 10^{-5}$.

Decay modes (BR)	$\tilde{t}_1 \to e^+ b$	$\tilde{t}_1 \to \mu^+ b$	$\tilde{t}_1 \to \tau^+ b$	Loop	Four-body
(A)	0.030	0.024	0.158	0.69	0.10
(B)	0.040	0.004	0.153	0.70	0.11
(C)	0.039	0.163	0.007	0.69	0.10

Table 2. Typical sizes of L_{ij} and L_i events at the Tevatron from top squark pair production using the BRs in table 1.

No. of events	L_{11}	L_{12}	L_{13}	L_{22}	L_{23}	L_{33}	L_1	L_2	L_3
(A)	3	5	34	2	27	91	152	121	804
(B)	5	1	44	0	4	86	206	20	709
(C)	5	46	2	97	8	0	198	829	35

Table 3. BRs of different decay modes of the LSP in the higgsino-dominated model and the gaugino-dominated model.

Decay modes	BR (%) in higgsino model	BR (%) in gaugino model
$\tilde{\chi}_1^0 \to \not{E}_T b\bar{b}$	12.5	79.7
$\tilde{\chi}_1^0 \to te\bar{b}$	19.3	3.7
$\tilde{\chi}_1^0 \to t\mu\bar{b}$	67.7	16.2
$\tilde{\chi}_1^0 \to t\tau\bar{b}$	0.5	0.4

RUN-II at a fixed $\tilde{t}_1$ mass. The signal $\tilde{t}_1\tilde{t}_1^* \to l_i^+\bar{b}l_j^- b$ is abbreviated as L_{ij}. We have also discussed another interesting signal L_i which arises if one of the produced top squarks decays via the RPV mode while the other decays via the loop-induced mode followed by the LSP decay ($\tilde{\chi}_1^0 \to \nu_i b\bar{b}$) leading to $\tilde{t}_1\tilde{t}_1^* \to l_i^+ bc\nu b\bar{b}$ or $l_i^- \bar{b}\bar{c}\nu b\bar{b}$. The BRs of various $\tilde{t}_1$ decay modes are given in table 1.

The number of signal events for Tevatron RUN II are presented in table 2.

3. LSP decay

Unless $m_{\tilde{\chi}_1^0} > m_t$, LSP decay ($\tilde{\chi}_1^0 \to \nu_i b\bar{b}$) alone cannot provide detailed information about the L-violating nature of the underlying model of m_ν.

If $m_{\tilde{\chi}_1^0} > m_t$ the following additional decay modes open up:

$$\text{(a) } \tilde{\chi}_1^0 \to e\bar{b}t, \quad \text{(b) } \tilde{\chi}_1^0 \to \mu\bar{b}t, \quad \text{(c) } \tilde{\chi}_1^0 \to \tau\bar{b}t. \tag{7}$$

We have compared the BRs of different leptonic decay channels of the LSP considering the gaugino-dominated model and the higgsino-dominated model in table 3.

We have studied gaugino pair production followed by cascades from RPC and RPV decays in the higgsino-dominated model at the LHC [2]. We have also checked that apart from a small region of the APS the LSP decay will be inside the detector.

4. Future prospects

We can estimate the RPC parameters from the edges of various kinematical distributions and by reconstructing the mass from fully visible events (e.g., $\tilde{t}_1 \to l_i^+ b$). Determination of RPV parameters from the measured BRs can test the underlying model. The BRs can be determined more accurately at the ILC and even rare decay modes may be useful.

References

[1] For a recent review, see for e.g., S Rakshit, *Mod. Phys. Lett.* **A19**, 2239 (2004)

[2] For details, notations and further references, see S P Das, Amitava Datta and S Poddar, *Phys. Rev.* **D73**, 075014 (2006)

[3] A Abada and M Losada, *Phys. Lett.* **B492**, 310 (2000)

[4] For neutrino oscillation data, see for e.g., M Maltoni *et al*, *New. J. Phys.* **6**, 122 (2004)

PRAMANA
— journal of
physics

© Indian Academy of Sciences

Vol. 69, No. 5
November 2007
pp. 843–847

Testing the supersymmetric QCD Yukawa coupling in a combined LHC/ILC analysis

A FREITAS[1,*] and P Z SKANDS[2]
[1]Institut für Theoretische Physik, Universität Zürich, Winterthurerstrasse 190, CH-8057 Zürich
[2]Theoretical Physics, Fermi National Accelerator Laboratory, Batavia, IL 60510-0500, USA
*E-mail: afreitas@physik.unizh.ch

Abstract. In order to establish supersymmetry (SUSY) at future colliders, the identity of gauge couplings and the corresponding Yukawa couplings between gauginos, sfermions and fermions needs to be verified. A first phenomenological study for determining the Yukawa coupling of the SUSY-QCD sector is presented here, using a method which combines information from LHC and ILC.

Keywords. Supersymmetry; quantum chromodynamics.

PACS Nos 11.30.Pb; 14.80.Ly; 13.85.-t

One of the fundamental relations in softly broken supersymmetric theories is the equality between the Yukawa coupling $\hat{g}$ of a gaugino interacting with a fermion and an sfermion and the corresponding standard model (SM) gauge coupling g of a gauge boson and two (s)fermions, $g = \hat{g}$. At colliders, this relation can be investigated through the production cross-sections for SUSY particles. Within the minimal supersymmetric standard model (MSSM), it has been shown [1–4] that the SUSY Yukawa couplings in the electroweak sector can be precisely tested at the per cent level at a high-energy e^+e^- collider (ILC).

However, the analysis of the SUSY Yukawa coupling $\hat{g}_s$ in the QCD sector is much more difficult. At the ILC this interaction could be studied in the process $e^+e^- \to q\tilde{q}^*\tilde{g}$, $\bar{q}\tilde{q}\tilde{g}$ [5], but suffers from very low rates and large backgrounds. At the LHC on the other hand, squarks and gluinos with masses below 2–3 TeV are abundantly produced, and their pair production cross-sections depend directly on $\hat{g}_s$. However, measurements of total cross-sections are exceedingly difficult at hadron colliders, with typically only one or two specific decay channels of the squarks and gluinos experimentally accessible [6].

In this contribution, a combination of ILC and LHC measurements is considered, where the relevant branching ratios are to be determined at ILC and combined with exclusive cross-section measurements in selected channels at the LHC.

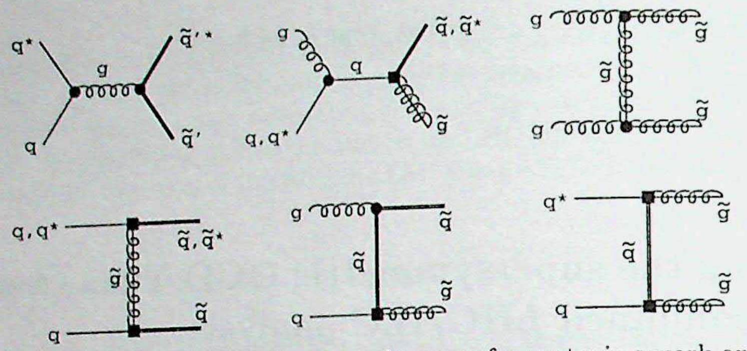

Figure 1. Examples for Feynman diagrams for partonic squark and gluino production in pp collisions. Dots indicate the gauge coupling g_s, squares the Yukawa coupling $\hat{g}_s$.

In pp collisions, squarks and gluinos can be produced in various combinations (see figure 1). The production of same-sign squarks ($\tilde{u}_L\tilde{u}_L, \ldots$) is especially interesting, since it only proceeds through the diagram in the lower left of figure 1, and thus depends solely on the SUSY Yukawa coupling $\hat{g}_s$. In pp collisions this process dominantly produces $\tilde{u}$ and $\tilde{d}$ squarks, in direct proportion to the quark content of the proton.

While the typically lighter $\tilde{q}_R$ almost exclusively decays directly into the lightest neutralino and a quark jet, thus not allowing charge tagging, for the heavier $\tilde{q}_L$ the charge of the squark can be tagged through a chargino decay chain,

$$\tilde{u}_L \to d\tilde{\chi}_1^+ \to dl^+\nu_l\tilde{\chi}_1^0, \quad \tilde{d}_L \to u\tilde{\chi}_1^- \to ul^-\bar{\nu}_l\tilde{\chi}_1^0. \tag{1}$$

The production of same-sign squarks with this decay channel will thus lead to two same-sign leptons, two hard jets and missing transverse energy in the final state. Other direct squark production processes on the other hand will tend to produce opposite-sign leptons.

A very problematic background can come from gluino pair and mixed gluino-squark production if $m_{\tilde{g}} > m_{\tilde{q}_L}$. In this case, gluinos can decay into quarks and squarks, $\tilde{g} \to q\tilde{q}_L$, generating a component of two same-sign squarks plus additional jets. This background is very challenging if the mass difference $m_{\tilde{g}} - m_{\tilde{q}_L}$ is small, since then the additional jets from the gluino decay will be soft. In the following we will only consider a scenario where the mass difference $m_{\tilde{g}} - m_{\tilde{q}_L}$ is sufficiently large to allow a veto on additional jets for gluino background reduction. We use a modification of the SPS1a scenario [7], where the gluino mass is raised to 700 GeV.

The most important backgrounds from standard model sources are $W^\pm W^\pm jj$, where j is a light-flavor jet, and semi-leptonic $t\bar{t}$, with the second lepton coming from the decay of a b quark. Due to the large total $t\bar{t}$ cross-section, this can result in a sizable background.

We compute numerical results for expected signal and background levels including some simple estimates for the detector response and resolution (see [8] for details), but do not perform a real experimental analysis. In our scenario, the chargino mainly decays into scalar taus, which subsequently decay into taus. To trace the charge explicitly, here we only consider the leptonic tau branching fraction in the decay chain

Table 1. Signal and background cross-sections for progressive application of cuts.

Cross-sections $\sum_{q=u,d,s,c} \sigma$ (fb)	Signal $\tilde{q}_{\rm L}\tilde{q}_{\rm L}$	Backgrounds **Sum**	$t\bar{t}$	$W^{\pm}W^{\pm}jj$	$\tilde{q}_{\rm L}\tilde{g}$	$\tilde{q}_{\rm L}\tilde{q}_{\rm L}^{*}$	$\tilde{g}\tilde{g}$
Total	2100	–	8×10^5	–	7000	1350	3200
Preselection	49.2	384.6	177.7	–	136.4	23.2	47.3
b-veto	17.1	31.4	13.0	–	10.3	7.1	1.0
$\not{E} > 150$ GeV	15.1	22.2	6.1	–	9.0	6.2	0.9
$p_{{\rm T},j_3} < 50$ GeV	7.8	5.9	2.4	N/A	1.0	2.5	0.03
$p_{{\rm T},j_1} > 200$ GeV	**7.0**	**<4.9**	1.0	<0.7	0.8	2.3	0.03

$$\tilde{u}_{\rm L} \xrightarrow{65\%} d\,\tilde{\chi}_1^+ \xrightarrow{100\%} d\,\tau^+\,\nu_\tau\,\tilde{\chi}_1^0 \xrightarrow{35\%} d\,\ell^+ + \not{E}, \quad \ell = e,\,\mu, \tag{2}$$

and similarly for $\tilde{d}_{\rm L}$. Both signal and top and gluino backgrounds were simulated with PYTHIA 6.326 [9], while the $WWjj$ background was generated with MADEVENT [10]. The cross-sections for squark, gluino and top production were normalized with the K-factors for next-to-leading order QCD corrections [11], while for the $W^{\pm}W^{\pm}jj$ background only leading order results are available.

As a first step, the following pre-selection cuts are applied: at least 100 GeV transverse missing energy, at least 2 jets with $p_{{\rm T},j} > 100$ GeV, and two isolated leptons $\ell = e, \mu$ with $p_{{\rm T},\ell} > 7$ GeV. At this level, most backgrounds are still larger than the signal (see table 1).

Using a b-veto is effective against the gluino and $t\bar{t}$ backgrounds. A high efficiency of $\epsilon = 90\%$ reduces the background substantially, at the price of a high mistagging $D = 25\%$ rate for the signal. The large SM backgrounds can be further suppressed by a cut on the missing transverse energy $\not{E}$, with $\not{E} > 150$ GeV. At this point, the gluino-related backgrounds dominate. They are reduced by a cut on hard additional jets. By rejecting all events with $p_{{\rm T},j3} > 50$ GeV, the ratio of the signal to gluino background is markedly improved. Finally, increasing the transverse momentum cut on the first jet to $p_{{\rm T},j1} > 200$ GeV, the top background is suppressed further, resulting in the cross-section estimate in table 1. The signal-to-background ratio is 1.4, sufficient to allow a meaningful measurement. With an integrated luminosity of 100 fb^{-1}, the statistical error on the same-sign squark cross-section is 4.9%.

In order to obtain from the measured rates at the LHC the total squark production cross-section, the individual branching ratios (BRs) in the decay chain (eq. (2)) must be determined. Here we explore, how these could be extracted from measurements at ILC.

The chargino BRs can be determined from chargino pair production. Due to the large cross-section for that process, all possible chargino decay channels can be easily separated from backgrounds, and the expected error on the BR is about 1%.

In the given scenario the L-squarks are slightly too heavy to be accessible at a 1 TeV linear collider. Here, we instead analyse the production of squarks for a hypothetical e^+e^- collider with a center-of-mass energy of about 1.5 TeV.

The L-squarks can decay into the whole spectrum of charginos and neutralinos. While in our scenario the light charginos and neutralinos decay into taus, the heavier

Table 2. Combination of statistical and systematic errors for the same-sign squark cross-section at the LHC and the derivation of the strong SUSY-Yukawa coupling.

	$\sigma(\tilde{q}_{\rm L}\tilde{q}_{\rm L})$ (%)	$\hat{g}_{\rm s}/g_{\rm s}$ (%)
LHC signal statistics	4.9	1.3
SUSY-QCD Yukawa coupling in $\tilde{q}_{\rm L}\tilde{g}$ background	2.4	0.6
PDF uncertainty	10	2.4
NNLO corrections	8	2.0
Squark mass $\Delta m_{\tilde{q}_{\rm L}} = 9$ GeV	6	1.5
$\mathrm{BR}(\tilde{q}_{\rm L} \to q'\,\tilde{\chi}_1^{\pm})$	8.2	2.0
	17.3	4.1

states have large BRs into gauge bosons, and can be distinguished through these channels (see [8] for details). The tau leptons in the final state can be identified in their hadronic decay mode with roughly 80% tagging efficiency.

For this work, Monte-Carlo samples for squark pair production in the different squark decay channels have been generated at the parton level with the tools of ref. [4]. Also the most relevant backgrounds have been simulated, stemming from double and triple gauge boson production as well as $t\bar{t}$ production. It is assumed that an integrated luminosity of 500 fb^{-1} is spent for a polarization combination $P(e^+)/P(e^-) = +50\%/-80\%$, which enhances the production cross-section both for $\tilde{u}_{\rm L}$ and $\tilde{d}_{\rm L}$ production. Here $\mp$ indicates left/right-handed polarization. The BRs are obtained from measuring the cross-sections of all accessible decay modes of the squarks and identifying the fraction of decays into one specific decay mode out of these.

Since the squarks are produced in charge-conjugated pairs, it is *a priori* difficult to distinguish up- and down-squarks in the final state. However, assuming universality between the first two generations, a separation between up- and down-type squarks can be obtained through charm tagging. According to ref. [12], a c-tagging efficiency of 40% is achievable for a purity of 90%. By combining the different decay channels, the following final state signatures are identified as interesting: $jj(n\tau)\not{E}$ with $n \in \{1,2,3,4\}$, $cc(n\tau)\not{E}$ with $n \in \{2,4\}$, $jj\tau\tau(Z/W)\not{E}$, $cc\tau\tau Z\not{E}$, where j indicates an untagged jet, c a tagged charm jet, and Z/W a hadronically decaying gauge boson where the invariant mass of the two jets combines to the given gauge boson mass. Since several squark decay channels can contribute to most of the final states above, one has to solve a linear equation system in order to derive the individual contributions. With this procedure we estimate the precision for the BRs of the squarks into charginos to be $\mathrm{BR}(\tilde{u}_{\rm L} \to d\tilde{\chi}_1^+) = (67.7 \pm 3.2)\%$ and $\mathrm{BR}(\tilde{d}_{\rm L} \to u\tilde{\chi}_1^-) = (63.9 \pm 5.2)\%$.

Based on the simulations for squark production at the LHC and the ILC presented above, one can now derive an estimate for the precision for the determination of the strong SUSY Yukawa coupling $\hat{g}_{\rm s}$. The statistical uncertainty is combined with the most important systematic error sources in table 2. We considered the following systematic error sources. The remaining background from gluino production at the LHC introduces a systematic error since it depends on $\hat{g}_{\rm s}$, which is estimated by varying $\hat{g}_s$. The uncertainty from the proton parton distribution functions (PDFs) is evaluated by comparing results for different CTEQ PDFs [13]. The uncertainty of the missing $\mathcal{O}(\alpha_s^2)$ radiative corrections are estimated by varying the renormalization scale of the $\mathcal{O}(\alpha_s)$ corrected cross-section within a factor two. Furthermore, the cross-section depends on the values of the squark masses, which according to ref. [6] can be determined with an error better than $\Delta m_{\tilde{q}_L} = 9$ GeV. Finally, the expected error for the determination of the squark branching ratios at the linear collider must be included. Combining all error sources in quadrature, it is found that the SUSY-QCD Yukawa coupling $\hat{g}_s$ can be determined with an error 4.1% in the given scenario.

References

[1] J L Feng, M E Peskin, H Murayama and X Tata, *Phys. Rev.* **D52**, 1418 (1995)

[2] S Y Choi *et al*, *Euro. Phys. J.* **C14**, 535 (2000)
S Y Čhoi, J Kalinowski, G Moortgat-Pick and P M Zerwas, *Euro. Phys. J.* **C22**, 563 (2001)

[3] M M Nojiri, K Fujii and T Tsukamoto, *Phys. Rev.* **D54**, 6756 (1996)
H C Cheng, J L Feng and N Polonsky, *Phys. Rev.* **D57**, 152 (1998)

[4] A Freitas, A v Manteuffel and P M Zerwas, *Euro. Phys. J.* **C34**, 487 (2004); **C40**, 435 (2005)

[5] A Brandenburg, M Maniatis and M M Weber, hep-ph/0207278

[6] LHC/LC Study Group: G Weiglein *et al*, hep-ph/0410364

[7] B C Allanach *et al*, *Euro. Phys. J.* **C25**, 113 (2002)

[8] A Freitas and P Z Skands, hep-ph/0606121

[9] T Sjöstrand, L Lönnblad, S Mrenna and P Skands, hep-ph/0308153

[10] F Maltoni and T Stelzer, *J. High Energy Phys.* **0302**, 027 (2003)

[11] W Beenakker, R Höpker, M Spira and P M Zerwas, *Nucl. Phys.* **B492**, 51 (1997)

[12] S M Xella Hansen *et al*, LC-PHSM-2003-061, www-flc.desy.de/lcnotes/

[13] J Pumplin *et al*, *J. High Energy Phys.* **0207**, 012 (2002)

PRAMANA
— journal of
physics

© Indian Academy of Sciences

Vol. 69, No. 5
November 2007
pp. 849–854

Probing space–time structure of new physics with polarized beams at the international linear collider

B ANANTHANARAYAN
Centre for High Energy Physics, Indian Institute of Science, Bangalore 560 012, India
E-mail: anant@cts.iisc.ernet.in

Abstract. At the international linear collider large beam polarization of both the electron and positron beams will enhance the signature of physics due to interactions that are beyond the standard model. Here we review our recently obtained results on a general model-independent method of determining for an arbitary one-particle inclusive state the space–time structure of such new physics through the beam polarization dependence and angular distribution of the final state particle.

Keywords. e^+e^- collisions; polarization; beyond the standard model interactions.

PACS Nos 13.88.+e; 13.66.-a; 12.60.-i

1. Introduction

At the international linear collider, the possibility of considerable beam polarization has led to a series of investigations on using this as a diagnostic aid for new physics arising due to beyond the standard model interactions (BSM) (for a recent review, see ref. [1]). We recently considered the possibility of observing CP-violating asymmetries in $t\bar{t}$ production with transversely polarized beam [2]. It was shown that only interactions that transform under the Lorentz transformations as pseudoscalar (P), scalar (S) and tensor (T) interactions could contribute. The fact that axial-vector (A) and vector (V) interactions will not contribute to CP-violating asymmetries with transverse beam polarization could have partly been deduced from some general results available in the literature for a general single-particle inclusive process, albeit for the case that the 'new physics' amplitudes interfere with the QED part of the standard model (SM) amplitudes [3].

These general results do not directly apply to other processes of interest, e.g., $Z\gamma$ production, where the SM production goes via t- and u-channel amplitudes, in contrast to the case of $t\bar{t}$ production where the SM production goes via s-channel amplitudes. Therefore, the general results available in the literature do not apply to the latter process and a case by case study has had to be performed [4–6].

Indeed, as mentioned earlier, general results involving both the QED as well as the neutral current amplitudes for single-particle inclusive process would be of general interest, as well as the extension to t- and u-channel processes. Here we review our recently obtained results on the subject [7]. It may also be noted that our results are sufficiently general to permit a discussion of features of, e.g., chargino and neutralino production in the minimal supersymmetric standard model (MSSM).

We note here that we do not give an extended bibliography on the subject and instead refer to the same in ref. [7].

2. Correlations and their features

The process of interest to us here is the one-particle inclusive process

$$e^-(p_-) + e^+(p_+) \to H(p) + X,$$

where H is a final-state particle, whose momentum p is measured, but not the spin, and X is an inclusive state. The process is assumed to occur through an s-channel exchange of a γ and a Z in the SM, and through a new current whose coupling to e^+e^- can be of the type V, A, or S, P, or T. We calculate the relevant factor in the interference between the standard model currents with the BSM currents as

$$\mathrm{Tr}[(1-\gamma_5 h_+ + \gamma_5 \not{s}_+)\not{p}_+ \gamma_\mu (g_\mathrm{V}^e - g_\mathrm{A}^e \gamma_5)(1+\gamma_5 h_- + \gamma_5 \not{s}_-)\not{p}_- \Gamma_i] H^{i\mu}.$$

Here $g_\mathrm{V}^e, g_\mathrm{A}^e$ are the vector and axial-vector couplings of the photon or Z to the electron current, and Γ_i is the corresponding coupling to the new physics current, $p_\pm$ are the four-momenta of $e^\pm$, $h_\pm$ are the helicities (in units of $\frac{1}{2}$) of $e^\pm$, and $s_\pm$ are respectively their transverse polarizations. For details on the notation which are spelt out in great detail, see ref. [7]. We should of course add the contributions coming from photon exchange and Z exchange, with the appropriate propagator factors. However, we give here the results for Z exchange, from which the case of photon can be deduced as a special case. The tensor $H^{i\mu}$ stands for the interference between the couplings of the final state to the SM current and the new physics current, summed over final-state polarizations, and over the phase space of the unobserved particles X. It is only a function of the momenta $q = p_- + p_+$ and p. The implied summation over i corresponds to a sum over the forms V, A, S, P, T, together with any Lorentz indices that these may entail.

We now determine the forms of the matrices Γ_i and the tensors $H^{i\mu}$ in the various cases, using only Lorentz covariance properties. We set the electron mass to zero. Consider now the three cases:

1. *Scalar and pseudoscalar case*: In this case, there is no free Lorentz index for the leptonic coupling. Consequently, we can write it as

$$\Gamma = g_\mathrm{S} + i g_\mathrm{P}\gamma_5.$$

The tensor $H^{i\mu}$ for this case has only one index, viz., μ. Hence the most general form for H is

$$H_\mu^\mathrm{S} = F(q^2, p\cdot q)p_\mu,$$

where F is a function of the Lorentz-invariant quantities q^2 and $p \cdot q$.

2. *Vector and axial-vector case*: The leptonic coupling for this case can be written as

$$\Gamma_\mu = \gamma_\mu (g_{\rm V} - g_{\rm A}\gamma_5).$$

The tensor H for this case has two indices, and can be written as

$$H^{\rm V}_{\mu\nu} = -g_{\mu\nu} W_1(q^2, p\cdot q) + p_\mu p_\nu W_2(q^2, p\cdot q) + \epsilon_{\mu\nu\alpha\beta} q^\alpha p^\beta W_3(q^2, p\cdot q),$$

where now there are three invariant functions, W_1, W_2, W_3.

3. *Tensor case*: In the tensor case, the leptonic coupling is

$$\Gamma_{\mu\nu} = g_{\rm T}\sigma_{\mu\nu}.$$

The tensor H for this case can be written in terms of the four invariant functions F_1, F_2, PF_1, PF_2 as

$$\begin{aligned} H^{\rm T}_{\mu\rho\tau} = {} & (q_\rho p_\tau - q_\tau p_\rho) p_\mu F_1(q^2, p\cdot q) + (g_{\rho\mu} p_\tau - g_{\tau\mu} p_\rho) F_2(q^2, p\cdot q) \\ & + \epsilon_{\rho\tau\alpha\beta} p^\alpha q^\beta p_\mu PF_1(q^2, p\cdot q) + \epsilon_{\rho\tau\mu\alpha} p^\alpha PF_2(q^2, p\cdot q). \end{aligned}$$

Evaluating the trace in each case, we present the results in tables 1–3, with $\vec{K} \equiv (\vec{p}_- - \vec{p}_+)/2 = E\hat{z}$, where $\hat{z}$ is a unit vector in the z-direction, E is the beam energy, and $\vec{s}_\pm$ lie in the x–y plane for $g^e_{\rm A}$ alone. The tables corresponding to $g^e_{\rm V}$ alone are not given, and was the case considered in ref. [3] for the interference of QED amplitudes with physics due to the then undetermined amplitude of the neutral current due to Z.

In tables 1–3, are also given the charge conjugation C and parity P properties of the various correlations, under the assumption that the final-state particle observed is self-conjugate, viz., $H = \bar{H}$. If it is not self-conjugate, then the C factor given in the tables would apply to the sum of the cross-sections for production of H and $\bar{H}$. The difference of these cross-sections would take a C factor of the opposite sign. The counting of the number of independent correlations for the vector and axial-vector cases turns out to be subtle, and is described at length in ref. [7].

We might like to use the behaviour of the differential cross-section to construct asymmetries which can test symmetry properties like CP. Tables 1–3 may be employed to make some predictions for what to expect. It is possible to make general deductions in the special case when the final state is a two-particle state. Within that, we consider two possibilities:

Table 1. List of S, P correlations for $g^e_{\rm A}$.

Term	Correlation	P	C
$\mathrm{Im}(g_{\rm P}F)$	$2E^2(h_+\vec{s}_- + h_-\vec{s}_+)\cdot\vec{p}$	+	+
$\mathrm{Im}(g_{\rm S}F)$	$2E[\vec{K}\cdot(h_+\vec{s}_- - h_-\vec{s}_+)\times\vec{p}]$	−	+
$\mathrm{Re}(g_{\rm S}F)$	$2E^2\,\vec{p}\cdot(\vec{s}_+ + \vec{s}_-)$	−	+
$\mathrm{Re}(g_{\rm P}F)$	$2E\,[\vec{K}\cdot(\vec{s}_+ - \vec{s}_-)\times\vec{p}]$	+	+

Table 2. List of V, A correlations for g_A^e.

Term	Correlation	P	C
$\mathrm{Re}(g_V W_1)$	$4E^2(h_+ - h_-)$	$-$	$-$
$\mathrm{Re}(g_A W_1)$	$-4E^2(h_+h_- - 1)$	$+$	$+$
$\mathrm{Re}(g_V W_2)$	$2(\vec{K}\cdot\vec{K}\,\vec{p}\cdot\vec{p} - (\vec{p}\cdot\vec{K})^2)(h_+ - h_-)$	$-$	$-$
$\mathrm{Re}(g_A W_2)$	$-2[-2E^2\vec{p}\cdot\vec{s}_-\vec{p}\cdot\vec{s}_+ + (\vec{K}\cdot\vec{K}\,\vec{p}\cdot\vec{p} - (\vec{p}\cdot\vec{K})^2)$ $(h_+h_- - 1 + \vec{s}_+\cdot\vec{s}_-)]$	$+$	$+$
$\mathrm{Im}(g_V W_3)$	$-8E^2(\vec{p}\cdot\vec{K})(h_+h_- - 1)$	$+$	$-$
$\mathrm{Im}(g_A W_3)$	$8E^2(\vec{p}\cdot\vec{K})(h_+ - h_-)$	$-$	$+$
$\mathrm{Im}(g_V W_2)$	$-2E(\vec{p}\cdot\vec{s}_+[\vec{K}\cdot\vec{s}_- \times \vec{p}] + \vec{p}\cdot\vec{s}_-[\vec{K}\cdot\vec{s}_+ \times \vec{p}])$	$-$	$-$

Table 3. List of T correlations for g_A^e.

Term	Correlation	P	C
$\mathrm{Im}(g_T F_1)$	$-8E^2\vec{p}\cdot\vec{K}[\vec{p}\cdot(\vec{s}_+ + \vec{s}_-)]$	$-$	$-$
$\mathrm{Im}(g_T F_2)$	$-4E^2\vec{p}\cdot(\vec{s}_+ - \vec{s}_-)$	$-$	$-$
$\mathrm{Im}(g_T PF_1)$	$-8E\vec{p}\cdot\vec{K}[\vec{K}\cdot(\vec{s}_+ - \vec{s}_-)\times\vec{p}]$	$+$	$-$
$\mathrm{Im}(g_T PF_2)$	$4E[\vec{K}\cdot(\vec{s}_+ + \vec{s}_-)\times\vec{p}]$	$+$	$-$
$\mathrm{Re}(g_T F_1)$	$8E\vec{p}\cdot\vec{K}[\vec{K}\cdot(h_+\vec{s}_- - h_-\vec{s}_+)\times\vec{p}]$	$-$	$-$
$\mathrm{Re}(g_T F_2)$	$-4E[\vec{K}\cdot(h_+\vec{s}_- + h_-\vec{s}_+)\times\vec{p}]$	$-$	$-$
$\mathrm{Re}(g_T PF_1)$	$8E^2\vec{p}\cdot\vec{K}[\vec{p}\cdot(h_+\vec{s}_- + h_-\vec{s}_+)]$	$+$	$-$
$\mathrm{Re}(g_T PF_2)$	$4E^2\vec{p}\cdot(h_+\vec{s}_- - h_-\vec{s}_+)$	$+$	$-$

Case 1: $H = \bar{H}$. The simplest case to consider is when H is self-conjugate, i.e., $H = \bar{H}$.

Case 2: $H \neq \bar{H}$. As mentioned earlier, in this case, the C properties in the tables refer to the sum

$$\Delta\sigma^+ = \Delta\sigma + \Delta\bar{\sigma},$$

where $\Delta\sigma$ and $\Delta\bar{\sigma}$ are partial cross-sections corresponding respectively to H and $\bar{H}$ production. The difference of these,

$$\Delta\sigma^- = \Delta\sigma - \Delta\bar{\sigma},$$

will have the opposite C property.

We have further considered two special cases: when the final state consists of a pair of conjugate particles $H\bar{H}$, and when it consists of two particles $H\bar{H}'$, where $H' \neq H$.

Case 2a: $X \equiv \bar{H}$.

Case 2b: $X \equiv \bar{H}'$, $H \neq H'$.

The specific properties are discussed in great detail in ref. [7].

3. Extensions and applications

So far we have dealt with a scenario where the SM interactions take place through s-channel γ and Z exchanges. This is most suitable for production of particles which have no direct coupling to e^- and e^+. However, for production of gauge bosons in the SM, which couple directly to e^+e^-, there would be a t-channel and/or u-channel lepton exchange. In ref. [7] we have provided a detailed discussion on what conclusions one may draw regarding the correlations for this process and the CP properties thereof, for the particular case of $Z\gamma$ production. The crucial factor in this adaptation is the fact that for $m_e = 0$, the only contributions which survive correspond to opposite e^- and e^+ helicities. For, any final-state particles which may be emitted from an electron line with a flip of electron helicity (as for example, a Higgs boson) will have vanishing coupling in the limit of $m_e = 0$. We are thus left in the most general case with only chirality-conserving combinations of Dirac matrices, sandwiched between electron and positron spinors of opposite helicities. Such a combination of Dirac matrices is a product of odd number of them. For massless spinors, they can always be reduced to a linear combination of γ_μ and $\gamma_\mu\gamma_5$. We are thus back to the case of V and A couplings in the s-channel considered in the foregoing, except that the coefficients $g_{\rm V}^e$ and $g_{\rm A}^e$ would now be replaced by something more complicated. In fact, they could contain tensors constructed out of momenta occurring in the process. It is possible to absorb these tensors into the definition of the H tensor, and the final result would be that we could still use the tables we have obtained so far, with appropriate redefinitions of $g_{\rm V}^e$, $g_{\rm A}^e$ and the form factors.

One further application presented in ref. [7] is for the S, P and T case, where it is possible to have CP-odd observables, and of the possible ones listed therein, the ones which occur in the special case of lowest-dimensional observables are $\mathrm{Re}(g_{\rm P}F)$ and $\mathrm{Re}(g_{\rm T}F_2)$, corresponding respectively to the four-Fermi couplings $\mathrm{Im}(S_{RR})$ and $\mathrm{Im}(T_{RR})$ in the notation of [2]. The special features observed in that work, viz., that the four-Fermi scalar coupling terms occur with only the $g_{\rm A}^e$ coupling at the electron vertex, and that the tensor coupling terms occur with only the $g_{\rm V}^e$ at the electron vertex, are borne out by our general results.

In ref. [7], it was further shown that some features of our treatment can be carried over to an extension of SM, like the MSSM, using as illustrations chargino and neutralino pair productions. We have also considered popular scenarios for BSM physics, resulting from either extra-dimensional models or from non-commutative models.

The work reviewed here is presently being extended to the processes $e^+e^- \to h_1(p_1)h_2(p_2)X$ and to $e^+e^- \to h(p,s)X$.

Acknowledgements

We thank the Council for Scientific and Industrial Research for support during the course of these investigations under scheme number 03(0994)/04/EMR-II, as well as the Department of Science and Technology, Government of India, and K Shivaraj and A Upadhyay for reading the manuscript.

References

[1] G A Moortgat-Pick *et al*, arXiv:hep-ph/0507011

[2] B Ananthanarayan and S D Rindani, *Phys. Rev.* **D70**, 036005 (2004), arXiv:hep-ph/0309260

[3] G V Dass and G G Ross, *Nucl. Phys.* **B118**, 284 (1977)
G V Dass and G G Ross, *Phys. Lett.* **B57**, 173 (1975)

[4] B Ananthanarayan, S D Rindani, R K Singh and A Bartl, *Phys. Lett.* **B593**, 95 (2004); Erratum, *Phys. Lett.* **B608**, 274 (2005), arXiv:hep-ph/0404106

[5] B Ananthanarayan and S D Rindani, *Phys. Lett.* **B606**, 107 (2005), arXiv:hep-ph/0410084

[6] B Ananthanarayan and S D Rindani, *J. High Energy Phys.* **0510**, 077 (2005), arXiv:hep-ph/0507037

[7] B Ananthanarayan and S D Rindani, *Euro. Phys. J.* **C46**, 705 (2006), arXiv:hep-ph/0601199

PRAMANA
— journal of
physics

© Indian Academy of Sciences

Vol. 69, No. 5
November 2007
pp. 855–860

Signals of universal extra dimension at the international linear collider

BIPLOB BHATTACHERJEE
Department of Physics, Calcutta University, 92 A.P.C. Road, Kolkata 700 009, India
E-mail: biplobb81@yahoo.co.in

Abstract. In the minimal universal extra dimension model, single production of $n = 2$ gauge bosons provides a unique discriminating feature from supersymmetry. We discuss how the proposed international linear collider can act as a $n = 2$ factory, much in the same vein as LEP.

Keywords. Universal extra dimension; electron–positron collider.

PACS Nos 11.25.Mj; 14.80.Cp

1. Introduction

In the simplest universal extra dimension (UED) model proposed by Appelquist *et al* [1], there is only one extra dimension, denoted by y, compactified on a circle (S_1) of radius R. All SM particles can access this dimension. To get chiral fermions at low-energy, one must impose a further $\mathcal{Z}_2$ symmetry $(y \leftrightarrow -y)$, so that finally we have an $S_1/\mathcal{Z}_2$ orbifold. As is well-known, a higher dimension theory is nonrenormalisable and should be treated in the spirit of an effective theory valid up to a scale $\Lambda > R^{-1}$. All fields have five space-time components; when brought down to four dimensions, for each low-mass (zero-mode) standard model (SM) particle of mass m_0, we get an associated Kaluza–Klein (KK) tower, the nth level (this n is the KK number of the particle) of which has a mass given by $m_n^2 = m_0^2 + \frac{n^2}{R^2}$. This is a tree-level relationship and gets modified once we take into account the radiative corrections. The KK number is conserved in the tree-level theory; this means that the lowest-mass $n = 1$ particle, which turns out to be the $n = 1$ photon, is absolutely stable. Such a lightest KK particle (LKP), just like the lightest supersymmetric particle (LSP), is an excellent candidate for dark matter.

Radiative corrections to the masses of the KK particles have been computed in [2–4]. These papers, in particular [3], show that the almost mass-degenerate spectrum for any KK level splits up due to such correction terms. There are two types of corrections; the first one, which results just from the compactification of the extra dimension, is in general small (zero for fermions) and is constant for all n levels. We will call this the bulk correction. The second one, which we will call boundary correction, is comparatively large (goes as $\ln \Lambda^2$ and hence, in principle, can be divergent), and plays a major role in determining the exact spectrum and possible decay modes. The boundary correction terms are related with the interactions present only at the fixed points $y = 0$ and $y = \pi R$. If the interaction is symmetric under the exchange of these fixed points (this is another Z_2 symmetry, but not the Z_2 of $y \leftrightarrow -y$), the conservation of KK number breaks down to the conservation of KK parity, defined as $(-1)^n$. Thus, LKP is still stable, but it is possible to produce an $n = 2$ state from two $n = 0$ states. This particular feature will be of central interest to this talk. With the proposed reach of ILC in mind, we will focus on the range 300 GeV $< R^{-1} <$ 500 GeV. A more detailed discussion and relevant references can be found in [5,6].

Let us mention here that though the main focus is on the ILC, an identical study may be performed for CLIC. Clearly, the reach of CLIC will be much higher.

It has been pointed out [7] that a 'smoking gun' signal of UED would be the production of $n = 2$ states. Pair production of such states is difficult even at the LHC energy, and is surely out of reach for ILC. However, one can produce a single γ_2 or Z_2. These will be narrow peaks, closely spaced, and probably not resolvable at LHC. Here ILC will perform a much better job, and if it can sit on these resonances, it may even repeat the LEP-I story. Such precision measurements will definitely determine the model parameters, even if it is not the simplest UED model. There are a couple of points that the reader should note.

- If a collider is energetic enough to pair produce $n = 1$ excitations, single production of $n = 2$ states is also possible. Since it is not possible to produce only one $n = 1$ UED state, it is a none-or-both situation.
- Decay of a $n = 2$ state to two $n = 0$ states is allowed by KK parity conservation, but this is suppressed by boundary-to-bulk ratio. However, there is no phase space suppression, not even if the final state is a $t\bar{t}$ pair. On the other hand, the coupling is large for the KK number conserving decays ($2 \to 2 - 0, 1 - 1$, where the numbers are for the generic KK levels), but there is a heavy kinematic suppression. Ultimately it turns out that both suppressions are of equal importance [3] and hence both KK-conserving and KK-violating decays are to be taken into account.

In this talk we will discuss the role that ILC may play in studying this resonance physics.

2. The KK-number violating interactions

A consistent formulation of UED needs the inclusion of interaction terms that exist only at the fixed points [2,3]. In the simplest UED model, these terms are taken to be universal, symmetric about the fixed points, and vanishing for energy $\Lambda \gg R^{-1}$. This introduces only two new parameters in the model, Λ and R^{-1}, and ensures the conservation of KK parity. (In fact, there is a third parameter, $\bar{m}_h^2$, the Higgs mass term induced on the fixed points. In the minimal UED model this is assumed to be zero, but its precise value may be probed through a precision study [6].)

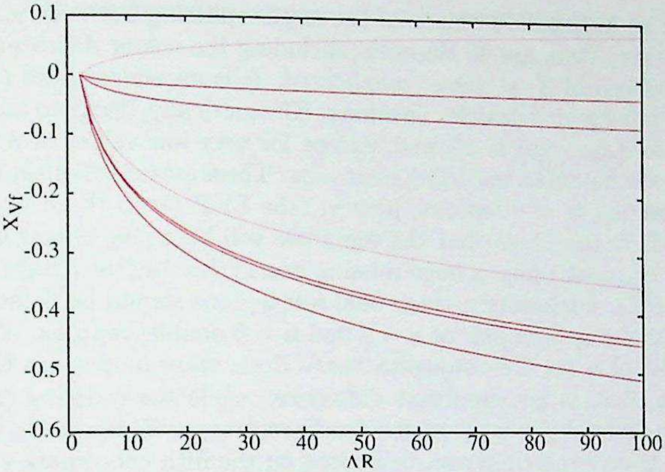

Figure 1. X_{Vf}, the KK-number violating couplings, as a function of ΛR, for $R^{-1} = 300$ GeV (the values are independent of R). From top to bottom, the curves are for X_{ZL}, $X_{\gamma e}$, $X_{\gamma L}$, X_{ZQ}, $X_{\gamma d}$, $X_{\gamma u}$, and $X_{\gamma Q}$ respectively. For their definitions, see text.

The excited states of Z and photon are obtained by diagonalising the mass matrix of W_3 and B. It has been shown in [3] that for all practical purposes, the $n = 2$ excitation of Z is almost W_3 (so that it is a pure $SU(2)$ triplet and couples only to the left-handed fermions) while the $n = 2$ excitation for photon is almost a pure B (so that it couples with different strengths to left- and right-handed fermions).

We will be interested in the coupling of $n = 2$ gauge bosons with an $n = 0$ fermion–antifermion pair. This coupling is given by [3]

$$(-ig\gamma^\mu T_a P_+)\,\frac{\sqrt{2}}{2}\left(\frac{\bar{\delta}(m_{V_2}^2)}{m_2^2} - 2\frac{\bar{\delta}(m_{f_2})}{m_2}\right), \tag{1}$$

where g is the generic gauge coupling, T_a is the group generator (third component of isospin, or hypercharge), and P_+ is the Z_2-even projection operator, which is $P_{\mathrm{L}} = (1-\gamma_5)/2$ for Z_2, but can be either P_{L} or P_{R} for γ_2. V can be either Z or γ. The expressions for the boundary corrections, $\bar{\delta}$, can be found in [3].

It is easy to check that for any level, the excitation of the photon, γ_n, is the lowest-lying particle. Thus, γ_2 cannot decay into a pair of $n = 0$ and $n = 2$ fermions. In fact, the decay to an $n = 1$ pair is also kinematically forbidden, for all choices of Λ and R. Thus, the only possible way to decay is to an $n = 0$ fermion–antifermion pair. Here, both right- and left-handed pairs (of quarks and leptons, including neutrinos) are included, albeit with different strengths, as obtained from eq. (1). In figure 1, we show how the function X_{Vf}, defined as

$$X_{Vf} = \frac{\sqrt{2}}{2}\left(\frac{\bar{\delta}(m_{V_2}^2)}{m_2^2} - 2\frac{\bar{\delta}(m_{f_2})}{m_2}\right), \tag{2}$$

varies for $V = \gamma, Z$ and $f = u_i, d_i, e_i$ ($SU(2)$ singlet states) and L_i, Q_i ($SU(2)$ doublet states), where i is the generation index. It is obvious that γ_2 should decay almost entirely to a $q\bar{q}$ pair, because of the larger splitting between γ_2 and $n = 2$ quarks. Altogether, there are 45 channels, including the colour degrees of freedom.

The decay pattern of Z_2 is more complicated. It is an almost pure $(W_3)_2$, so it couples only to left-handed doublet fermions. Kinematically, decay to an $n = 1$ pair of lepton doublet (Z_2-even) is allowed, except for very low values of Λ ($\Lambda R < 3$). There are six such channels, including neutrinos. These states will ultimately decay to the corresponding $n = 0$ leptons, plus γ_1, the LKP (even the $n = 1$ neutrino can decay in this channel), so that the signature will be a pair of soft leptons (for charged lepton channels) plus a huge missing energy (excited neutrinos, of course, will go undetected). Fortunately, these final soft leptons should be detectable [8,9]. Similarly, Z_2 can decay to a pair of $n = 2$ and $n = 0$ doublet leptons. Again, there are six channels, plus six CP-conjugate ones. Both these modes are KK-number conserving, but there is an important difference: while the coupling is the usual g for the latter channels, it is $g/\sqrt{2}$ for the former ones. This can be checked by integrating the trigonometric terms dependent on the fifth coordinate y.

Just like γ_2, Z_2 has its own share of KK-number violating modes, but it can only decay to a left-handed pair. Since the lower limit on R^{-1} is about 300 GeV, both these gauge bosons can decay even to the $n = 0$ $t\bar{t}$ pair. However, KK-number conserving Z_2 decays to electroweak bosons are forbidden from kinematic considerations.

In the minimal UED model, $\bar{m}_{\rm h}^2 = 0$, Z_2 cannot decay through the Bjorken channel to $Z_1 h_1$, purely from kinematic considerations. (The three-body channels, with a virtual Z_1 or h_1, will be even more suppressed.) However, if $\bar{m}_{\rm h}^2 < 0$, all the Higgs masses will be lowered, and one can just be able to produce a neutral CP-even Higgs excitation through this channel. The decay channel of h_1 is dominantly a right-handed τ pair (assuming the mixing in the $n = 1$ level to be small) plus LKP, and if the τs are soft enough, they may escape detection, leading to an invisible decay mode of h_1.

3. Production and decay of $n = 2$ neutral gauge bosons

The gauge bosons are produced as s-channel resonances in e^+e^- collision through KK-number violating couplings. This suppression brings down the peak cross-section to an otherwise expected nanobarn level to about 35–45 pb for Z_2 and about 63 pb for γ_2 (for $R^{-1} = 300$ GeV, and the variation is due to that of Λ). For $R^{-1} = 450$ GeV, these numbers drop to 16–21 pb and 28 pb, respectively. The reason for a higher production cross-section for γ_2 is its narrower width compared to Z_2. However, it will be almost impossible to detect γ_2 at LHC since it decays almost entirely to two jets which will be swamped by the QCD background, and moreover the resonance is quite narrow. Z_2 has a better chance, since there are a number of hadronically quiet channels, and soft leptons with energy greater than 2 GeV should be detectable. But for a precision study of these resonances we must turn to ILC (or CLIC). These machines should be able to measure precisely the positions and the widths of these two peaks, and hence entirely determine the spectrum, since there are only two unknown parameters (hopefully the Higgs mass will already be measured by LHC). These measurements, in conjunction with the precise determination of $n = 1$ levels, should be able to discriminate, not only

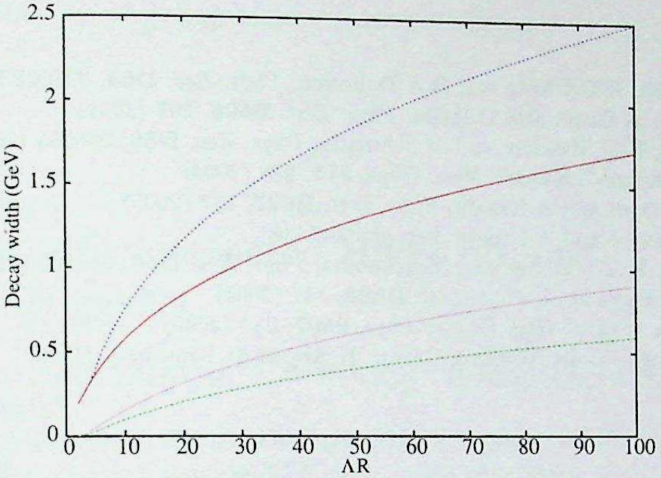

Figure 2. Decay widths of Z_2 (upper pair) and γ_2 (lower pair) as a function of ΛR, for $R^{-1} = 450$ and 300 GeV (upper and lower curves in a pair).

between UED and supersymmetry, but even the minimal version of UED from its variants.

In figure 2 we show the decay widths of Z_2 and γ_2, plotted for two different values of R^{-1} and as a function of ΛR. They increase logarithmically, because of the $\log \Lambda^2$ dependence of the couplings, but no new channel opens up. For small values of ΛR (2-3), the KK-number conserving channels for Z_2 are still closed, and Z_2 can be very long-lived, even to leave a displaced vertex. (As discussed earlier, for $\Lambda R = 2$, a somewhat fine-tuned value, Z_2 is almost stable, and the peak is correspondingly narrow and hence difficult to detect.)

We emphasise that this study will be meaningful only if LHC finds some signal of new physics, which may look like UED, and for which the pair production of $n = 1$ states is not beyond the reach of ILC. In that case a careful scan about $\sqrt{s} = 2/R$ should reveal these two peaks. The points that one would like to verify are:

(i) On the Z_2 peak, $\mathcal{R}$, the ratio of e^+e^- to two jets to $e^+e^- \to \mu^+\mu^-$ would show a sharp dip, in particular if we include the missing energy events. The reason is that the Z_2-width is dominated by the channel to a pair of $n = 1$ leptons, and quarks can appear only from KK-number violating interactions. On the other hand, $\mathcal{R}$ should show a sharp peak on the γ_2 resonance.

(ii) The cross-section would show a kink between the two peaks; this is the position where the KK-number conserving channels open up.

(iii) With the polarised beam option, the behaviour of the two peaks will be quite different. Since Z_2 couples only to the left-handed fermions, with suitable polarisation the peak may vanish altogether, or may get enhanced by a factor of 3 (assuming 80% e^- polarisation and 60–70% e^+ polarisation). The γ_2 peak will get enhanced by about a factor of 2 with left-polarised e^- beam, but will never vanish altogether.

Let us also note that the SM background, coming from the continuum, is less than 10 pb for $\sqrt{s} = 600$–900 GeV [10], and may be further reduced by suitable cuts.

References

[1] T Appelquist, H C Cheng and B A Dobrescu, *Phys. Rev.* **D64**, 035002 (2001)
[2] H Georgi, A K Grant and G Hailu, *Phys. Lett.* **B506**, 207 (2001)
[3] H C Cheng, K T Matchev and M Schmaltz, *Phys. Rev.* **D66**, 036005 (2002)
[4] M Puchwein and Z Kunszt, *Ann. Phys.* **311**, 288 (2004)
[5] B Bhattacherjee and A Kundu, *Phys. Lett.* **B627**, 137 (2005)
[6] B Bhattacherjee and A Kundu, hep-ph/0605118
[7] H C Cheng, K T Matchev and M Schmaltz, *Phys. Rev.* **D66**, 056006 (2002)
[8] G Bhattacharyya *et al*, *Phys. Lett.* **B628**, 141 (2005)
[9] M Battaglia *et al*, *J. High Energy Phys.* **0507**, 033 (2005)
[10] ACFA Linear Collider Working Group: K Abe *et al*, hep-ph/0109166

PRAMANA
— journal of
physics

© Indian Academy of Sciences

Vol. 69, No. 5
November 2007
pp. 861–869

Higher-order corrected Higgs bosons in FeynHiggs2.4

T HAHN[1], S HEINEMEYER[2,*], W HOLLIK[1], H RZEHAK[3], G WEIGLEIN[4] and K WILLIAMS[4]
[1]Max-Planck-Institut für Physik, Föhringer Ring 6, D-80805 Munich, Germany
[2]Instituto de Fisica de Cantabria (CSIC-UC), Santander, Spain
[3]Paul Scherrer Institut, Würenlingen und Villigen, CH-5232 Villigen PSI, Switzerland
[4]IPPP, University of Durham, Durham DH1 3LE, UK
*E-mail: Sven.Heinemeyer@cern.ch

Abstract. Large higher-order corrections enter the Higgs boson sector of the MSSM via Higgs-boson self-energies. Their effects have to be taken into account for the correct treatment of loop-corrected Higgs-boson mass eigenstates as external (on-shell) or internal particles in Feynman diagrams. We review how the loop corrections, including momentum dependence and imaginary contributions, are correctly taken into account for external (on-shell) Higgs boson and how effective couplings can be derived. The procedures are implemented in the code FeynHiggs2.4.

Keywords. Minimal supersymmetric standard model; Higgs, higher-order corrections.

PACS Nos 11.30.Pb; 14.80.Cp; 12.60.Fr

1. Introduction

The search for Higgs bosons is a crucial test of supersymmetry (SUSY) which can be performed with the present and the next generation of accelerators. A precise prediction for the production and decay processes of the Higgs bosons in terms of the relevant SUSY parameters is necessary in order to determine the discovery and exclusion potential of the Tevatron [1–3], and for physics at the LHC [4–7] and the ILC [8–12]. A precise prediction of Higgs-boson properties is also required as input for (current) electroweak precision analyses (see e.g. refs [13,14]).

Since the soft SUSY-breaking parameters can in general be complex, it is necessary to take into account the effects of complex phases. In the minimal supersymmetric standard model with complex parameters (cMSSM) Higgs physics is affected by complex parameters entering via loop corrections. In particular, these are the Higgs mixing parameter, μ, the trilinear couplings, A_f, $f = t, b, \tau, \ldots$, and the gaugino mass parameters M_1, M_2, M_3, where $|M_3| \equiv m_{\tilde{g}}$ (the gluino mass). As a consequence, once loop corrections are taken into account the neutral Higgs bosons are no longer $\mathcal{CP}$-eigenstates, but mix with each other [15],

$$(h, H, A) \to h_1, h_2, h_3. \tag{1}$$

As tree-level input parameters in the Higgs sector (besides the gauge couplings and the Z boson mass), it is convenient to choose the mass of the charged Higgs boson, $M_{H^\pm}$, and the ratio of the two vacuum expectation values, $\tan\beta$.

In order to obtain the prediction for the Higgs masses beyond lowest order, the poles of the Higgs propagators have to be determined. Since the propagator poles are located in the complex plane, we define the physical mass of each particle according to the real part of the complex pole.

Neglecting the mixing with the Goldstone bosons and the longitudinal parts of the Z boson (see ref. [16] for details) one can write the propagator matrix of the neutral Higgs bosons h, H, A as a 3×3 matrix, $\Delta_{hHA}(p^2)$. It is related to the 3×3 matrix of the irreducible vertex functions by

$$\Delta_{hHA}(p^2) = -\left(\hat{\Gamma}_{hHA}(p^2)\right)^{-1}, \tag{2}$$

where

$$\hat{\Gamma}_{hHA}(p^2) = \mathrm{i}\left[p^2 \mathbb{1} - \mathbf{M}_n(p^2)\right], \tag{3}$$

$$\mathbf{M}_n(p^2) = \begin{pmatrix} m_h^2 - \hat{\Sigma}_{hh}(p^2) & -\hat{\Sigma}_{hH}(p^2) & -\hat{\Sigma}_{hA}(p^2) \\ -\hat{\Sigma}_{hH}(p^2) & m_H^2 - \hat{\Sigma}_{HH}(p^2) & -\hat{\Sigma}_{HA}(p^2) \\ -\hat{\Sigma}_{hA}(p^2) & -\hat{\Sigma}_{HA}(p^2) & m_A^2 - \hat{\Sigma}_{AA}(p^2) \end{pmatrix}. \tag{4}$$

Inversion of $\hat{\Gamma}_{hHA}(p^2)$ yields the diagonal Higgs propagators ($i = h, H, A$)

$$\Delta_{ii}(p^2) = \frac{i}{p^2 - m_i^2 + \hat{\Sigma}_{ii}^{\rm eff}(p^2)}, \tag{5}$$

where $\Delta_{hh}(p^2)$, $\Delta_{HH}(p^2)$, $\Delta_{AA}(p^2)$ are the 11, 22, 33 elements of the 3×3 matrix $\Delta_{hHA}(p^2)$, respectively. The structure of eq. (5) is formally the same as for the case without mixing, but the usual self-energy is replaced by the effective quantity $\hat{\Sigma}_{ii}^{\rm eff}(p^2)$ which contains mixing contributions of the three Higgs bosons. It reads (no summation over i, j, k)

$$\begin{aligned} &\hat{\Sigma}_{ii}^{\rm eff}(p^2) \\ &= \hat{\Sigma}_{ii}(p^2) - \mathrm{i}\frac{2\hat{\Gamma}_{ij}(p^2)\hat{\Gamma}_{jk}(p^2)\hat{\Gamma}_{ki}(p^2) - \hat{\Gamma}_{ki}^2(p^2)\hat{\Gamma}_{jj}(p^2) - \hat{\Gamma}_{ij}^2(p^2)\hat{\Gamma}_{kk}(p^2)}{\hat{\Gamma}_{jj}(p^2)\hat{\Gamma}_{kk}(p^2) - \hat{\Gamma}_{jk}^2(p^2)}, \end{aligned} \tag{6}$$

where $\hat{\Gamma}_{ij}(p^2)$ are the elements of the 3×3 matrix $\hat{\Gamma}_{hHA}(p^2)$ as specified in eq. (3).

For completeness, we also state the expression for the off-diagonal Higgs propagators. It reads ($i \neq j$, no summation over i, j, k)

$$\Delta_{ij}(p^2) = \frac{\hat{\Gamma}_{ij}\hat{\Gamma}_{kk} - \hat{\Gamma}_{jk}\hat{\Gamma}_{ki}}{\hat{\Gamma}_{ii}\hat{\Gamma}_{jj}\hat{\Gamma}_{kk} + 2\hat{\Gamma}_{ij}\hat{\Gamma}_{jk}\hat{\Gamma}_{ki} - \hat{\Gamma}_{ii}\hat{\Gamma}_{jk}^2 - \hat{\Gamma}_{jj}\hat{\Gamma}_{ki}^2 - \hat{\Gamma}_{kk}\hat{\Gamma}_{ij}^2}, \tag{7}$$

where we have dropped the argument p^2 of the $\hat{\Gamma}_{ij}(p^2)$ appearing on the right-hand side for ease of notation.

The complex pole $\mathcal{M}^2$ of each propagator is determined as the solution of

$$\mathcal{M}_i^2 - m_i^2 + \hat{\Sigma}_{ii}^{\text{eff}}(\mathcal{M}_i^2) = 0. \tag{8}$$

Writing the complex pole as

$$\mathcal{M}^2 = M^2 - iM\Gamma, \tag{9}$$

where M is the mass of the particle and Γ its width, and expanding up to first order in Γ around M^2 yields the following equation for M_i^2:

$$M_i^2 - m_i^2 + \text{Re}\hat{\Sigma}_{ii}^{\text{eff}}(M_i^2) + \frac{\text{Im}\,\hat{\Sigma}_{ii}^{\text{eff}}(M_i^2)\left(\text{Im}\,\hat{\Sigma}_{ii}^{\text{eff}}\right)'(M_i^2)}{1 + \left(\text{Re}\hat{\Sigma}_{ii}^{\text{eff}}\right)'(M_i^2)} = 0. \tag{10}$$

The short-hand notation $f'(p^2) \equiv \mathrm{d}f(p^2)/(\mathrm{d}p^2)$ has been used, and M_i denotes the loop-corrected mass, while m_i is the lowest-order mass ($i = h, H, A$).

We define the loop-corrected mass eigenvalues according to

$$M_{h_1} \leq M_{h_2} \leq M_{h_3}. \tag{11}$$

In our numerical analysis (and in the code FeynHiggs2.4) we determine the mass eigenvalues using an iterative diagonalization procedure, which avoids the expansion in the width Γ used for deriving eq. (10) (see ref. [17] for further details).

The effects of the imaginary parts of the Higgs-boson self-energies on Higgs phenomenology can be especially relevant if the masses are close to each other. This has been analyzed in ref. [18] taking into account the mixing between the two heavy neutral Higgs-bosons, where the complex mass matrix has been diagonalized with a complex mixing angle, resulting in a non-unitary mixing matrix. The effects of imaginary parts of the Higgs-boson self-energies on physical processes with s-channel resonating ('on-shell') Higgs bosons are discussed in refs [18–20]. In ref. [18] only the one-loop corrections from the $t/\tilde{t}$ sector have been taken into account for the H–A mixing, analyzing the effects on resonant Higgs production at a photon collider. In ref. [19] the full one-loop imaginary parts of the self-energies have been evaluated for the mixing of the three neutral MSSM Higgs bosons. The effects have been analyzed for resonant Higgs production at the LHC, the ILC and a photon collider (however, the corresponding effects on the Higgs-boson masses have been neglected). In ref. [20] the $\tilde{t}/\tilde{b}$ one-loop contributions (neglecting the t/b corrections) on the H–A mixing for resonant Higgs production at a muon collider have been discussed. Our calculation incorporates for the first time the complete effects arising from the imaginary parts of the one-loop self-energies in the neutral Higgs-boson propagator matrix, including their effects on the Higgs masses and the Higgs couplings in a consistent way.

Since the mass M_i^2 appears as argument of the self-energies in eq. (10), solving this equation for M_i^2 is in general non-trivial. It is therefore of interest to consider also approximate methods for determining the Higgs-boson masses. Instead of keeping the full momentum dependence in eq. (4), the 'p^2 on-shell' approximation consists of setting the arguments of the self-energies appearing in eq. (4) to the tree-level masses according to $(i, j = h, H, A)$

$$p^2 \text{ on-shell approximation:} \quad \begin{aligned} &\hat{\Sigma}_{ii}(p^2) \to \hat{\Sigma}_{ii}(m_i^2) \\ &\hat{\Sigma}_{ij}(p^2) \to \hat{\Sigma}_{ij}((m_i^2 + m_j^2)/2). \end{aligned} \tag{12}$$

In this way the Higgs-boson masses can simply be obtained as the eigenvalues of the (momentum-inpendent) matrix of eq. (4). The 'p^2 on-shell' approximation has the benefit that it removes all residual dependencies on the field renormalization constants that cannot be avoided in the iterative procedure.

Instead of setting the momentum argument of the renormalized self-energies to the tree-level masses, in the '$p^2 = 0$' approximation the momentum dependence of the self-energies is neglected completely $(i, j = h, H, A)$,

$$p^2 = 0 \text{ approximation:} \quad \begin{aligned} &\hat{\Sigma}_{ii}(p^2) \to \hat{\Sigma}_{ii}(0) \\ &\hat{\Sigma}_{ij}(p^2) \to \hat{\Sigma}_{ij}(0). \end{aligned} \tag{13}$$

In the '$p^2 = 0$' approximation the masses are identified with the eigenvalues of $\mathbf{M}_n(0)$ (see eq. (4)) instead of the true pole masses. This approximation is mainly useful for comparisons with effective-potential calculations. The matrix $\mathbf{M}_n(0)$ is Hermitian by construction.

2. Amplitudes with external Higgs bosons

In evaluating processes with external (on-shell) Higgs bosons beyond lowest order one has to account for the mixing between the Higgs bosons in order to ensure that the outgoing particle has the correct on-shell properties such that the S matrix is properly normalized. This gives rise to finite wave function normalization factors [22]. For the case of 2×2 mixing appearing in the MSSM with real parameters (rMSSM) for the mixing between the two neutral $\mathcal{CP}$-even Higgs bosons h and H, which is analogous to the mixing of the photon and Z boson in the standard model, the relevant wave function normalization factors are well-known (see e.g. refs [24,25]). An amplitude with an external Higgs boson, i, receives the corrections $(i, j = h, H$, no summation over $i, j)$

$$\sqrt{\hat{Z}_i}\left(\Gamma_i + \hat{Z}_{ij}\Gamma_j\right), \quad i \neq j, \tag{14}$$

where $\Gamma_{i,j}$ denote the one-particle irreducible Higgs vertices, and

$$\hat{Z}_i = \left[1 + \text{Re } \hat{\Sigma}'_{ii}(p^2) - \text{Re}\left(\frac{\left(\hat{\Sigma}_{ij}(p^2)\right)^2}{p^2 - m_j^2 + \hat{\Sigma}_{jj}(p^2)}\right)'\right]^{-1}_{\Big|p^2 = M_i^2}, \tag{15}$$

$$\hat{Z}_{ij} = -\frac{\hat{\Sigma}_{ij}(M_i^2)}{M_i^2 - m_j^2 + \hat{\Sigma}_{jj}(M_i^2)}. \tag{16}$$

As before m_j denotes the tree-level mass, while M_i is the loop-corrected mass.

In the case of the cMSSM, the formulas above need to be extended to the case of 3×3 mixing. A vertex with an external Higgs boson, i, has the form (with i, j, k all different, $i, j, k = h, H, A$, and no summation over indices)

$$\sqrt{\hat{Z}_i}\left(\Gamma_i + \hat{Z}_{ij}\Gamma_j + \hat{Z}_{ik}\Gamma_k\right). \tag{17}$$

The finite Z factors are given by

$$\hat{Z}_i = \frac{1}{1 + \left(\mathrm{Re}\hat{\Sigma}_{ii}^{\mathrm{eff}}\right)'(M_i^2)}, \tag{18}$$

$$\begin{aligned}\hat{Z}_{ij} &= \frac{\Delta_{ij}(p^2)}{\Delta_{ii}(p^2)}\Bigg|_{p^2=M_i^2} \\ &= \frac{\hat{\Sigma}_{ij}(M_i^2)\left(M_i^2 - m_k^2 + \hat{\Sigma}_{kk}(M_i^2)\right) - \hat{\Sigma}_{jk}(M_i^2)\hat{\Sigma}_{ki}(M_i^2)}{\hat{\Sigma}_{jk}^2(M_i^2) - \left(M_i^2 - m_j^2 + \hat{\Sigma}_{jj}(M_i^2)\right)\left(M_i^2 - m_k^2 + \hat{\Sigma}_{kk}(M_i^2)\right)},\end{aligned} \tag{19}$$

where the propagators $\Delta_{ii}(p^2)$, $\Delta_{ij}(p^2)$ have been given in eqs (5) and (7), respectively. Using eq. (17) with Z factors specified in eqs (18), (19) and adding to this expression the mixing contributions of the Higgs bosons with the Goldstone bosons and the gauge bosons (see refs [16,21] for more details) yields the correct normalization of the outgoing Higgs bosons in the S matrix.

For convenience we define a matrix $\tilde{\mathbf{Z}}_n$ based on the wave function normalization factors. Its elements are given by (with $\hat{Z}_{ii} = 1$, $i, j = h, H, A$, and no summation over i)

$$(\tilde{\mathbf{Z}}_n)_{ij} := \sqrt{\hat{Z}_i}\,\hat{Z}_{ij}. \tag{20}$$

Performing a re-ordering of the lines of $\tilde{\mathbf{Z}}_n$ such that they correspond to the mass ordering of eq. (11) results in the matrix $\mathbf{Z}_n$. A vertex with an external (on-shell) Higgs boson h_i is then given by

$$(\mathbf{Z}_n)_{i1}\Gamma_h + (\mathbf{Z}_n)_{i2}\Gamma_H + (\mathbf{Z}_n)_{i3}\Gamma_A. \tag{21}$$

3. Effective couplings

In a general amplitude with Higgs bosons, the structure describing the Higgs part is given by $\sum_{ij}\Gamma_i\Delta_{ij}\Gamma_j$, where $\Gamma_{i,j}$ are the one-particle irreducible Higgs vertices as above, and the propagators Δ_{ij} are as given in eqs (5) and (7). For phenomenological analyses it is often convenient to use approximations of improved-Born type with effective couplings incorporating leading higher-order effects. There is no unique prescription how to define such effective coupling terms. One possibility would be to consider the matrix $\mathbf{Z}_n$, defined through eqs (20) and (21), as mixing matrix. The elements of the matrix $\mathbf{Z}_n$, however, are in general complex, so that the $\mathbf{Z}_n$ is a non-unitary matrix. Therefore, it cannot be interpreted as a rotation matrix. If one wants to introduce effective couplings by means of a (unitary) rotation matrix, it is necessary to make further approximations.

A possible choice leading to a unitary rotation matrix is the '$p^2 = 0$' approximation, which is used in the effective potential approach. As before, we first consider the case of 2×2 mixing relevant for the rMSSM. In the '$p^2 = 0$' approximation defined in eq. (13) the momentum dependence in the renormalized self-energies is set to the respective tree-level Higgs boson masses, so that the derivative in eq. (15) acts only on the p^2 term in the propagator factor. In this limit $\hat{Z}_i$ simplifies to [26,27]

$$p^2 = 0 \text{ approximation, } 2 \times 2 \text{ mixing:} \qquad \hat{Z}_i = \frac{1}{1 + \hat{Z}_{ij}^2} \,. \tag{22}$$

For the mixing between the neutral $\mathcal{CP}$-even Higgs bosons h, H this yields $\hat{Z}_h = \hat{Z}_H = \cos^2 \Delta\alpha$. This corresponds to an effective coupling approximation where the tree-level mixing angle α appearing in the couplings of the neutral $\mathcal{CP}$-even Higgs bosons is replaced by $\alpha_{\text{eff}} = \alpha + \Delta\alpha$ [26,27].

It is easy to verify that for the 3×3 mixing case eq. (18) in the '$p^2 = 0$' approximation simplifies to

$$p^2 = 0 \text{ approximation, } 3 \times 3 \text{ mixing:} \qquad \hat{Z}_i = \frac{1}{1 + \hat{Z}_{ij}^2 + \hat{Z}_{ik}^2} \,, \tag{23}$$

as a direct generalization of eq. (22).

The matrix $\mathbf{Z}_n$ defined through eqs (20) and (21) goes over into a unitary matrix $\mathbf{R}_n$ in this approximation,

$$\begin{gathered} p^2 = 0 \text{ approximation, } 3 \times 3 \text{ mixing:} \\ \mathbf{Z}_n \to \mathbf{R}_n, \quad \mathbf{R}_n = \begin{pmatrix} R_{11} & R_{12} & R_{13} \\ R_{21} & R_{22} & R_{23} \\ R_{31} & R_{32} & R_{33} \end{pmatrix} . \end{gathered} \tag{24}$$

The matrix $\mathbf{R}_n$ diagonalizes the matrix $\mathbf{M}_n(0)$ arising from eq. (4) in the '$p^2 = 0$' approximation. $\mathbf{R}_n$ can therefore be used to connect the mass eigenstates h_1, h_2, h_3 with the original states h, H, A,

$$\begin{gathered} \begin{pmatrix} h_1 \\ h_2 \\ h_3 \end{pmatrix}_{p^2=0} = \mathbf{R}_n \cdot \begin{pmatrix} h \\ H \\ A \end{pmatrix}, \\ \mathbf{R}_n \mathbf{M}_n(0) \mathbf{R}_n^\dagger = \begin{pmatrix} M_{h_1\,p^2=0}^2 & 0 & 0 \\ 0 & M_{h_2\,p^2=0}^2 & 0 \\ 0 & 0 & M_{h_3\,p^2=0}^2 \end{pmatrix} . \end{gathered} \tag{25}$$

Since $\mathbf{M}_n$ is Hermitian, the matrix $\mathbf{R}_n$ is unitary.

As shown in ref. [16], a better approximation of the full result can be achieved by defining the effective couplings in the 'p^2 on-shell' approximation. The unitary matrix $\mathbf{U}_n$ is defined such that it diagonalizes the matrix $\mathrm{Re}(\mathbf{M}_n(p^2 \text{ on-shell}))$ arising from eq. (4) in the 'p^2 on-shell' approximation and neglecting the imaginary parts. This yields

$$p^2 \text{ on-shell approx.:} \quad \begin{pmatrix} h_1 \\ h_2 \\ h_3 \end{pmatrix}_{p^2 \text{ on-shell}} = \mathbf{U}_n \cdot \begin{pmatrix} h \\ H \\ A \end{pmatrix},$$

$$\mathbf{U}_n = \begin{pmatrix} U_{11} & U_{12} & U_{13} \\ U_{21} & U_{22} & U_{23} \\ U_{31} & U_{32} & U_{33} \end{pmatrix}, \tag{26}$$

$$\mathbf{U}_n \, \mathrm{Re}(\mathbf{M}_n(p^2 \text{ on-shell})) \, \mathbf{U}_n^\dagger = \begin{pmatrix} M^2_{h_1,p^2 \text{ on-shell}} & 0 & 0 \\ 0 & M^2_{h_2,p^2 \text{ on-shell}} & 0 \\ 0 & 0 & M^2_{h_3,p^2 \text{ on-shell}} \end{pmatrix}.$$

The elements of $\mathbf{U}_n$ can be used to quantify the extent of $\mathcal{CP}$-violation. For example, U_{13}^2 can be understood as the $\mathcal{CP}$-odd part in h_1, while $U_{11}^2 + U_{12}^2$ make up the $\mathcal{CP}$-even part. The unitarity of $\mathbf{U}_n$ ensures that both parts add up to 1.

The elements of $\mathbf{U}_n$ can be interpreted as effective couplings of internal Higgs bosons in a loop diagram, which take into account leading higher-order contributions. As an example we show the couplings of a neutral Higgs boson to two gauge bosons, $VV = ZZ, W^+W^-$. Beyond the lowest order in the cMSSM all three neutral Higgs bosons have a $\mathcal{CP}$-even component, so that all three Higgs bosons have non-vanishing couplings to two gauge bosons. The couplings normalized to the SM values are given by

$$g_{h_i VV} = U_{i1} \sin(\beta - \alpha) + U_{i2} \cos(\beta - \alpha) . \tag{27}$$

4. Conclusions

Large higher-order corrections enter the Higgs-boson sector of the MSSM via Higgs-boson self-energies. Their effects have to be taken into account for the correct treatment of loop-corrected Higgs-boson mass eigenstates as external (on-shell) or internal particles in loop diagrams. We have shown how the loop corrections can be taken into account in the treatment of external (on-shell) Higgs bosons, and how effective couplings, taking into account leading higher-order effects, can be constructed.

The procedure presented here is implemented in the code FeynHiggs2.4 [16,28–30]. For the Higgs-boson self-energies the complete one-loop corrections [16,31–33] are supplemented by the available two-loop corrections in the Feynman-diagrammatic approach for the MSSM with real parameters [28,29,34] and a re-summation of the leading (s)bottom corrections for complex parameters [35]. Higgs boson decays and production cross-sections [36] are evaluated using $\mathbf{Z}_n$ (20,21), ensuring the on-shell properties of the external particles. Effective Higgs boson couplings are obtained with the help of $\mathbf{U}_n$ (26). In this way FeynHiggs provides a precise prediction of Higgs-boson production and decay properties and the respective couplings.

References

[1] D0 Collaboration: V Abazov *et al*, hep-ex/0504018

[2] CDF Collaboration: A Abulencia *et al*, hep-ex/0508051

[3] CDF Collaboration: hep-ex/0510065

[4] ATLAS Collaboration: Detector and Physics Performance Technical Design Report, CERN/LHCC/99-15 (1999), see atlasinfo.cern.ch/Atlas/GROUPS/PHYSICS/TDR/access.html

[5] S Abdullin *et al*, *Euro. Phys. J.* **C39S2**, 41 (2005)
CMS Physics TDR, see: cmsinfo.cern.ch/Welcome.html/CMSdocuments/CMSplots/

[6] M Dührssen, S Heinemeyer, H Logan, D Rainwater, G Weiglein and D Zeppenfeld, *Phys. Rev.* **D70**, 113009 (2004), hep-ph/0407190

[7] M Schumacher, *Czech. J. Phys.* **54**, A103 (2004), hep-ph/0410112

[8] J Aguilar-Saavedra *et al*, hep-ph/0106315, see tesla.desy.de/tdr

[9] American Linear Collider Working Group Collaboration: T Abe *et al*, hep-ex/0106056

[10] ACFA Linear Collider Working Group Collaboration: K Abe *et al*, hep-ph/0109166, see lcdev.kek.jp/RMdraft

[11] LHC/ILC Study Group: G Weiglein *et al*, *Phys. Rep.* **426**, 47 (2006)

[12] S Heinemeyer *et al*, hep-ph/0511332
S Heinemeyer, *These Proceedings*

[13] S Heinemeyer, W Hollik, D Stöckinger, A M Weber and G Weiglein, *J. High Energy Phys.* **0608**, 052 (2006); *These Proceedings*

[14] J Ellis, S Heinemeyer, K Olive and G Weiglein, *J. High Energy Phys.* **0502**, 013 (2005); **0605**, 005 (2006)
S Heinemeyer, *These Proceedings*

[15] A Pilaftsis, *Phys. Rev.* **D58**, 096010 (1998); *Phys. Lett.* **B435**, 88 (1998)

[16] M Frank, T Hahn, S Heinemeyer, W Hollik, H Rzehak and G Weiglein, *J. High Energy Phys.* **0702**, 047 (2007)

[17] T Hahn, physics/0607103

[18] S Choi, J Kalinowski, Y Liao and P Zerwas, *Euro. Phys. J.* **C40**, 555 (2005)

[19] J Ellis, J Lee and A Pilaftsis, *Phys. Rev.* **D70**, 075010 (2004); *Nucl. Phys.* **B718**, 247 (2005); *Phys. Rev.* **D72**, 095006 (2005)

[20] J Bernabeu, D Binosi and J Papavassiliou, hep-ph/0604046

[21] K Williams *et al*, *in preparation*

[22] The introduction of these factors can in principle be avoided by using a renormalization scheme where all involved particles obey on-shell conditions from the start, but it is often more convenient to work in a different scheme like the $\overline{\mathrm{DR}}$ scheme for the field renormalizations [23].

[23] M Frank, S Heinemeyer, W Hollik and G Weiglein, hep-ph/0202166

[24] A Dabelstein, *Nucl. Phys.* **B456**, 25 (1995); *Z. Phys.* **C67**, 495 (1995)

[25] T Hahn, S Heinemeyer and G Weiglein, *Nucl. Phys.* **B652**, 229 (2003)

[26] S Heinemeyer, W Hollik and G Weiglein, *Euro. Phys. J.* **C16**, 139 (2000)

[27] S Heinemeyer, W Hollik, J Rosiek and G Weiglein, *Euro. Phys. J.* **C19**, 535 (2001)

[28] S Heinemeyer, W Hollik and G Weiglein, *Euro. Phys. J.* **C9**, 343 (1999)

[29] G Degrassi, S Heinemeyer, W Hollik, P Slavich and G Weiglein, *Euro. Phys. J.* **C28**, 133 (2003)

[30] S Heinemeyer, W Hollik and G Weiglein, *Comp. Phys. Commun.* **124**, 76 (2000)
T Hahn, S Heinemeyer, W Hollik and G Weiglein, hep-ph/0507009, see www.feynhiggs.de

[31] S Heinemeyer, *Euro. Phys. J.* **C22**, 521 (2001)

[32] M Frank, S Heinemeyer, W Hollik and G Weiglein, hep-ph/0212037

[33] S Heinemeyer, *Int. J. Mod. Phys.* **A21**, 2659 (2006)

[34] S Heinemeyer, W Hollik and G Weiglein, *Phys. Rev.* **D58**, 091701 (1998); *Phys. Lett.* **B440**, 296 (1998)

[35] M Carena, D Garcia, U Nierste and C Wagner, *Nucl. Phys.* **B577**, 577 (2000)

[36] T Hahn, F Maltoni, S Heinemeyer, G Weiglein and S Willenbrock, hep-ph/0607308

PRAMANA
— journal of
physics

© Indian Academy of Sciences

Vol. 69, No. 5
November 2007
pp. 871–876

Extra dimension searches at hadron colliders to next-to-leading order-QCD

M C KUMAR[1,2], PRAKASH MATHEWS[1,*] and V RAVINDRAN[3]
[1]Saha Institute of Nuclear Physics, 1/AF Bidhan Nagar, Kolkata 700 064, India
[2]School of Physics, University of Hyderabad, Hyderabad 500 046, India
[3]Harish-Chandra Research Institute, Chhatnag Road, Jhunsi, Allahabad 211 019, India
*E-mail: prakash.mathews@saha.ac.in

Abstract. The quantitative impact of NLO-QCD corrections for searches of large and warped extra dimensions at hadron colliders are investigated for the Drell-Yan process. The K-factor for various observables at hadron colliders are presented. Factorisation, renormalisation scale dependence and uncertainties due to various parton distribution functions are studied. Uncertainties arising from the error on experimental data are estimated using the MRST parton distribution functions.

Keywords. Parton distribution function and scale uncertainties; large and warped extra dimensions.

PACS Nos **11.10.Kk; 12.10.-g; 12.38.-t; 13.60.Hb**

1. Introduction

The gauge hierarchy problem has been one of the main motivations for physics beyond the standard model (SM). The apparent weakness of gravity can be accounted for by the existence of either large extra spatial dimensions ADD model [1] or warped extra dimension RS model [2]. In either case the fundamental Planck scale could be of the order of a few TeV and hence a possible explanation of the hierarchy. In both these models only gravity is allowed to propagate the extra dimensions while the SM particles are constrained on a 3-brane. Due to different methods of compactification of the extra dimensions in ADD and RS models, their Kaluza–Klein (KK) spectrum and their effective interactions with the SM model particles are distinct. Experimental signature of extra dimensions would correspond to deviation from SM predictions due to the virtual exchange of KK modes or direct production of KK modes at a collider.

At hadron colliders, it is important to have a precise knowledge of the parton distribution functions (PDFs) to predict production cross-sections of both signals and backgrounds. These universal PDFs are non-perturbative inputs that are extracted from global fits to available data on DIS, DY and other hadronic processes.

Parametrisation of PDFs to a particular order in QCD would involve various theoretical and experimental uncertainties. Recently there has been a series of papers [3–5] which for the first time have calculated the next-to-leading order (NLO) QCD corrections to various distributions of the DY process for both ADD and RS model. These NLO results would certainly reduce one aspect of the theoretical uncertainties as results prior to this calculation were only to leading order (LO) in QCD for process involving gravity.

2. Theoretical uncertainties

In the QCD improved parton model the hadronic cross-section can be expressed in terms of the partonic cross-section convoluted with appropriate parton distribution function. The subprocess cross-section is a perturbative expansion in the strong coupling constant $\alpha_s(\mu_R)$. The partonic flux is non-perturbative and is given in terms of the parton distribution function $f_a(z, \mu_F)$. In perturbative QCD, the unknown higher-order corrections and the scale uncertainties are strongly correlated. The factorisation of mass singularities from the perturbatively calculable partonic cross-sections leads to the introduction of factorisation scale μ_F in both non-perturbative parton densities $f_a(x, \mu_F)$ as well as the finite partonic cross-sections $d\hat{\sigma}_{ab}(x, \mu_F)$. The value of the scale is arbitrary and one demands that the physical cross-sections be independent of them. In addition to the factorisation scale, the partonic cross-sections are dependent on the renormalisation scale μ_R. This is the scale at which the bare parameters of the theory become finite renormalised ones. The choice of the scale is again arbitrary. Gravity couples to the SM fields via its energy momentum tensor, and the calculations are done in the high energy limits where masses of the SM particles are ignored. The only parameter that requires UV renormalisation is the strong coupling constant. The scale uncertainties come about from the truncation of the perturbative series.

2.1 *PDF uncertainty*

Unlike the perturbatively calculable partonic cross-sections, the PDFs being non-perturbative in nature are extracted from various experiments. These are fitted at a scale of the experiments and then evolved according to the Altarelli–Parisi evolution equations to any other relevant scale. They are not only sensitive to experimental errors but also to theoretical uncertainties that enter through the partonic cross-section calculations and the splitting functions that are known only to certain orders in strong coupling constant in perturbative QCD. There are various groups that are involved in parametrising these PDFs taking the uncertainties into account. These groups use not only different experiments but also different methods to parametrise these PDFs. Here, we mainly concentrate on the uncertainties coming from the various PDFs, viz. Alekhin [6], CTEQ [7] and MRST [8], in detail and quantify their impact on the new physics searches in extra dimensional models. Differences among the various PDFs would translate as uncertainties on the physical observables. To

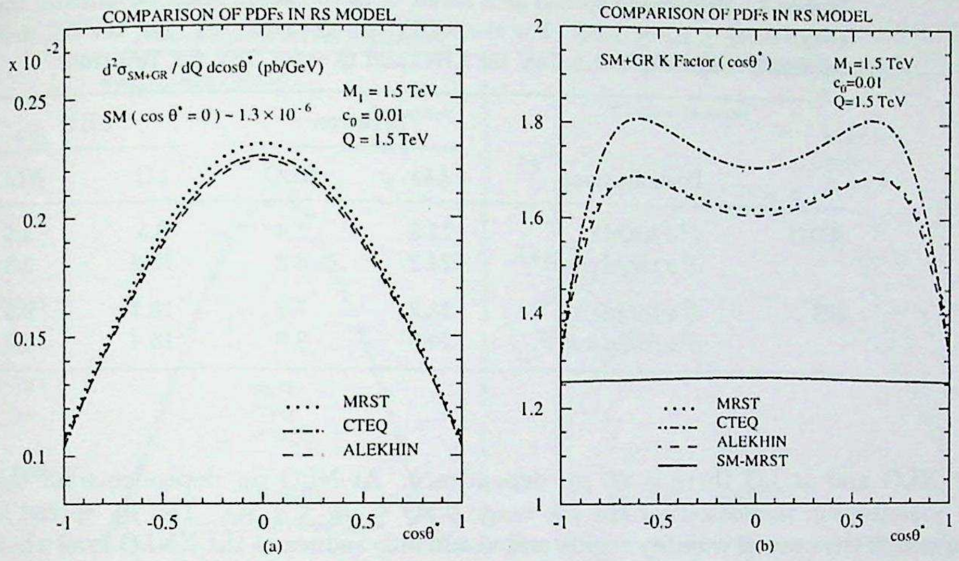

Figure 1. (**a**) In the region of first RS resonance, the double differential with respect to invariant mass and angular distribution of the lepton is plotted for various PDFs at LHC. (**b**) The corresponding K-factor for various PDFs.

NLO in QCD for various PDFs, we consider the following differential distributions [9]:

$$\frac{\mathrm{d}\sigma}{\mathrm{d}Q}, \quad \frac{\mathrm{d}^2\sigma}{\mathrm{d}Q\ \mathrm{d}Y}, \quad \frac{\mathrm{d}^2\sigma}{\mathrm{d}Q\ \mathrm{d}\cos\theta^*}, \tag{1}$$

where Q is the invariant mass, Y is the rapidity and θ^* is the angle between the final-state lepton momenta and the initial state hadron momenta in the c.o.m frame of the lepton pair. The corresponding K-factor which is the ratio of NLO to LO of the above distributions are also plotted for various PDFs. The K-factor is as large as about 1.6. This clearly shows the need to go beyond LO in QCD in these models [3–5,9].

2.2 *Renormalisation/factorisation scale uncertainties*

The μ_{F} variation is studied by varying μ_{F} in the range $0.5Q \leq \mu_{\mathrm{F}} \leq 1.5Q$. We see that for both the ADD and RS models in going from LO to NLO in QCD, the uncertainties due to μ_{F} variation considerably get reduced [9]. The spread of K-factor with μ_{F} is much smaller for the SM as compared to SM+GR. This certainly indicates the need to go beyond NLO. In table 1 we tabulate the percentage spread of the factorisation scale μ_{F} dependence of various distributions at LHC and Tevatron. On the average at LHC and Tevatron, the percentage spread of the scale variation gets reduced by about 2.88 times in going from LO to NLO. The dependence of cross-section on μ_{R} comes from the strong coupling constant

Table 1. Percentage spread as a result of factorisation scale variation in the range $0.5Q \leq \mu_{\rm F} \leq 1.5Q$. For the ADD case $Q = 0.7$ TeV. For the RS, first resonance region $Q = 1.5$ TeV for LHC and $Q = 0.7$ TeV for Tevatron.

		Tevatron		LHC	
	Distributions	LO	NLO	LO	NLO
ADD	$\mathrm{d}^2\sigma/\mathrm{d}Q\mathrm{d}Y$	22.8	7.4	9.5	3.5
	$\mathrm{d}^2\sigma/\mathrm{d}Q\mathrm{d}\cos\theta$	24.2	8.2	10.9	3.8
RS	$\mathrm{d}^2\sigma/\mathrm{d}Q\mathrm{d}Y$	23.2	7.7	18.7	6.9
	$\mathrm{d}^2\sigma/\mathrm{d}Q\mathrm{d}\cos\theta$	24.2	8.0	18.4	6.8

at NLO and at LO there is no $\mu_{\rm R}$ dependence. At NLO $\mu_{\rm R}$ dependence for the Y distribution is plotted for the $\mu_{\rm R}$ range $0.5Q \leq \mu_{\rm R} \leq 1.5Q$. The $\mu_{\rm R}$ spread is largest in the central rapidity region and would only reduce at the NNLO level when the $\mu_{\rm R}$ dependences would be compensated for by the dependence coming from the coefficient functions. We have studied the K-factor for SM and SM+GR and see its dependence on $\mu_{\rm R}$. The uncertainties due to $\mu_{\rm R}$ are much larger when the gravity is included. The percentage spread is of the order of 3.5% which is comparable to the $\mu_{\rm F}$ spread at NLO.

3. Experimental uncertainties

In addition to the theoretical uncertainties that we have described in the previous section, there are uncertainties due to errors on the data. Various groups have studied the experimental errors and have estimated the uncertainties on the PDFs within NLO-QCD framework [10,11]. Now that NLO-QCD results are also available for extra dimension searches [3] for the dilepton production, we consider some of the distributions and estimate the uncertainties due to the experimental error. We have plotted the error band for the MRST 2001 PDF [11] in the ADD model for the dilepton invariant mass distribution at LHC. This error band is comparable to the spread associated with different sets of PDFs [9]. At $Q = 1$ TeV the percentage of experimental error is 7.5% for SM+GR while the pure SM error is about 3.3%. For the RS case at LHC in the first resonance region at $Q = 1.5$ TeV the experimental error is about 12.8%. At Tevatron the ADD model experimental error is 7.4% at $Q = 1$ TeV. In figure 2a we have plotted PDF comparison plots for the double differential distribution with respect to invariant mass and rapidity at a fixed value of $Q = 0.7$ TeV. The experimental error for this distribution for the central rapidity region is about 3.5% and is indicated in figure 2a by the thin line band.

4. Conclusions

We have studied the impact of various parton density sets at NLO in QCD on the Drell-Yan production of dileptons at hadron colliders such as LHC and Tevatron.

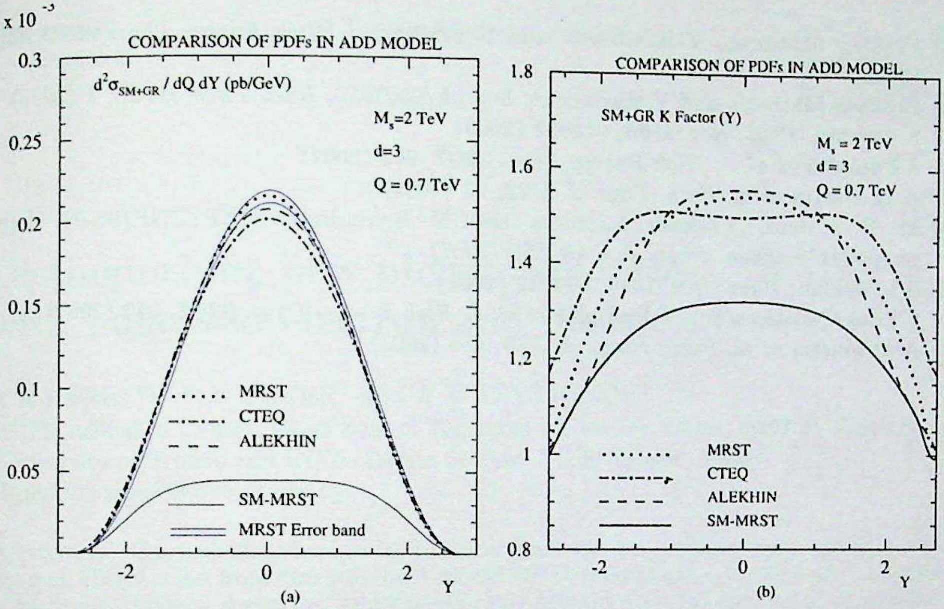

Figure 2. The comparison plots for the various PDF sets for $Q = 0.7$ TeV at LHC. (**a**) The double differential cross-section with respect to invariant mass and rapidity as a function of rapidity. The thin line band gives the range of experimental error on the MRST PDF. (**b**) The corresponding K-factor as a function of rapidity.

This process can probe the physics beyond the SM through exchange of new particles that these theories predict. At hadron colliders, the precise measurement of DY production cross-sections is possible. In this context, we have studied the theories of extra dimensions such as ADD and RS which attempt to explain gauge hierarchy problem in the SM. We have discussed various theoretical uncertainties that enter through renormalisation, factorisation scales and the parton density sets. We have quantified the uncertainties coming from various parton density sets using the recent results on NLO-QCD corrections to parton level cross-sections and recent PDF sets that take into account various theoretical and experimental errors. Our entire analysis is model-independent, thanks to the factorisation of QCD radiative corrections from the model-dependent contributions. We find that the K-factor for various observables depends on the choice of PDFs.

References

[1] N Arkani-Hamed, S Dimopoulos and G Dvali, *Phys. Lett.* **B249**, 263 (1998)
I Antoniadis, N Arkani-Hamed, S Dimopoulos and G Dvali, *Phys. Lett.* **B436**, 257 (1998)
[2] L Randall and R Sundrum, *Phys. Rev. Lett.* **83**, 3370 (1999)
W D Goldberger and M B Wise, *Phys. Rev. Lett.* **83**, 4922 (1999)
[3] Prakash Mathews, V Ravindran, K Sridhar and W L van Neerven, *Nucl. Phys.*, **B713**, 333 (2005)

[4] Prakash Mathews, V Ravindran and K Sridhar, *J. High Energy Phys.* **0510**, 031 (2005)
[5] Prakash Mathews and V Ravindran, hep-ph/0507250, *Nucl. Phys.* **B753**, 1 (2006)
[6] S Alekhin, *Phys. Rev.* **D68**, 014002 (2003)
[7] J Pumplin *et al*, *J. High Energy Phys.* **0207**, 012 (2002)
[8] A D Martin *et al*, *Euro. Phys. J.* **C23**, 73 (2002)
[9] M C Kumar, Prakash Mathews and V Ravindran, SINP/TNP/06-08, hep-ph/0604135, *Euro. Phys. J.* **C49**, 599 (2007)
[10] S I Alekhin, *Phys. Rev.* **D63**, 094022 (2001)
CTEQ Collaboration: J Pumplin *et al*, *J. High Energy Phys.* **0207**, 012 (2002)
[11] A D Martin *et al*, *Euro. Phys. J.* **C28**, 455 (2003)

PRAMANA
— journal of
physics

© Indian Academy of Sciences

Vol. 69, No. 5
November 2007
pp. 877–881

Distinguishing new physics scenarios with polarized electron and positron beams

A A PANKOV[1,*], N PAVER[2] and A V TSYTRINOV[1]
[1]ICTP Affiliated Centre, Pavel Sukhoi Technical University, Gomel 246746, Belarus
[2]University of Trieste and INFN-Trieste Section, 34100 Trieste, Italy
[*]E-mail: pankov@gstu.gomel.by

Abstract. Contact-like nonstandard interactions can be revealed only through deviations of observables from the standard model (SM) predictions. We consider a number of such nonstandard scenarios, and discuss their identification as sources of deviations in fermion-pair production processes at the international linear collider (ILC), if they were observed. We emphasize the role of e^- and e^+ polarization in enhancing the identification reaches.

Keywords. Polarized e^+e^- collisions; models beyond the standard model.

PACS Nos 12.60.-i; 12.60.Rc; 12.60.Cn

1. Introduction

New physics (NP) beyond the standard model is expected to show up at the LHC and ILC colliders either *directly* through production of new particles, or *indirectly* through *deviations* of cross-sections and asymmetries from the SM predictions. The latter case is typical of interactions mediated by exchanges of heavy mass objects, such that the energy is not sufficient for their direct production. The corresponding corrections to the SM predictions are most conveniently parametrized in terms of negative powers of the characteristic large mass scales Λ, times matrix elements of effective, contact-like, Lagrangians.

The so-called *discovery reach*, i.e., the maximum value of Λ for which a deviation could be observed within the foreseeable experimental accuracy, gives an indication of the expected sensitivity of an observable to the various NP scenarios. On the other hand, in principle different NP models can cause similar deviations. Therefore, it should be interesting to assess the *identification reach* on the individual models, i.e., the maximum value of Λ for which a novel interaction not only produces observable deviations, but also can be discriminated, as the source of the observed deviations, from the other nonstandard interactions for all values of their characteristic mass scale parameters. Clearly, by definition, the identification reach is expected to be smaller than the discovery reach. Here we discuss the differential cross-sections for the following processes at the ILC with both beams longitudinally polarized:

$$e^+ + e^- \to \bar{f} + f, \quad f = e, \mu, \tau, c, b. \tag{1}$$

All these processes can receive corrections from the contact-like interactions considered here, and their sensitivity is significantly enhanced by the initial e^- and e^+ polarizations [1–4]. This facility is envisaged at the planned ILC [5].

The nonstandard scenarios we consider are the following:
(a) The ADD large compactified extra dimensions scenario [6–8], where only gravity can propagate in the extra spatial dimensions, and correspondingly a tower of graviton KK states is exchanged in the four-dimensional space [9,10]. The relevant, dimension-8, effective Lagrangian can be expressed as [11]

$$\mathcal{L}^{\mathrm{ADD}} = i\frac{4\lambda}{\Lambda_H^4} T^{\mu\nu} T_{\mu\nu}, \tag{2}$$

with $T_{\mu\nu}$ being the energy–momentum tensor of the SM particles and Λ_H a phenomenological cut-off on the summation over the KK spectrum, expected in the (multi) TeV region. Here, $\lambda = \pm 1$.
(b) Gravity in TeV^{-1}-scale extra dimensions, in which the SM gauge bosons can also propagate. The relevant contact-like effective Lagrangian can be parametrized by a 'compactification scale' M_{C}, and for one extra dimension it reads [12,13]:

$$\begin{aligned}\mathcal{L}^{\mathrm{TeV}} = -\frac{\pi^2}{3M_{\mathrm{C}}^2}&[Q_e Q_f(\bar{e}\gamma_\mu e)(\bar{f}\gamma^\mu f) \\ &+(g_{\mathrm{L}}^e \bar{e}_{\mathrm{L}}\gamma_\mu e_{\mathrm{L}} + g_{\mathrm{R}}^e \bar{e}_{\mathrm{R}}\gamma_\mu e_{\mathrm{R}})(g_{\mathrm{L}}^f \bar{f}_{\mathrm{L}}\gamma^\mu f_{\mathrm{L}} + g_{\mathrm{R}}^f \bar{f}_{\mathrm{R}}\gamma^\mu f_{\mathrm{R}})].\end{aligned} \tag{3}$$

(c) The dimension-6 four-fermion contact interactions (CI) [14,15], with $\Lambda_{\alpha\beta}$ 'compositeness' mass scales ($\alpha, \beta = \mathrm{L}, \mathrm{R}$ and $\eta_{\alpha\beta} = \pm 1, 0$):

$$\mathcal{L}^{\mathrm{CI}} = \frac{4\pi}{1+\delta_{ef}} \sum_{\alpha,\beta} \frac{\eta_{\alpha\beta}}{\Lambda_{\alpha\beta}^2} \left(\bar{e}_\alpha \gamma_\mu e_\alpha\right)\left(\bar{f}_\beta \gamma^\mu f_\beta\right). \tag{4}$$

Current experimental lower bounds on the above mass scales at the 95% C.L. are $\Lambda_H > 1.1$–1.3 TeV and $M_{\mathrm{C}} > 6.8$ TeV [16] while, generically, those on Λs of eq. (4) are in the range 10–15 TeV [17].

2. Derivation of discovery reaches

For an extensive presentation of the analysis and a full account of the numerical results for the expected discovery and identification reaches we refer to [1]. Basically, for the polarized angular distributions, $\mathcal{O} = \mathrm{d}\sigma/\mathrm{d}\cos\theta$, we introduce the relative deviations from the SM predictions and the corresponding χ^2:

$$\Delta(\mathcal{O}) = \frac{\mathcal{O}(\mathrm{SM+NP}) - \mathcal{O}(\mathrm{SM})}{\mathcal{O}(\mathrm{SM})}; \quad \chi^2(\mathcal{O}) = \sum_{\mathrm{bins}} \left(\frac{\Delta(\mathcal{O})^{\mathrm{bin}}}{\delta\mathcal{O}^{\mathrm{bin}}}\right)^2. \tag{5}$$

Table 1. 95% C.L. discovery reaches (in TeV). Left and right entries refer to the polarization configurations $(|P^-|, |P^+|) = (0, 0)$ and $(0.8, 0.6)$, respectively.

	Process			
Model	$e^+e^- \to e^+e^-$	$e^+e^- \to l^+l^-$	$e^+e^- \to \bar{b}b$	$e^+e^- \to \bar{c}c$
	$\sqrt{s} = 0.5$ TeV, $\mathcal{L}_{\text{int}} = 100$ fb^{-1}			
Λ_H	4.1; 4.3	3.0; 3.2	3.0; 3.4	3.0; 3.2
Λ^{ef}_{VV}	76.2; 86.4	89.7; 99.4	76.1; 96.4	84.0; 94.1
Λ^{ef}_{AA}	47.4; 69.1	80.1; 88.9	76.7; 98.2	76.5; 85.9
Λ^{ef}_{LL}	37.3; 52.5	53.4; 68.3	63.6; 72.7	54.5; 66.1
Λ^{ef}_{RR}	36.0; 52.2	51.3; 68.3	42.5; 71.2	46.3; 66.8
Λ^{ef}_{LR}	59.3; 69.1	48.5; 62.8	51.3; 68.7	37.0; 57.7
Λ^{ef}_{RL}	$\Lambda^{ee}_{\text{RL}} = \Lambda^{ee}_{\text{LR}}$	48.7; 63.6	46.8; 60.1	52.2; 60.7
M_{C}	12.0; 13.8	20.0; 22.2	6.6; 10.7	10.4; 12.0

Here, the angular range has been divided into ten equal-sized bins, and $\delta\mathcal{O}^{\text{bin}}$ denotes the expected relative uncertainty, statistical plus systematic ones, in each bin. The discovery reaches on models (2)–(4) can be assessed by assuming nonobservation of deviations and, accordingly, are determined by the condition $\chi^2(\mathcal{O}) < \chi^2_{\text{CL}}$. Here, we take $\chi^2_{\text{CL}} = 3.84$ for a 95% C.L. In table 1 we present numerical results for an ILC with parameters as specified in the caption. The assumed reconstruction efficiencies are 100% for e^+e^- final pairs; 95% for l^+l^- events $(l = \mu, \tau)$; 35% and 60% for $c\bar{c}$ and $b\bar{b}$, respectively. The major systematic uncertainties originate from uncertainties on beam polarizations and on the time-integrated luminosity, for which we have assumed $\delta P^-/P^- = \delta P^+/P^+ = 0.2\%$ and $\delta\mathcal{L}_{\text{int}}/\mathcal{L}_{\text{int}} = 0.5\%$, respectively. The results in table 1 clearly show the enhancement in sensitivity to NP models allowed, at a given c.m. energy, by beams polarization. In particular, this effect is dramatic in the case of the CI models (4).

3. Assessment of expected identification reaches

In ref. [18], the identification reaches at ILC on contact-like interactions were obtained from a Monte Carlo-based analysis of the unpolarized leptonic processes (1). Here we consider polarized beams and also quark final states. Continuing the previous χ^2-based analysis, we now assume that a deviation has been observed, for example consistent with the ADD scenario (2) with some value of Λ_H. To assess the level at which the ADD model can be identified from the other models potential sources of the deviation, we choose, for example, the AA model of eq. (4), and introduce relative deviations $\tilde{\Delta}$ and corresponding $\tilde{\chi}^2$ similar to eq. (5):

$$\tilde{\Delta}(\mathcal{O}) = \frac{\mathcal{O}(\text{AA}) - \mathcal{O}(\text{ADD})}{\mathcal{O}(\text{ADD})}; \quad \tilde{\chi}^2(\mathcal{O}) = \sum_{\text{bins}} \left(\frac{\tilde{\Delta}(\mathcal{O})^{\text{bin}}}{\tilde{\delta}\mathcal{O}^{\text{bin}}} \right)^2. \qquad (6)$$

Table 2. 95% C.L. identification reaches (in TeV). Left and right entries refer to the polarization configurations $(|P^+|,|P^-|) = (0, 0)$ and $(0.8, 0.6)$.

	Process			
Model	$e^+e^- \to e^+e^-$	$e^+e^- \to l^+l^-$	$e^+e^- \to \bar{b}b$	$e^+e^- \to \bar{c}c$
	$\sqrt{s} = 0.5$ TeV, $\mathcal{L}_{\rm int} = 100$ fb^{-1}			
Λ_H	2.5; 3.1	2.7; 2.8	3.0; 3.1	2.7; 2.9
$\Lambda^{ef}_{\rm VV}$	26.8; 41.0	57.6; 63.9	20.3; 82.7	56.3; 64.4
$\Lambda^{ef}_{\rm AA}$	41.1; 60.9	63.2; 70.2	20.4; 84.7	62.2; 75.5
$\Lambda^{ef}_{\rm LL}$	—; 44.3	—; 56.0	—; 62.2	—; 59.0
$\Lambda^{ef}_{\rm RR}$	—; 45.2	—; 58.0	—; 61.1	—; 59.9
$\Lambda^{ef}_{\rm LR}$	31.3; 48.5	—; 57.5	—; 49.0	—; 46.9
$\Lambda^{ef}_{\rm RL}$	$\Lambda^{ee}_{\rm RL} = \Lambda^{ee}_{\rm LR}$	—; 58.3	—; 56.2	—; 53.1
$M_{\rm C}$	4.2; 6.5	8.8; 14.4	4.5; 7.7	6.0; 8.3

In eq. (6), $\tilde{\delta}\mathcal{O}^{\rm bin}$ is the expected relative uncertainty, the statistical part being related to the ADD model prediction. Accordingly, $\tilde{\chi}^2$ is a function of λ/Λ_H^4 and $\eta/\Lambda^2_{\rm AA}$, and we can determine, in the plane of these parameters, the *confusion region* where the AA model can be considered as consistent with the ADD. At the 95% C.L., one determines such confusion region from the condition $\tilde{\chi}^2 < 3.84$. The contour of the confusion region identifies a maximal value of $|\lambda/\Lambda_H^4|$ (equivalently, a minimum value of Λ_H), for which the AA model can *exclude* at the 95% C.L. for any value of $\eta/\Lambda^2_{\rm AA}$. This value, $\Lambda_H^{\rm AA}$, is the *exclusion reach* on the AA model. Figure 1 (left panel) shows an example of confusion region obtained by different polarization. This procedure can be repeated for all other interactions in eqs (3) and (4), to determine the individual exclusion reaches $\Lambda_H^{\rm VV}$, $\Lambda_H^{\rm RR}$, $\Lambda_H^{\rm LL}$, $\Lambda_H^{\rm LR}$, $\Lambda_H^{\rm RL}$ and $\Lambda_H^{\rm TeV}$. Finally, the *identification reach* on the ADD scenario corresponds to the *minimum* of the *exclusion reaches*, $\Lambda_H^{\rm ID} = \min\{\Lambda_H^{\rm VV}, \Lambda_H^{\rm AA}, \Lambda_H^{\rm RR}, \Lambda_H^{\rm LL}, \Lambda_H^{\rm LR}, \Lambda_H^{\rm RL}, \Lambda_H^{\rm TeV}\}$. Clearly, for $\Lambda_H < \Lambda_H^{\rm ID}$ all composite-like CI models as well as the TeV^{-1} gravity model can be excluded as explanations of the deviation or, equivalently, the ADD model can be identified. This simple χ^2 procedure can be applied in turn to all the individual sources of corrections to the SM in eqs (3) and (4), and the expected identification reaches the corresponding Λ mass parameters and can be determined analogously. Figure 1 (right panel) shows an example, relevant to CI models, where a restricted confusion region can be determined only with initial beams polarization.

The numerical results for the expected identification reaches are shown in table 2. Here, blank entries refer to models for which the identification reach is found to fall below the current limits.

4. Concluding remarks

In the previous section we have considered the problem of distinguishing the New Physics scenarios represented by the contact-like effective Lagrangians (2)–(4) from one another at the ILC, by analyzing polarized differential cross-sections for fermion-pair production processes. The discovery reaches as well as

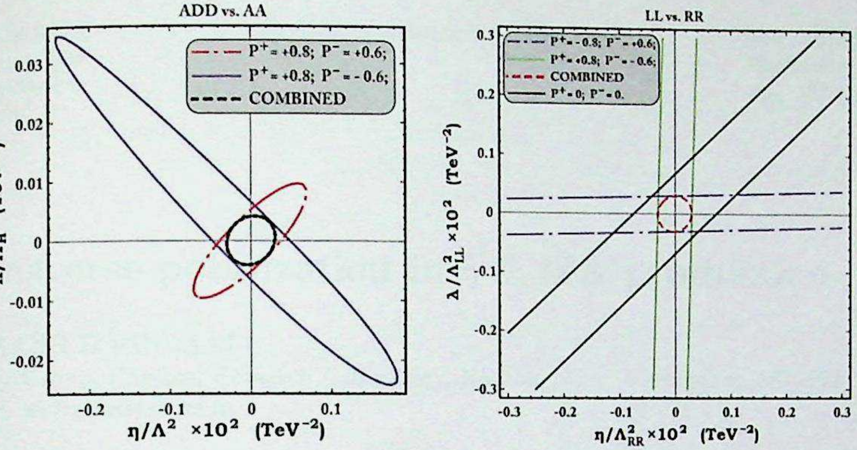

Figure 1. Left panel: $\Lambda_{\rm H}$ vs. $\Lambda_{\rm AA}$ confusion region from $e^+e^- \to e^+e^-$. Right panel: $\Lambda_{\rm LL}$ vs. $\Lambda_{\rm RR}$ confusion region from $e^+e^- \to l^+l^-$ $(l = \mu, \tau)$. $\sqrt{s} = 0.5$ TeV, $\mathcal{L}_{\rm int} = 100$ fb^{-1}.

the identification reaches are rather high compared to the current bounds, depending on energy and luminosity, and can increase by factors 2.5–3 for an ILC with $\sqrt{s} = 1\,$TeV and $\mathcal{L}_{\rm int} = 1000\,{\rm fb}^{-1}$ [1]. The role of polarization in the various cases is shown by figure 1 and table 2. It has an appreciable role in enhancing the identification sensitivity to the ADD model (figure 1, left panel). The enhancement is dramatic for models (3) and (4). Actually, as indicated by the blank entries in table 2, polarization should be essential for the identification of some of the contact interaction scenarios (4), which would not be possible with unpolarized beams (figure 1, right panel).

References

[1] A A Pankov, N Paver and A V Tsytrinov, *Phys. Rev.* **D73**, 115005 (2006)
[2] A A Pankov and N Paver, *Phys. Rev.* **D72**, 035012 (2005)
[3] P Osland, A A Pankov and N Paver, *Phys. Rev.* **D68**, 015007 (2003)
[4] A A Pankov and N Paver, *Euro. Phys. J.* **C29**, 313 (2003)
[5] G Moortgat-Pick *et al*, arXiv:hep-ph/0507011
[6] N Arkani-Hamed, S Dimopoulos and G R Dvali, *Phys. Lett.* **B429**, 263 (1998)
[7] N Arkani-Hamed, S Dimopoulos and G R Dvali, *Phys. Rev.* **D59**, 086004 (1999)
[8] I Antoniadis, N Arkani-Hamed, S Dimopoulos and G R Dvali, *Phys. Lett.* **B436**, 257 (1998)
[9] G F Giudice, R Rattazzi and J D Wells, *Nucl. Phys.* **B544**, 3 (1999)
[10] T Han, J D Lykken and R J Zhang, *Phys. Rev.* **D59**, 105006 (1999)
[11] J L Hewett, *Phys. Rev. Lett.* **82**, 4765 (1999)
[12] K M Cheung and G Landsberg, *Phys. Rev.* **D65**, 076003 (2002)
[13] T G Rizzo and J D Wells, *Phys. Rev.* **D61**, 016007 (2000)
[14] E Eichten, K D Lane and M E Peskin, *Phys. Rev. Lett.* **50**, 811 (1983)
[15] R Rückl, *Phys. Lett.* **B129**, 363 (1983)
[16] For a review see, e.g., K Cheung, arXiv:hep-ph/0409028
[17] Particle Data Group: S Eidelman *et al*, *Phys. Lett.* **B502**, 1 (2004)
[18] G Pasztor and M Perelstein, arXiv:hep-ph/0111471

PRAMANA
— journal of
physics

© Indian Academy of Sciences

Vol. 69, No. 5
November 2007
pp. 883–887

Transverse polarization in $\gamma Z, HZ$ production

SAURABH D RINDANI
Theory Group, Physical Research Laboratory, Navrangpura, Ahmedabad 380 009, India
E-mail: saurabh@prl.res.in

Abstract. With the use of transverse polarization (TP), a CP-odd and T-odd observable can be constructed when the final-state particles are self-conjugate. In the case of HZ production, this observable can be used to probe a certain effective four-point e^+e^-ZH CP-violating coupling, not accessible without TP. Effective CP-violating ZZH coupling does not contribute to this observable. A similar observable in γZ production can be used to probe $e^+e^-\gamma Z$ four-point couplings.

Keywords. Transverse polarization at electron–positron collider; Higgs production; beyond standard model; Z boson.

PACS Nos 11.30.Er; 13.66.Fg; 13.88.+e

1. The process $e^+e^- \to HZ$

In a theory with an extended Higgs sector and new mechanisms of CP violation, the physical Higgs bosons are not necessarily eigenstates of CP. In such a case, the production of a physical Higgs can proceed through more than one channel, and the interference between two channels can give rise to a CP-violating signal in the production. Here we consider in a general model-independent way the production of a Higgs mass eigenstate H through the process $e^+e^- \to HZ$, an important mechanism for the production of the Higgs. $e^+e^- \to HZ$ gets contribution from a diagram with an s-channel exchange of Z. At the lowest order, the ZZH vertex in this diagram is simply a point-like coupling. It may be modified by interactions beyond SM by means of a form factor, and/or more complicated momentum-dependent anomalous interactions [1–3].

We consider a beyond-SM contribution represented by a four-point e^+e^-ZH coupling. This is general enough to include the effects of the diagram with anomalous ZZH vertex with s-channel Z exchange. In addition it can include effects of box diagrams, or diagrams with t-channel exchange of new particles. We obtain the angular distributions in the presence of polarized beams and examine how angular asymmetries can be used to constrain the form factors of the four-point coupling. Details may be found in [4]. In earlier works, it has been observed that polarization does not give any new information about the anomalous ZZH couplings when they are assumed real [3]. However, with four-point couplings, we find that there are new CP-odd terms in the distribution when both e^- and e^+ beams have transverse polarization (TP). Thus, TP would be most useful in isolating such terms.

The most general chirality conserving (CC) four-point vertex for the process $e^-(p_1) + e^+(p_2) \to Z^\alpha(q) + H(k)$ consistent with Lorentz invariance can be written as (we neglect the electron mass everywhere)

$$M^3 \Gamma^\alpha_{\rm CC} = -M^2 \gamma^\alpha (V_1 + \gamma_5 A_1) + \not{k}(V_2 + \gamma_5 A_2) k^\alpha \\ -i \not{q}(V_3 + \gamma_5 A_3)(p_2 - p_1)^\alpha . \tag{1}$$

In the above expression, V_i and A_i are form factors, which, for simplicity, we treat as tants. The terms containing V_3 and A_3 are CP violating, whereas the remaining CP conserving. M is a parameter with dimensions of mass, put in to render the form factors dimensionless.

We obtain, for arbitrary polarizations, analytic expressions for the angular distribution [4] of Z arising from SM and from the interference between the SM amplitude and the amplitude arising from the four-point couplings of (1). We neglect terms bilinear in the four-point couplings, which are assumed small compared to the SM ones.

The z-axis is chosen along the direction of the e^- momentum, and the xz plane to coincide with the production plane. The positive x axis is chosen to be along the direction of the e^- TP. θ and ϕ are then the polar and azimuthal angles of the momentum of Z. The e^+ polarization direction is chosen anti-parallel to the e^- polarization direction.

The V_3 and A_3 terms in the distribution can be determined using a simple forward–backward asymmetry:

$$A_{\rm FB}(\theta_0) = (1/\sigma_0)[\Delta\sigma(\theta_0, \pi/2) - \Delta\sigma(\pi/2, \pi - \theta_0)], \tag{2}$$

with $\Delta\sigma(\theta, \theta') \equiv \int_\theta^{\theta'} ({\rm d}\sigma/{\rm d}\theta){\rm d}\theta$, where $\sigma_0 \equiv \Delta\sigma(\theta_0, \pi - \theta_0)$ is the integrated cross section, and θ_0 is a cut-off in the forward and backward directions needed to keep away from the beam pipe, and chosen to optimize the sensitivity. This asymmetry is odd under CP and is proportional to the combination $g_V \,{\rm Im}\, V_3 - g_A \,{\rm Im}\, A_3$.

The distribution with TP of beams has new ϕ-dependent terms occurring with a factor of $P_{\rm T}\bar{P}_{\rm T}$. Hence both beams need to have TP for nontrivial azimuthal dependence. We define two asymmetries, which serve to measure two different combinations of CP-violating couplings:

$$A^{\rm T}_{\rm FB}(\theta_0) = \frac{1}{\sigma_0} \sum_{n=0}^{3} (-1)^n \int_{\pi n/2}^{\pi(n+1)/2} {\rm d}\phi A_{\rm FB}(\theta_0; \phi), \tag{3}$$

$$A'^{\rm T}_{\rm FB}(\theta_0) = \frac{1}{\sigma_0} \sum_{n=0}^{3} (-1)^n \int_{\pi(2n-1)/4}^{\pi(2n+1)/4} {\rm d}\phi A_{\rm FB}(\theta_0; \phi), \tag{4}$$

where $A_{\rm FB}(\theta_0; \phi)$ is a differential form of the asymmetry in eq. (2), before integration over ϕ, and for nonzero TP. The integrals in the above can be easily evaluated. The result shows that $A^{\rm T}_{\rm FB}(\theta_0)$ and $A'^{\rm T}_{\rm FB}(\theta_0)$ are respectively proportional to $g_V \,{\rm Re}\, A_3 + g_A \,{\rm Re}\, A_3$ and $g_V \,{\rm Im}\, V_3 + g_A \,{\rm Im}\, A_3$. Both are proportional to $P_{\rm T}\bar{P}_{\rm T}$. We find that if one considers only a modification of the ZZH vertex as in

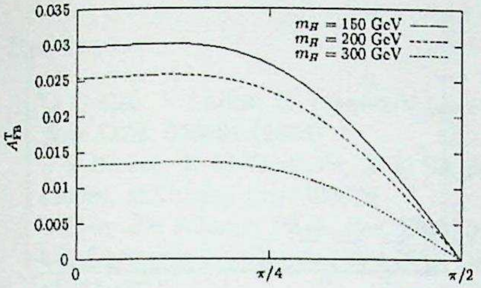

Figure 1. The asymmetry $A^{\rm T}_{\rm FB}$ for transverse polarizations $P_{\rm T} = 0.8$ and $\bar{P}_{\rm T} = 0.6$ plotted against θ_0 for $\mathrm{Re}\,V_3 = 0.1$, $\mathrm{Re}\,A_3 = 0$.

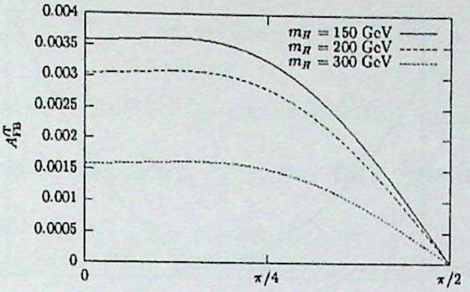

Figure 2. The asymmetry $A'^{\rm T}_{\rm FB}$ for transverse polarizations $P_{\rm T} = 0.8$ and $\bar{P}_{\rm T} = 0.6$ plotted against θ_0 for $\mathrm{Im}\,V_3 = 0.1$, $\mathrm{Im}\,A_3 = 0$.

refs [1–3], $A^{\rm T}_{\rm FB}$ and $A'^{\rm T}_{\rm FB}$ vanish. This result for $A^{\rm T}_{\rm FB}$ was obtained in [3]. Thus, observation of a nonzero asymmetry would signal the presence of a CP-violating four-point interaction.

We now describe our numerical results. We use the value $M = 1$ TeV. This choice is simply for convenience, and is not simply related to any assumption about the scale of new physics – a change in M can always be compensated by changes in the form factors. For the linear collider, we assume $\sqrt{s} = 500$ GeV, $P_{\rm T} = 0.8$, $\bar{P}_{\rm T} = 0.6$, and an integrated luminosity of 500 fb^{-1}. We show results for three values of the Higgs mass, $m_{\rm H} = 150$ GeV, 200 GeV and 300 GeV.

The asymmetries $A^{\rm T}_{\rm FB}$ and $A'^{\rm T}_{\rm FB}$ are shown as functions of θ_0 in figures 1 (for $\mathrm{Re}\,V_3 = 0.1$, $\mathrm{Re}\,A_3 = 0$) and 2 (for $\mathrm{Im}\,V_3 = 0.1$, $\mathrm{Im}\,A_3 = 0$). We now examine the accuracy in which these couplings can be constrained. We find that the 90% confidence level (C.L.) limit that can be placed on $\mathrm{Re}\,V_3$ from the asymmetry $A^{\rm T}_{\rm FB}$ for a typical value of $\theta_0 = 45°$ ranges from 3.9×10^{-2} for $m_{\rm H} = 150$ GeV, to 1.3×10^{-1} for $m_{\rm H} = 300$ GeV. The corresponding limits on $\mathrm{Re}\,A_3$ are a factor $|g_A/g_V| \approx 8.3$ higher. In case of $A'^{\rm T}_{\rm FB}$ it is $\mathrm{Im}\,A_3$ which has the limits mentioned above for $\mathrm{Re}\,V_3$, and limits on $\mathrm{Im}\,V_3$ are a factor of about 8.3 higher.

2. The process $e^+e^- \to \gamma Z$

γZ production has a significant SM cross section at the planned ILC energies. We discuss contributions to the differential cross section due to general, model-independent, gauge and Lorentz invariant, chirality conserving (CC) four-point interactions. Details may be found in [5]. In particular, one of these interactions generates precisely the same contributions as from anomalous CP-violating triple-gauge boson vertices studied in a similar context [6].

The process considered is $e^-(p_-, s_-) + e^+(p_+, s_+) \to \gamma(k_1, \alpha) + Z(k_2, \beta)$. The chirality-conserving anomalous four-point vertex for this process contains 12 form factors [5], which we label as v_i, a_i $(i = 1, \dots, 6)$. We assume for simplicity that the form-factors are all constants. The combinations $v_1, v_2 - v_5, v_3 - v_4$ and $a_1, a_2 - a_5, a_3 - a_4$ are CP conserving, while $v_2 + v_5, v_3 + v_4, v_6$ and $a_2 + a_5, a_3 + a_4, a_6$ are CP violating.

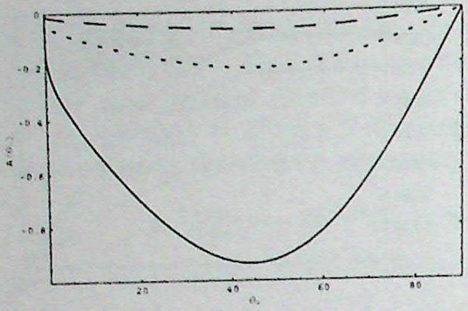

Figure 3. The asymmetries $A^{\mathrm{T}}_{\mathrm{FB}}(\theta_0)$ (solid line), $A'^{\mathrm{T}}_{\mathrm{FB}}(\theta_0)$ (dashed line) and $A_{\mathrm{FB}}(\theta_0)$ (dotted line), plotted as functions of the cut-off θ_0 for Re v_6 = Im $v_6 = 1$.

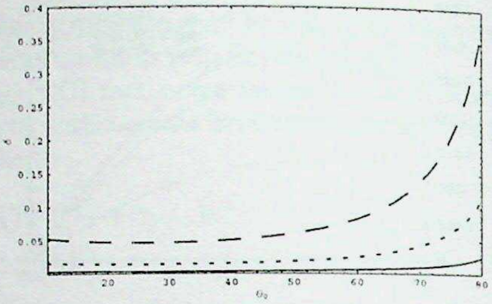

Figure 4. 90% C.L. limit on Re v_6 from the asymmetry $A^{\mathrm{T}}_{\mathrm{FB}}(\theta_0)$ (solid line), and on Im v_6 from $A'^{\mathrm{T}}_{\mathrm{FB}}(\theta_0)$ (dashed line) and $A_{\mathrm{FB}}(\theta_0)$ (dotted line), plotted as functions of the cut-off θ_0.

We use the same CP-odd asymmetries as in the previous section, with θ and ϕ referring to the polar and azimuthal angles of γ. Two of these again require both beams to have TP. Figure 3 shows the asymmetries as functions of the cut-off when the anomalous couplings Re v_6 (for the case of $A^{\mathrm{T}}_{\mathrm{FB}}(\theta_0)$) and Im v_6 (for the case of $A'^{\mathrm{T}}_{\mathrm{FB}}(\theta_0)$ and $A_{\mathrm{FB}}(\theta_0)$) alone are set to unity. 90% C.L. limits on couplings, denoted by δ, are shown in figure 4 for a choice of 26° for θ_0. The results for other CP-violating combinations of couplings can be deduced from this case. From the asymmetry $A^{\mathrm{T}}_{\mathrm{FB}}(\theta_0)$, we get the limits (in units of 10^{-3}) $|\mathrm{Re}\, v_{3,4}| \leq 0.21$, $|\mathrm{Re}\, v_6| \leq 3.1$, and $|\mathrm{Re}\, a_{3,4}| \leq 3.1$, $|\mathrm{Re}\, a_6| \leq 46$. The asymmetry $A'^{\mathrm{T}}_{\mathrm{FB}}(\theta_0)$ yields limits which are obtained from these by the replacement of the real part by imaginary part and interchange of v_i and a_i. The asymmetry $A_{\mathrm{FB}}(\theta_0)$ with unpolarized beams yields the limits (in units of 10^{-3}) $\mathrm{Im}\, v_{2,5} \leq 0.93$, $\mathrm{Im}\, v_6 \leq 14$ and $\mathrm{Im}\, a_{2,5} \leq 0.064$, $\mathrm{Im}\, a_6 \leq 0.96$.

3. Conclusions

In conclusion, we have considered in all generality the role of chirality conserving four-point couplings due to new physics in the processes $e^+e^- \to HZ$ and $e^+e^- \to \gamma Z$ with polarized beams. We found that in the presence of TP, there is a CP-odd and T-odd contribution to the angular distribution, dependent on coupling combinations which cannot be determined without TP. Moreover, in the case of HZ production, this contribution does not exist when only ZZH anomalous couplings are considered. Hence such a term, if observed, would be a unique signal of CP-violating four-point interaction.

Acknowledgement

This work was partly supported by the IFCPAR project no. 3004-2. The work in section 1 was done in collaboration with Kumar Rao. The work in section 2 was done in collaboration with B Ananthanarayan.

References

[1] Q H Cao, F Larios, G Tavares-Velasco and C P Yuan, arXiv:hep-ph/0605197, *Phys. Rev.* **D74**, 056001 (2006)
S S Biswal, R M Godbole, R K Singh and D Choudhury, *Phys. Rev.* **D73**, 035001 (2006), arXiv:hep-ph/0509070
T Han and J Jiang, *Phys. Rev.* **D63**, 096007 (2001), arXiv:hep-ph/0011271
G J Gounaris, F M Renard and N D Vlachos, *Nucl. Phys.* **B459**, 51 (1996), arXiv:hep-ph/9509316
A Skjold and P Osland, *Nucl. Phys.* **B453**, 3 (1995), arXiv:hep-ph/9502283

[2] V Barger, T Han, P Langacker, B McElrath and P Zerwas, *Phys. Rev.* **D67**, 115001 (2003), arXiv:hep-ph/0301097
W Kilian, M Kramer and P M Zerwas, arXiv:hep-ph/9605437; *Phys. Lett.* **B381**, 243 (1996), arXiv:hep-ph/9603409

[3] K Hagiwara and M L Stong, *Z. Phys.* **C62**, 99 (1994), arXiv:hep-ph/9309248

[4] K Rao and S D Rindani, arXiv:hep-ph/0605298, *Phys. Lett.* **B642**, 85 (2006)

[5] B Ananthanarayan and S D Rindani, *Phys. Lett.* **B606**, 107 (2005), arXiv:hep-ph/0410084; *J. High Energy Phys.* **0510**, 077 (2005), arXiv:hep-ph/0507037

[6] D Choudhury and S D Rindani, *Phys. Lett.* **B335**, 198 (1994), arXiv:hep-ph/9405242
B Ananthanarayan, S D Rindani, R K Singh and A Bartl, *Phys. Lett.* **B593**, 95 (2004); Erratum, *Phys. Lett.* **B608**, 274 (2005), arXiv:hep-ph/0404106

PRAMANA
— journal of
physics

© Indian Academy of Sciences

Vol. 69, No. 5
November 2007
pp. 889–894

Higher curvature effects in Arkani-Hamed–Dimopoulos–Dvali and Randall–Sundrum models

T G RIZZO
Stanford Linear Accelerator Center, 2575 Sand Hill Rd., Menlo Park, CA 94025, USA
E-mail: rizzo@slac.stanford.edu

Abstract. We explore the collider phenomenology of terascale extra-dimensional models with gravitational actions that contain higher curvature terms. In particular, we examine how the classic collider signatures of the models of Arkani-Hamed, Dimopoulos and Dvali (ADD) and of Randall and Sundrum (RS) are altered by these modifications to the usual Einstein–Hilbert (EH) action. Not only are the detailed signatures for gravitationally induced processes altered but new contributions are found to arise due to the existence of additional scalar Kaluza–Klein (KK) states in the spectrum.

Keywords. Extra dimensions; gravity; colliders.

PACS Nos 11.25.Wx; 12.60.-i

1. Introduction

Over the last few years several extra-dimensional models have been introduced in an attempt to deal with the hierarchy problem. These models can lead to rather unique and spectacular signatures at terascale colliders such as the LHC and ILC. The ADD and RS models, though quite distinct, have many common features including a constant curvature bulk, localized standard model (SM) fields and the assumption of the validity of the EH action as a description of gravitational interactions.

It is well-known that the EH action can only be regarded as an effective theory, so we may on general grounds expect that as one probes energies approaching the fundamental scale, M, (as one will do so at the LHC/ILC for both models) significant deviations from EH expectations are likely to appear. From a bottom-up approach we can claim ignorance of what a more complete gravitational theory may be like but we would expect that the leading deviations from EH would appear as higher dimensional operators involving various invariants constructed from the curvature tensor. This motivates us to consider a more general class of gravitational actions of the $D = 4 + n$-dimensional form

$$S_g = \frac{M^{D-2}}{2} \int \mathrm{d}^D x \sqrt{g}\, F(R, P, Q), \tag{1}$$

where $P = R_{AB}R^{AB}$ and $Q = R_{ABCD}R^{ABCD}$. Various actions of this generic type have been examined in the literature within a variety of contexts including black holes, cosmology, modifications of gravity within the solar system as well as at short-distances scales which are of interest to us here [1]. It will be assumed in what follows that at low energies $F \to R$ so that the EH action, with all its successes, is recovered.

In both the ADD and RS models we wish to know the graviton KK spectrum and wave functions as well as their couplings to SM fields. We also need to know how $\bar{M}_{\rm Pl}$ and the more fundamental scale M are related. To this end it can be shown that for spaces with constant curvature the above action is the most general one; furthermore it can be shown that we can obtain all of the desired information by expanding this action around the constant background metric to quadratic order [1]. Performing this expansion then yields an effective action of the form

$$S_{\rm eff} = \frac{M^{D-2}}{2} \int {\rm d}^D x \sqrt{g}\, \left[\Lambda + a_1 R + a_2 R^2 + a_3 C + a_4 G\right], \tag{2}$$

where $G = R^2 - 4R_{AB}R^{AB} + R_{ABCD}R^{ABCD} = R^2 - 4P + Q$ is the Gauss–Bonnet invariant and $C = C_{ABCD}C^{ABCD} = Q - 4P/(n+2) + 2R^2/(n+3)(n+2)$ is the square of the Weyl tensor. This simplification is obtainable from the direct expansion $F = F_0 + (R - R_0)F_R + (P - P_0)F_P + (Q - Q_0)F_Q$ + quadratic terms, where F_0 is a constant corresponding to the evaluation of F itself in the fixed curvature background metric and $F_X = \partial F/\partial X|_0$; a quantity X_0 here means that X is to be evaluated in terms of the background metric which we assume to be a space of constant curvature as is the case in both the ADD and the RS models. Thus the quantities R_0, P_0, Q_0, F_X and F_{XY} are just numbers which depend on the explicit form of the metric and the number of extra dimensions. This procedure directly gives us constants Λ, a_i [1] in terms of F and its derivatives evaluated in the background metric as we will see below.

2. ADD

For the action F, the D-dimensional field content consists of a massless tensor field (i.e., the 'usual' graviton) as well as a massive scalar field and a massive tensor ghost field with bulk masses directly calculable from F itself. This can be seen most clearly in, e.g., the ADD model where the full exchange amplitude between two localized SM sources (before KK summation) can be written as $A \sim [T_{\mu\nu}T^{\mu\nu} - T^2/(n+2)]/(k^2 - m_n^2) - [T_{\mu\nu}T^{\mu\nu} - T^2/(n+3)]/(k^2 - (m_{\rm T}^2 + m_n^2)) + T^2/(n+2)(n+3)[k^2 - (m_{\rm S}^2 + m_n^2)]$. Here $T_{\mu\nu}$ is the localized SM stress-energy tensor and T is its trace. Ghost fields are potentially very dangerous in perturbation theory and can cause unitarity violations so we may want to rid ourselves of this massive tensor field. To remove this ghost state from the spectrum it is sufficient to force the bulk tensor mass $m_{\rm T}$ to infinity; this will make all of the fields in its entire KK tower decomposition have infinite mass. In this simple ADD case one finds that $m_{\rm T}^2 = -F_R/(n+2)(F_P + 4F_Q)$ and thus we see that to make $m_{\rm T}$ infinitely large it is sufficient to demand that F be only a function of R and the combination $P - 4Q$. These results can also be shown to hold qualitatively in the case of the RS

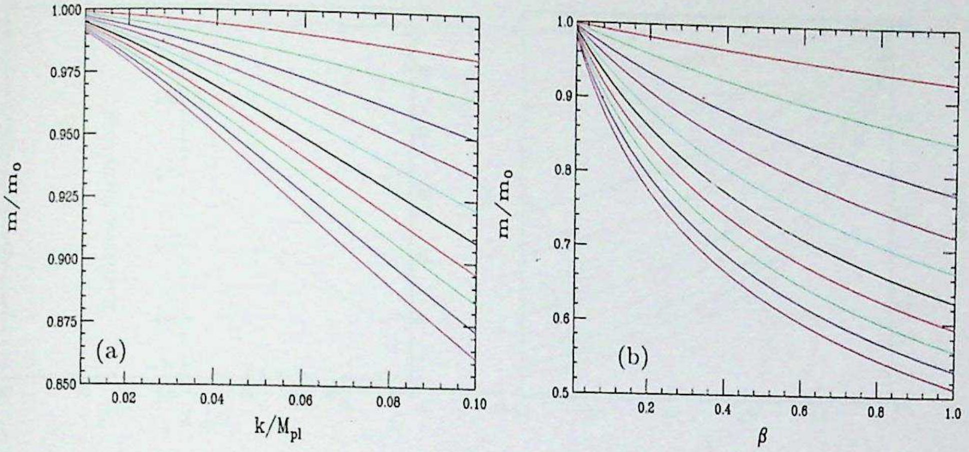

Figure 1. Shifts in the RS KK graviton masses due to finite β corrections: (**a**) As a function of c with $\beta = 0.1$–1 in steps of 0.1 from top to bottom and (**b**) as a function of β for $c = 0.01$–0.1 in steps of 0.01 from top to bottom.

model and the $P - 4Q$ dependence of F will be assumed in the discussion below. Of course, we still need to insure that the usual KK gravitons and the new KK scalars are non-tachyonic so that $F_R > 0$ will also be required. For either ADD or RS model, one now in general finds that $a_3 = 0$ and

$$\begin{aligned}
\Lambda &= F_0 - R_0 F_R + F_{RR} R_0^2/2 + \lambda R_0^2 [F_Q - R_0 F_{QQ} + \lambda F_{QQ} R_0^2/2] \\
a_1 &= F_R - R_0 F_{RR} + \lambda R_0^2 F_{RQ} \\
a_2 &= -F_Q + F_{RR}/2 + R_0 F_{RQ} - \lambda R_0^2 F_{QQ} \\
a_4 &= -a_2 + F_{RR}/2 \,. \qquad (3)
\end{aligned}$$

The ADD case is particularly easy to analyze as the space is flat and there is no bulk cosmological constant. Here the expansion of F to quadratic order is quite simple: $F \to F_R R + \big[-F_Q + F_{RR}/2\big] R^2 + F_Q G$.

In ADD there are two major modifications due to $R \to F$. First, due to the existence of the D-dimensional bulk scalar which produces its own KK tower there are new exchanges between SM sources and new emissions that can lead to missing energy signatures. However, the effect of these new states on these conventional signatures is quite suppressed as scalars couple to the trace of the energy–momentum tensor. For SM fields the ratio $T^2/T_{\mu\nu}T^{\mu\nu} \sim (m^2/s)^k$, with m a SM particle mass and $k = 1, 2$. Further suppression occurs since the KK spectrum of the scalars begins at the value of the bulk mass m_S; for most reasonable choices of F it can be shown that m_S is naturally $\sim M \sim$ TeV. For example, if $F = R + \beta R^2/M^2$, we find that the value of m_S^2 is $(n+2)M^2/(4\beta(n+3))$; thus we see that with β of $O(1)$, $m_S \sim M$.

The second effect is to modify the usual ADD relation to

$$\bar{M}_{\rm Pl}^2 = V_n M^{n+2} F_R \,, \qquad (4)$$

where we expect F_R is $O(1)$ and $V = (2\pi R)^n$ for a torus. Since $\bar{M}_{\rm Pl}$ is fixed, for a given M the effect of $F_R \neq 1$ is to shift the value of R which leads to a modification

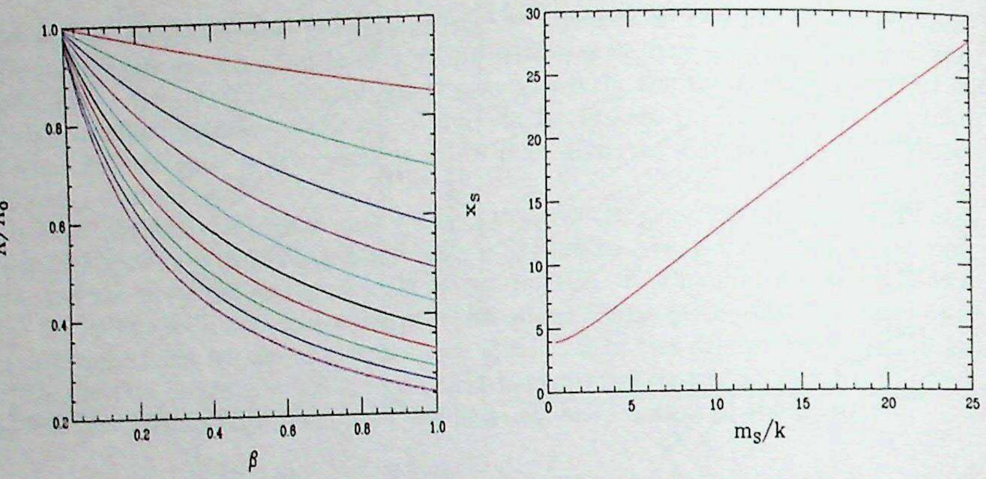

Figure 2. (**a**) Shift in the cosmological constant in RS due to finite β for $c =$ 0.01–0.10 from top to bottom in 0.01 steps. (**b**) Root for the determination of mass of the lightest KK state corresponding to the new RS scalar as a function of the scaled bulk mass. As a point of comparison the first KK graviton has a root of $\simeq$3.83.

of the KK spectrum as $m_{KK} \sim 1/R$, i.e., $m_{KK} \to m_{KK} F_R^{1/n}$. Similar arguments lead to rescalings of the graviton emission amplitude, $\mathrm{d}\sigma_{\mathrm{ADD}} \to F_R^{-1} \mathrm{d}\sigma_{\mathrm{ADD}}$ as well as the amplitude for graviton KK exchange, $A_{KK} \to F_R^{-1} A_{KK}$, both of which can lead to important experimental consequences, i.e., $O(1)$ modifications to anticipated ADD search reaches at colliders.

3. RS

In RS the bulk is of constant background curvature with $R_0 = -20k^2$, k being defined via the metric $\mathrm{d}s^2 = \mathrm{e}^{-2k|y|}\eta_{\mu\nu}\mathrm{d}x^\mu \mathrm{d}x^\nu - \mathrm{d}y^2$ induced by a bulk cosmological constant Λ. For general $F(R, P-4Q)$, the equations of motion lead to a relationship between F, k, M and Λ: $224k^4 F_Q + 8k^2 F_R + F_0 = 2\Lambda/M^3$ from which k as a function of Λ (or the other way around) can be extracted. It is important to remember here that $F_{0,R,Q}$ are themselves functions of k. For example, if we assume that $F = R + R^2/M^2$, we obtain

$$k^2 = \frac{3M^2}{40\beta}\left[1 \pm \left(1 + \frac{40\Lambda}{9M^5}\beta\right)^{1/2}\right], \tag{5}$$

for which the negative root goes over to the usual EH result as the parameter $\beta \to 0$. Further analysis of the equations of motion shows that the basic RS relationship between the 5d fundamental scale and $\bar{M}_{\mathrm{Pl}}$ is also altered by $F \neq R$; we now find that

$$H(k)\frac{M^3}{k} = \bar{M}_{\mathrm{Pl}}^2, \tag{6}$$

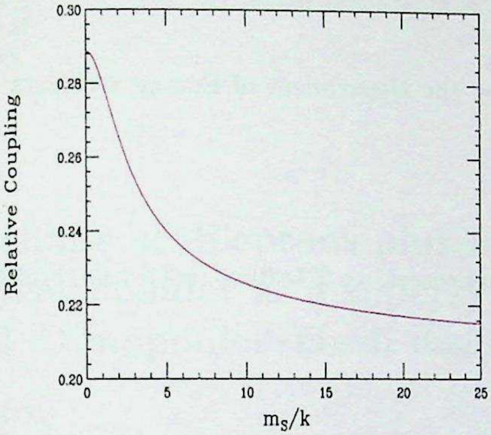

Figure 3. Estimate of the relative wave function suppression for the lightest scalar KK coupling to matter in comparison to the corresponding KK graviton. Recall that scalars couple to T whereas gravitons couple to $T_{\mu\nu}$.

where in general $H = F_R + 36k^2F_Q + 1000k^4F_{RQ} + 10080k^6F_{QQ}$. If, for example, $F = R + R^2/M^2$, then $H = 1 - 40\beta k^2/M^2$. Since $\bar{M}_{\rm Pl}$ is known, for a fixed value of M the two expressions above lead to shifts in the values of both k and Λ as compared to standard RS expectations and, consequently, to a shift in the KK graviton spectrum. This is shown in figure 1 for our simple example of $F = R + \beta R^2/M^2$ where the KK mass shift is explicitly given by

$$\frac{m}{m_0} = (80\beta c^{4/3})^{-1}\left[-1 + (1 + 160\beta c^{4/3})^{1/2}\right]. \qquad (7)$$

Here we have defined $c = k_0/\bar{M}_{\rm Pl}$, where k_0 is the value obtained in the usual RS model employing the EH action. The corresponding shift in Λ is shown in figure 2.

As in ADD, the new scalar obtains a bulk mass which in RS case is given by

$$m_S^2 = \frac{3}{8}\,\frac{F_R + 20k^2F_{RR} + 280k^4F_{RQ}}{F_{RR} - 2F_Q - 40k^2F_{RQ} - 560k^4F_{QQ}}. \qquad (8)$$

Within a given model this value can be used to obtain the scalar KK spectrum by solving for the roots of the equation $(2-\nu)J_\nu(x_n) + x_nJ_{\nu-1}(x_n) = 0$ with J the usual Bessel function and $\nu^2 = 4 + m_S^2/k^2$ in the usual RS fashion; the KK masses are then given by $m_n = x_nk{\rm e}^{-\pi kr_c}$. Figure 2 shows the root for the lightest KK scalar state, x_S, as a function of m_S/k. We thus naturally expect these scalar KK states to be more massive than the corresponding more familiar graviton excitations. Since their couplings are suppressed as in the ADD case they might be difficult to detect experimentally; this is made even more so by the small value of the scalar KK wave function evaluated at the TeV brane where the SM matter is assumed to be localized. This further relative suppression is shown in figure 3.

Hopefully new dimensions will be discovered at the Terascale.

Acknowledgments

This work supported in part by the Department of Energy, Contract DE-AC02-76SF00515.

References

[1] For more details and original references, see T G Rizzo, arXiv:hep-ph/0603242

PRAMANA
— journal of
physics

© Indian Academy of Sciences

Vol. 69, No. 5
November 2007
pp. 895–901

Event-shape of dileptons plus missing energy at a linear collider as a supersymmetry/Arkani-Hamed–Dimopoulos–Dvali discriminant

PROBIR ROY
Tata Institute of Fundamental Research, Homi Bhabha Road, Mumbai 400 005, India
E-mail: probir@theory.tifr.res.in

Abstract. An event-shape analysis of the dileptons in the process $e^+e^- \to \ell^+\ell^- \not\!\!E$, studied in ILC or CLIC, can clearly discriminate between a supersymmetric or a large extra dimensional (ADD) production mechanism.

Keywords. Linear collider; supersymmetry; large extra dimensions; event-shape.

PACS Nos 04.50.+h; 11.10.Kk; 11.25.Mj; 12.60.Jv; 13.66.Hk; 14.80.Ly

1. Objective

This talk is based on work done with Partha Konar [1]. New physics is widely expected to emerge at TeV energies on the basis of naturalness, gauge hierarchy and WIMP dark matter considerations. Among possible scenarios, supersymmetry (SUSY) [2] and large extra dimensions [3] of the Arkani-Hamed–Dimopoulos–Dvali (ADD) model [4] are in the limelight. This is because they promise a large number of new states to be explored at the LHC as well as ILC and CLIC. The signature of these states is the occurrence of multilepton, multijet events with a large missing energy $\not\!\!E$ or missing transverse energy $\not\!\!E_{\rm T}$. The question of discrimination between the two scenarios on the basis of such events is thus an important issue.

2. Signal cross-section

We consider the lepton sector where the LHC will not be a powerful probe. Hence we zero in on ILC ($\sqrt{s} = 500$ GeV) and CLIC ($\sqrt{s} = 3$ TeV). Our process is $e^+e^- \to \ell^+\ell^- \not\!\!E$, where ℓ is an electron or a muon. For SUSY, we take the MSSM with the parameters $\tan\beta$, $m_{\tilde{e}_{\rm L,R}}$, $m_{\tilde{\mu}_{\rm L,R}}$, μ, M_1 and M_2 in standard notation, with all mass parameters expected to be $\gtrsim \mathcal{O}$ (100 GeV). The production of a pair of charged sleptons $\tilde{\ell}^{\pm}_{\rm L,R}$ and their subsequent decays into $\ell^{\pm}\tilde{\chi}^0_1$ lead to our signal in this scenario. Signal sensitivity to $\tan\beta$ turns out to be very mild and we fix the

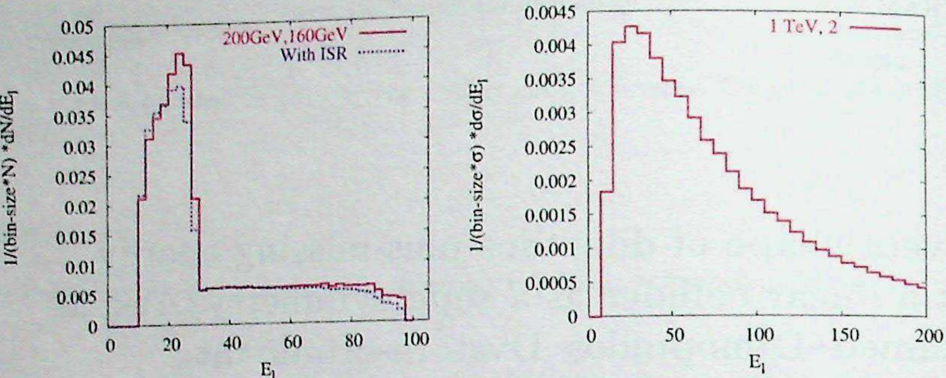

Figure 1. Lepton energy spectrum: SUSY (ADD) in left (right) panel with M_2 and M_1 ($M_{\rm S}$ and d) specified.

latter at 10. Thus we have a 4-parameter SUSY model. Turning to the ADD case, we take d extra spatial dimensions (with $d = 2, 3, 4, 5$), all compactified on a d-torus with the same radius R_c of compactification for each. All standard model fields are assumed to lie on a 3-brane while only gravity is taken to propagate in the bulk. The parameters d, R_c and the fundamental 'string' scale $M_{\rm S}$ in higher dimensions are related by $M_{\rm S}^{2+d} = (4\pi)^{d/2}\Gamma(d/2)G_{\rm N}^{-1}R_c^{-d}$, $G_{\rm N}$ being Newton's constant, so that one can take d and $M_{\rm S}$ to be the two independent parameters of this model.

A reliable discriminant between the SUSY and ADD scenarios, apart from being a measurable quantity, needs to have robust features distinguishing between them. Such is not the case with the lepton energy spectrum here. For appropriate parameters and with ISR corrections, the famous box-shaped lepton energy spectrum from slepton decay can get squeezed [5] into a hump (figure 1a), not too unlike that in the ADD case (figure 1b). Lepton angular distributions also tend to be flat and somewhat similar in both scenarios for most of the allowed range. In contrast, event-shape distributions like those of sphericity and thrust are robust with respect to ISR/FSR corrections and differ significantly for the two scenarios.

All lowest-order diagrams, relevant to the process $e^+e^- \to \ell^+\ell^- \not{E}$ in the ADD (SUSY) case are shown in the left (right) panel of figure 2. For the former, one can write

$$\begin{aligned}\sigma(e^+e^- \to \ell^+\ell^- \not{E}) &= \Sigma_n \sigma(e+e^- \to \ell^+\ell^- G_n)\\ &\simeq \int_0^{\sqrt{s}} {\rm d}m\ \sigma(m)\left[2R_c^d m^{d-1}(4\pi)^{-d/2}/\Gamma(d/2)\right],\end{aligned}$$

m being the mass of the graviton mode with $\sigma(m)$ being the corresponding production cross-section. The latter has been calculated with the subroutine HELAS. For the SUSY case, the rate for the process $e^+e^- \to \tilde{\ell}^+_{\rm L,R}\tilde{\ell}^-_{\rm L,R} \to \ell^+\ell^-\tilde{\chi}^0_1\tilde{\chi}^0_1$ has been calculated using the package COMPHEP. Typical cross-sections for the two scenarios, computed with cuts described in the next section, are listed in table 1. Values for SUSY and ADD show considerable overlap both for ILC (upper half) and CLIC (lower half).

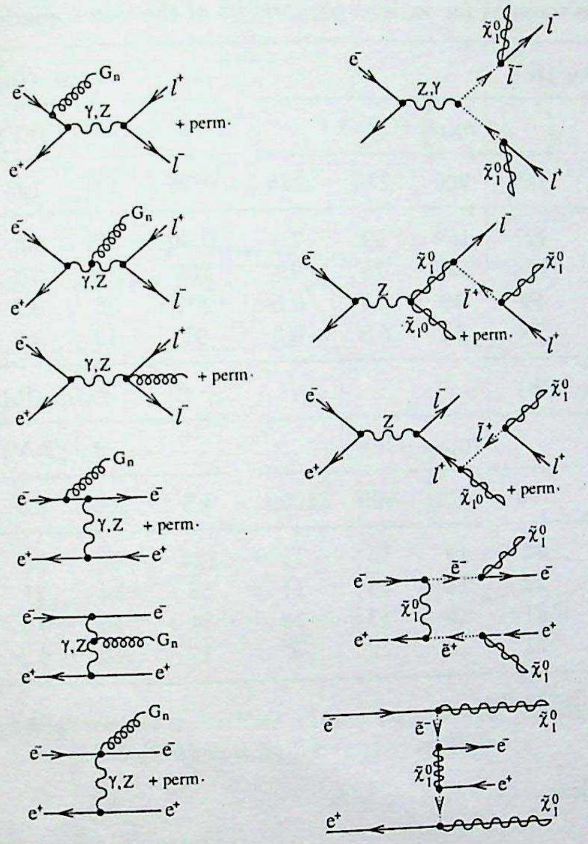

Figure 2. Lowest-order diagrams for our process in the two cases.

3. SM background and chosen cuts

The main background to our signal comes from the reactions $e^+e^- \to \ell^+\ell^- Z$, $Z \to \nu_\ell\bar{\nu}_\ell$ and $e^+e^- \to W^+W^-$, $W \to \ell\nu_\ell$. The first can be eliminated by a missing mass cut clearly excluding M_Z. The second is kinematically reconstructible, modulo a 2-fold ambiguity, and can then be explicitly subtracted. The signal-to-background ratio gets further enhanced on account of our cuts chosen as follows. (1) Each ℓ must be at least 10° from the beam pipe to control beamsstrahlung effects and collinear singularities from t-channel photon exchange. (2) For each ℓ, p_{T}^{ℓ} must exceed 10 GeV (ILC) or 20 GeV (CLIC). (3) The corresponding acceptance lower limits for $p_{\mathrm{T}}^{\mathrm{miss}}$ are chosen as 15 GeV and 25 GeV respectively. (4) The isolation criterion $\Delta R \equiv (\Delta\eta^2 + \Delta\phi^2)^{1/2} > 0.2$ is chosen. (5) The opening angle acceptance range is taken as $5^\circ < \theta_{\ell^+\ell^-} < 175^\circ$. (6) The missing mass cut is chosen to be $M_{\mathrm{miss}} > 150$ GeV for ILC and 450 GeV for CLIC. With these cuts, the SM background is about 36 fb (ILC) and 72 fb (CLIC) to be compared with the signal numbers in table 1. For an integrated luminosity of 100 fb^{-1} (ILC) and 1000 fb^{-1} (CLIC), a minimum signal cross-section of 1.8 fb and 0.8 fb would achieve $S/\sqrt{B} \simeq 3$.

Table 1. Cross-sections for various parameters of the two scenarios.

σ_{SUSY} (fb)						σ_{ADD} (fb)				
$\tan\beta = 10$		m_{slep} (GeV)				M_S (TeV)				
M_2, M_1 (GeV)	μ (GeV)	155	205	225	245	0.75	1.0	1.5	2.0	d
200, 100	−400	427	164	59	7.8	1090	345	68	22	2
300, 150	−400	144	137	75	19	455	108	14	3.3	3
400, 200	−150	92	40	13	0.6	202	36	3.2	0.6	4
400, 200	−100	79	32	6.9	0.3	97	13	0.8	0.1	5
σ_{SUSY} (fb)						σ_{ADD} (fb)				
$\tan\beta = 10$		m_{slep} (GeV)				M_S (TeV)				
M_2, M_1 (GeV)	μ (GeV)	700	800	900	1000	4.5	5.0	5.5	6.0	d
200, 100	−500	24	19	15	11	124	81	56	39	2
400, 190	−500	22	18	15	11	58	34	21	14	3
600, 290	−500	21	16	13	10	31	16	9.2	5.5	4
800, 380	−500	21	18	12	8	17	8.3	4.2	2.3	5

SM bkgd ~ 36 fb (72 fb).

4. Event-shape variables

The idea of using event-shape variables arises from the following expectation. Decay products from a slepton pair, produced not far from threshold, are likely to be more isotropic as compared with the somewhat more spiked configurations of bremsstrahlung-like graviton emission in the ADD case. We define a sphericity tensor S_{ij} and a scalar parameter thrust T as

$$S_{ij} = \frac{p^i_{\ell^+} p^j_{\ell^+} + p^i_{\ell^-} p^j_{\ell^-}}{\mathbf{p}^2_{\ell^+} + \mathbf{p}^2_{\ell^-}}, \quad T = \max \frac{\hat{\mathbf{n}} \cdot (\mathbf{p}_{\ell^+} + \mathbf{p}_{\ell^-})}{|\mathbf{p}_{\ell^+}| + |\mathbf{p}_{\ell^-}|},$$

where the thrust axis unit vector $\hat{\mathbf{n}}$ is chosen to maximize the numerator of T. The allowed range for the latter is $1/2 \leq T \leq 1$ and a spiked (isotropic) event has $T \sim 1$ (1/2). On the other hand, if $\lambda_{1,2,3}$ are the eigenvalues of S_{ij}, defined with $\lambda_1 \geq \lambda_2 \geq \lambda_3 \geq 0$, $\lambda_1 + \lambda_2 + \lambda_3 = 1$, the sphericity S of the event can be defined as

$$S = \frac{3}{2}(\lambda_2 + \lambda_3)$$

with $0 \leq S \leq 1$, where $S = 1, 0$ for an ideally spherical, linear event. For our process, the planar nature of two-body production implies that $\lambda_3 = 0$. Thus the shape of an isotropic event is circular (rather than spherical) for $S_{\max} = 3/4$. However, ISR/FSR effects can, in principle, push S beyond the maximum and towards unity.

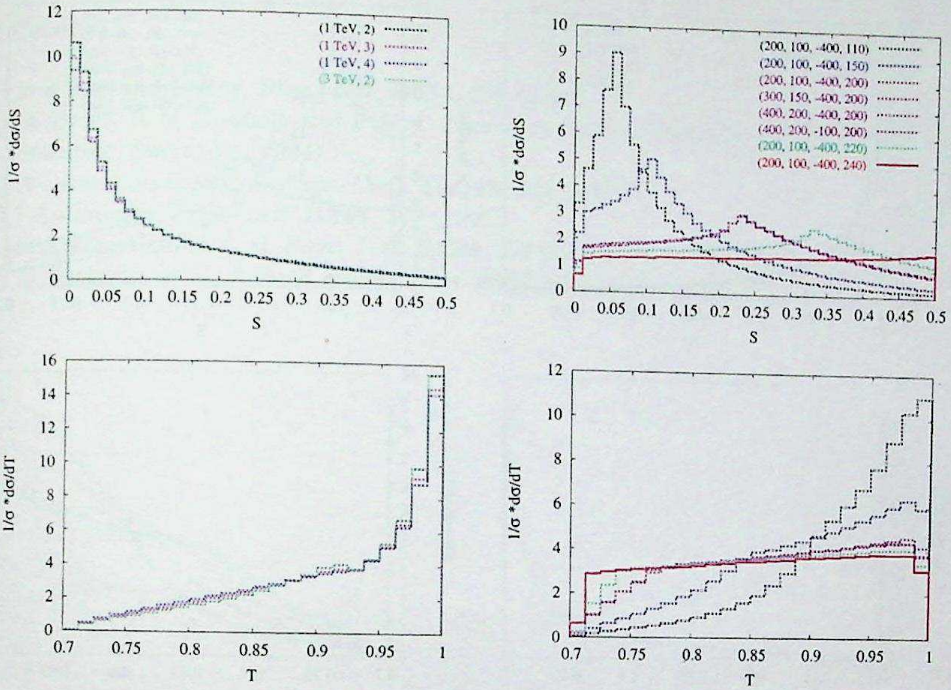

Figure 3. Sphericity (upper panels) and thrust (lower panels) distributions for ADD (left) and SUSY (right) at ILC.

5. Results and discussion

The resultant sphericity and thrust distributions for the two scenarios relevant to ILC is shown in figure 3 and CLIC is shown in figure 4. We have cross-checked the SUSY plots by redoing [1] the calculation in PYTHIA with ISR/FSR effects taken into account. The observed changes are small, showing the robustnes of these event-shape variables with respect to such corrections.

An examination of these plots clarifies the distinction between the two scenarios. Both S and T distributions are flatter in the SUSY case, showing structure in terms of a peak in S and a break in T. In contrast, they are monotonic for ADD with maxima at $S = 0$ and $T = 1$ (spiked event), followed by a continuous fall and rise respectively. It is a fact that the discrimination is more spectacular via S than via T. In the SUSY case, the location of the sphericity peak is uniquely correlated with the slepton mass $m_{\tilde{\ell}}$, being insensitive to other MSSM parameters. This is demonstrated in the scatter plot of figure 5 displaying the cross-section against the said location. In contrast, the maxima for all ADD parametric choices are strictly at $S = 0$.

In summary, a clear discrimination between SUSY and ADD will be possible in $e^+e^- \to \ell^+\ell^- \not{E}$ at a linear collider by means of ISR/FSR-insensitive sphericity distributions. A peaked structure, with the peak location uniquely specifying the slepton mass, characterizes SUSY. In contrast, a structureless monotonic fall-off from a maximum at $S = 0$ is the hallmark of ADD.

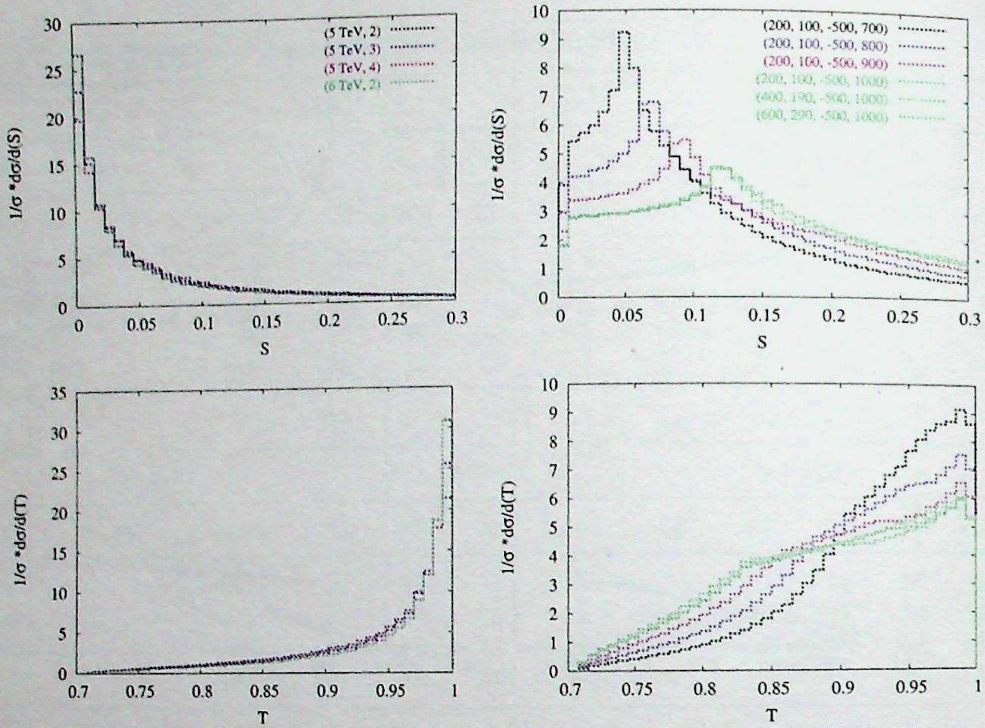

Figure 4. Sphericity (upper panels) and thrust (lower panels) distributions for ADD (left) and SUSY (right) at CLIC.

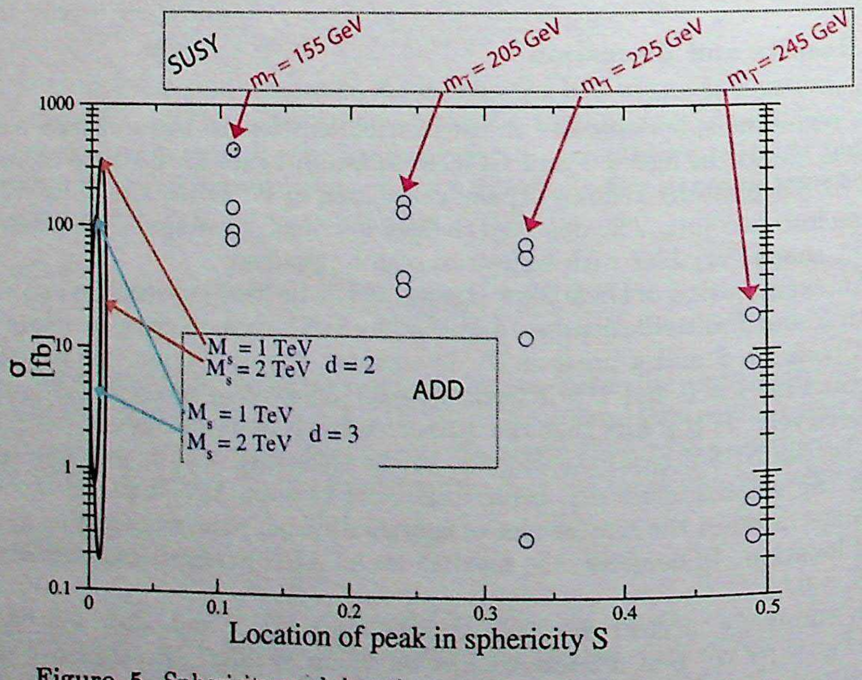

Figure 5. Sphericity peak location.

References

[1] P Konar and P Roy, *Phys. Lett.* **B634**, 295 (2006)

[2] M Drees, R M Godbole and P Roy, *Theory and phenomenology of sparticles* (World Scientific, Singapore, 2004)

[3] A Perez-Lorenzana, *J. Phys. Conf. Ser.* **18**, 224 (2005)

[4] I Antoniadis, *Phys. Lett.* **B246**, 377 (1990)
N Arkani-Hamed *et al*, *Phys. Lett.* **B429**, 263 (1998); *Phys. Rev.* **D59**, 086004 (1999)

[5] M Battaglia *et al*, *J. High Energy Phys.* **0507**, 033 (2005)

PRAMANA
— journal of
physics

© Indian Academy of Sciences

Vol. 69, No. 5
November 2007
pp. 903–907

Probing universal extra dimension at the international linear collider*

GAUTAM BHATTACHARYYA
Saha Institute of Nuclear Physics, 1/AF Bidhan Nagar, Kolkata 700 064, India
E-mail: Gautam.Bhattacharyya@saha.ac.in

Abstract. We consider the UED scenario and study the detectability of the first KK electron–positron pair at the ILC. A few hundred GeV KK electron decays into a nearly degenerate KK photon, which carries away missing energy, and the standard electron. The mass splitting between the KK electron and KK photon is controlled by the bulk- and brane-induced radiative corrections. We look for the signal event e^+e^-+ large missing energy for $\sqrt{s} = 1$ TeV and observe that with a few hundred fb^{-1} luminosity the signal can be deciphered from the standard model background. We briefly outline how the UED signals may be distinguished from the supersymmetric signals.

Keywords. Extra dimension; Kaluza–Klein; linear collider.

PACS Nos 12.60.-i; 14.60.Hi

1. Introduction

We consider universal extra dimension (UED) models [2] with just one extra compactified dimension in the range $R^{-1} = 250$–450 GeV. This extra dimension is accessed by all the standard model (SM) fields. In this context, we examine production of the first Kaluza–Klein (KK) electron–positron pair ($E_1^+E_1^-$) in the e^+e^- international linear collider (ILC) [3]. The heavy modes $E_1^{\pm}$ would decay into the SM (zero modes) $e^{\pm}$ and the first KK photon (γ_1), the latter being stable escapes the detector giving rise to missing energy. The splitting between $E_1^{\pm}$ and γ_1 arises from the bulk and brane-localized radiative corrections. The cross-section of the final state e^+e^- plus missing energy is in the pb range and the SM background is tractable, so that even with a one year run of the upgraded ILC at $\sqrt{s} = 1$ TeV with approximately 300 fb^{-1}, enough evidence may be garnered to support the UED hypothesis. Angular distribution of the final electrons can be used to discriminate the KK leptons from the supersymmetric particles.

---

*This talk is based on a work the author did with Paramita Dey, Anirban Kundu and Amitava Raychaudhuri [1].

2. Simplest universal extra dimension

The extra dimension here is actually an orbifold S^1/Z_2. The orbifolding is necessary to generate zero mode chiral fermions. The tree-level mass of the nth KK state is given by $M_n^2 = M_0^2 + n^2/R^2$, where M_0 is the zero mode mass. The momentum along y, quantized as n/R, is a conserved quantity at all tree-level interactions. But what is conserved at all order is the KK parity defined as $(-1)^n$, and as a result even states mix with even states via loops, and odd mix with odd. Therefore, (i) the lightest Kaluza–Klein particle (LKP) is stable, and (ii) a single KK state (e.g. $n = 1$ state) cannot be produced by tree-level couplings. Thus KK parity is quite similar to R-parity in supersymmetry. Phenomenological constraints on the UED scenario (see ref. [1]) indicate that $R^{-1} \gtrsim 250$ GeV. So we consider only the first level $E_1^+ E_1^-$ pair production and their subsequent decays. In the next section, we shall see how the degeneracy between $E_1^{\pm}$ and γ_1 is lifted by radiative corrections.

3. Radiative corrections and the spectrum

The above-mentioned degeneracy ($M_n = n/R$), barring zero mode masses, is only a tree-level result. Radiative corrections lift this degeneracy [4]. For intuitive understanding, we consider the kinetic term of a 5D scalar field as $L_{\rm kin} = Z\partial_\mu\phi\partial^\mu\phi - Z_5\partial_5\phi\partial^5\phi$, where Z and Z_5 are wave-function renormalizations. Recall, tree-level KK masses ($M_n = n/R$) originate from the kinetic term in the y-direction. If $Z = Z_5$, there is no correction to those KK masses. But this equality is lost due to Lorentz violation leading to $\Delta M_n \propto (Z - Z_5)$. One actually encounters two kinds of radiative corrections.

(a) *Bulk corrections*: These corrections are finite, and nonzero only for bosons. They arise when the internal loop lines wind around the compactified direction. The correction turns out to be $\Delta M_n^2 \propto \beta/16\pi^4 R^2$, where β is a symbolic representation of the collective β-function contributions of the gauge and matter KK fields floating inside the loop. Since the β-functions are different for particles in different representations, the KK degeneracy is lifted causing splitting around n/R. For the KK fermions this correction is zero.

(b) *Orbifold corrections*: Orbifolding breaks translational invariance in the y-direction, and generates interactions localized at the fixed points. These corrections are log divergent. Such boundary terms can be thought of as counterterms whose finite parts are *assumed* to vanish at some cut-off Λ. The correction is given by $\Delta M_n \sim M_n(\beta/16\pi^2)\ln(\Lambda^2/\mu^2)$, where μ is the low energy where we compute these corrections. The KK states are thus further split, now with an additional dependence on Λ. The orbifold corrections are numerically dominant (see table 1 for mass spectrum including both types of corrections).

4. Production and decay modes of KK leptons

The KK fermions are vector-like. The $SU(2)$ doublet KK states are $(\mathcal{N}_n, \mathcal{E}_n)^T_{\rm L,R}$, and $SU(2)$ singlets are $(\hat{\mathcal{E}}_n)_{\rm L,R}$, where n is the KK index. Below we denote $\mathcal{E}_1^{\pm}$ and $\hat{\mathcal{E}}_1^{\pm}$ collectively by $E_1^{\pm}$.

Table 1. $n = 1$ KK masses in GeV for different cases.

R^{-1}	ΛR	$M_{\hat{\mathcal{E}}_1}$	$M_{\mathcal{E}_1}$	M_{W_1}	M_{Z_1}	M_{γ_1}
250	20	252.7	257.5	276.5	278.1	251.6
	50	253.6	259.7	280.6	281.9	251.9
350	20	353.8	360.4	379.0	379.7	351.4
	50	355.0	363.6	384.9	385.4	351.5
450	20	454.9	463.4	482.9	483.3	451.1
	50	456.4	467.5	490.6	490.8	451.1

The process $e^+e^- \to E_1^+E_1^-$ proceeds through s- (γ/Z mediated) and t-channel (γ_1/Z_1) graphs. E_1 decays into e and γ_1. The splitting between E_1 and γ_1 masses is sufficient for the decay to occur within the detector with a 100% branching ratio (BR). It may be possible to observe even a displaced vertex (e.g., $\hat{\mathcal{E}}_1$ decays, with $R^{-1} = 250$ GeV). So in the final state we have $e^+e^- + 2\gamma_1$ ($\equiv$ missing energy). The same final states can be obtained from $e^+e^- \to W_1^+W_1^-$, but this will be BR suppressed.

SM background: The main background comes from $\gamma^*\gamma^* \to e^+e^-$ events, where γ^*s arise from the initial e^+e^- pair while the latter go undetected down the beam pipe [5]. The $\gamma^*\gamma^*$ production cross-section is $\sim 10^4$ pb. About half of these events go to final-state e^+e^- pair as visible particles. The background e^+e^- pairs are usually quite soft and coplanar with the beam axis. An acoplanarity cut significantly removes this background without much affecting the signal. For example, excluding events which deviate from coplanarity within 40 mrad reduces only 7% of the signal cross-section. For another strategy to handle backgrounds, see footnote 1 in [1]. Numerically much less significant backgrounds would come from $e^+e^- \to W^+W^-$, $e\nu W$, e^+e^-Z, followed by the appropriate leptonic decays of W and Z.

Collider parameters: The study is performed in the context of the ILC, running at $\sqrt{s} = 1$ TeV (upgraded option), and with a polarization efficiency of 80% for e^- and 50% for e^+ beams. We impose kinematic cuts on the lower and upper energies of the final-state electrons/positrons as 0.5 GeV (for identification) and 20 GeV (for reducing SM background) respectively. We also employ a rapidity cut rejecting all final-state electrons which are within 15° of the beam pipe.

Cross-sections: The cross-section for e^+e^- plus missing energy final state has been plotted in figure 1. Varying the beam polarizations does create a detectable difference. The cross-section enhances as we increase ΛR from 2 to 20; this is due to the change in θ_{W1} (the weak angle for $n = 1$ KK gauge bosons). The cuts tend to reduce the cross-section which is why the curve for $\Lambda R = 50$ lies between the ones for $\Lambda R = 2$ and 20.

Forward-backward (FB) asymmetries: The FB asymmetries of the final-state electrons, defined as $A_{\mathrm{FB}} = (\sigma_{\mathrm{F}} - \sigma_{\mathrm{B}})/(\sigma_{\mathrm{F}} + \sigma_{\mathrm{B}})$, are plotted in figure 2. The first-stage process $e^+e^- \to E_1^+E_1^-$ is forward-peaked, and for smaller $1/R$, i.e. lighter KK electrons, the final state $e^\pm$ are boosted more along the direction of the parent $E_1^\pm$. As $1/R$ increases the boost drops and the distribution loses its original

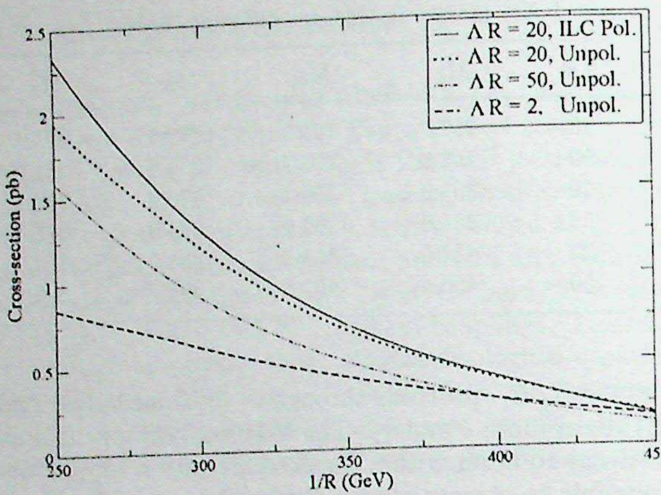

Figure 1. Cross-section vs. $1/R$ for the process $e^+e^- \to e^+e^- +$ missing energy.

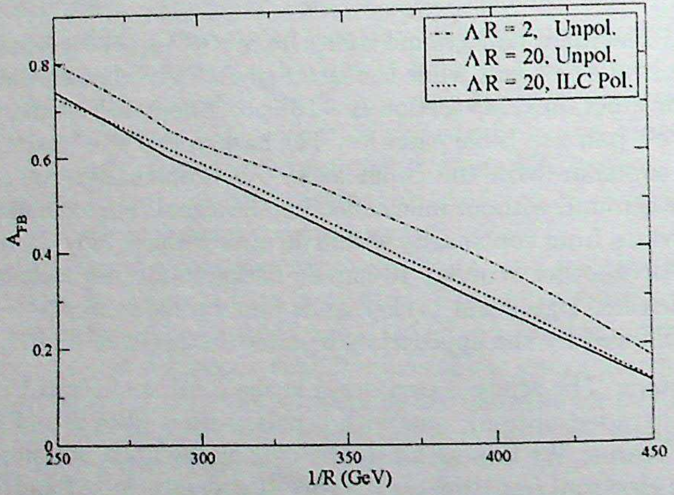

Figure 2. A_{FB} vs. $1/R$ for the same process as in figure 1.

forward-peaked nature. A point to note is that the electrons coming from the two-photon background will be FB symmetric.

5. Discriminating UED from other new physics

$n = 1$ KK spectrum [6] closely resembles supersymmetry spectrum if the latter is pretty degenerate. Still, even if the LSP weighs above 250 GeV and is almost degenerate with a selectron, the latter can be discriminated from a KK lepton from the decay angular distributions on account of their different spins. We demonstrate this with a simple toy scenario. Compare the pair production of (a) generic heavy fermions and (b) generic heavy scalars in an e^+e^- collider. Assume $\sqrt{s} \gg m$, where m is the mass of the heavy lepton/scalar, so that only the t-channel diagrams, with a heavy gauge boson in case (a) and a heavy fermion in case (b) as propagators, are dominant. The heavy states are produced with sufficient boost, and therefore the tagged leptons they decay into have roughly the same angular distributions as them. Then the cross-section ratio $\mathrm{d}\sigma/\mathrm{d}\cos\theta$ (case (a)$\div$ case (b)) $= (A + B\cos\theta + C\cos^2\theta) \div (\sin^2\theta)$, where A, B, C are parameter-dependent numbers, clearly indicates that angular distributions can discriminate the two cases. Moreover, the UED fermion pair production cross-section is about a factor of 4 to 5 larger than the scalar production cross-section for similar couplings and masses. While dealing with selectrons, one must take into account the detailed neutralino structure, but the above basic arguments go through.

6. LHC/ILC synergy and conclusions

For improved precision in the measurements of masses, decay widths, mixing angles, etc., ILC would be an ideal machine following the discovery runs at LHC. The accuracy of measuring the mass of a 200 GeV selectron is about 5 GeV at LHC, but it could be as low as 0.2 to 1 GeV at ILC [7]. Similar precisions may be expected for similar KK electron masses as well. A spin correlation study [8] to distinguish UED from supersymmetry at LHC concluded that spin assignments are extremely difficult if the observed spectrum turns out to be quasi-degenerate. A factor of 4 to 5 larger production cross-section for UED compared to supersymmetry will then be a better discriminator. The clinching evidence of UED would of course be the discovery of the single production of $n = 2$ KK modes (see [9] for details) which have no supersymmetry analog.

To conclude, ILC is important for precision studies in the post-LHC era. Studying the physics interplay between the LHC and ILC constitutes a very important particle physics research topic.

References

[1] G Bhattacharyya, P Dey, A Kundu and A Raychaudhuri, *Phys. Lett.* **B628**, 141 (2005)
[2] T Appelquist, H C Cheng and B A Dobrescu, *Phys. Rev.* **D64**, 035002 (2001)
[3] D J Miller, arXiv:hep-ph/0410306
[4] H C Cheng, K T Matchev and M Schmaltz, *Phys. Rev.* **D66**, 036005 (2002)
M Puchwein and Z Kunszt, *Ann. Phys.* **311**, 288 (2004)
[5] See the website: http://hep-www.colorado.edu/SUSY
[6] H C Cheng, K T Matchev and M Schmaltz, *Phys. Rev.* **D66**, 056006 (2002)
[7] LHC/LC Study Group: G Weiglein *et al*, arXiv:hep-ph/0410364
[8] J M Smillie and B R Webber, *J. High Energy Phys.* **0510**, 069 (2005)
[9] B Bhattacherjee and A Kundu, *Phys. Lett.* **B627**, 137 (2005)

PRAMANA
— journal of
physics

© Indian Academy of Sciences

Vol. 69, No. 5
November 2007
pp. 909–913

Littlest Higgs model and *W* pair production at international linear collider

P POULOSE
Indian Institute of Technology Guwahati, Guwahati 781 039, India
E-mail: poulose@iitg.ernet.in

Abstract. Among the viable alternatives to the standard Higgs mechanism is the recently proposed Little Higgs model. The advantage here is that the model has an elementary light neutral scalar particle, which arises dynamically as against its *ad hoc* introduction in the standard model. The model also avoids hierarchy problem. We have investigated the W pair production at ILC to study the littlest Higgs model using different observables. Specifically, polarization fraction of W boson is expected to be measured very accurately at ILC. We use this to put limit on the scale parameter, f, in the model.

Keywords. Electroweak symmetry breaking; littlest Higgs, W polarization fraction.

PACS No. **12.90.+b**

1. Introduction

Study of electroweak symmetry breaking mechanism is one of the central problems of particle physics today. The SM Higgs mechanism is simple, but *ad hoc*-ly introduces an elementary scalar particle in the theory. Mass of the Higgs particle is expected, from theoretical and experimental considerations, to be in the range of 10^2 GeV. But at one-loop level Higgs mass square acquire quadratically diverging corrections; a difficulty known as hierarchy problem. Models including supersymmetric extensions of the standard model, composite Higgs models, strongly interacting EW scenario, Higgs-less models, little Higgs models, etc. suggest different ways to take care of the hierarchy problem. Of these, we will be concerned here with the little Higgs models [1]. Unlike supersymmetric theories, little Higgs theories work on the gauge sector of the theory. An appealing aspect of the scenario is that the scalars are not introduced ad hoc-ly, and the symmetry breaking is generated dynamically.

Although LHC is expected to investigate the electroweak symmetry breaking (EWSB) mechanism, it will require the clean environment of the proposed international linear collider (ILC) to study the details and, for example, distinguish between different scenarios.

In this write-up we will discuss W pair production at ILC within the framework of one version of the little Higgs models, known as the littlest Higgs models [2]. In the next section we will introduce the littlest Higgs model. In §3 we will discuss the process $e^+e^- \to W^+W^-$ and the observables that are sensitive to the littlest Higgs model.

2. The little Higgs models

The scenario is analogous to the description of low-energy hadronic interactions by a non-linear realization of the chiral symmetry $SU(2)_{\mathrm{L}} \times SU(2)_{\mathrm{R}}$ broken down to $SU(2)_{\mathrm{I}}$ at energy scale f. Pions (π) are taken to be the Nambu–Goldstone bosons (NGB) of the symmetry breaking, and their dynamics can be defined by a non-linear sigma model.

In little Higgs models [1], similarly, we consider the non-linear realization of some global symmetry G broken down to H. The Nambu–Goldstone bosons (NGB) of the symmetry breaking are candidate Higgs field. In a specific model, called littlest Higgs (LH) model [2] $G \equiv SU(5)$ is broken down to $H \equiv SO(5)$. This leaves us $24 - 10 = 14$ NGBs. Interaction of NGBs are described by non-linear sigma model, which is an effective theory valid below the cut-off $\Lambda \sim 4\pi f$. To identify some of these NGBs as Higgs particles we gauge a subgroup of $SU(5)$. In the original version of the littlest Higgs model $[SU_1(2) \times U_1(1)] \times [SU_2(2) \times U_2(1)] \subset SU(5)$ is gauged, which is broken down to the standard model (SM) gauge group $SU(2)_{\mathrm{L}} \times U(1)_{\mathrm{Y}}$. Under the SM gauge group, the 14 NGBs transform as $(\mathbf{1}, 0) + (\mathbf{3}, 0) + (\mathbf{2}, \frac{1}{2}) + (\mathbf{3}, 1)$. SM gauge bosons, $\vec{W}_L^\mu$ and B_L^μ remain massless at this stage, while the gauge bosons belonging to the broken sector, $\vec{W}_H^\mu$ and B_H^μ, become massive after absorbing the singlet and the real triplet (with hypercharge, $Y = 0$). The doublet NGB field has all the correct quantum numbers to be identified as the standard Higgs doublet. At tree level, they have only derivative couplings. Quantum corrections at one-loop level will generate Coleman–Weinberg potential with quadratic and quartic terms. Gauge symmetry is constructed such that, in the absence of any one (original) gauge interaction, Higgs is massless at all orders. This also ensures that quadratically divergent contributions to the mass square term at one-loop level are canceled between the two gauge bosons from the two sectors. Logarithmically divergent terms contribute to the potential. In order to avoid quadratic divergence due to top quark loop, a pair of (weak-singlet) Weyl quark $U_{\mathrm{L}}, U_{\mathrm{R}}$ is introduced, which mix with the ordinary left- and right-quarks to give the mass eigenstates. Here again, it is arranged such that the quadratic divergence coming from the standard top quark is canceled by its heavy counterpart, and the logarithmically diverging part adds to the Coleman–Weinberg potential. The triplet left over NGBs also add logarithmically diverging quadratic terms to the potential. Presence of triplet in the loop also generates quartic terms in the potential. The Higgs potential thus generated breaks the $SU(2)_{\mathrm{L}} \times U(1)_{\mathrm{Y}}$ symmetry spontaneously. At the same time, Higgs mass is protected from acquiring quadratically divergent mass corrections at one loop.

Precision electroweak measurements constrain this model to have $f > 4$ TeV, leaving the cut-off $\Lambda > 12$ TeV, thwarting the original motivation of solving hierarchy problem. There are variations that avoid this difficulty; two among them are (i) introduce T-Parity [3], (ii) change the gauge sector [4]. In the second approach, which we will be concerned here with the gauge group considered is

$SU_1(2) \times SU_2(2) \times U_Y(1)$, which is broken down to the standard $SU_L(2) \times U_Y(1)$. Situation is similar to the earlier case, but without B_H. In this model we have three heavy gauge bosons; $W_H^{\pm}$ and Z_H, in addition to the standard $W^{\pm}$, Z and A. Masses of the new gauge bosons are given by

$$M_{W_H} = M_{Z_H} = \frac{g}{\sin 2\theta}\, f, \tag{1}$$

where $g = g_1 g_2/\sqrt{g_1^2 + g_2^2}$ is the standard $SU(2)_L$ coupling and θ is the mixing angle between $SU_1(2)$ and $SU_2(2)$. Electroweak precision measurements allow $f > 1$ TeV with $\cos\theta \sim 1/3$. Some of the phenomenological studies of little Higgs models in the context of LHC and ILC are listed in ref. [5].

3. The process: $e^+e^- \to W^+W^-$

We will now consider the effect of this scenario in W pair production at a high energy linear e^+e^- collider. Apart from the standard channels, this process gets contribution from a Z_H mediated s-channel. Along with this, there could also be differences between the SM predictions and the littlest Higgs model predictions through changed couplings. The SM gauge couplings ($g_{WW\gamma}, g_{WWZ}$) and the W couplings to the fermions are unchanged, but the fermionic couplings of the standard model Z boson pick up an additional contribution of the order of v^2/f^2. The vector and axial vector couplings of Z to the electrons are given respectively by

$$c^v_{eeZ} = \frac{g}{2c_W}\left[\left(-\frac{1}{2} + 2x_W\right) + \frac{v^2}{f^2}\,\frac{\sin 4\theta}{8}\right] \tag{2}$$

$$c^a_{eeZ} = \frac{g}{2c_W}\left[\frac{1}{2} - \frac{v^2}{f^2}\,\frac{\sin 4\theta}{16}\cot\theta\right]. \tag{3}$$

Couplings of the heavy Z_H with W and electrons are given by

$$g_{WWZ_H} = \frac{gv^2}{8f^2}\,\sin 4\theta, \tag{4}$$

$$c^v_{eeZ_H} = \frac{-g}{4}\,\cot\theta, \quad c^a_{eeZ_H} = \frac{g}{4}\,\cot\theta. \tag{5}$$

We will now present our results. In the first place, we study the deviation of total cross-section from the SM value. In figure 1 (left) we plot the total cross-section against the centre-of-mass energy. In order to get an estimate of how far we can probe the scale f at ILC, we consider two c.m. energy values, 500 GeV and 800 GeV, and assume a luminosity of 1 ab^{-1}. At 1σ level we can probe f up to 6 TeV at both energies. LEP has measured the fractional cross-section of the polarized Ws very precisely [6]. AT ILC this precision is expected to be even better. Defining the polarization fractions as

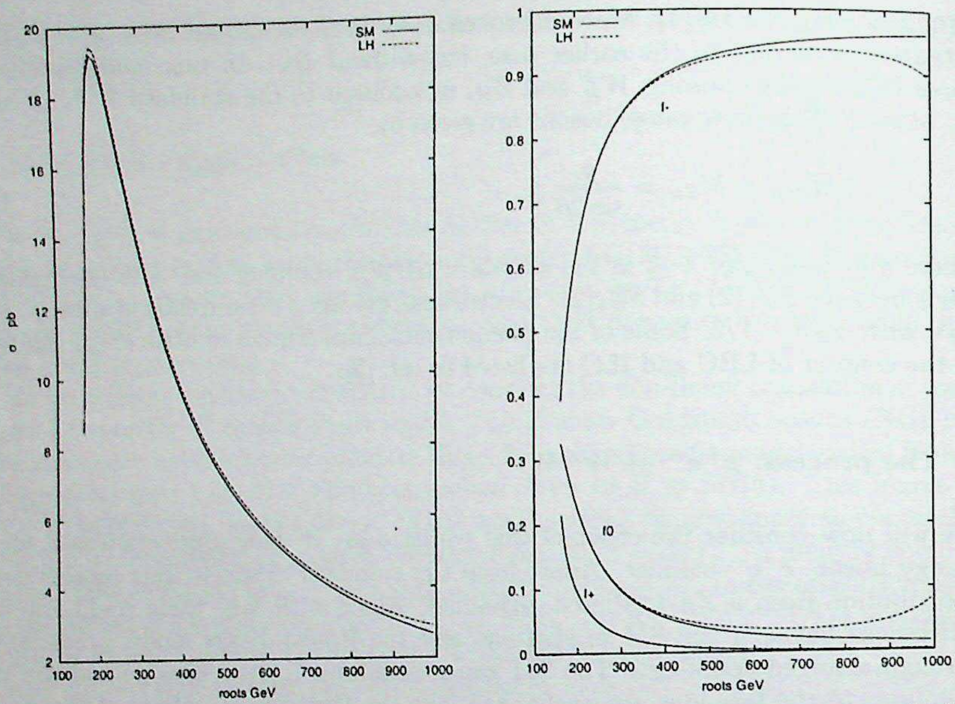

Figure 1. Unpolarized cross-section (left) and polarization fractions (right) against centre-of-mass energy. Solid line corresponds to SM, while the dashed line corresponds to the littlest Higgs model.

$$f^0 = \frac{\sigma(e^+e^- \to W^+W_{\rm L}^-)}{\sigma_{\rm unpol}}, f^T = \frac{\sigma(e^+e^- \to W^+W_{\rm T}^-)}{\sigma_{\rm unpol}}, \tag{6}$$

where L refers to the longitudinal polarization and T = ± refers to the transverse polarizations, we plot them in figure 1 (right). We find that the longitudinal fraction is changed from 3.8% to 4.4%, and from 1.9% to 4.0% at centre-of-mass energies 500 GeV and 800 GeV respectively.

It is clear that beam polarization can be used to switch off the dominant t-channel production to which LH model does not add any new contribution. This will enhance the sensitivity considerably. One could also consider different observables, including forward–backward asymmetry to probe the fermionic couplings of the gauge bosons. Work on this is in progress.

References

[1] N Arkani-Hamed, A G Cohen, T Gregoire and J G Wacker, *J. High Energy Phys.* **0208**, 020 (2002), hep-ph/0202089
N Arkani-Hamed, A G Cohen, E Katz, A E Nelson, T Gregoire and J G Wacker, *J. High Energy Phys.* **0208**, 021 (2002), hep-ph/0206020
[2] N Arkani-Hamed, A G Cohen, E Katz and A E Nelson, *J. High Energy Phys.* **0207**, 034 (2002), hep-ph/0206021

M Schmaltz and D Tucker-Smith, *Ann. Rev. Nucl. Part. Sci.* **55**, 229 (2005), hep-ph/0502182

M Perelstein, hep-ph/0512128

[3] H C Cheng and I Low, *J. High Energy Phys.* **0309**, 051 (2003)

J Hubisz, P Meade, A Noble and M Perelstein, *J. High Energy Phys.* **0601**, 135 (2006), hep-ph/0506042

[4] R Barbieri, A Pomarol, R Rattazzi and A Strumia, *Nucl. Phys.* **B703**, 127 (2004)

M Perelstein, M E Peskin and A Pierce, *Phys. Rev.* **D69**, 075002 (2004), hep-ph/0310039

C Csaki, J Hubisz, G D Kribs, P Meade and J Terning, *Phys. Rev.* **D68**, 035009 (2003), hep-ph/0303236

[5] T Han, H E Logan, B McElrath and L T Wang, *Phys. Rev.* **D67**, 095004 (2003), hep-ph/0301040

T Han, H E Logan, B McElrath and L T Wang, *Phys. Lett.* **B563**, 191 (2003), hep-ph/0302188, Erratum, *Phys. Lett.* **B603**, 257 (2004)

J L Hewett, F J Petriello and T G Rizzo, *J. High Energy Phys.* **0310**, 062 (2003)

C Csaki, J Hubisz, G D Kribs, P Meade and J Terning, *Phys. Rev.* **D67**, 115002 (2003)

T Han, H E Logan and L T Wang, *J. High Energy Phys.* **0601**, 099 (2006), hepph/0506313

J S Conley, J A Hewett and My Phuong Le, *Phys. Rev.* **D72**, 115014 (2005), hep-ph/0507198

[6] L3 Collaboration: *Phys. Lett.* **B474**, 194 (2000), hep-ex/0001016

PRAMANA
— journal of
physics

© Indian Academy of Sciences

Vol. 69, No. 5
November 2007
pp. 915–919

Lepton distribution in top decay: A probe of new physics and top-polarization

ROHINI M GODBOLE[1,*], SAURABH D RINDANI[2] and RITESH K SINGH[3]
[1]Center for High Energy Physics, Indian Institute of Science, Bangalore 560 012, India
[2]Physical Research Laboratory, Ahmedabad 380 009, India
[3]Laboratoire de Physique Théoretique, 91405 Orsay Cedex, France
*E-mail: godbolerm@gmail.com

Abstract. We investigate the possibilities of studying new physics in various processes of t-quark production using kinematical distributions of the secondary lepton coming from decay of t quarks. We show that the angular distributions of the secondary lepton are insensitive to the anomalous tbW vertex and hence are pure probes of new physics in a generic process of t-quark production. The effects of t polarization on the distributions of the decay lepton are demonstrated for top-pair production process at a $\gamma\gamma$-collider mediated by a heavy Higgs boson.

Keywords. Top; polarization; anomalous top coupling.

PACS Nos 14.65.Ha; 13.88.+e; 13.85.Qk

1. Introduction

As a result of the large mass of top quark and the consequent large coupling to the longitudinal component of the W boson, it decays prior to hadronization. Hence, the spin of the decaying top quark leaves its imprint on the kinematical distributions of the decay products: the W boson and the b quark. Possible new physics of electro-weak symmetry breaking (EWSB) may alter t quark coupling with the W boson leading to changed decay width and distributions. Further, new physics may also appear in its production process potentially affecting kinematical distributions and possibly polarization. The simultaneous presence of new physics both in production and decay processes of top quark may complicate the analysis and it may become difficult to probe new physics couplings of top quark. However, if one can construct observables that are sensitive to production and decay mechanism independent of each other, the analysis can be greatly simplified. It has been shown that the angular distribution of the leptons from the decay of top quark is insensitive to the anomalous tbW coupling in the $2 \to 2$ processes of top quark production [1] and also for a general process [2]. Here we extend the result by relaxing the approximations used in the earlier analysis, for a general $2 \to n$ process [3].

2. Anomalous tbW interaction and lepton distribution

We treat the tbW vertex in a model independent way by parameterizing it as

$$\Gamma^\mu = \frac{-ig}{\sqrt{2}}\left[\gamma^\mu(f_{1L}P_L + f_{1R}P_R) - \frac{i\sigma^{\mu\nu}}{m_W}(p_t - p_b)_\nu(f_{2L}P_L + f_{2R}P_R)\right]. \tag{1}$$

For the SM we have $f_{1L} = 1$ and the anomalous couplings $f_{1R} = f_{2L} = f_{2R} = 0$. Further we note that the contribution from f_{1R} and f_{2L} is proportional to m_b and will be absent in the vanishing m_b limit. To show the decoupling of lepton angular distribution from anomalous top coupling we assume

1. t-quark is on-shell, i.e. using narrow-width approximation for top quark and
2. anomalous couplings f_{1R}, f_{2R} and f_{2L} are small, we retain terms linear in them.

Using narrow-width approximation for top quark we can write the matrix element square as

$$|M|^2 = \frac{\pi\delta(p_t^2 - m_t^2)}{m_t\Gamma_t}\sum_{\lambda,\lambda'}\rho(\lambda,\lambda')\Gamma(\lambda,\lambda'); \qquad \begin{array}{c}\rho(\lambda,\lambda') = M_\rho(\lambda)M_\rho^*(\lambda')\\ \Gamma(\lambda,\lambda') = M_\Gamma(\lambda)M_\Gamma^*(\lambda').\end{array} \tag{2}$$

With this the differential cross-section for $2 \to n$ process of top production followed by its decay can be written as

$$\begin{aligned}\mathrm{d}\sigma = \sum_{\lambda,\lambda'}&\left[\frac{(2\pi)^4}{2I}\rho(\lambda,\lambda')\delta^4\left(k_A + k_B - p_t - \sum_i^{n-1} p_i\right)\frac{\mathrm{d}^3p_t}{2E_t(2\pi)^3}\prod_i^{n-1}\frac{\mathrm{d}^3p_i}{2E_i(2\pi)^3}\right]\\ &\times\left[\frac{1}{\Gamma_t}\left(\frac{(2\pi)^4}{2m_t}\Gamma(\lambda,\lambda')\delta^4(p_t - p_b - p_\nu - p_\ell)\frac{\mathrm{d}^3p_b}{2E_b(2\pi)^3}\,\frac{\mathrm{d}^3p_\nu}{2E_\nu(2\pi)^3}\right)\frac{\mathrm{d}^3p_\ell}{2E_\ell(2\pi)^3}\right].\end{aligned} \tag{3}$$

The first term in eq. (3) can be written as $\mathrm{d}\sigma_{2\to n}(\lambda,\lambda')\,\mathrm{d}E_t\,\mathrm{d}\cos\theta_t$ after integration in the lab frame, while we integrate the second term in the rest frame of the decaying top quark as

$$\begin{aligned}&\frac{1}{\Gamma_t}\frac{(2\pi)^4}{2m_t}\int\frac{\mathrm{d}^3p_\ell}{2E_\ell(2\pi)^3}\frac{\mathrm{d}^3p_b}{2E_b(2\pi)^3}\frac{\mathrm{d}^3p_\nu}{2E_\nu(2\pi)^3}\\ &\qquad\times\Gamma(\lambda,\lambda')\delta^4(p_t - p_b - p_\nu - p_\ell)\\ &\qquad= \frac{1}{32\Gamma_t m_t}\frac{E_\ell}{(2\pi)^4}\frac{\langle\Gamma(\lambda,\lambda')\rangle}{m_t E_\ell}\mathrm{d}E_\ell\mathrm{d}\Omega_\ell\ \mathrm{d}p_W^2.\end{aligned} \tag{4}$$

Here the angular brackets indicate averaging over azimuthal angle between b quark and decay lepton. In the rest frame of the top quark we have

$$\langle \Gamma(\lambda, \lambda') \rangle = g^4 m_t E^0_\ell |\Delta_W(p_W^2)|^2 A(\lambda, \lambda') \times F(E^0_\ell), \tag{5}$$

where $\Delta_W(p^2_W) = \frac{1}{p^2_W - m^2_W + i\Gamma_W m_W}$ is the W-propagator, $A(\pm, \pm) = (1 \pm \cos\theta_\ell)$, $A(\pm, \mp) = \sin\theta_\ell e^{\pm \phi_\ell}$ is the pure angular factor and $F(E^0_\ell)$ is given as

$$F(E^0_\ell) = \left[(m_t^2 - m_b^2 - 2p_t \cdot p_l) \left(|f_{1L}|^2 + \Re(f_{1L} f^*_{2R}) \frac{m_t}{m_W} \frac{p^2_W}{p_t \cdot p_l} \right) \right.$$
$$\left. - \, 2\Re(f_{1L} f^*_{2L}) \frac{m_b}{m_W} p^2_W - \Re(f_{1L} f^*_{1R}) \, \frac{m_b m_t}{p_t \cdot p_l} p^2_W \right], \tag{6}$$

is angle independent factor that depends upon the lepton energy. It should be noted here that all the anomalous couplings appear only in $F(E^0_\ell)$. Combining the production and decay part, we have

$$\mathrm{d}\sigma = \frac{1}{32 \; \Gamma_t m_t (2\pi)^4} \left[\sum_{\lambda, \lambda'} \mathrm{d}\sigma_{2 \to n}(\lambda, \lambda') \times g^4 A^{\mathrm{c.m.}}(\lambda, \lambda') \right]$$
$$\times \mathrm{d}E_t \; \mathrm{d}\cos\theta_t \; \mathrm{d}\cos\theta_\ell \; \mathrm{d}\phi_\ell \times E_\ell F(E_\ell) \; \mathrm{d}E_\ell \; \mathrm{d}p^2_W. \tag{7}$$

Further, we have $\Gamma_t \propto \int E_\ell F(E_\ell) \, \mathrm{d}E_\ell \, \mathrm{d}p^2_W$. Thus, if we integrate over E_ℓ in eq. (7), the factor containing anomalous couplings cancels between the numerator and Γ_t in the denominator. This proves that the differential rates are independent of anomalous tbW couplings once we integrate over lepton energy. Hence, the angular distribution of lepton is independent of anomalous tbW couplings in any inertial frame of reference and thus sensitive only to the production mechanism and possible new physics therein. On the other hand, the energy distribution of the decay lepton in the lab frame depends on the tbW vertex, i.e. possible new physics in top decay, and also on energy-angular distribution of the produced top quarks, i.e. possible new physics in top production. However, the E^0_ℓ distribution in the rest frame of the decaying top quark is given by $\mathrm{d}\sigma/\mathrm{d}E^0_\ell \propto \int E^0_l F(E^0_l) \, \mathrm{d}p^2_W$, hence sensitive only to the decay vertex with proportionality constant absorbing the information about production mechanism. In other words, the E^0_ℓ distribution (in the rest frame of top quark) provides sensitivity to the anomalous tbW coupling independent of the production mechanism of top quark. To summarize, the decay lepton distribution can provide separate and pure probes of possible new physics in production and decay of top quarks.

3. Polarization of top quark

Denoting the first line of eq. (3) by $\sigma(\lambda, \lambda')$, one can write the polarization density matrix of the top quark as

$$P_t = \frac{1}{2} \begin{pmatrix} 1 + \eta_3 & \eta_1 - i\eta_2 \\ \eta_1 + i\eta_2 & 1 - \eta_3 \end{pmatrix}, \quad \text{where} \quad \begin{aligned} \eta_3 &= (\sigma(+,+) - \sigma(-,-))/\sigma_{\mathrm{tot}}, \\ \eta_1 &= (\sigma(+,-) + \sigma(-,+))/\sigma_{\mathrm{tot}}, \\ i\,\eta_2 &= (\sigma(+,-) - \sigma(-,+))/\sigma_{\mathrm{tot}} \end{aligned} \tag{8}$$

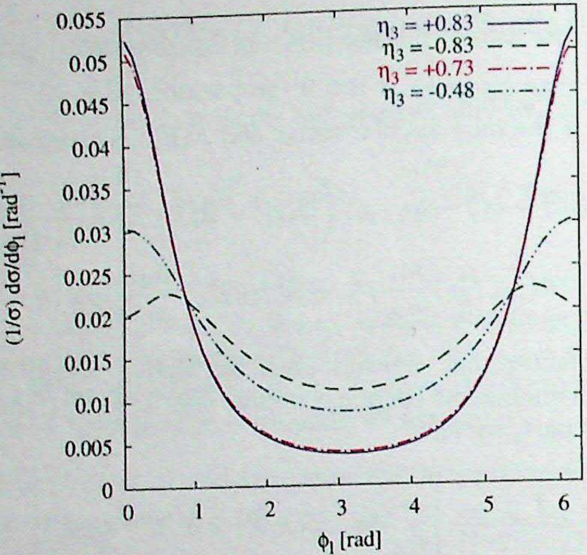

Figure 1. The distribution in the azimuthal angle of the lepton in the lab frame for different top polarizations.

and $\sigma_{\text{tot}} = \sigma(+,+) + \sigma(-,-)$. Here η_3 is the longitudinal polarization of the top quark or the average helicity, η_2 is the transverse polarization normal to the production plane and η_1 is the transverse polarization in the production plane. These polarizations can be calculated from the angular distribution of leptons as

$$\frac{\eta_i}{2} = \frac{\sigma(p_\ell \cdot s_i < 0) - \sigma(p_\ell \cdot s_i > 0)}{\sigma(p_\ell \cdot s_i < 0) + \sigma(p_\ell \cdot s_i > 0)}, \quad \text{for } i = 1,2,3 \tag{9}$$

where $s_i \cdot s_j = -\delta_{ij}$ and $p_t \cdot s_i = 0$. For $p_t^\mu = E_t(1, \beta_t \sin\theta_t, 0, \beta_t \cos\theta_t)$, we have $s_1^\mu = (0, -\cos\theta_t, 0, \sin\theta_t)$, $s_2^\mu = (0,0,1,0)$ and $s_3^\mu = E_t(\beta_t, \sin\theta_t, 0, \cos\theta_t)/m_t$. The measurement of η_i requires knowledge of s_is. In other words, one requires to fully or partially reconstruct top momentum in the lab frame. Alternatively, one can look at the azimuthal distribution of leptons with respect to the top production plane as (at least) a qualitative probe of top polarization. For demonstration, we choose $\gamma\gamma \to t\bar{t}$ with and without Higgs mediation and polarized photon beams. With the help of variation in the photon polarization and the presence and absence of Higgs exchange we generate ensemble of top quarks with varying polarization and show the decay lepton azimuthal distribution in figure 1. We note that for this example we have $\eta_1 = \eta_2 = 0$ and the values of η_3 are indicated on the plot. We see that the distribution is peaked at the top production plane ($\phi_\ell = 0,\ 2\pi$) for positively polarized top and the height of peak decreases as polarization changes from positive to negative value. For large negative value of polarization (-0.83) there is a dip in the distribution in place of the peak near the top production plane. This qualitative feature of the azimuthal distribution can be converted into quantitative measure after establishing the correlation between η_3 and height of the peak for a given process.

To conclude, we show that the lepton angular distribution is sensitive to top polarization and production mechanism independent of anomalous tbW couplings and E_ℓ^0 distribution is sensitive to anomalous tbW coupling independent of top production mechanism. Further, we show that azimuthal distribution of decay lepton in the lab frame can be used to probe polarization of decaying top quark.

References

[1] S D Rindani, *Pramana – J. Phys.* **54**, 791 (2000)
B Grzadkowski and Z Hioki, *Phys. Lett.* **B476**, 87 (2000)
Z Hioki, hep-ph/0104105
K Ohkuma, *Nucl. Phys. (Proc. Suppl.)* **B111**, 285 (2002)
R M Godbole, S D Rindani and R K Singh, *Phys. Rev.* **D67**, 095009 (2003), Erratum, *Phys. Rev.* **D71**, 039902 (2005)
B Grzadkowski and Z Hioki, *Phys. Lett.* **B529**, 82 (2002)

[2] B Grzadkowski and Z Hioki, *Phys. Lett.* **B557**, 55 (2003)
Z Hioki, hep-ph/0210224

[3] R M Godbole, S D Rindani and R K Singh, arXiv:hep-ph/0605100

PRAMANA
— journal of
physics

© Indian Academy of Sciences

Vol. 69, No. 5
November 2007
pp. 921–926

Scalar top study: Detector optimization

C MILSTÉNE[1] and A SOPCZAK[2,*]
[1]Fermi National Laboratory, Batavia, Il-60510, USA
[2]Department of Physics, Lancaster University, LA1 4YW, UK
E-mail: caroline@fnal.gov; andre.sopczak@cern.ch

Abstract. A vertex detector concept of the linear collider flavour identification (LCFI) collaboration, which studies pixel detectors for heavy quark flavour identification, has been implemented in simulations for *c*-quark tagging in scalar top studies. The production and decay of scalar top quarks (stops) is particularly interesting for the development of the vertex detector as only two *c*-quarks and missing energy (from undetected neutralinos) are produced for light stops. Previous studies investigated the vertex detector design in scenarios with large mass differences between stop and neutralino, corresponding to large visible energy in the detector. In this study we investigate the tagging performance dependence on the vertex detector design in a scenario with small visible energy for the international linear collider (ILC).

Keywords. Supersymmetry; scalar top quarks; CCD detector; vertex detector; linear collider flavour identification; detector concept; linear collider; beam delivery system; radiation damage; multiple scattering.

PACS Nos 12.20.Pb; 14.80.ty; 29.00.00; 14.65.DW; 13.66.JN

1. Introduction

The development of a vertex detector for a linear collider is an important and challenging enterprise. A key aspect is the distance of the innermost layer to the interaction point, which is related to radiation hardness and beam background. Another key aspect is the number of radiation lengths the particles go through, since it determines the multiple scattering which affects the vertex reconstruction.

The optimization of the vertex detector tagging performance is of great importance for studies of physics processes. While mostly at previous and current accelerators (e.g. SLC, LEP, Tevatron) *b*-quark tagging has revolutionized many searches and measurements, *c*-quark tagging will be very important at a future linear collider, for example, in studies of supersymmetric dark matter [1]. Therefore, *c*-quark tagging could be a benchmark for vertex detector developments. The scalar top

---

[*] Speaker

Table 1. Number of background events.

Thickness	Layers	12% Signal efficiency	25% Signal efficiency
Single	5 (4)	68 (82)	2300 (2681)
Double	5 (4)	69 (92)	2332 (2765)

production and decay process, and the implemented vertex detector geometry are shown in ref. [2].

The analysis for a large mass difference with the SPS-5 parameter point (ISAJET) $m_{\tilde{t}_1} = 220.7$ GeV, $m_{\tilde{\chi}^0_1} = 120$ GeV and $\cos\theta_{\tilde{t}} = 0.5377$ was previously performed [3]. For 25% (12%) efficiency 3800 (1800) signal events and 5400 (170) background events without c-quark tagging were obtained, while the background was reduced to 2300 (68) events with c-quark tagging.

The vertex detector radiation length was varied between single thickness (TESLA TDR) and double thickness. In addition, the number of vertex detector layers was varied between five layers (innermost layer at 1.5 cm as in the TESLA TDR) and four layers (innermost layer at 2.6 cm). For SPS-5 parameters, the following number of background events remain as shown in table 1 [3].

A significantly larger number of background events was expected if the first layer of the vertex detector is removed. The distance of the first layer to the interaction point is also an important aspect from the accelerator physics (beam delivery) perspective. The interplay between the beam delivery and vertex detector design in regard to critical tolerances like hardware damage of the first layer and occupancy (unable to use the data of the first layer) due to beam background goes beyond the scope of this study and will be addressed in the future.

For large visible energy (large mass difference) no significant increase in the expected background was observed for doubling the thickness of the vertex detector layers [3,4]. In this study the effect of the vertex detector design on the events with smaller visible energy in the detector is addressed.

2. Signal and background simulations

The production of simulated light stops at a 500 GeV linear collider is analyzed using high luminosity $\mathcal{L} = 500\ \text{fb}^{-1}$. The signature for stop pair production at an e^+e^- collider is two charm jets and large missing energy:

$$e^+e^- \to \tilde{t}_1 \bar{\tilde{t}}_1 \to c\,\tilde{\chi}^0_1\,\bar{c}\,\tilde{\chi}^0_1. \tag{1}$$

For small $\Delta m = m_{\tilde{t}_1} - m_{\tilde{\chi}^0_1}$, the jets are relatively soft and separation from backgrounds is very challenging. Backgrounds arising from various standard model processes can have cross-sections that are several orders of magnitude larger than the signal. Thus, it is necessary to study this process with a realistic detector simulation. Signal and background events are generated with PYTHIA 6.129 [5], including a scalar top signal generation [6] previously used in ref. [7]. The detector simulation is based on the fast simulation SIMDET [8], describing a typical ILC detector. Good agreement in comparisons with SGV [9] detector simulations was obtained [3,4].

Cross-sections for the signal process and the relevant backgrounds have been computed with a code used in ref. [10] and by GRACE 2.0 [11], with cross-checks to COMPHEP 4.4 [12]. A minimal transverse momentum cut, $p_t > 5$ GeV, is applied for the two-photon background, to avoid the infra-red divergence. Details of the event selection are given in ref. [1].

The c-tagging with the LCFI detector is based on vertex identification and a neural network application [13]. The vertex identification considered three cases for each jet independently:

(a) *Only a primary vertex.* In this case, the two tracks with the largest separation in the r–ϕ plane are considered and for these tracks the neural network variables include the impact parameter and its significance (impact parameter divided by uncertainty) both in the r–ϕ plane and in the z-direction, their momenta, and the joined probability in r–ϕ plane and z-direction.

(b) *One secondary vertex.* In addition to the previous variables, the decay length significance of the secondary vertex, the multiplicity and momenta of all associated tracks, and the P_t corrected mass of the secondary vertex (corrected for neutral hadrons and neutrinos), the P_t of the decay products perpendicular to the flight direction between primary and secondary vertex, and the joint probability in r–ϕ and z-direction.

(c) *More than one secondary vertex.* Two secondary vertices are considered, where the tracks are assigned to the vertex closest to the primary vertex, and the neural network input variables are defined as in case (b).

The neural network is tuned to 255,000 simulated signals and 240,000 $We\nu$ background events. The signal events are a combination of all simulated signal events for the scalar top mass range between 120 and 220 GeV and for $\Delta m = 5, 10$ and 15 GeV.

After a preselection which substantially reduces the background while keeping about 70% of the signal, six sequential cuts are applied: number of jets, missing energy, acollinearity, thrust angle, transverse momentum, and the jet–jet invariant mass and c-tagging [1]. The background consists of the following processes: W^+W^-, ZZ, $We\nu$, eeZ, $q\bar{q}(q \neq t)$, $t\bar{t}$, and two-photon. After all the cuts, the total background of about 5680 events is dominated by about 5044 $We\nu$ events [1]. A scalar top signal of 120 GeV has been simulated with a neutralino mass of 110 GeV. The selection efficiency is about 20% [14] and 11,500 signal events are expected for a standard LCFI vertex detector configuration as given in the TESLA TDR.

3. Varying the vertex detector design

This study of the vertex detector design is based on 50,000 simulated 120 GeV signals and 210,000 $We\nu$ background events for each detector design. After preselection 29,842 signals and 53,314 $We\nu$ events are selected, corresponding to 34,318 and 779,450 events per 500 fb^{-1}, respectively. This preselection signal efficiency of

59.7% does not depend on the vertex detector design. Four detector designs are compared:

- VX_{12}: The TESLA TDR design with 5 layers and a single layer (0.064% X_0 radiation length per layer).
- VX_{22}: Four layers (the innermost layer removed). This scenario could for example occur if the vertex detector is exposed to a large dose of machine background from the accelerator. The optimization of the radius of the innermost layer is an important aspect in the design of a vertex detector for a linear collider.
- VX_{32}: Five layers and double material thickness (0.128% X_0 radiation length per layer). As the rigidity of the sensitive elements and the support structure is another important aspect in the detector design, the material budget has to be taken into account.
- VX_{42}: Four layers (the innermost layer removed) and double thickness (0.128% X_0 radiation length per layer).

The c-tagging efficiency per event is normalized to the number of signal events after the preselection and requiring two jets. At least one c-tagged jet is required and the efficiency is given in figure 1 and table 2 as a function of the purity, where purity is defined as the ratio of the number of simulated signal events after c-tagging to all the c-tagged events assuming the same luminosity for signal and background. The different purities are obtained by varying the cut on the c-tagging neural network variable. The effect of the detector design variation increases with increasing purity (harder c-tagging neural network cut). For the second set of points in the plot with purities about 18% and c-tagging efficiencies between 85% and 90%, the variation of the signal efficiency and the number of $We\nu$ background events are given in table 2 after all selection cuts.

4. Results

These results for small visible energy ($\Delta m = 10$ GeV) lead to the same observation as for large visible energy (SPS-5 scenario with $\Delta m = 100.7$ GeV). The radius of the innermost layer of the vertex detector has a large effect on the c-quark tagging performance. Curves VX_{12} and VX_{22} in figure 1 show the performance for radii 15 and 26 mm, respectively. There is no significant effect on the c-quark tagging performance from doubling the material budget (e.g. curves VX_{12} and VX_{32} of

Table 2. Expected signal efficiency and number of $We\nu$ background events for the four detector designs. The statistical uncertainties are also given.

Thickness	Layers	Signal efficiency (in %)	$We\nu$/210 k	$We\nu$/500 fb^{-1}
Single	5 (4)	20.46 (19.67)	364 (369)	5322 (5396)
Double	5 (4)	20.32 (19.52)	366 (385)	5352 (5630)
		±0.18	±19	±280

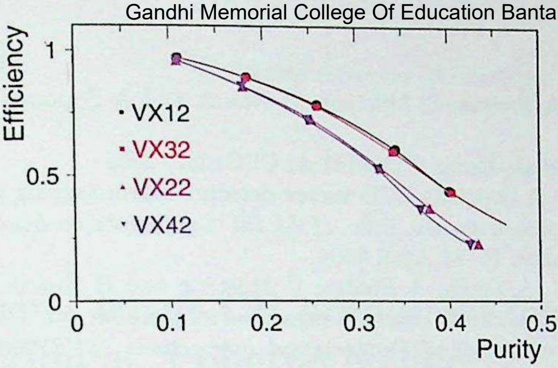

Figure 1. Scalar top c-tagging efficiency and purity with $We\nu$ background for different detector designs. The VX_{12} curve is for a detector design with five layers (innermost at 15 mm) and single density, curve VX_{22} is for a detector design with four layers (innermost at 26 mm). Curves VX_{32} and VX_{42} are for double density (0.128% X_0 radiation length per layer) with four and five layers, respectively.

figure 1). The increase of multiple scattering is not significant between single and double thicknesses (0.128% X_0 radiation length per layer).

In order to quantitatively estimate the multiple scattering effect, the number of tracks per signal event and the visible energy have been determined. The minimum visible energy per event is about 10 GeV and the maximum number of tracks is about 20, therefore the minimum track energy is about 0.5 GeV. The analytical calculation of the multiple scattering angle is given by $\theta \approx 13.6/P \cdot \sqrt{x/X_0}$, where the track momentum P is given in MeV. The displacement at the interaction point is $d \approx R\theta$, where R is the radius of the innermost layer of the vertex detector. For $P = 500$ MeV, $x/X_0 = 0.128\%$ and $R = 15$ mm, $d = 15$ μm. This small value compared to the flight distance of charm mesons explains the insignificant effect on the c-quark tagging from the multiple scattering increase by doubling the vertex detector layer thickness.

5. Conclusions

In conclusion, studies with a small visible energy signal lead to the same results as in the previous study for large visible energy regarding the vertex detector design. A strong dependence on the detector performance on the radius of the innermost vertex detector layer has been observed, while doubling the material thickness has no significant effect on the c-quark tagging performance in scalar top studies at the ILC. The optimization of the radius of the innermost vertex detector layer will have to take into account the accelerator background which depends on the machine optics and the collimation system.

Acknowledgements

The author AS would like to thank the organizers of the workshop for making this presentation possible.

References

[1] M Carena, A Finch, A Freitas, C Milstène, H Nowak and A Sopczak, *Phys. Rev.* **D72**, 115008 (2005)

[2] C Milsténe and A Sopczak, Econf C0508141:ALCPG1431, 2005

[3] A Finch, H Nowak and A Sopczak, CCD vertex detector charm-tagging performance in studies of scalar top quark decays, *Proc. of the Int. Conference on Linear Colliders (LCWS 04)*, Paris, France, 19–24 April 2004

[4] A Sopczak, M Carena, A Finch, A Freitas, C Milsténe and H Nowak, Scalar top quark studies with various visible energies, presented at the *13th Int. Conference on Supersymmetry and Unification of Fundamental Interactions (SUSY'05)*, Durham, UK, 18–23 July 2005

[5] T Sjöstrand *et al*, *Comput. Phys. Commun.* **135**, 238 (2001)

[6] A Sopczak, in PHYSICS AT LEP2, Event Generators for Discovery Physics, CERN Yellow Report CERN 96-01

[7] A Finch, H Nowak and A Sopczak, contributed paper EPS370, *Int. Conference on High-Energy Physics (HEP 2003)*, Aachen, Germany, 17–23 July 2003 (LC Note LC-PHSM-2003-075)

[8] M Pohl and H J Schreiber, hep-ex/0206009

[9] M Berggren, Simulation Grand Vitesse (SGV), http://berggren.home.cern.ch/berggren/sgv.html

[10] A Freitas, D J Miller and P M Zerwas, *Euro. Phys. J.* **C21**, 361 (2001)
A Freitas, A von Manteuffel and P M Zerwas, *Euro. Phys. J.* **C34**, 487 (2004)

[11] F Yuasa *et al*, *Prog. Theor. Phys. Suppl.* **138**, 18 (2000)

[12] CompHEP Collaboration: E Boos *et al*, *Nucl. Instrum. Methods* **A534**, 250 (2004)

[13] T Kuhl, Hadronic branching ratio of a SM-like Higgs boson at a future linear collider, *Proc. of the Int. Conference on Linear Colliders (LCWS 04)*, Paris, France, 19–24 April 2004

[14] The re-tuning of the c-tagging neural network increased the selection efficiency from 19% [1] to 20% and the $We\nu$ background from 5044 [1] to 5322 ± 280 events

PRAMANA
— journal of
physics

© Indian Academy of Sciences

Vol. 69, No. 5
November 2007
pp. 927–930

Measuring Higgs CP properties through top quark production at a photon collider

ERI ASAKAWA
Theory Group, KEK, Tsukuba, Ibaraki 305-0801, Japan
E-mail: eri_asakawa@yahoo.co.jp

Abstract. We study resonant effects of heavy Higgs bosons on the top-pair production process at a photon linear collider. Observables which can be obtained by circular polarization of colliding photons and polarization measurement through the angular distribution of the top quark decays are useful not only for measuring the Higgs CP parity but also for resolving degeneracy of Higgs bosons.

Keywords. Higgs; beyond the standard model.

PACS Nos 12.60.Fr; 14.80.Cp

1. Introduction

The Higgs sector of the standard model (SM) can be extended by additional Higgs multiplets. In such models, neutral CP-even Higgs boson(s) (H) as well as neutral CP-odd Higgs boson(s) (A) appear. Models like the minimal supersymmetric extension of the SM (MSSM) are expected to have almost degenerate masses for H and A if they are heavy in comparison with m_Z.

On the other hand, a photon collider can be an ideal device for production of neutral Higgs bosons H and A. Its reach for the mass of Higgs bosons is about 80% of the parent e^+e^- collider. Even if the heavy neutral Higgs bosons cannot be detected at the LHC, and even if they are too heavy to be detected at the e^+e^- collider, it may be possible to detect them at a photon collider [1].

In this talk, we study observables which can be obtained by circular polarization of colliding photons and polarization measurement through the angular distribution of the top quark decays in the $\gamma\gamma \to t\bar{t}$ process at a photon collider. It will be shown that special linear combinations for these observables are useful for measuring the Higgs CP parity and for resolving degeneracy of heavy neutral Higgs bosons [2].

2. Observables for the process $\gamma\gamma \to t\bar{t}$

When the $\gamma\gamma$ collision energy reaches around mass of the Higgs bosons H and A, the helicity amplitudes for the process $\gamma_{\lambda_1}\gamma_{\lambda_2} \to t_\sigma \bar{t}_{\bar{\sigma}}$ can be expressed as

$$M^{\sigma\bar{\sigma}}_{\lambda_1\lambda_2} = [M_H]^{\sigma\bar{\sigma}}_{\lambda_1\lambda_2} + [M_A]^{\sigma\bar{\sigma}}_{\lambda_1\lambda_2} + [M_t]^{\sigma\bar{\sigma}}_{\lambda_1\lambda_2}\,, \tag{1}$$

where the first term $M_{H,A}$ stands for the s-channel H, A-exchange amplitudes and the latter term M_t stands for the t- and u-channel top-quark-exchange amplitudes. The resonant helicity amplitudes are calculated by using the lowest-dimensional effective Lagrangian of the form

$$L_{\phi\gamma\gamma} = \frac{1}{m_\phi}\left(b_\gamma^H A_{\mu\nu}A^{\mu\nu} + b_\gamma^A \widetilde{A}_{\mu\nu}A^{\mu\nu}\right)\phi. \tag{2}$$

By considering the decay angular distribution of $t\bar{t}$ pairs, we can derive the convoluted four observables, Σ_1 to Σ_4,

$$\begin{aligned}\Sigma_i(\sqrt{\hat{s}}) = \int \mathrm{d}\sqrt{\hat{s}} \sum_{\lambda_1,\ \lambda_2}\left(\frac{1}{L_{0.8}}\frac{\mathrm{d}L^{\lambda_1\lambda_2}}{\mathrm{d}\sqrt{\hat{s}}}\right) \\ \times\left(\frac{3\beta}{32\pi\hat{s}}\int S^i_{\lambda_1\lambda_2}(\Theta,\sqrt{\hat{s}})\mathrm{d}\cos\Theta\right),\end{aligned} \tag{3}$$

for $i = 1-4$, where $\hat{s}$ is the total energy-squared in the rest frame of $\gamma\gamma$ collisions and the functions $S^i_{\lambda_1\lambda_2}$ contain all the information about the $\gamma\gamma \to t\bar{t}$ helicity amplitudes:

$$\begin{aligned}&S^1_{\lambda_1\lambda_2} = \left|M^{RR}_{\lambda_1\lambda_2}\right|^2, \quad S^2_{\lambda_1\lambda_2} = \left|M^{LL}_{\lambda_1\lambda_2}\right|^2, \\ &S^3_{\lambda_1\lambda_2} = 2\Re\left[M^{RR}_{\lambda_1\lambda_2}\left(M^{LL}_{\lambda_1\lambda_2}\right)^*\right], \quad S^4_{\lambda_1\lambda_2} = 2\Im\left[M^{RR}_{\lambda_1\lambda_2}\left(M^{LL}_{\lambda_1\lambda_2}\right)^*\right],\end{aligned} \tag{4}$$

the $\gamma\gamma$ luminosity integrated over $z \geq 0.8z_m$ is denoted by $L_{0.8}$ and the luminosity distribution for each $\gamma\gamma$ helicity combination is expressed by $\mathrm{d}L^{\lambda_1\lambda_2}/\mathrm{d}\sqrt{\hat{s}}$.

For the collider parameters, here we use $E_e = 250$ GeV, $P_l = -1.0$, $P_e = 0.9$ and $x = 4.8$, where colliding photons are highly polarized to be + around $\sqrt{\hat{s}} = 400$ GeV. In this case, among the four combinations for $\lambda_1\lambda_2$, the ++ combination largely dominates around $\sqrt{\hat{s}} = 400$ GeV, and the quantities S^{1-4} in (4) can be expressed by $M_{H,A}$ and M_t which are the abbreviated notations for $[M_{H,A}]^{RR}_{++}$ and $[M_t]^{RR}_{++}$;

$$\begin{aligned}S^1_{++} &= |M_t|^2 + |M_A|^2 + |M_H|^2 \\ &+2M_t\Re[M_A] + 2M_t\Re[M_H] + 2\Re[M_A^*M_H],\end{aligned} \tag{5}$$

$$\begin{aligned}S^2_{++} &= \left(\frac{1-\beta}{1+\beta}\right)^2|M_t|^2 + |M_A|^2 + |M_H|^2 \\ &+2\frac{1-\beta}{1+\beta}M_t\Re[M_A] - 2\frac{1-\beta}{1+\beta}M_t\Re[M_H] - 2\Re[M_A^*M_H],\end{aligned} \tag{6}$$

$$\begin{aligned}S^3_{++} &= 2\frac{1-\beta}{1+\beta}|M_t|^2 + 2|M_A|^2 - 2|M_H|^2 \\ &+2\left(\frac{1-\beta}{1+\beta}+1\right)M_t\Re[M_A] + 2\left(\frac{1-\beta}{1+\beta}-1\right)M_t\Re[M_H],\end{aligned} \tag{7}$$

$$\begin{aligned}S^4_{++} &= 2\left(\frac{1-\beta}{1+\beta}-1\right)M_t\Im[M_A] + 2\left(\frac{1-\beta}{1+\beta}+1\right)M_t\Im[M_H] \\ &+4\Im[M_A^*M_H],\end{aligned} \tag{8}$$

where β is the velocity of the top quarks.

3. Measuring Higgs CP parity

If we assume that the top-quark decays are essentially described by the SM amplitudes, it is straightforward to extract all the four observables Σ_1 to Σ_4 which are proportional to $S^1_{\lambda_1\lambda_2} - S^4_{\lambda_1\lambda_2}$. As you see in (5)–(8), S^2, S^3 and S^4 include the terms which differ in sign for H and A. Therefore, if we observe the difference between H and A, it is possible to determine the Higgs CP parity from the observables [2,3].

The observables are also sensitive to the complex phase of the $\gamma\gamma H$ and $\gamma\gamma A$ vertices. Since variation in the phase modifies the magnitudes of the observables and the $\sqrt{\hat{s}}$ values where the observables have peaks and bottoms, we can receive new information about the Higgs couplings to new heavy charged particles which give extra contribution to the $\gamma\gamma H$ and/or $\gamma\gamma A$ vertices [2].

4. Resolving degeneracy of Higgs bosons

In the above discussion, we studied four observables separately. Once they are derived individually, we can obtain their arbitrary linear combinations. The most powerful combinations for probing the CP parity of Higgs bosons are $\Sigma_1 + \Sigma_2 + \Sigma_3$ and $\Sigma_1 + \Sigma_2 - \Sigma_3$ which are approximately proportional to

$$S^1_{++} + S^2_{++} + S^3_{++} = \left(\frac{2}{1+\beta}\right)^2 |M_t|^2 + 4|M_A|^2 + 4\frac{2}{1+\beta} M_t \Re[M_A], \tag{9}$$

$$S^1_{++} + S^2_{++} - S^3_{++} = \left(\frac{2\beta}{1+\beta}\right)^2 |M_t|^2 + 4|M_H|^2 + 4\frac{2\beta}{1+\beta} M_t \Re[M_H]. \tag{10}$$

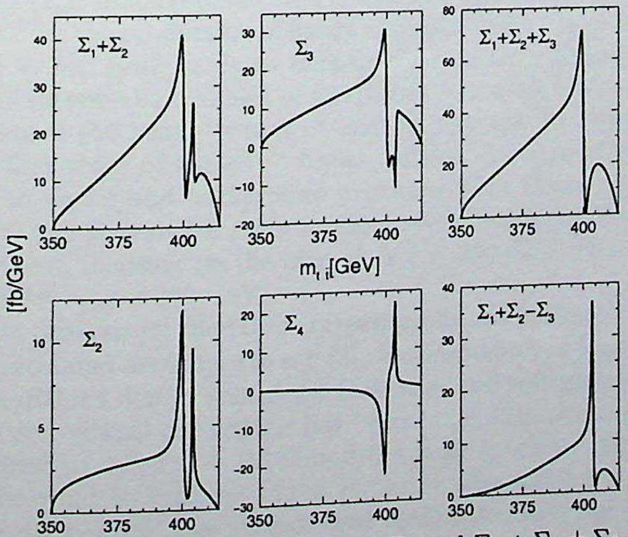

Figure 1. The observables Σ_1 to Σ_4 and $\Sigma_1 + \Sigma_2 \pm \Sigma_3$.

The former combination receives contribution only from the CP-odd resonance, while the latter only from the CP-even resonance when CP is conserved. It is therefore straightforward to separate the CP-even and CP-odd resonances, even when their masses are degenerate.

The four observables Σ_1 to Σ_4 and the linear combination $\Sigma_1 + \Sigma_2 \pm \Sigma_3$ are shown in figure 1. When we draw the figure, we adopt a MSSM prediction as an example where the parameters are taken as follows: $m_A = 400$ GeV, $\tan\beta = 3$, $m_{\tilde{f}} = 1$ TeV, $M_2 = 500$ GeV, $\mu = -500$ GeV. Then we find

$$\begin{aligned} & m_A = 400\ \text{GeV}, \quad \Gamma_A = 1.75\ \text{GeV}, \\ & \text{Br}(A \to \gamma\gamma) = 1.53 \times 10^{-5}, \quad \text{Br}(A \to t\bar{t}) = 0.946, \end{aligned} \tag{11}$$

$$\begin{aligned} & m_H = 403.8\ \text{GeV}, \quad \Gamma_H = 0.79\ \text{GeV}, \\ & \text{Br}(H \to \gamma\gamma) = 0.99 \times 10^{-5}, \quad \text{Br}(H \to t\bar{t}) = 0.742 \end{aligned} \tag{12}$$

for the above parameters [4]. In the left four figures, contributions from both H and A bosons whose masses are almost degenarate can be found. It may be impossible to tell the existence of two Higgs bosons under the energy resolution of the detector from those observables. On the other hand, in the right two figures, contributions from the H and A bosons are resolved. Then it is obvious that both H and A bosons exist around $\sqrt{\hat{s}} = 400$ GeV.

References

[1] M M Muhlleitner, M Kramer, M Spira and P M Zerwas, *Phys. Lett.* **B508**, 311 (2001)
D M Asner, J B Gronberg and J F Gunion, *Phys. Rev.* **D67**, 035009 (2003)

[2] E Asakawa and K Hagiwara, *Euro. Phys. J.* **C31**, 351 (2003)

[3] E Asakawa, J Kamoshita, A Sugamoto and I Watanabe, *Euro. Phys. J.* **C14**, 335 (2000)

[4] A Djouadi, J Kalinowski and M Spira, *Comm. Phys. Commun. Res.* **108**, 56 (1998)

PRAMANA
— journal of
physics

© Indian Academy of Sciences

Vol. 69, No. 5
November 2007
pp. 931–935

Heavy neutral MSSM Higgs bosons at the photon linear collider – a comparison of two analyses

M SPIRA[1], P NIEŻURAWSKI[2], M KRAWCZYK[3,*] and A F ŻARNECKI[2]
[1]Paul-Scherrer-Institut, CH-5232 Villigen PSI, Switzerland
[2]Institute of Experimental Physics, Warsaw University, ul. Hoża 69, 00-681 Warsaw, Poland
[3]Institute of Theoretical Physics, Warsaw University, ul. Hoża 69, 00-681 Warsaw, Poland
*E-mail: maria.krawczyk@fuw.edu.pl

Abstract. Measurement of the heavy neutral MSSM Higgs bosons H and A production in the process $\gamma\gamma \to A/H \to b\bar{b}$ at the Photon Linear Collider [1,2] has been considered in two independent analyses for the parameter range corresponding to the so-called 'LHC wedge'. Significantly different conclusions were obtained; signal-to-background ratio 36 vs. 2. Here assumptions and results of these two analyses are compared. We have found that differences in the final results are mainly due to different assumptions on $\gamma\gamma$-luminosity spectra, jet definitions and selection cuts.

Keywords. MSSM Higgs bosons; photon linear collider; LHC wedge.

PACS Nos 14.80.Cp; 13.87.Ce

A photon-collider option of the future e^+e^- linear collider offers a unique possibility to produce neutral Higgs bosons as s-channel resonances. In this contribution two analyses [1,2] are compared which estimate the precision of the cross-section measurement for the production of heavy neutral MSSM Higgs bosons in the process $\gamma\gamma \to A/H \to b\bar{b}$. Both analyses were focused on the so-called 'LHC wedge', i.e. the region of intermediate values of $\tan\beta$, $\tan\beta \approx 4$–10, and masses $M_{A/H}$ above 200 GeV, where the heavy bosons A and H may not be discovered at the LHC and at the first stage of the e^+e^- linear collider. In each of these analyses NLO corrections to signal and background processes were taken into account. As the results of the two approaches seem to differ significantly, we undertook the task of comparing them, focusing on the case of $M_A = 300$ GeV with MSSM parameters $tg\beta = 7$ and $M_2 = \mu = 200$ GeV.

In the first analysis [1] the NLO corrections to the background process $\gamma\gamma \to b\bar{b}$ have been calculated according to ref. [3]. Resummation of large Sudakov and non-Sudakov logarithms due to soft gluon radiation and soft gluon and bottom-quark exchange in the virtual corrections has been taken into account [4]. The NLO-α_s was normalized to $\alpha_s(M_Z) = 0.119$ and the scale given by the $\gamma\gamma$ invariant mass was used. In order to suppress gluon radiation slim two-jet configurations in the final state were selected; jets were defined within the Sterman–Weinberg criterion.

If the radiated gluon energy was larger than 10% of the total $\gamma\gamma$ invariant energy and if, at the same time, the opening angles between all three partons in the final state were larger than 20°, the event was classified as three-jet event and rejected. The interference between the signal and background processes has been taken into account properly. The NLO QCD corrections of the interference terms to quark final states including the resummation of the large (non-)Sudakov logarithms were calculated (for details, see [5]). The description of the $\gamma\gamma$-luminosity was based on the LO cross-section formula for the Compton process. It was assumed that the beam energy is tuned to obtain maximum luminosity at the value of the pseudoscalar Higgs mass M_A. In this analysis the selection of events was applied at the parton level. The background was reduced with a cut in the production angle of the bottom quark only, $|\cos\theta_b| < 0.5$. By collecting $b\bar{b}$ final states with a resolution in the invariant mass $M_A \pm 3$ GeV, the sensitivity to the combined A and H resonance peaks above the background was strongly increased. The result for the peak cross-section is shown in figure 1 as a function of M_A. It can be inferred from the figure that the background is strongly suppressed (signal-to-background ratio ≈ 36 for $M_A = 300$ GeV).

The second analysis [2] was based on realistic simulations of the $\gamma\gamma$-luminosity spectra for the PLC at the TESLA collider [6,7]. One-year run of PLC was assumed with the center-of-mass energy of the colliding electron beams optimized for the production of the pseudoscalar Higgs bosons. The distribution of the primary vertex and the beam crossing angle were taken into account. The total widths and branching ratios of the Higgs bosons and the H mass were calculated with the program HDECAY [8], taking into account decays to and loops of supersymmetric particles [9]. These results were used to calculate the signal cross-section in the resonance approximation. The events were generated with the PYTHIA program [10]. As the main background to Higgs-boson production heavy-quark pair production was considered; the event samples were generated using the program by Jikia [11] which includes exact one-loop QCD corrections to the lowest order processes $\gamma\gamma \to q\bar{q}(g)$ [12], and the non-Sudakov form factor in the double-logarithmic approximation, calculated up to 4 loops [13]. The JADE jet definition with a parameter $y_{\text{cut}}^J = 0.01$ is used to define 2- and 3-parton final states. The resummation of Sudakov logarithms due to soft gluon bremsstrahlung is omitted. In the calculation the LO-α_s normalized to $\alpha_s(M_Z) = 0.119$ was used at the scale given by the average of the squared transverse masses of the quark and anti-quark. Other background processes were also studied. As about two $\gamma\gamma \to$ hadrons events (so-called overlaying events) are expected per bunch crossing, they were generated with PYTHIA, and have been overlaid on signal and background events according to the Poisson distribution. On the detector level [14] jets were reconstructed using the Durham algorithm with $y_{\text{cut}}^D = 0.02$. Two or three jet events were accepted. To reduce the heavy-quark production background a cut on the polar angle for each jet was imposed: $|\cos\theta_{\text{jet}}| < 0.65$. Since the Higgs bosons are produced almost at rest, the ratio of the total longitudinal momentum calculated from all jets in the event, P_z, to the total measured energy, E, was required to be small: $|P_z|/E < 0.06$. Additional cuts to suppress the influence of overlaying events and the $\gamma\gamma \to W^+W^-$ background were also applied. A realistic b-tagging algorithm was used. All cuts were optimized. A more detailed description of event generation, simulation and selection cuts can be found in [16,17]. The result of the analysis is shown in figure 2 where the distribution of the corrected invariant mass, W_{corr} (correction for escaping neutrinos; see [18]), after imposing all selection cuts is presented for the signal and individual background contributions. From the number of signal and background events in the optimized W_{corr}-window the expected statistical precision of the cross-section measurement for $M_A = 300$ GeV is equal to 11%.

The results of both analyses differ significantly. In the first analysis the background contribution is negligible: the signal-to-background ratio $S/B \approx 36$ in the invariant mass window 297–303 GeV. For comparison in the second analysis $S/B \approx 2$ was obtained in the corrected invariant mass window 295–305 GeV if only the process $\gamma\gamma \to b\bar{b}$ is taken into account as the background. In order to understand the sources of those differences the cross-sections for the background process $\gamma\gamma \to b\bar{b}$ and signal process $\gamma\gamma \to A/H \to b\bar{b}$ were recalculated within both approaches with the same cuts and the same $\gamma\gamma$-luminosity spectrum.

The following conclusions emerged after investigation of the two calculations of the heavy quark background. With the polar angle cut imposed only on the quark b the 3-jet part is larger than the 2-jet part by more than an order of magnitude. However, if the cut on the anti-quark angle is added, the 2- and 3-jet cross-sections differ only by a factor 2 to 3. Thus, requiring only 2-jet events is less essential if the angular cut is applied for both quarks. This corresponds to the common cut on the jet polar angle which is usually applied on the detector level. The 2-jet cross-sections obtained in the two approaches agree within a factor of 2. Moreover, the full resummation of Sudakov and non-Sudakov logarithms does not modify the 2-jet numbers too much compared to the 4-loop expansion of the non-Sudakov logarithms. If the JADE algorithm is applied in both analyses then the obtained cross-sections agree within 15%. These residual differences can be mainly attributed to the different scale choices of the strong coupling α_s.

Next, the analogous comparison for the signal process was performed for $M_A = 300$ GeV. The same MSSM parameter set was used, i.e. $\tan\beta = 7$, $\mu = 200$ GeV, $M_2 = 200$ GeV, trilinear couplings equal to 1500 GeV, and common sfermion mass equal to 1 TeV were assumed. A top quark mass of 174 GeV has been adopted. Decays to supersymmetric particles and loops with them were taken into account. Small contributions from the decays $A/H \to gg^* \to gb\bar{b}$ were not added to the branching ratio $\text{BR}(A/H \to b\bar{b})$. With JADE jet definitions the results of both approaches agree within 5% for the total cross-section, and within 30% for the 2- and 3-jet classes separately. The differences in the separation of 2- and 3-jet classes mainly originate from the different approaches used in the two analyses. The second analysis used the resonance approximation and generated gluon radiation by parton showers, while the first analysis used a full NLO calculation for the signal process including soft gluon resummation for the 2-jet part.

Finally, we have compared the results for the invariant-mass window 297–303 GeV taking into account the assumed $\gamma\gamma$-luminosity spectra with the same normalization. Our first conclusion is that if the JADE jet definition were used in both analyses, the difference in the signal-to-background ratio between our analyses would be mainly due to the different contributions of $J_z = 0$ and $|J_z| = 2$ parts to the $\gamma\gamma$-luminosity. The $J_z = 0$ luminosity component of the realistic luminosity distribution used in the second analysis amounts only to 94% of the same

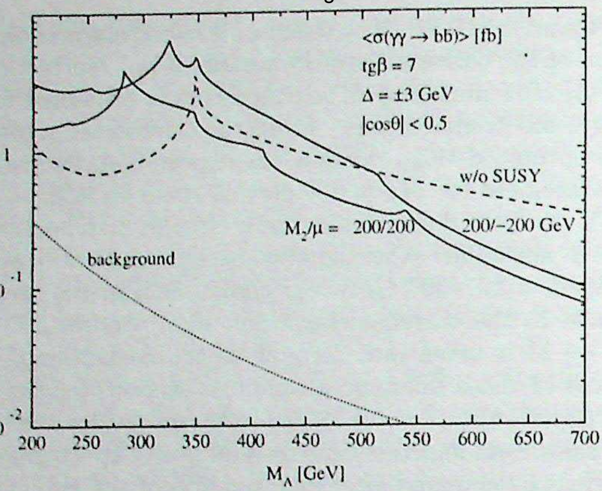

Figure 1. Average cross-sections in the invariant mass window ±3 GeV for resonant heavy Higgs boson H, A production in $\gamma\gamma$ collisions as a function of the pseudoscalar Higgs mass M_A with final decays into $b\bar{b}$ pairs, and the corresponding background cross-section. The maximum of the photon luminosity has been tuned to M_A. The MSSM parameters have been chosen as $tg\beta = 7, M_2 = \pm\mu = 200$ GeV; the limit of vanishing SUSY-particle contributions is shown for comparison (from ref. [1]).

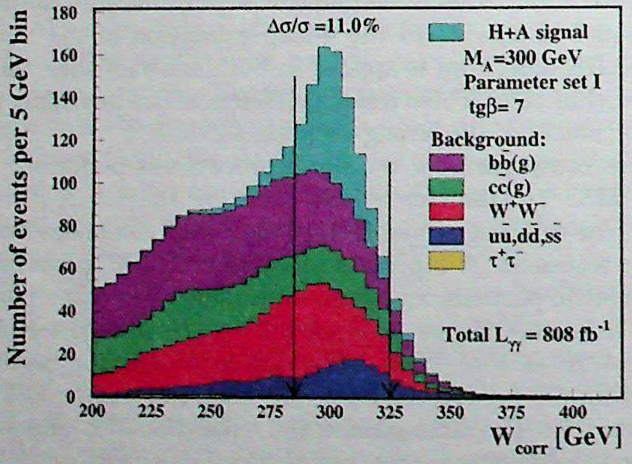

Figure 2. Distributions of the corrected invariant mass, W_{corr}, for signal and all considered background contributions, with overlaying events included. The best precision of 11% for $\gamma\gamma \to A/H \to b\bar{b}$ cross-section measurement is achieved in the W_{corr} window between 285 and 325 GeV (from ref. [2]).

component of the ideal spectrum used in the first analysis. What is more important is, in the realistic spectrum about 5.5 times more of the $|J_z| = 2$ component is taken into account relative to the same component in the ideal spectrum. If the JADE algorithm with $y^J_{\text{cut}} = 0.01$ is used, the signal-to-background ratio is around 12 in case of the first approach with angular cuts $|\cos\theta_{b/\bar{b}}| < 0.5$ applied for each quark and if 2- and 3-jet events are taken into account. In the second approach the ratio is around 6. However, if a correction accounting for the differences in the luminosity spectra is applied, the rescaled result of the second analysis is around 10, thus only 17% less than in the first analysis.

Our second observation is that the use of the Sterman–Weinberg jet definition leads to much higher rates of 2-jet events for the signal than for the background. This results in nearly two times higher signal-to-background ratios in comparison to the results obtained with the JADE jet definition if only 2-jet events are taken into account.

The measurement of the process $\gamma\gamma \to A/H \to b\bar{b}$ at the PLC is very promising, even for the realistic $\gamma\gamma$-luminosity spectrum, which is less advantageous than the ideal one. Use of the clustering algorithm based on the Sterman–Weinberg jet definition would lead to much higher signal-to-background ratios, if only 2-jet events were taken into account.

Acknowledgements

MK, AFZ and PN acknowledge partial support by Polish Ministry of Science and Higher Education, grant no. 1 P03B 040 26 and MS acknowledges partial support by the Swiss Bundesamt für Bildung und Wissenschaft.

References

[1] M Mühlleitner, M Krämer, M Spira and P Zerwas, *Phys. Lett.* **B508**, 311 (2001)
[2] P Nieżurawski, A F Żarnecki and M Krawczyk, *Acta Phys. Polon.* **B37**, 1187 (2006)
[3] B Kamal, Z Merebashvili and A P Contogouris, *Phys. Rev.* **D51**, 4808 (1995) and (E) *Phys. Rev.* **D55**, 3229 (1997)
[4] V S Fadin, V A Khoze and A D Martin, *Phys. Rev.* **D56**, 484 (1997)
M Melles and W J Stirling, *Phys. Rev.* **D59**, 094009 (1999); *Euro. Phys. J.* **C9**, 101 (1999); *Nucl. Phys.* **B564**, 325 (2000)
[5] M M Mühlleitner, Ph.D. thesis, DESY-THESIS-2000-033, hep-ph/0008127
[6] V I Telnov, http://www.desy.de/˜telnov/ggtesla/spectra/
[7] A F Żarnecki, *Acta Phys. Polon.* **B34**, 2741 (2003), hep-ex/0207021
[8] A Djouadi, J Kalinowski and M Spira, *Comput. Phys. Commun.* **108**, 56 (1998)
[9] The MSSM parameter set considered here was denoted in [2] as *I*
[10] T Sjöstrand *et al*, *Comput. Phys. Commun.* **135**, 238 (2001), hep-ph/0108264
[11] G Jikia and S Söldner-Rembold, *Nucl. Instrum. Methods* **A472**, 133 (2001)
[12] G Jikia and A Tkabladze, *Nucl. Instrum. Methods* **A355**, 81 (1995); *Phys. Rev.* **D54**, 2030 (1996)
[13] M Melles and W J Stirling, *Phys. Rev.* **D59**, 94009 (1999); *Euro. Phys. J.* **C9**, 101 (1999)
M Melles, W J Stirling and V A Khoze, *Phys. Rev.* **D61**, 54015 (2000)
M Melles, *Nucl. Instrum. Methods* **A472**, 128 (2001)
[14] The detector performance was simulated by the program SIMDET [15]
[15] M Pohl and H J Schreiber, DESY-02-061, hep-ex/0206009
[16] P Nieżurawski, hep-ph/0507004; hep-ph/0503295
[17] P Nieżurawski, A F Żarnecki and M Krawczyk, hep-ph/0507006
[18] P Nieżurawski, A Żarnecki and M Krawczyk, *Acta Phys. Polon.* **B34**, 177 (2003)

PRAMANA
— journal of
physics

© Indian Academy of Sciences

Vol. 69, No. 5
November 2007
pp. 937–941

Photon collider beam simulation with CAIN

ALEKSANDER FILIP ŻARNECKI
Institute of Experimental Physics, Warsaw University, Hoża 69, 00-681 Warszawa, Poland
E-mail: Filip.Zarnecki@fuw.edu.pl

Abstract. The CAIN simulation program was used to study the outgoing beam profile for the photon collider at ILC. The main aim of the analysis was to verify the feasibility of the photon linear collider running with 20 mrad electron beam crossing angle. The main problem is the distorted electron beam, which has to be removed from the interaction region. It is shown that with a new design of the final dipole, it should be possible to avoid large energy losses at the face of the magnet.

Keywords. Photon collider; crossing angle; Compton scattering; beam optics.

PACS Nos 29.27.-a; 41.85.-p

1. Introduction

A photon collider has been proposed as a natural extension of the e^+e^- linear collider [1]. The physics potential of a photon collider is very rich and complementary to the physics program of the e^+e^- and hadron–hadron colliders. Although the photon linear collider (PLC) is considered as one of the upgrade options of the ILC, it has specific requirements. Dedicated studies are being performed to verify that these requirements will be met by the ILC reference design and that the resulting running conditions at the PLC will allow to reach the proposed physics goal.

One of the PLC requirements is that the electron beam crossing angle is large enough to allow safe extraction of the electron beams distorted by scattering with the laser beams and with the opposing bunches [2]. For the photon collider at TESLA, the crossing angle of 34 mrad has been proposed as the optimum choice [3]. However, for the ILC baseline design, only the crossing angles of up to 20 mrad were considered. This contribution summarizes the study performed to verify if the proposed 20 mrad crossing angle solution is consistent with the PLC option.

2. Simulation

Photon linear collider beams were simulated using CAIN ver. 2.35 [4], compiled and run under Linux (Fedora Core 4). Beam configuration for e^-e^- running at

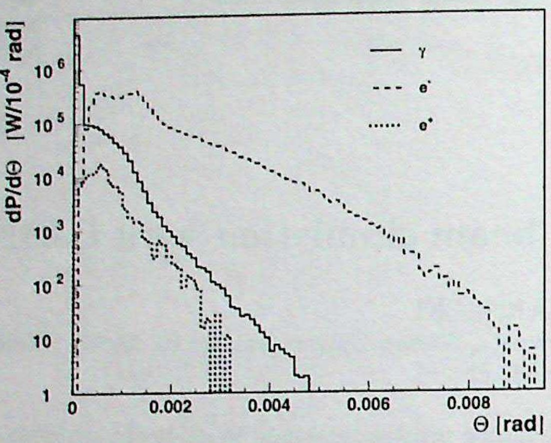

Figure 1. Profile of the beam leaving the $\gamma\gamma$ interaction region, for $\sqrt{s_{ee}} = 500$ GeV and the beam crossing angle of 34 mrad.

$\sqrt{s_{ee}} = 500$ GeV was based on the TESLA design, with optimized laser parameters [3]. Up to 200,000 macroparticles were used for detailed modeling of the incident beam bunches consisting of $2 \cdot 10^{10}$ electrons. It turned out that the simulation results are unstable if the colliding beams are assumed to be perfectly aligned. Therefore, a small vertical shift between the beams, $\Delta y = 0.1$ nm was introduced.

3. Beam profile

The expected profile of the outgoing PLC beam, after electron beam collision with the laser pulse and the beam–beam interaction, is presented in figure 1. Energy flow obtained from the simulation was scaled to the average beam power. After the Compton scattering, most of the incident electron beam power is transfered to the photon beam. However, the high-energy photons are very well-collimated along the incident electron beam direction and for angles greater than about 0.3 mrad the beam halo is dominated by electrons. It has to be noted that the electron beam distortion and the resulting background is much higher than in the case of e^+e^- or e^-e^- running with the same beam parameters. This is because the majority of electrons from the incident beam lose most of their energy in collisions with the laser photons, as shown in figure 2 (left). Although the electron scattering angles in the Compton scattering process are very small in the laboratory frame (∼10 μrad), low-energy electrons are deflected to much larger angles by the interaction with the opposite electron bunch, as shown in figure 2 (right).

4. Detector magnetic field

The largest contribution to the outgoing beam smearing is due to the interactions between two electron beams. Nevertheless, a cone with an opening angle of 10 mrad (which is consistent with the proposed design for the 20 mrad crossing angle) would

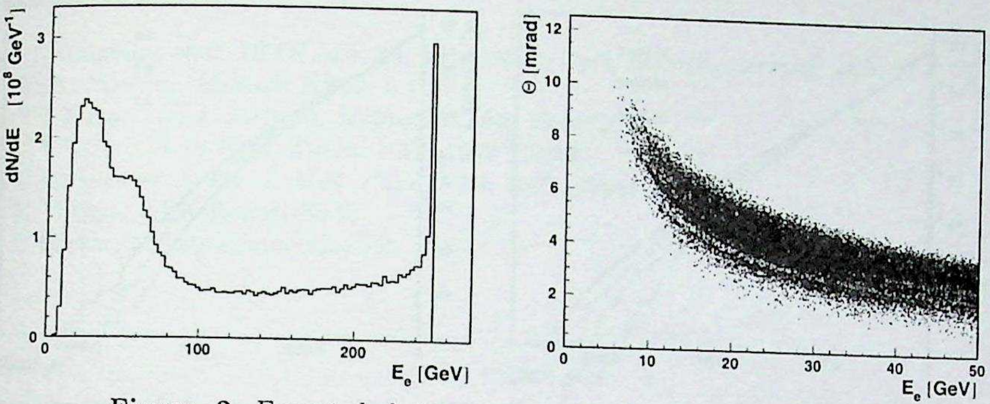

Figure 2. Expected electron energy distribution (left) and the correlation between electron energy and the deflection angle due to beam–beam interactions (right) for the electron beam leaving the $\gamma\gamma$ interaction region. Incident beam energy is 250 GeV.

be sufficient to accommodate all of the particles leaving the $\gamma\gamma$ interaction region (see figure 2 (right)). However, outgoing electrons and positrons are a subject to additional deflection in the detector magnetic field. Again, this effect is much more important at PLC than at ILC, as the average electron energy is smaller. Shown in figure 3 is the expected power dissipation due to particles going outside the cone with a given opening angle, for different values of the beam crossing angle and of the detector magnetic field. The distribution is calculated from the beam profile expected at $L^\star = 4.5$ m from the $\gamma\gamma$ interaction point, i.e. at the distance where the final focusing dipole should be located. The expected beam background decreases with decreasing beam crossing angle and magnetic field. However, even for a crossing angle of 20 mrad and a magnetic field of 3 T, an outgoing beam opening of at least 12 mrad is needed to avoid power dissipation greater than 10 W. A new design of the final dipole with 39 mm outer radius [5], decreases the opening angle needed for the incoming beam to about 9 mrad. Nevertheless, the results presented up to this point suggest that a crossing angle larger than 20 mrad is needed for PLC.

5. Proposed solution

Presented in figure 4(left) is the transverse profile of the outgoing beam expected at the distance of 4.5 m from the $\gamma\gamma$ interaction point. Both the beam–beam interaction between two flat beams and the effect of the detector magnetic field increase the size of the beam mainly in the vertical direction. Assuming a horizontal beam pipe opening of 10 mrad, we can still decrease the expected beam power losses below 10 W by increasing the vertical beam pipe opening, as indicated by the solid ellipse in figure 4. The dashed circle indicates the position of the final dipole with an outer radius of 39 mm. The expected power dissipation at the face of the final dipole, as a function of its outer radius, is presented in figure 4 (right).

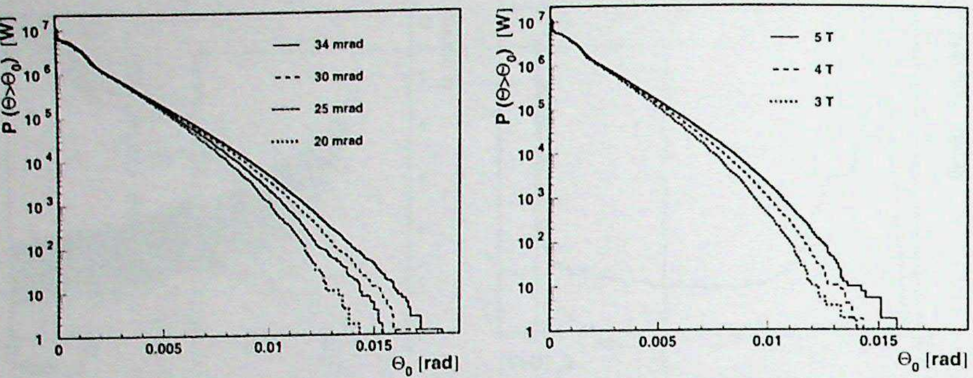

Figure 3. Power dissipation outside a given cone (around the nominal beam axis), for different values of the beam crossing angle and the detector magnetic field of 4 T (left), and for the beam crossing angle of 20 mrad and different values of the detector magnetic field (right). The distribution is calculated from the beam profile 4.5 m from the $\gamma\gamma$ interaction point.

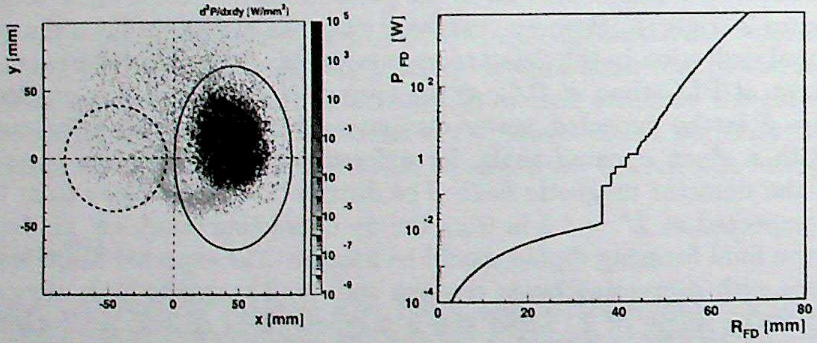

Figure 4. Left: the transverse profile of the beam 4.5 m from the $\gamma\gamma$ interaction point, for 20 mrad beam crossing angle and detector magnetic field of 4 T. Right: expected power dissipation at the face of the final dipole, as a function of its outer radius.

We conclude that horizontal opening of 11 mrad is sufficient to accommodate the outgoing beam for the photon linear collider running at 20 mrad crossing angle. This is consistent with $L^\star = 4.5$ m and the final dipole with up to 40 mm outer radius. Expected power dissipation at the magnet face is below 1 W. If smaller $L^\star$ or larger dipole radius is considered, 25 mrad crossing angle is required, as discussed in [2].

Acknowledgements

I would like to thank K Moenig, V Telnov, A Finch and other colleagues from the ECFA study groups. This work was partially supported by the Ministry of Science and Higher Education, Grant No. 1 P03B 040 26.

References

[1] I F Ginzburg *et al*, *JETP Lett.* **34**, 491 (1981); *Nucl. Instrum. Methods* **205**, 47 (1983); *Nucl. Instrum. Methods* **A219**, 5 (1984)
V I Telnov, *Nucl. Instrum. Methods* **A294**, 72 (1990)
[2] V I Telnov, *Acta Phys. Polon.* **B37**, 1049 (2006)
[3] B Badelek *et al*, *Int. J. Mod. Phys.* **A19**, 5097 (2004)
[4] K Yokoya, KEK-Report-85-9
[5] B Parker, private communication

PRAMANA
— journal of
physics

© Indian Academy of Sciences

Vol. 69, No. 5
November 2007
pp. 943–946

Results from GRACE/SUSY at one-loop

J FUJIMOTO[1], T ISHIKAWA[1], M JIMBO[2], T KANEKO[3],
T KON[3], Y KURIHARA[1], M KURODA[4], Y SHIMIZU[5] and Y YASUI[2,*]
[1]KEK, Oho, Tsukuba, Ibaraki 305-0801, Japan
[2]Tokyo Management College, Ichikawa, Chiba 272-0001, Japan
[3]Seikei University, Musashino, Tokyo 180-8633, Japan
[4]Meiji Gakuin University, Totsuka, Yokohama 244-8539, Japan
[5]The Graduate University for Advanced Studies, Hayama, Kanagawa 240-0193, Japan
[*]E-mail: yasui@tmc-ipd.ac.jp

Abstract. We report the recent development on the SUSY calculations with the help of GRACE system. GRACE/SUSY/1LOOP is the computer code which can generate Feynman diagrams in the MSSM automatically and compute one-loop amplitudes in the numerical way. We present new results of various two-body decay widths and chargino pair production at ILC (international linear collider) at one-loop level.

Keywords. Radiative corrections; supersymmetry.

PACS Nos **02.70.-c; 11.15.Bt; 12.38.Bx; 12.60.Jv**

1. Introduction

The supersymmetric (SUSY) theories are the prime candidates for the high energy particle physics beyond the standard model. The SUSY model is well motivated which was proposed as a solution of the hierarchy problem. Since the spectrum of the SUSY particles depends on the scenario of the model at higher energy scale, such as the GUT and the Planck scale, the detailed information of the SUSY parameters at the TeV scale may provide a probe to understand the nature of the early Universe.

Since we require that ILC has not only the capability to discover new physics, but also the potential to measure mass parameters and couplings precisely, precision measurements of the SUSY parameters will be one of the important issues at ILC experiment. We are to determine the mass parameters and couplings for SUSY particles within a few per cent precision [1]. To realize such precision measurements, in the theoretical side, the estimation of radiative corrections (RC) is essential.

Many authors have already discussed the RC studies of SUSY models [3–6]. However, the calculations of the RC in SUSY models are highly nontrivial. SUSY models include a large number of particles and couplings. Thus, a vast number of Feynman diagrams appear in the loop calculation. Performing such computation

Table 1. One-loop electroweak corrections on decay widths.

	Parent's mass (GeV)	Γ_0 (GeV)	$\delta\Gamma/\Gamma_0$ (%)
$H^0 \to d\bar{d}$	431.4	2.75×10^{-4}	+18
$H^0 \to b\bar{b}$	431.4	1.80	+9.7
$H^+ \to t\bar{b}$	438.4	1.45	+4.7
$H^+ \to \nu_\tau \tau^+$	438.4	8.75×10^{-2}	+16
$H^+ \to \tilde{\chi}_1^0 \tilde{\chi}_1^+$	438.4	1.21×10^{-1}	+4.0
$\tilde{e}_1^- \to e^- \tilde{\chi}_1^0$	123.2	7.80×10^{-2}	+7.8
$\tilde{\chi}_1^+ \to \nu_\tau \tilde{\tau}_1^+$	184.2	2.93×10^{-2}	+9.0
$\tilde{\chi}_2^+ \to Z^0 \tilde{\chi}_1^+$	421.1	7.53×10^{-1}	−2.8
$\tilde{\chi}_3^0 \to W^- \tilde{\chi}_1^+$	405.2	1.47	−4.2
$\tilde{\chi}_3^0 \to Z^0 \tilde{\chi}_1^0$	405.2	4.42×10^{-1}	+2.5
$\tilde{t}_1 \to b\tilde{\chi}_1^+$	347.4	1.35×10^{-1}	+13
$\tilde{t}_1 \to t\tilde{\chi}_1^0$	347.4	1.28×10^{-1}	+7.5
$\tilde{b}_1 \to t\tilde{\chi}_1^-$	469.4	1.22	+5.5
$\tilde{b}_1 \to b\tilde{\chi}_1^0$	469.4	1.65×10^{-1}	−1.4
$\tilde{u}_1 \to u\tilde{\chi}_1^0$	506.5	9.61×10^{-1}	+8.1

is absolutely beyond the human power if it should be done by hand. Since the procedure of a perturbation calculation is well established, computers must be able to take the place of human hand. In this decade, several groups have developed computer programs which generate Feynman diagrams and calculate cross-sections in the MSSM, like GRACE/SUSY [7,8], FeynArts-FormCalc [9] and CompHEP [10].

In this talk, we report the recent developments of the new system named GRACE/SUSY/1LOOP. This system, the upgraded version of GRACE/SUSY, can calculate full one-loop Feynman amplitudes in the minimal supersymmetric extension of the standard model (MSSM). In the next section, we show the results of the one-loop calculations for various two-body decay processes and the chargino pair production at e^+e^- colliders.

2. Physical results

To demonstrate the loop calculations, we adopt the gauge symmetric and on-shell renormalization scheme of the MSSM [11]. For the consistency check of the numerical results, we introduced the nonlinear gauge (NLG) fixing terms. This technique is the analogy of the NLG check which was used in the non-SUSY calculations with the GRACE/LOOP system [12]. We also tested the consistency checks of the ultraviolet finiteness and the infrared finiteness. All of these numerical tests have been done in the quadruple precision. Throughout the calculation we use the SPA1a' parameter sets [13].

First, we show the one-loop radiative corrections for various two-body decay widths of the Higgs and sparticles in table 1. We notice that the electroweak corrections $\delta\Gamma/\Gamma_0$ for the processes whose decay products include leptons are of the

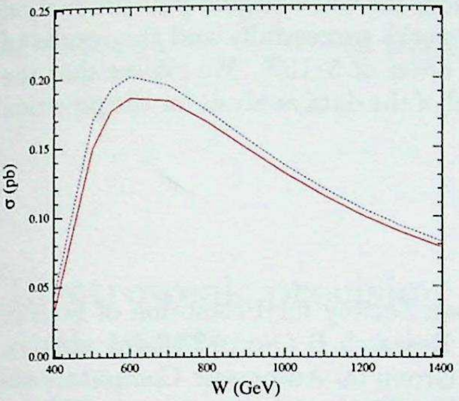

Figure 1. Total cross-section for chargino pair production. Solid and dotted lines denote $\sigma_{\rm elwk}$ and $\sigma_{\rm BORN}$, respectively.

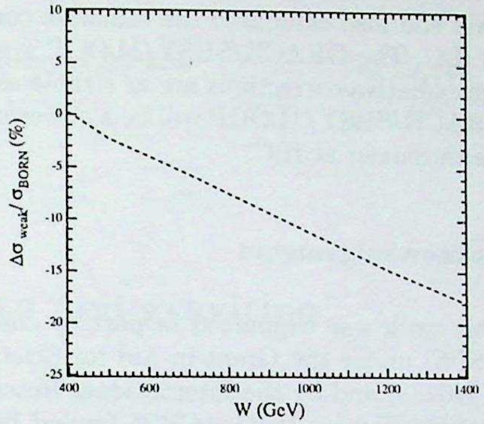

Figure 2. Weak correction for chargino pair production.

order of +10–+15%. For the processes where the Higgs or the gauginos decays into two heavy particles (weak gauge bosons or gauginos), $\delta\Gamma/\Gamma_0 \simeq -5$–$+5\%$. As for squarks decays, $\delta\Gamma/\Gamma_0$ sensitively depends on the masses and the mixing angles in the squark sector.

The next example is the one-loop calculation of the lighter chargino pair production at e^+e^- colliders. We show the energy dependence of the total cross-section in figure 1, where $W = \sqrt{s}$ and

$$\sigma_{\rm elwk} = \sigma_{\rm BORN}(1 + \delta_{\rm 1loop} + \delta_{\rm soft}) + \sigma_{\rm hard}. \tag{1}$$

The one-loop electroweak correction is of the order of −10%. We note that RC of this order can be detectable at the proposed ILC.

The RC on the chargino pair production in the SPA1a' scenario has already been studied by the Wien group [5]. Unfortunately, since they adopt different treatment of the photon emission correction, the direct comparison of our result with theirs is not possible. In figure 2 we show the energy dependence of the 'weak' correction $\Delta\sigma_{\rm weak}/\sigma_{\rm BORN}$ defined by

$$\Delta\sigma_{\rm weak} \equiv \sigma_{\rm elwk} - \sigma_{\rm BORN} * \delta_{\rm QED} - \sigma_{\rm hard}^{\rm initial}. \tag{2}$$

We find that our result is consistent with the values presented in [5]. From figure 2, we find that the weak correction becomes non-negligible, of the order of −5% for $\sqrt{s} = 600$ GeV.

3. Summary

GRACE/SUSY/1LOOP is the automatic computation system which can calculate full one-loop amplitudes for up to 2→2 processes in MSSM. Using this system, we demonstrated the systematic studies of several two-body decay widths at one-loop level and also estimated the radiative corrections for the chargino-pair production at ILC. The GRACE/SUSY/1LOOP system works successfully and the results of the radiative corrections are as sizable as the order of 5–15%. We expect that the GRACE/SUSY/1LOOP will be a powerful tool of the data analysis for the precision measurement at ILC.

Acknowledgements

This work was supported in part by the Japan Society for Promotion of Science (JSPS) under the Grant-in-Aid for Scientific Research B (No. 17340085 and No. 17540283) and by the International Research Group on Automatic Computational Particle Physics (IRG ACPP) funded by CNRS/Universities in France, KEK in Japan and MSU/RAS/MFBR in Russia.

References

[1] See for example: K Abe *et al*, GLC Project, KEK Report 2003-7 (2003)
[2] H P Nilles, *Phys. Rep.* **110**, 1 (1984)
H E Haber and G L Kane, *Phys. Rep.* **117**, 75 (1985)
[3] T Fritzsche and W Hollik, *Euro. Phys. J.* **C24**, 619 (2002); *Nucl. Phys. Proc. Suppl.* **135**, 102 (2004)
T Blank and W Hollik, hep-ph/0011092
W Hollik and H Rzehak, *Euro. Phys. J.* **C32**, 127 (2003)
A Arhrib and W Hollik, *J. High Energy Phys.* **0404**, 073 (2004)
J Guasch, W Hollik and J Sola, hep-ph/0307011
[4] H Eberl, W Majerotto and Y Yamada, *Phys. Lett.* **B597**, 275 (2004)
H Eberl, M Kincel, W Majerotto and Y Yamada, *Nucl. Phys.* **B625**, 372 (2002)
K Kovarik, C Weber, H Eberl and W Majerotto, *Phys. Lett.* **B591**, 242 (2004)
[5] W Öller, H Eberl and W Majerotto, *Phys. Rev.* **D71**, 115002 (2005)
[6] A Freitas and D J Miller, *eConf*, **C010630**, E3061 (2001)
[7] J Fujimoto *et al*, *Comput. Phys. Commun.* **111**, 185 (1998)
[8] J Fujimoto *et al*, *Comput. Phys. Commun.* **153**, 106 (2003); Program package GRACE/SUSY (GRACE v2.2.0) is available from http://minami-home.kek.jp/
[9] T Hahn, *Nucl. Phys. Proc. Suppl.* **89**, 231 (2000)
T Hahn, *Comput. Phys. Commun.* **140**, 418 (2001)
T Hahn and C Schappacher, *Comput. Phys. Commun.* **143**, 54 (2002)
[10] D S Gorbunov and A V Semenov, hep-ph/0111291.
A Semenov, *Nucl. Instrum. Methods* **A502**, 558 (2003)
[11] M Kuroda, in Research report to the Ministry of Education, Science and Culture, Japan, the Grant-in-Aid for Scientific Research C (No. 08640391) (1999) 127
[12] G Bélanger, F Boudjema, J Fujimoto, T Ishikawa, T Kaneko, K Kato and Y Shimizu, *Phys. Rep.* **430(3)**, 117 (2006)
[13] J A Aguilar-Saavedra *et al*, *Euro. Phys. J.* **C46**, 43 (2006)

PRAMANA
— journal of
physics

© Indian Academy of Sciences

Vol. 69, No. 5
November 2007
pp. 947–951

Electroweak precision data and gravitino dark matter

S HEINEMEYER
Instituto de Fisica de Cantabria (CSIC-UC), Santander, Spain
E-mail: Sven.Heinemeyer@cern.ch

Abstract. Electroweak precision measurements can provide indirect information about the possible scale of supersymmetry already at the present level of accuracy. We review present day sensitivities of precision data in mSUGRA-type models with the gravitino as the lightest supersymmetric particle (LSP). The χ^2 fit is based on M_W, $\sin^2\theta_{\text{eff}}$, $(g-2)_\mu$, BR($b \to s\gamma$) and the lightest MSSM Higgs boson mass, M_h. We find indications for relatively light soft supersymmetry-breaking masses, offering good prospects for the LHC and the ILC, and in some cases also for the Tevatron.

Keywords. Gravitino dark matter; fit; precision observables.

PACS Nos **12.60.Jv; 14.80.Ly**

1. Introduction

We have recently analyzed [1,2] the indications provided by current experimental data concerning the possible scale of supersymmetry (SUSY) within the framework of the minimal supersymmetric extension of the standard model (MSSM), assuming that the soft supersymmetry-breaking scalar masses m_0, gaugino masses $m_{1/2}$ and tri-linear parameters A_0 were each constrained to be universal at the input GUT scale, with the gravitino heavy and the lightest supersymmetric particle (LSP) being the lightest neutralino $\tilde{\chi}_1^0$ (CMSSM). (For other recent analyses, see ref. [3].) However, there are more scenarios for SUSY phenomenology. For example, the gravitino might be the LSP and constitute the dark matter [4], a framework known as the GDM [5].

Supersymmetry may provide an important contribution to loop effects that are rare or forbidden within the standard model. Especially sensitive in this respect are the observables M_W and $\sin^2\theta_{\text{eff}}$, the loop-induced quantities $(g-2)_\mu$ and BR($b \to s\gamma$), as well as the lightest MSSM Higgs boson mass, M_h (see ref. [6] for a review). Another important constraint is provided by the cold dark matter (CDM) density $\Omega_{\text{CDM}}h^2$ determined by WMAP and other observations. We analyze the precision observables in the context of the GDM, focusing on parameter combinations that fulfill $0.094 < \Omega_{\text{CDM}}h^2 < 0.129$ [7]. In order to simplify the analysis in a motivated manner, we furthermore restrict our attention to scenarios inspired by supergravity (mSUGRA), in which the gravitino mass is constrained to be equal to m_0 at the input GUT scale, and the trilinear and bilinear soft supersymmetry-breaking parameters are related by $A_0 = B_0 + m_0$. In the cases we review here, namely $A_0/m_0 = 0, 3/4, 3 - \sqrt{3}, 2$, the regions of the $(m_{1/2}, m_0)$ plane allowed by cosmological constraints then take the form of wedges located at small values of m_0 [5,8].

2. The χ^2 fit

In this section we review briefly the experimental data set that has been used for the fits. We focus on parameter points that yield the correct value of the cold dark matter density, $0.094 < \Omega_{\rm CDM}h^2 < 0.129$ [7], which is, however, not included in the fit itself. The top quark mass has been fixed to be $m_t = 172.7$ GeV [9], where the experimental uncertainty of $\delta m_t^{\rm exp} = 2.9$ GeV has been taken into account in the parametric uncertainty (see below). For the other observables we use the following experimental values (see ref. [2] and references therein)

$$\begin{aligned}
&M_W^{\rm exp} = 80.410 \pm 0.032 \text{ GeV},\\
&\sin^2\theta_{\rm eff}^{\rm exp} = 0.23153 \pm 0.00016,\\
&a_\mu^{\rm exp} - a_\mu^{\rm theo,SM} = (25.2 \pm 9.2) \times 10^{-10},\\
&{\rm BR}(b \to s\gamma) = (3.39^{+0.30}_{-0.27}) \times 10^{-4}.
\end{aligned} \tag{1}$$

An update to the most recent experimental values would not change our results in a qualitative manner (see e.g. ref. [10] for an analysis of the dependence on $m_t^{\rm exp}$ and $\delta m_t^{\rm exp}$). For M_h we use the complete likelihood information available from LEP [11]. Our starting points are the ${\rm CL}_s(M_h)$ values provided by the final LEP results on the SM Higgs boson search (see figure 9 in [11], where the χ^2 contribution is obtained by inversion ${\rm CL}_s(M_h)$ (see ref. [2] for details).

Assuming that the five observables listed above are uncorrelated, a χ^2 fit has been performed with

$$\chi^2 \equiv \sum_{n=1}^{4} \left(\frac{R_n^{\rm exp} - R_n^{\rm theo}}{\sigma_n} \right)^2 + \chi^2_{M_h}. \tag{2}$$

Here $R_n^{\rm exp}$ denotes the experimental central value of the nth observable (M_W, $\sin^2\theta_{\rm eff}$, $(g-2)_\mu$ and ${\rm BR}(b \to s\gamma)$), $R_n^{\rm theo}$ is the corresponding GDM prediction and σ_n denotes the combined error (experimental, parametric, intrinsic, refs [2,6]). $\chi^2_{M_h}$ denotes the χ^2 contribution coming from the lightest MSSM Higgs boson mass as described above. For details of the theory evaluations, see refs [6,12–15] and references therein.

3. Results in the GDM

In figure 1 we show total χ^2 as a function of $m_{1/2}$ and various SUSY particle masses. The global minimum of χ^2 for all the GDM models with $A_0/m_0 = 0, 0.75, 3 - \sqrt{3}$

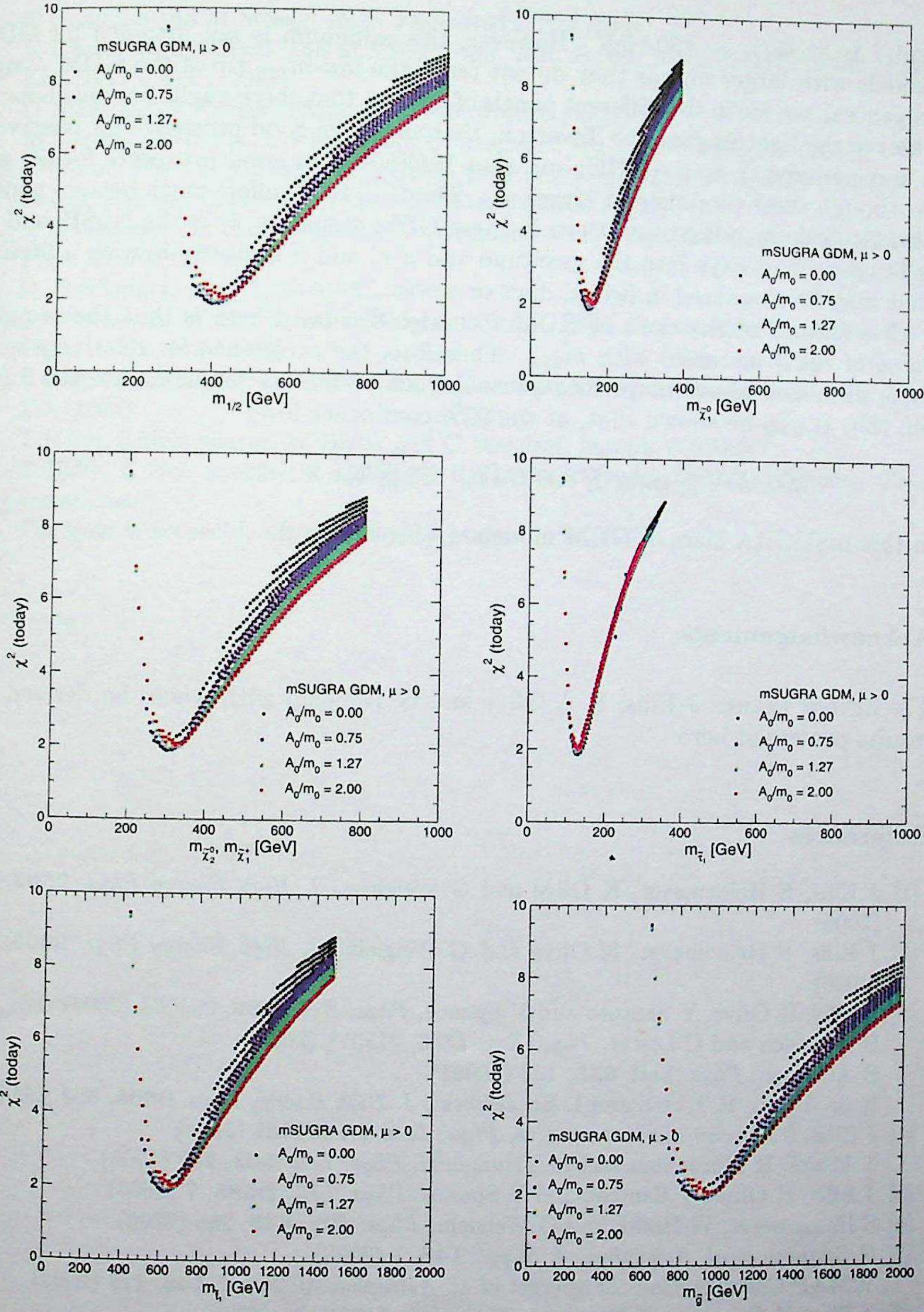

Figure 1. The dependence of the χ^2 function on $m_{1/2}$ for GDM scenarios with $A_0/m_0 = 0, 0.75, 3 - \sqrt{3}$ and 2, scanning the regions where the lighter stau $\tilde{\tau}_1$ is the NLSP, shown as a function of (**a**) $m_{1/2}$, (**b**) $m_{\tilde{\chi}_1^0}$, (**c**) $m_{\tilde{\chi}_2^0}$ and $m_{\tilde{\chi}_1^\pm}$, (**d**) $m_{\tilde{\tau}_1}$, (**e**) $m_{\tilde{t}_1}$, and (**f**) $m_{\tilde{g}}$.

and 2 is at $m_{1/2} \sim 450$ GeV. However, this minimum is not attained for GDM models with larger m_0, as they do not reach the low-$m_{1/2}$ tip of the GDM wedge. In general, we see in the different panels of figure 1 that there might be some hope to observe the lightest $\tilde{\tau}$ at the Tevatron, that there are good prospects for observing $\tilde{g}$ and perhaps $\tilde{t}_1$ at the LHC, and that ILC(500) has good prospects for $\tilde{\chi}^0_1$ and $\tilde{\tau}_1$, though these diminish for larger m_0. The ILC(1000) offers much better chances also for large m_0. We recall that, in these GDM scenarios, $\tilde{\tau}_1$ is the NLSP, and $\tilde{\chi}^0_1$ is heavier. $\tilde{\tau}_1$ decays into the gravitino and a τ, and is metastable with a lifetime that may be measured in hours, days or weeks.

One feature of the class of GDM scenarios discussed here is that the required value of $\tan\beta$ increases with $m_{1/2}$. Therefore, the preference for relatively small $m_{1/2}$ discussed above maps into an analogous preference for moderate $\tan\beta$ (see ref. [2]). It can be shown that, at the 95% confidence level

$$300 \text{ GeV} \lesssim \mathrm{m}_{1/2} \lesssim 800 \text{ GeV}, \quad 15 \lesssim \tan\beta \lesssim 27 \tag{3}$$

in this mSUGRA class of GDM models.

Acknowledgements

The author thanks J Ellis, K A Olive and G Weiglein with whom he derived the results presented here.

References

[1] J Ellis, S Heinemeyer, K Olive and G Weiglein, *J. High Energy Phys.* **0502**, 013 (2005)
[2] J Ellis, S Heinemeyer, K Olive and G Weiglein, *J. High Energy Phys.* **0605**, 005 (2006)
[3] J Ellis, K Olive, Y Santoso and V Spanos, *Phys. Rev.* **D69**, 095004 (2004)
B Allanach and C Lester, *Phys. Rev.* **D73**, 015013 (2006)
B Allanach, *Phys. Lett.* **635**, 123 (2006)
R de Austri, R Trotta and L Roszkowski, *J. High Energy Phys.* **0605**, 002 (2006)
[4] J Ellis, J Kim and D Nanopoulos, *Phys. Lett.* **B145**, 181 (1984)
T Moroi, H Murayama and M Yamaguchi, *Phys. Lett.* **303**, 289 (1993)
[5] J Ellis, K Olive, Y Santoso and V Spanos, *Phys. Lett.* **B588**, 7 (2004)
[6] S Heinemeyer, W Hollik and G Weiglein, *Phys. Rep.* **425**, 265 (2006)
[7] C Bennett *et al*, *Astrophys. J. Suppl.* **148**, 1 (2003)
WMAP Collaboration: D Spergel *et al*, *Astrophys. J. Suppl.* **148**, 175 (2003)
[8] J Ellis, K Olive and E Vangioni, *Phys. Lett.* **B619**, 30 (2005)
[9] CDF Collaboration, D0 Collaboration, Tevatron EWWG, hep-ex/0507091
[10] J Ellis, S Heinemeyer, K Olive and G Weiglein, hep-ph/0508169
[11] LEP Higgs Working Group, *Phys. Lett.* **B565**, 61 (2003)
[12] For a recent re-evaluation of M_W, see: S Heinemeyer, W Hollik, D Stöckinger, A M Weber and G Weiglein, *J. High Energy Phys.* **0608**, 052 (2006); *These proceedings*
[13] G Belanger, F Boudjema, A Pukhov and A Semenov, hep-ph/0405253
C Degrassi, P Gambino and G Giudice, *J. High Energy Phys.* **0012**, 009 (2000)

P Gambino and M Misiak, *Nucl. Phys.* **B611**, 338 (2001)
K Chetyrkin, M Misiak and M Münz, *Phys. Lett.* **B400**, 206 (1997); Erratum, *Phys. Lett.* **B425**, 414 (1998)
G Hiller and F Krüger, *Phys. Rev.* **D69**, 074020 (2004)
M Carena, D Garcia, U Nierste and C Wagner, *Phys. Lett.* **B499**, 141 (2001)

[14] T Moroi, *Phys. Rev.* **D53**, 6565 (1996); Erratum, *Phys. Rev.* **D56**, 4424 (1997)
G Degrassi and G Giudice, *Phys. Rev.* **D58**, 053007 (1998)
S Heinemeyer, D Stöckinger and G Weiglein, *Nucl. Phys.* **B690**, 62 (2004); *Nucl. Phys.* **B699**, 103 (2004)
D Stöckinger, hep-ph/0609168

[15] S Heinemeyer, W Hollik and G Weiglein, *Comp. Phys. Comm.* **124**, 76 (2000); *Euro. Phys. J.* **C9**, 343 (1999)
G Degrassi, S Heinemeyer, W Hollik, P Slavich and G Weiglein, *Euro. Phys. J.* **C28**, 133 (2003)
T Hahn, S Heinemeyer, W Hollik and G Weiglein, hep-ph/0507009
T Hahn, S Heinemeyer, W Hollik, H Rzehak, G Weiglein and K Williams, *These proceedings*
The code is accessible via www.feynhiggs.de

List of participants

Abrams Robert, Indiana University, USA
Acharya B S, TIFR, Mumbai, India
Adolphsen Chris, SLAC, USA
Agrawal Pankaj, IOP, Bhubaneswar, India
Agrawal Ujjawala, BEL, India
Ananthanarayan Balasubramanian, IISc, Bangalore, India
Andricek Ladislav, MPI Munich, Germany
Angal-Kalinin Deepa, CCLRC, Daresbury Laboratory, UK
Angarano Matteo, CAEN spa, Italy
Appleby Rob, The Cockcroft Institute, UK
Arora Shilpee, University of Delhi, Delhi, India
Asakawa Eri, KEK, Japan
Asiri Fred, SLAC, USA
Augustin Jean-Eudes, LPNHE-Paris, France
Aziz Tariq, TIFR, Mumbai, India

Bacala Angelina, Mindanao State University, Iligan City, Philippines
Bailey David, University of Manchester, UK
Banerjee Sunanda, TIFR, Mumbai, India
Bardeen Marjorie, Fermilab, USA
Barish Barry, Caltech, USA
Barklow Timothy, SLAC, USA
Basu Rahul, IMSc, Chennai, India
Beard Carl, ASTeC, Daresbury Laboratory, UK
Behnke Ties, DESY, Germany
Berger Edmond, Argonne National Laboratory, USA
Bhandari Rakesh, VECC, Kolkata, India
Bharadwaj Vinod, SLAC, USA
Bhattacharya Satyaki, University of Delhi, Delhi, India
Bhattacharyya Gautam, SINP, India
Bhattacherjee Biplob, University of Calcutta, Kolkata, India
Bheesette Satyanarayana, TIFR, Mumbai, India
Biagini Maria Enrica, INFN-LNF, Italy
Bialowons Wilhelm, DESY, Germany
Biswal Sudhansu, IISc, Bangalore, India
Blair Grahame, Royal Holloway, Univ. of London, UK
Bose Suvadeep, TIFR, Mumbai, India
Brau James, Univ. of Oregon, USA
Buesser Karsten, DESY, Germany
Burrows Philip, John Adams Institute, Oxford University, UK

Carter Harry, Fermi National Accelerator Laboratory, USA
Carwardine John, Argonne National Laboratory, USA
Chattopadhyay Subhasis, VECC, Kolkata, India
Choudhary Brajesh, Fermilab, USA
Choudhury Debajyoti, University of Delhi, Delhi, India
Christian Glenn, John Adams Institute for Accelerator Science, UK
Clements Elizabeth, Fermilab, USA
Coe Paul, University of Oxford, UK
Colas Paul, CEA Saclay/DAPNIA, France
Contarato Devis, Lawrence Berkeley National Laboratory, USA
Cooper William, Fermilab, USA
Corriveau Francois, IPP/McGill University, Canada
Cvach Jaroslav, Institute of Physics ASCR, Prague, Czech Republic

Dahiya Harleen, Panjab University, Chandigarh, India
Dahiya Mamta, SGTB Khalsa College, University of Delhi, India
Dainton John, Cockcroft Institute, UK
Das Prasanta, IMSc, Chennai, India
Das Sibaprasad, Jadavpur University, India
Datta Anindya, HRI, Allahabad, India
Datta Asesh, HRI, Allahabad, India
de Lataille Christophe, IN2P3/LAL Orsay, France
Delahaye Jean-Pierre, CERN, Switzerland

Delerue Nicolas, John Adams Institute, University of Oxford, UK
Demarteau Marcel, Fermilab, USA
Desch Klaus, University of Freiburg, Germany
Dey Malay, VECC, DAE, India
Dhawan Satish, Yale University, USA
Diaz Marco Aurelio, Universidad Catolica de Chile, Chile
Dixit Sudhir, John Adams Institute, University of Oxford, UK
Djouadi Abdelhak, LPT Orsay, France
Druhakou Uladzimir, NC PHEP, Minsk/DESY, Belarus
Dugan Gerald, Cornell University, USA
Dutta Sharada, IISc, Bangalore, India
Dutta Sukanta, SGTB Khalsa College, University of Delhi, India

Eckerlin Guenter, DESY, Germany
Ehrlichmann Heiko, DESY, Germany
Elsen Eckhard, DESY, Germany
Enomoto Atsushi, KEK, Japan

Ferrari Arnaud, Uppsala University, Sweden
Finch Alexander, Lancaster University, UK
Fisk Henry, Fermilab, USA
Fleury Julien, LAL-Orsay, France
Foster Brian, University of Oxford, UK
Freitas Ayres, University of Zurich, Zurich, Switzerland
Funk Warren, Jefferson Lab, USA

Gao Jie, IHEP, Beijing, China
Gao Yuanning, Tsinghua University, China
Garbincius Peter, Fermilab, USA
Gatto Corrado, INFN Lecce, Italy
Gaur Naveen, University of Delhi, Delhi, India
Gautam Sanjeev, Panjab University, Chandigarh, India
Gavai Rajiv, TIFR, Mumbai, India
Gay Pascal, LPC-UBP-IN2P3, France
Gaycken Goetz, LLR-Ecole Polytechnique, France
Godbole Rohini, IISc, Bangalore, India
Grah Christian, DESY, Germany
Grancagnolo Francesco, INFN-Lecce, Italy
Grannis Paul, US DOE, USA
Greenshaw Tim, Liverpool University, UK
Gronberg Jeffrey, LLNL, USA
Guchait Monoranjan, TIFR, Mumbai, India
Guiducci Susanna, INFN-LNF, Italy
Gupta Rameshwar
Gupta Sudhir, HRI, Allahabad, India
Gurtu Atul, TIFR, Mumbai, India

Hansen Jorgen, Denmark
Hartin Tony, John Adams Institute, University of Oxford, UK
Hauptman John, Iowa State University, USA
Hayano Hitoshi, KEK, Japan
Heinemeyer Sven, University of Zaragoza, Spain
Heusch Clemens, SCIPP, UC Santa Cruz, USA
Hewett JoAnne, SLAC/Stanford, USA
Higo Toshiyasu, KEK, Japan
Himel Tom, SLAC, USA
Hronek Maxine, Fermilab, USA

Ikematsu Katsumasa, DESY, Germany
Irikura Masao, Toshiba Electron Tubes & Devices Co., Ltd., Japan

Jacosalem Editha, MSU-IIT, Philippines
Jaros John, SLAC, USA
Jean-Luc Baldy, CERN, Switzerland
Jindal Pratima, Panjab University, Chandigarh, India
Jones Roger, Cockcroft Institute, University of Manchester, UK
Joshi Satish, RRCAT, Indore, India
Jung Dong-Won, KIAS, Seoul, Korea

Kanjilal Dinakar, IUAC, Delhi, India
Karlen Dean, University of Victoria & TRIUMF, Canada
Karmarkar Mangesh, RRCAT, Indore, India
Kephart Robert, Fermilab, USA
Khare Avinash, IOP, Bhubaneswar, India
Kim DongHee, Kyungpook National University, Korea
Kim HyoungSuk, Kyungpook National University, Korea
Kim Kwang-Je, Argonne National Laboratory, USA

Kim Young-Kee, University of Chicago, USA
Kobayashi Makoto, KEK, Japan
Komamiya Sachio, University of Tokyo, Japan
Koscielniak Shane, TRIUMF, Canada
Krawczyk Maria, Warsaw University, Poland
Krishnagopal Srinivas, CAT, Indore, India
Kubo Kiyoshi, KEK, Japan
Kuchler Vic, Fermilab, USA
Kumar Alok, IMSc, Chennai, India
Kuriki Masao, KEK, Japan
Kurokawa Shin-ichi, KEK, Japan
Kurup Balakrishna, TIFR, Mumbai, India
Kush Pradeep, RRCAT, Indore, India

Lackowski Tom, Fermilab, USA
Laihem Karim, DESY, Germany
Laktineh Imad, IPN de Lyon, France
Larsen Ray, SLAC, USA
Lebrun Paul, Fermilab, USA
LeDiberder Francois, CNRS/IN2P3, France
Ledu Patrick, DAPNIA CEA, France
Li Weiguo, IHEP, Beijing, China
Lilje Lutz, DESY, Germany
Liu Qian, IHEP, Beijing, China
Loew Gregory, SLAC, USA
Lohmann Wolfgang, DESY, Germany
Lutz Pierre, DAPNIA/Saclay, France

Magnan Anne-Marie, Imperial College, London
Maity Manas, Visva-Bharati, India
Majumder Gobinda, TIFR, Mumbai, India
Maki Akihiro, KEK, Japan
Mallik Chaturanan, VECC, Kolkata, India
Mallik Usha, The University of Iowa, USA
Markiewicz Thomas, SLAC, USA
Martin Jean-Pierre, University of Montreal, Canada
Martin Victoria, University of Edinburgh, UK
Mathews Prakash, SINP, Kolkata, India
Matsumoto Shigeki, KEK, Japan
Matsunaga Hiroyuki, University of Tsukuba, Japan
Matsuoka Masanori, Mhi, Japan
Mavromanolakis Georgios, Univ. of Cambridge, UK
Mazumdar Kajari, TIFR, Mumbai, India
McBride Patricia, Fermi National Acceleartor Lab, USA
Meshkov Igor, JINR, Dubna, Russia
Michael Poehler, CERN, Switzerland
Mishra Shekhar, Fermilab, USA
Misra Basudha, IMSc, Chennai, India
Miyamoto Akiya, KEK, Japan
Mnich Joachim, DESY, Germany
Moenig Klaus, DESY, Germany
Mondal Naba, Tata Institute, India
Morgunov Vasily, DESY/ITEP, Germany
Mori Toshinori, University of Tokyo, Japan
Morita Youhei, KEK, Japan
Moser Hans-Guenther, MPI fuer Physik, Germany
Mukherjee Asmita, IIT, Bombay, India
Mukhopadhyaya Biswarup, HRI, Allahabad, India
Myneni Ganapati Rao, Jefferson Lab., USA

Namkung Won, POSTECH, Korea
Napoly Olivier, CEA/Saclay, France
Nelson Tony, Wah Chang, USA
Nishi Masatsugu, Linear Collider Forum of Japan, Japan
Nitoh Osamu, Tokyo University of Agriculture and Technology, Japan
Noguchi Shuichi, KEK, Japan
Nozaki Mitsuaki, Kobe University, Japan
Nyffeler Andreas, HRI, Allahabad, India

Oddone Piermaria, Fermilab, USA
Oh Sun-Kun, Konkuk University, Korea
Ohuchi Norihito, KEK, High Energy Accelerator Research Organization, Japan
Okada Nobuchika, KEK, Japan
Okada Yasuhiro, KEK, Japan
Omori Tsunehiko, KEK, Japan
Oreglia Mark, University of Chicago, USA

Padamsee Hasan, Cornell University, USA
Pagani Carlo, University and INFN Milano, Italy
Pandit Vijay-Shanker, VECC, Kolkata, India
Pandita Pran, North Eastern Hill University, India
Pankov Alexander, Techn. Univ. of Gomel, Belarus
Para Adam, Fermilab, USA
Park Hwanbae, Kyungpook National University, Korea
Paterson Ewan, SLAC, USA
Pauletta Giovanni, University/INFN Udine, Italy
Peiniger Michael, ACCEL Instruments GmbH, Germany
Penzo Aldo, Trieste/INFN, Italy
Peterson Robert, Fermilab, USA
Peterson Thomas, Fermi National Accelerator Laboratory, USA
Phinney Nan, SLAC, USA
Pillay Raj, TIFR, Mumbai, India
Poddar Sujoy, Jadavpur University, India
Polak Ivo, Institute of Physics, Prague, Czech Republic
Popescu Sorina, IFIN-HH/CERN, Switzerland
Poulose Poulose, IIT, Guwahati, India
Prabhakara Rao Y P, BEL, India

Rai Santosh, HRI, Allahabad, India
Ramadas T S, Avasarala Technologies Ltd., India
Rangarajan Govindan, IISc, Bangalore, India
Rani Rejeena, BEL, India
Rao Kumar, PRL, Ahmedabad, India
Raspereza Alexei, MPI Munich, Germany
Raubenheimer Tor, SLAC, USA
Raychaudhuri Sreerup, IIT, Kanpur, India
Reidy Jim, US Dept of Energy-HEP, USA
Reserva Rosario, MSU-IIT, Philippines
Richard Francois, LAL/IN2P3, France
Riemann Sabine, DESY, Germany
Rindani Saurabh, PRL, Ahmedabad, India
Rizzo Thomas, SLAC, USA
Ronan Michael, LBNL, Berkeley
Rosca Aura, West University of Timisoara, Romania
Ross Marc, SLAC, USA
Roy Amit, Inter-University Accelerator Centre, New Delhi, India
Roy Durgaprasad, TIFR, Mumbai, India
Roy Probir, TIFR, Mumbai, India
Roychowdhury Samadrita, Duke University, USA
Royole-Degieux Perrine, LAL, France

Saito Kenji, KEK, Japan
Sanjeev Ganesh, Microtron Centre, Mangalore University, Mangalore, India
Sanuki Tomoyuki, University of Tokyo, Japan
Saveliev Valeri, Obninsk State Uni/DESY, Russia
Savoy-Navarro Aurore, LPNHE-Paris, France
Schaelicke Andreas, DESY, Germany
Schulte Daniel, CERN, Switzerland
Sefkow Felix, DESY, Germany
Sen D, IISc, Bangalore, India
Seryi Andrei, SLAC, USA
Settles Ron, Max-Planck-Institute for Physics, Munich/Desy, Germany
Shankaranarayana N P, BEL, India
Sharma Chandradew, IMSc, Chennai, India
Sharma Chandrasen, Indo-German Tool Room
Sharma Nikhil, BEL, India
Sharma Seema, TIFR, Mumbai, India
Shidara Tetsuo, KEK, Japan
Shirkov Grigori, JINR, Dubna, Russia
Shivpuri Ram, University of Delhi, Delhi, India
Shrinath B V, Avasarala Technologies Ltd., India
Shrivastava Purushottam, RRCAT, Indore, India
Sinev Nikolai, University of Oregon, USA
Singh Jasbir, Panjab University, Chandigarh, India
Singh Ritesh, LPT Orsay, France
Sinha Nita, IMSc, Chennai, India
Solyak Nikolay, Fermilab, USA

Som Sumit, VECC, Kolkata, India
Sopczak Andre, Lancaster University, UK
Sridhar K, TIFR, Mumbai, India
Srikanth Raghavendra, HRI, Allahabad, India
Stanek Rich, Fermilab, USA
Stefanov Konstantin, Rutherford Appleton Laboratory, UK
Sugahara Ryuhei, KEK, Japan
Sugimoto Yasuhiro, KEK, Japan
Sugiyama Akira, Saga University, Japan
Swarna Kotaiah, RRCAT, Indore, India

Takeshita Tohru, Shinshu University, Japan
Tanaka Masami, KEK, Japan
Targett-Adams Christopher, Calice, UK
Tauchi Toshiaki, KEK, Japan
Tavian Laurent, CERN, Switzerland
Taylor Geoffrey, University of Melbourne, Australia
Telnov Valery, INP, Novosibirsk, Russia
Terunuma Nobuhiro, KEK, Japan
Thomson Mark, University of Cambridge, USA
Toge Nobukazu, KEK, Japan
Tonutti Manfred, RWTH Aachen, Germany
Tonwar Suresh, TIFR, Mumbai, India
Topkar Anita, BARC, Mumbai, India
Tripathi Mani, University of California, Davis, USA

Urakawa Junji, KEK, Japan

Vaidya Sachindeo, IISc, Bangalore, India
Varma Raghava, IIT, Bombay, India
Videau Henri, LLR-Ecole Polytechnique, France
Vila Ivan, Instituto de Fisica de Cantabria, Spain
Vogel Hanspeter, ACCEL Instruments GmbH, Germany

Wagner Albrecht, DESY, Germany
Walker Nicholas, DESY, Germany
Watanabe Isamu, Akita Keizaihoka Univ., Japan
Weerts Hendrik, Argonne National Laboratory, USA
Wendt Oliver, DESY, Germany
White Andrew, University of Texas at Arlington, USA
Wierba Wojciech, Institute of Nuclear Physics PAS, Cracow, Poland
Willeke Ferdinand, DESY, Germany
Willis William, Columbia University, USA
Winter Marc, IRES/CNRS, Strasbourg
Worm Steve, RAL, UK

Yamamoto Hitoshi, Tohoku University, Japan
Yamashita Satoru, University of Tokyo, Japan
Yasui Yoshiaki, Tokyo Management College, Japan
Yokoya Kaoru, KEK, Japan
Yoshioka Tamaki, University of Tokyo, Japan
Yu Jaehoon, University of Texas at Arlington, USA

Zalesak Jaroslav, Institute of Physics ASCR, Prague, Czech Republic
Zhang Bin, Tsinghua University, China
Zhang Qingmin, Institute of High Energy Physics, Beijing, China
Zhang Zhiqing, LAL, Orsay, France
Zhao Tianchi, University of Washington, USA
Zutshi Vishnu, Northern Illinois University, USA

(Continued from back page)

Photon collider beam simulation with CAIN .... *Aleksander Filip Żarnecki* 937

Loop Calculations

Results from GRACE/SUSY at one-loop .... *J Fujimoto, T Ishikawa, M Jimbo, T Kaneko, T Kon, Y Kurihara, M Kuroda, Y Shimizu and Y Yasui* 943

Electroweak precision data and gravitino dark matter .... *S Heinemeyer* 947

List of Participants i

(*Continued from inside back cover*)

New Physics at TeV Scale and Electroweak Precision Test

Probing space–time structure of new physics with polarized beams at the international linear collider .... *B Ananthanarayan* 849

Signals of universal extra dimension at the international linear collider .... *Biplob Bhattacherjee* 855

Higher-order corrected Higgs bosons in FeynHiggs2.4 .... *T Hahn, S Heinemeyer, W Hollik, H Rzehak, G Weiglein and K Williams* 861

Extra dimension searches at hadron colliders to next-to-leading order-QCD .... *M C Kumar, Prakash Mathews and V Ravindran* 871

Distinguishing new physics scenarios with polarized electron and positron beams .... *A A Pankov, N Paver and A V Tsytrinov* 877

Transverse polarization in $\gamma Z, HZ$ production .... *Saurabh D Rindani* 883

Higher curvature effects in Arkani-Hamed–Dimopoulos–Dvali and Randall–Sundrum models .... *T G Rizzo* 889

Event-shape of dileptons plus missing energy at a linear collider as a supersymmetry/Arkani-Hamed–Dimopoulos–Dvali discriminant .... *Probir Roy* 895

Probing universal extra dimension at the international linear collider .... *Gautam Bhattacharyya* 903

Littlest Higgs model and W pair production at international linear collider .... *P Poulose* 909

Top and Quantum Chromodynamics

Lepton distribution in top decay: A probe of new physics and top-polarization .... *Rohini M Godbole, Saurabh D Rindani and Ritesh K Singh* 915

Scalar top study: Detector optimization ... *C Milsténe and A Sopczak* 921

$\gamma\gamma\ e^-e^-$ Physics

Measuring Higgs CP properties through top quark production at a photon collider .... *Eri Asakawa* 927

Heavy neutral MSSM Higgs bosons at the photon linear collider – a comparison of two analyses .... *M Spira, P Nieżurawski, M Krawczyk and A F Żarnecki* 931

G.M. College of Education
Raipur, Bantalab
Jammu.
Acc No.....5283.......
Dated.......19/12/2024

(*Continued on back page*)

(*Continued from back cover*)

Probing CP-violating Higgs contributions in $\gamma\gamma \to f\bar{f}$ .... *Rohini M Godbole, Sabine Kraml, Saurabh D Rindani and Ritesh K Singh* 771

Anomalous VVH interactions at a linear collider .... *Sudhansu S Biswal, Debajyoti Choudhury, Rohini M Godbole and Ritesh K Singh* 777

Testing the minimal supersymmetric standard model with the mass of the W boson .... *S Heinemeyer, W Hollik, D Stöckinger, A M Weber and G Weiglein* 783

Partially composite two-Higgs doublet model .... *Dong-Won Jung* 789

Probing anomalous Higgs couplings at an $e\gamma$ collider using unpolarised beams .... *Debajyoti Choudhury and Mamta* 795

Search for Higgs boson in beyond standard model scenarios at large hadron collider .... *Kajari Mazumdar* 801

Associated single photons and doubly-charged scalars at linear e^-e^- colliders .... *Biswarup Mukhopadhyaya and Santosh Kumar Rai* 809

Identifying new physics contributions in the Higgs sector at linear e^+e^- colliders .... *Santosh Kumar Rai* 815

Higgs self-coupling in the fusion channel at the international linear collider .... *K Moenig and A Rosca* 819

SUSY Particles

Phenomenology of non-universal gaugino masses and implications for the Higgs boson decay .... *K Huitu, J Laamanen, P N Pandita and Sourov Roy* 823

Low-scale gravity mediation in warped extra dimension and collider phenomenology on hidden sector .... *H Itoh, N Okada and T Yamashita* 829

Model-independent approach for dark matter phenomenology: Signatures in linear colliders and cosmic positron experiments .... *Shigeki Matsumoto and Nobuchika Okada* 835

Top squark and neutralino decays in a R-parity violating model constrained by neutrino oscillation data .... *Sujoy Poddar* 839

Testing the supersymmetric QCD Yukawa coupling in a combined LHC/ILC analysis .... *A Freitas and P Z Skands* 843

(*Continued on opposite page*)

PRAMANA
journal of
physics

Vol. 69 (No. 5), November 2007

CONTENTS

Special Issue on

Proceedings of the Linear Collider Workshop (LCWS06) – Part I

Foreword 693

Plenary

The LDC detector concept .... *Ties Behnke* 697

Gamma gamma technology group .... *Alexander John Finch* 703

Physics overview: Introduction to international linear collider physics .... *Yasuhiro Okada* 707

Physics beyond the standard model and cosmological connections: A summary from LCWS06 .... *K Sridhar* 719

The road towards the international linear collider: Higgs, top/quantum chromodynamics, loops .... *S Heinemeyer* 727

Forward tracking detectors .... *Klaus Mönig* 735

Higgs and Electroweak Symmetry Breaking

Photon pairs: Quantum chromodynamics continuum and the Higgs boson .... *Edmond L Berger* 743

The standard model Higgs search at the large hadron collider .... *Satyaki Bhattacharya* 749

Little Higgs model effects in $\gamma\gamma \to \gamma\gamma$ .... *S Rai Choudhury, Ashok Goyal, A S Cornell and Naveen Gaur* 753

Charged and neutral minimal supersymmetric standard model Higgs boson decays and measurement of tan β at the compact linear collider .... *E Coniavitis and A Ferrari* 759

Power losses in the international linear collider 20 mrad extraction line at 1 TeV .... *A Ferrari and Yuri Nosochkov* 765

(*Continued on inside back cover*)

Indexed in CURRENT CONTENTS ISSN 0304-4289
Edited and published by N Mukunda for the Indian Academy of Sciences, Bangalore 560080
Printed at Tholasi Prints India Pvt. Ltd., Bangalore
Registered with Registrar of Newspapers in India, Vide Regn No. [illegible]
Regn. No. CPMG/KA/BGE-337/2006-2008 WPP No. 49
Posted at PSO, Mysore Road, Bangalore 560026 16/11/2007

Rs. 50/-